

## University of Southampton Research Repository

Copyright © and Moral Rights for this thesis and, where applicable, any accompanying data are retained by the author and/or other copyright owners. A copy can be downloaded for personal non-commercial research or study, without prior permission or charge. This thesis and the accompanying data cannot be reproduced or quoted extensively from without first obtaining permission in writing from the copyright holder/s. The content of the thesis and accompanying research data (where applicable) must not be changed in any way or sold commercially in any format or medium without the formal permission of the copyright holder/s.

When referring to this thesis and any accompanying data, full bibliographic details must be given, e.g.

Thesis: Author (Year of Submission) "Full thesis title", University of Southampton, name of the University Faculty or School or Department, PhD Thesis, pagination.

Data: Author (Year) Title. URI [dataset]



**UNIVERSITY OF SOUTHAMPTON**

FACULTY OF ENVIRONMENTAL AND LIFE SCIENCES

School of Biological Sciences



**THE CONTRIBUTION OF SRC FAMILY KINASES TO SYNAPTIC FUNCTION AND  
PLASTICITY IN ADULT WILD-TYPE MICE AND AN INDUCIBLE MOUSE MODEL OF  
ALZHEIMER'S DISEASE**

by

**Lauren McNicholas**

Thesis for the degree of Doctor of Philosophy

February 2023





## **Abstract**

Alzheimer's disease (AD) is the most common cause of dementia, yet there are no drugs available that can prevent or slow disease progression. One reason for this could be because research focussed on treating individuals with mid-to-late AD who present with extensive and potentially irreversible damage. Increasing research is now investigating therapies to target much earlier pathological events in earlier stages of AD. By the point of AD diagnosis, >50% of CA1 hippocampal synapses have already been lost. Furthermore, synaptic plasticity deficits occur before and could be causative of synapse loss. Therefore, understanding the mechanisms driving synaptic plasticity deficits in AD is an attractive area of research that could aid the discovery of new treatments for early AD intervention.

One potential candidate contributing to plasticity and synapse loss is Fyn kinase (Fyn), a member of the Src family kinases (SFKs). Post-mortem AD tissue and AD mouse models show increased Fyn activity or phosphorylation of Fyn targets. Fyn phosphorylates Y1472 of GluN2B subunits of the NMDAR, stabilising NMDARs at the synapse. Enhanced Fyn activity in AD is proposed to over-stabilise GluN2B-containing NMDARs and increase NMDAR signalling, which could promote excitotoxicity and contribute to the loss of plasticity and synapses.

Using an inducible mouse model of AD (Line 102) to induce APP<sub>Swe/Ind</sub> expression in adult mice, we analysed mice when synaptic plasticity deficits first arise in CA3-CA1 synapses (after 3 weeks of APP<sub>Swe/Ind</sub> expression). We show enhanced GluN2B pY1472, consistent with increased Fyn activity. To test whether increased Fyn activity contributes to reduced synaptic plasticity, we measured long-term potentiation (LTP) in hippocampal slices from these mice following inhibition of Fyn with Saracatinib, a drug approved for human use with repurposing potentials for AD.

Acute Saracatinib treatment reduced Y1472-GluN2B phosphorylation, and whilst it did not alter LTP in adult WT mice, it rescued the LTP impairment in Line 102 mice. This suggests that increased Fyn activity may contribute to plasticity impairments in this model. However, since Saracatinib is a broad SFK inhibitor, further research is required using more Fyn-specific drugs to determine whether Fyn inhibition is responsible for rescuing plasticity. Acute Saracatinib treatment did not rescue impaired synaptic transmission that occurred later in Line 102 mice, suggesting a narrow therapeutic window of Saracatinib. This thesis supports the evidence suggesting increased Fyn activity in AD, and our results suggest that this increase may occur early in disease progression, possibly before symptom onset. The findings in this project contribute to our understanding of the mechanisms that underlie early AD pathology and add further support to the future use of SFK inhibitors to treat AD.



# Table of Contents

<b>Table of Contents</b> .....	<b>i</b>
<b>Table of Tables</b> .....	<b>vii</b>
<b>Table of Figures</b> .....	<b>ix</b>
<b>Research Thesis: Declaration of Authorship</b> .....	<b>xiii</b>
<b>Acknowledgements</b> .....	<b>xv</b>
<b>Definitions and Abbreviations</b> .....	<b>xvii</b>
<b>Chapter 1 Introduction</b> .....	<b>1</b>
1.1 Alzheimer's disease.....	1
1.1.1 The role of A $\beta$ in Alzheimer's disease .....	3
1.1.2 The role of tau in Alzheimer's disease .....	6
1.2 The Hippocampus .....	8
1.2.1 Hippocampal layers.....	9
1.3 Excitatory neurotransmission .....	12
1.3.1 AMPA and NMDA receptors.....	12
1.3.1.1 AMPA receptors .....	12
1.3.1.2 NMDA receptor structure and properties .....	13
1.3.1.3 NMDA receptor subunits.....	15
1.3.1.4 NMDA receptor allosteric modulation .....	16
1.4 Synaptic plasticity.....	17
1.5 The NMDAR subunit composition may alter the type of plasticity induced .....	20
1.6 Synapse loss and synaptic dysfunction in AD.....	21
1.6.1 Synaptic dysfunction in the Line 102 mouse model.....	24
1.7 SFK structure and regulation.....	27
1.8 Fyn activity is increased in AD .....	30
1.8.1 Evidence from humans.....	30
1.8.2 Evidence from model systems .....	30
1.8.2.1 Cell culture .....	30
1.8.2.2 Mouse Models.....	31

## Table of Contents

1.9	A $\beta$ -Fyn-Tau interaction.....	33
1.10	Increased Fyn activity may contribute to AD pathology via GluN2B-containing NMDARs .....	36
1.10.1	Fyn-mediated GluN2B phosphorylation increases cell-surface expression of GluN2B-containing NMDARs .....	37
1.10.2	Fyn-mediated GluN2B phosphorylation increases synaptic contribution of GluN2B-containing NMDARs .....	39
1.10.3	Src enhances NMDAR-mediated currents .....	42
1.10.4	Increased Fyn activity may promote excitotoxicity .....	44
1.10.5	Src and Fyn modulate synaptic plasticity .....	47
1.11	Inhibiting Fyn in AD: Saracatinib.....	51
1.12	Aims and Objectives .....	58
<b>Chapter 2</b>	<b>Methods .....</b>	<b>59</b>
2.1	Animals .....	59
2.1.1	Animal husbandry.....	59
2.1.2	Line 102 .....	59
2.2	Genotyping .....	60
2.2.1	DNA extraction .....	61
2.2.2	PCR .....	61
2.2.3	Agarose gel electrophoresis .....	63
2.3	Electrophysiology .....	64
2.3.1	Solutions .....	64
2.3.2	Brain extraction .....	64
2.3.3	Preparation of hippocampal slices .....	65
2.3.4	Field recordings rig setup .....	66
2.3.5	Eliciting field excitatory postsynaptic potentials (fEPSPs) .....	67
2.3.6	Input-Output response .....	67
2.3.7	Paired-pulse ratio .....	68
2.3.8	Theta-burst induced LTP .....	68
2.4	Drug application .....	69

2.4.1 Saracatinib for <i>ex vivo</i> application .....	69
2.4.2 Saracatinib for <i>in vivo</i> administration .....	70
2.4.3 DHPG .....	70
2.4.4 TAT-Fyn(39-47).....	71
2.5 Western blotting .....	71
2.5.1 Protein extraction .....	71
2.5.2 Sample preparation.....	72
2.5.3 SDS-polyacrylamide gel electrophoresis (PAGE) .....	72
2.5.4 Electroblotting of protein to nitrocellulose membrane .....	73
2.5.5 Antibody labelling .....	74
2.5.6 Quantification and data analysis.....	75
2.6 Statistics .....	75
<b>Chapter 3 The effect of SFK inhibition on synaptic function and plasticity in WT mice</b>	<b>77</b>
3.1 Chapter aims .....	77
3.2 Results.....	78
3.2.1 Antibody validation .....	78
3.2.2 Acute application of Saracatinib reduces GluN2B pY1472 in adult WT hippocampal slices .....	79
3.2.3 Acute application of Saracatinib does not alter basal synaptic transmission in adult WT hippocampal slices.....	83
3.2.4 Acute application of Saracatinib does not alter basal synaptic plasticity in adult WT hippocampal slices.....	85
3.2.5 <i>In vivo</i> administration of Saracatinib in adult WT mice .....	87
3.3 Discussion.....	91
3.3.1 Acute Saracatinib application reduces GluN2B phosphorylation.....	92
3.3.2 Acute Saracatinib application does not alter basal synaptic transmission .....	94
3.3.3 Acute Saracatinib application does not alter synaptic plasticity.....	95
3.3.4 <i>In vivo</i> administration of Saracatinib.....	96
3.3.5 Conclusions .....	97
<b>Chapter 4 GluN2B phosphorylation in a mouse model of early Alzheimer's Disease ..</b>	<b>99</b>

## Table of Contents

4.1	Chapter aims .....	100
4.2	Results .....	100
4.2.1	GluN2B Y1742 phosphorylation is increased after 3 weeks, but not 12 or 16 weeks, off dox in adult onset Line 102 mice .....	100
4.2.2	Acute treatment of Line 102 hippocampal slices with Saracatinib .....	106
4.2.3	The effect of slicing on GluN2B Y1472 phosphorylation .....	108
4.3	Discussion .....	112
4.3.1	GluN2B Y1472 phosphorylation in Line 102 mice following 3 and 12 weeks of APP <sub>Swe/Ind</sub> expression .....	112
4.3.2	Application of Saracatinib to slices from Line 102 mice following 3 weeks of APP <sub>Swe/Ind</sub> expression .....	115
4.3.3	Conclusions .....	117
<b>Chapter 5 The effect of SFK inhibition in Line 102 mice .....</b>		<b>119</b>
5.1	Chapter aims .....	120
5.2	Saracatinib rescues plasticity deficits in Line 102 mice following 3 weeks of A $\beta$ accumulation .....	120
5.3	Saracatinib does not alter basal synaptic transmission in Line 102 mice following 3 and 12 weeks of A $\beta$ accumulation .....	123
5.4	Replicating LTP impairments in 16-week off dox Line 102 mice .....	126
5.5	Acute application of Saracatinib does not rescue impaired basal synaptic transmission in 16-week off dox Line 102 mice .....	128
5.6	Discussion .....	130
5.6.1	The effect of acute Saracatinib application to CA3-CA1 synapses of Line 102 mice following 3 weeks of APP <sub>Swe/Ind</sub> expression .....	130
5.6.2	The effect of acute Saracatinib application to CA3-CA1 synapses of Line 102 mice following 16 weeks of APP <sub>Swe/Ind</sub> expression .....	132
5.7	Conclusions .....	134
<b>Chapter 6 Overall conclusions and future work .....</b>		<b>137</b>
6.1	Research question and main findings .....	137
6.2	Limitations of this study and recommendations for future research .....	138

6.2.1	Using mouse models to study Alzheimer's Disease .....	138
6.2.2	Measuring GluN2B Y1472 phosphorylation as a readout of Fyn activity.....	139
6.2.3	Which kinase is responsible for the rescue of LTP by Saracatinib.....	140
6.2.4	Which SFK target protein(s) is responsible for the rescue of LTP by Saracatinib? .....	141
6.2.5	Pyk2 may contribute to the beneficial effects of Saracatinib .....	142
6.2.5.1	The synergistic relationship between Fyn and Pyk2 .....	143
6.2.5.2	Pyk2 and synaptic plasticity.....	143
6.2.5.3	AD relevance .....	144
6.2.5.4	Experimental proposal .....	145
6.2.6	Does chronic Saracatinib prevent synapse loss in Line 102 .....	146
6.2.6.1	Experimental proposal .....	146
6.3	Conclusions and perspective.....	148
<b>Appendix A The effect of sex on GluN2B pY1472 in Line 102 mice .....</b>		<b>151</b>
<b>List of References .....</b>		<b>155</b>





## Table of Tables

Table 1 GluN2 subunits alter the pharmacological and biophysical properties of NMDARs.....	15
Table 2 SFKs inhibited by 2 $\mu$ M Saracatinib .....	52
Table 3 Decreasing Fyn activity alters NMDAR phosphorylation, plasticity, cell viability and behaviour in mice. ....	56
Table 4 Mouse models of AD relevant to this project .....	57
Table 5 PCR components for genotyping Line 102 mice.....	61
Table 6 PCR reaction conditions .....	63
Table 7 Reagents and their volumes to make one 7% gel for Western blot.....	72
Table 8 Primary antibodies used for Western blotting.....	74



## Table of Figures

Figure 1.1 Cognitive decline in AD measured by MMSE score .....	2
Figure 1.2 Amyloid precursor protein processing.....	4
Figure 1.3 Tau gene and six isoforms in the human brain .....	7
Figure 1.4 The hippocampal formation .....	9
Figure 1.5 The rodent hippocampus.....	11
Figure 1.6 Structure of the GluN1/GluN2B NMDAR .....	14
Figure 1.7 Doxycycline controls the expression of APPSwe/Ind in APPtTA mice.....	25
Figure 1.8 Structure and activation of SFKs .....	28
Figure 1.9 A $\beta$ mediates toxic effects via the PrPc-mGluR5-Fyn complex. ....	33
Figure 1.10 D1 receptor activation by SKF81297.....	40
Figure 1.11 Mechanism of action of Fyn(39-57) .....	42
Figure 1.12 Src and Fyn activity enhance NMDAR currents.....	44
Figure 2.1. APP expression upon dox diet removal in Line 102 mice. ....	60
Figure 2.2 Genotyping Line 102 mice .....	64
Figure 2.3 Preparation of hippocampal slices for field recordings .....	65
Figure 2.4 Measuring the postsynaptic response .....	67
Figure 2.5 Paired-pulse ratio.....	68
Figure 2.6 Theta burst stimulation protocol .....	69
Figure 2.7 Arrangement of materials for SDS-PAGE protein transfer.....	73
Figure 3.1 Western blot image of hippocampal slices from adult WT mice following incubation in aCSF (veh), 2 $\mu$ M Saracatinib (2 hours) or 0.1 mM Na <sub>3</sub> VO <sub>4</sub> (10 minutes). ....	79
Figure 3.2 Saracatinib reduces GluN2B phosphorylation at Y1472 in WT adult hippocampal slices .....	80

## Table of Figures

Figure 3.3 The level of GluN2B and pY1472 GluN2B in hippocampal slices from adult WT mice following acute application of TAT-Fyn(39-57) peptide inhibitor .....	82
Figure 3.4 Acute application of Saracatinib does not alter basal synaptic transmission in WT adult hippocampal slices .....	84
Figure 3.5 Acute application of Saracatinib does not alter LTP in WT adult hippocampal slices	85
Figure 3.6 Acute application of Saracatinib does not alter DHPG-induced LTD in WT adult hippocampal slices .....	86
Figure 3.7 The level of GluN2B and pY1472 GluN2B in the hippocampus and cortex from adult WT mice following in vivo treatment with 5mg/kg/day or 20mg/kg/day Saracatinib for 3 days.....	88
Figure 3.8 The level of GluN2B and pY1472 GluN2B in the hippocampus and cortex from adult WT mice following in vivo treatment with 5mg/kg/day Saracatinib for 3 days ....	90
Figure 4.1 The level of GluN2B and pY1472 GluN2B in the hippocampus and cortex of Line 102 mice after 3 weeks of Dox removal.....	101
Figure 4.2 The level of GluN2B and pY1472 GluN2B in the hippocampus and cortex of Line 102 mice after 12 weeks of Dox removal.....	102
Figure 4.3 The level of GluN2B and pY1472 GluN2B in the hippocampus and cortex of Line 102 mice after 16 weeks of Dox removal.....	103
Figure 4.4 The levels of GluN2B and pY1472 GluN2B in hippocampal slices from Line 102 mice following acute application of Saracatinib .....	107
Figure 4.5 The effect of slicing on GluN2B Y1472 phosphorylation .....	109
Figure 4.6 The effect of slicing in aCSF containing kynurenic acid on GluN2B Y1472 phosphorylation .....	111
Figure 5.1 The effect of acute Saracatinib treatment on LTP in hippocampal slices from Line 102 mice after 3 weeks of dox removal .....	122
Figure 5.2 The effect of acute Saracatinib treatment on basal synaptic transmission in hippocampal slices from Line 102 mice after 3 weeks of dox removal.....	125
Figure 5.3 The level of LTP in hippocampal slices from Line 102 mice after 16 weeks of dox removal .....	127

Figure 5.4 The effect of acute Saracatinib treatment on basal synaptic transmission in hippocampal slices from Line 102 mice after 16 weeks of dox removal .....	129
Figure 6.1 Experiment design for administration of Saracatinib in vivo using Line 102 mice ..	147



## Research Thesis: Declaration of Authorship

Print name:

Title of thesis:

I declare that this thesis and the work presented in it are my own and has been generated by me as the result of my own original research.

I confirm that:

1. This work was done wholly or mainly while in candidature for a research degree at this University;
2. Where any part of this thesis has previously been submitted for a degree or any other qualification at this University or any other institution, this has been clearly stated;
3. Where I have consulted the published work of others, this is always clearly attributed;
4. Where I have quoted from the work of others, the source is always given. With the exception of such quotations, this thesis is entirely my own work;
5. I have acknowledged all main sources of help;
6. Where the thesis is based on work done by myself jointly with others, I have made clear exactly what was done by others and what I have contributed myself;
7. None of this work has been published before submission
8. Signature:                      Date:





## Acknowledgements

First, I would like to express my gratitude to my supervisors, Dr Mariana Vargas-Caballero and Dr Katrin Deinhardt, for their consistent help and encouragement throughout the past four years. Thank you for giving me this opportunity and trusting me with this project. Thank you also to the funders of this project, The Gerald Kerkut Trust and Alzheimer's Research UK.

Thank you to all lab members, past and present, for their academic and personal support. Good luck to all remaining in the lab as you continue your research. A special thanks to Hannah and Dianne, who started this process alongside me and have been the best lab partners and friends. Working in Ephys would not have been the same without you both. Even though now we go our separate ways into the "real world", I am sure we will keep in touch. I would also like to extend my sincere thanks to the technical staff at the BRF, especially Lorraine, who was a great help with the *in vivo* work presented in this thesis.

Last but not least, thank you to my family and friends outside of Southampton. Thanks especially to Hannah and Emma for always being at the end of the phone, congratulating me when things went well and motivating me when things got tough. To Sam for your unwavering patience and source of encouragement. Thank you for being there through my highs and lows and listening to me rant about science. Thank you to my parents, without whom none of this would have been possible. You have always believed in me, even when I did not believe in myself and I am forever grateful to have you both as my parents. To my grandfathers, who unfortunately will not get to see me close this chapter of my life, I hope I have made you proud.



## Definitions and Abbreviations

-/-	Knockout
A $\beta$	Amyloid $\beta$
A $\beta$ o	Amyloid $\beta$ oligomer
aCSF	Artificial cerebrospinal fluid
AD	Alzheimer's disease
AICD	APP intracellular C-terminal domain
AMPA	Alpha-amino-3-hydroxyl-5-methyl-4-isoxadole-propionate receptor
ANOVA	Analysis of variance
APP	Amyloid precursor protein
APV	Amino-5-phosphovalerate
BBB	Blood brain barrier
CA-Fyn	Constitutively active Fyn
CA	Cornu Ammonis
CaM	Calmodulin
CaMKII	Ca <sup>2+</sup> -calmodulin dependent kinase II
CNS	Central nervous system
CTD	C-terminal domain
CTF	C-terminal fragment
D1R	Dopamine 1 receptor
DG	Dentate gyrus
Dox	Doxycycline
EC	Entorhinal cortex
EPSC	Excitatory postsynaptic current
EPSP	Excitatory postsynaptic potential
FAD	Familial Alzheimer's disease
fEPSP	Field excitatory postsynaptic potential

## Definitions and Abbreviations

GABA .....	Gamma-aminobutyric acid
GPCR.....	G-protein coupled receptor
HFS .....	High frequency stimulation
IO .....	Input output
LBD .....	Ligand binding domain
LDH .....	Lactate dehydrogenase release
LTD .....	Long-term depression
LTP.....	Long-term potentiation
MAP .....	Microtubule associated protein
Mapt.....	Microtubule associated protein tau
MCI .....	Mild cognitive impairment
mGluR.....	Metabotropic glutamate receptor
MMSE .....	Mini mental state examination
MWM .....	Morris water maze
NFT .....	Neurofibrillary tangles
NMDAR.....	N-methyl-D-aspartate receptor
PKA .....	Protein kinase A
PPR .....	Paired pulse ratio
PrP .....	Prion protein
PSD .....	Postsynaptic density
PSD-95 .....	Postsynaptic density-95
PTK .....	Protein tyrosine kinase
SDS .....	Sodium dodecyl sulphate
SEM .....	Standard error of the mean
SFK.....	Src family kinase
SH .....	Src homology
SLM.....	Stratum lacunosum-moleculare
SM .....	Stratum moleculare

SO .....	Stratum oriens
SP .....	Stratum pyramidale
SR .....	Stratum radiatum
STEP .....	Striatal enriched tyrosine phosphatase
TBS .....	Theta burst stimulus
TMD .....	Transmembrane domain
tTA .....	Tetracycline transactivator
WT.....	Wild type



# Chapter 1 Introduction

## 1.1 Alzheimer's disease

Alzheimer's disease (AD) is a progressive neurodegenerative disease that is characterised by the presence of amyloid beta ( $A\beta$ ) plaques, tau neurofibrillary tangles, overt neurodegeneration, inflammation and cerebral amyloid angiopathy. Together these pathological hallmarks drive dysfunction and loss of neurons. As synapses and neurons are lost over the course of AD, individuals present with a gradual decline in cognitive ability that affects memory, judgment, decision making, orientation and language (Nussbaum et al., 2003). By the later stages of the disease, individuals are unable to live independently. This is not only devastating for families but also creates an economic burden which was estimated to be around £34.7 billion a year in 2019 in the UK (Wittenberg et al., 2019). Currently, there are no available drugs that can reverse or slow AD progression and only drugs that provide short-term symptomatic relief are available.

Cognitive impairment in individuals with AD is assessed using rating scales. The Mini-Mental State Examination (MMSE) is a widely used rating scale that assesses a person's mental capacity, including attention, short-term memory, language skills, visuospatial ability and the ability to understand and follow instructions. The maximum score for the test is 30, and a score of 25 or higher is considered normal. The severity of cognitive impairment is represented by the MMSE score as follows: mild AD:21-26, moderate AD:10-20, moderately severe AD: 10-14, severe AD: <10 (National Institute for Health and Clinical Excellence, 2011). The decrease in MMSE score during AD progression is illustrated in Figure 1.1.

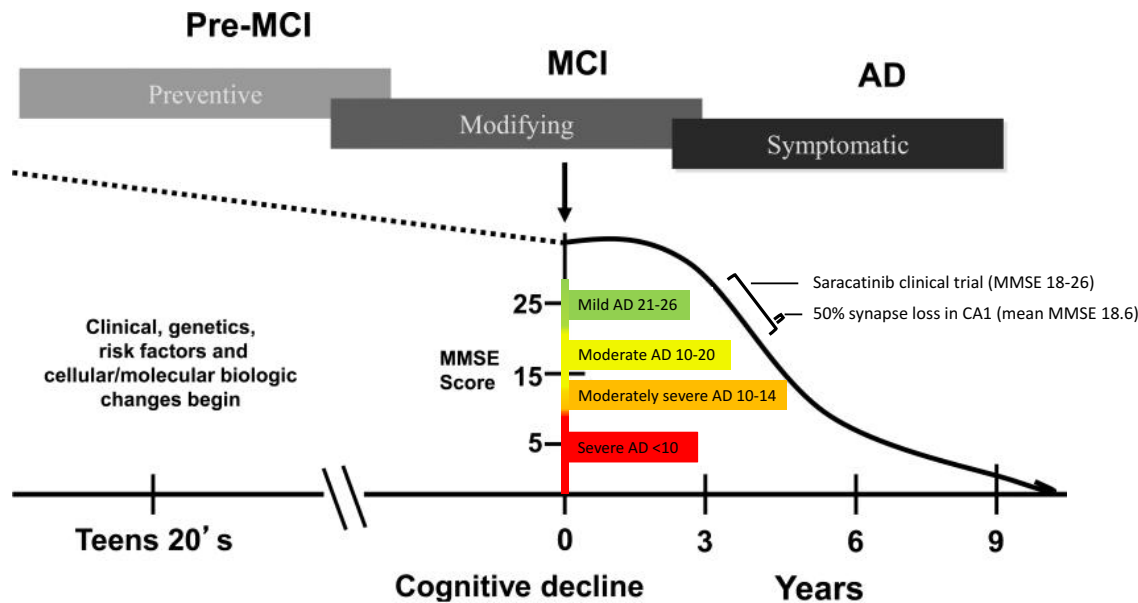


Figure 1.1 Cognitive decline in AD measured by MMSE score

A schematic to illustrate the extensive preclinical stage of AD followed by a progressive decline in MMSE score as memory function declines. The MMSE score can be divided into groups to define mild AD: MMSE 21-26 (green), moderate AD: MMSE 10-20 (yellow), moderately severe AD: MMSE 10-14 (orange), and severe AD: MMSE <10 (red). 50% of synapses in CA1 of the hippocampus are lost in early AD (MMSE 18.6). A Src family kinase inhibitor, Saracatinib, entered clinical trials and was tested on individuals with mild-moderate AD (18-26) (Van Dyck et al., 2019). Diagram adapted from Mufson et al., 2016.

Epidemiology analyses of brain pathology and cognitive impairment in the general population suggest that A $\beta$  deposition occurs in the brains of patients up to 15 years before MMSE scores decrease (Sperling et al., 2011). The failure of clinical trials could be attributed, at least in part, to testing disease-modifying drugs on individuals that are too late in the progression of AD. For example, the first active immunotherapy against A $\beta$  using AN1792 was tested on individuals with broad MMSE scores ranging from 14-16 (Orgogozo et al., 2003). However, current research is shifting to understand pathological events that occur much earlier in the disease, for example, before synapse loss and cognitive impairment. A better understanding of pathological events early in AD may lead to more effective therapeutic interventions that could act to protect against future neuronal damage, for example, by preventing synapse loss.



### 1.1.1 The role of A $\beta$ in Alzheimer's disease

A $\beta$  plaques are found extracellularly and close to neurons and are comprised of A $\beta$  peptides derived from cleavage of the amyloid precursor protein (APP), a type I transmembrane protein. The APP gene is located on chromosome 21, and alternative splicing results in 3 major isoforms; APP695 APP751 and APP770. Unlike the ubiquitously expressed APP751 and APP770 isoforms, APP695 is expressed exclusively in neurons. All 3 isoforms can be processed to produce A $\beta$ , however it is suggested that A $\beta$  is preferentially produced through the processing of APP695 (Belyaev et al., 2010).

As illustrated in Figure 1.2, APP is processed via the amyloidogenic or non-amyloidogenic pathway (reviewed by Chen et al., 2017). The production of A $\beta$  peptides occurs via the amyloidogenic pathway by sequential cleavage of APP by  $\beta$ -secretase and  $\gamma$ -secretase. The first cleavage step in the amyloidogenic pathway by  $\beta$ -secretase results in the release of a soluble fragment of APP (APP-s $\beta$ ). The remaining membrane fragment (CTF $\beta$ ) is cleaved by  $\gamma$ -secretase which can occur at multiple sites, giving rise to A $\beta$  fragments of various amino acid lengths (37-51 amino acids). Some of these fragments can be cleaved by  $\gamma$ -secretase to produce the most common A $\beta$  species; A $\beta$ 40 and A $\beta$ 42. A $\beta$ 42 is the most fibrillogenic and predominant component of A $\beta$  plaques (Meisl et al., 2014).

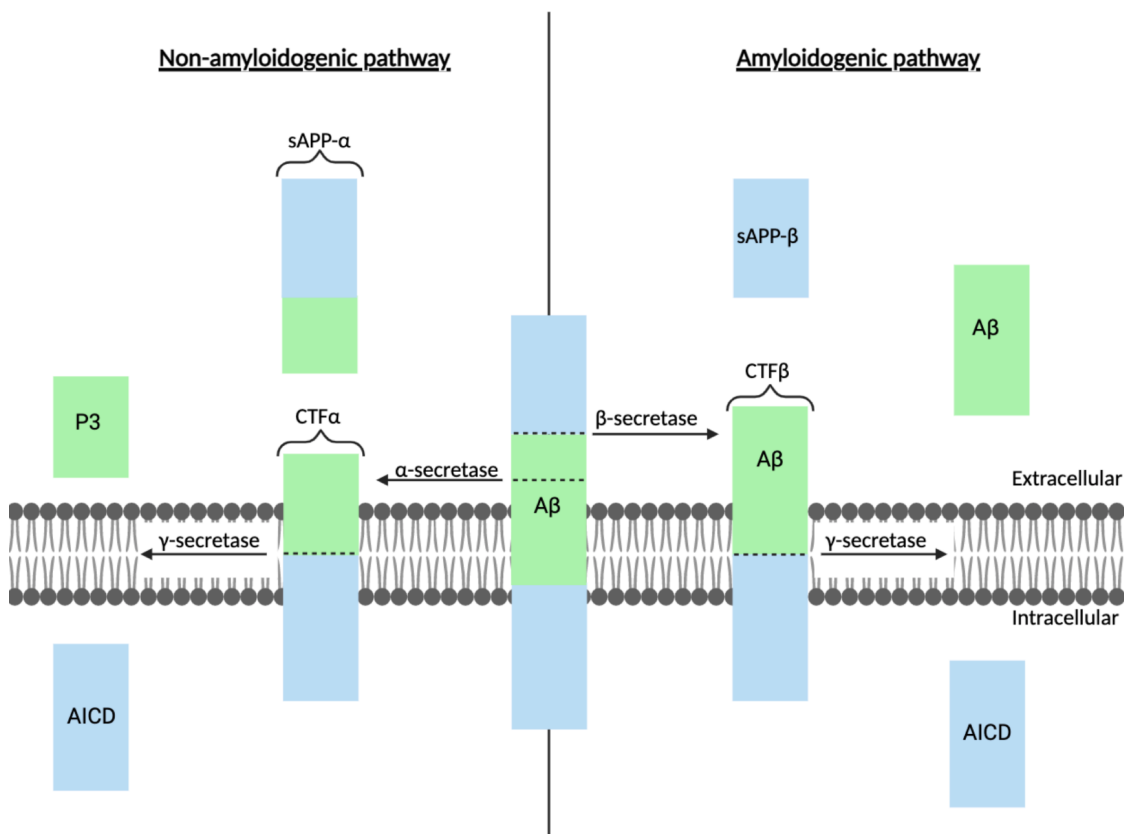


Figure 1.2 Amyloid precursor protein processing

APP can be cleaved via the amyloidogenic or non-amyloidogenic pathway. In the amyloidogenic pathway, APP is first cleaved  $\beta$ -secretase (BACE1), resulting in the secretion of a soluble fragment of APP (sAPP $\beta$ ) and a membrane-bound C-terminal fragment (CTF $\beta$ ). CTF $\beta$  is cleaved by  $\gamma$ -secretase, resulting in an APP intracellular C-terminal domain (AICD) and A $\beta$  peptide. In the non-amyloidogenic pathway, APP is cleaved by  $\alpha$ -secretase within the A $\beta$  domain, impeding A $\beta$  formation. This results in the release of a soluble fragment (s-APP $\alpha$ ) and a membrane-bound C-terminal fragment (CTF $\alpha$ ). Subsequent cleavage of CTF- $\alpha$  by  $\gamma$ -secretase gives rise to an AICD and P3 fragment. Created using Biorender.com.

Both amyloidogenic and non-amyloidogenic cleavage of APP occurs under physiological conditions, and A $\beta$  immunoreactivity has been detected in the cerebral spinal fluid (CSF) of 13-50-year-old healthy individuals (Seubert et al., 1992). However, the physiological function of A $\beta$  remains unclear, with many potential functions suggested, including antimicrobial activity, tumour suppression, sealing leaks in the blood brain barrier (BBB), promoting recovery from brain injury and regulating synaptic function (reviewed by Brothers et al., 2018). The physiological role of APP is also unclear. Some of the suggested functions of APP include playing a role in neurite

outgrowth and synaptogenesis, axonal protein trafficking and transmembrane signal transduction (reviewed by Zheng et al., 2006).

Under physiological conditions the production and clearance of A $\beta$  in the brain are rapid. However, under pathological conditions, such as AD, A $\beta$  monomers accumulate and aggregate to form soluble A $\beta$  oligomers (A $\beta$ o) which further aggregate into insoluble fibrils and plaques. A $\beta$  accumulation may occur due to decreased A $\beta$  clearance and/or increased A $\beta$  production. The clearance rate of A $\beta$  in the central nervous system (CNS) can be measured by metabolic labelling of A $\beta$ . This technique shows impaired clearance rates for both A $\beta$ 42 and A $\beta$ 40 in individuals with sporadic AD compared to healthy controls (Mawuenyega et al., 2010). Increased A $\beta$  production could also contribute towards A $\beta$  accumulation in AD. This is supported by the occurrence of familial AD (FAD) in individuals carrying various mutations in genes that encode APP,  $\gamma$ -secretase complex proteins (presenilin 1 and 2) and the increased prevalence of AD in individuals with Down's syndrome who have enhanced APP production as a result of triplication of chromosome 21 (Weggen et al., 2012)(Lott et al., 2019). In all scenarios, there is an increased production of A $\beta$  or A $\beta$ 42:A $\beta$ 40 ratio. A $\beta$ 42 accumulation is critical for AD pathogenesis, and increased A $\beta$ 42:A $\beta$ 40 ratios correlate with early onset FAD caused by presenilin mutations (Kumar-Singh et al., 2006).

Further evidence comes from the APP Iceland (A673T) genetic mutation, which is protective against AD. The A673 residue of APP is close to the  $\beta$ -secretase recognition site and forms part of the A $\beta$  peptide. The A673T mutation renders APP less favourable for  $\beta$ -secretase cleavage, and even when cleavage does occur, the resulting A $\beta$  peptides are less prone to aggregation. For example, HEK-293T cells transfected with mutant A673T APP showed a significant reduction in the formation of A $\beta$ 40 and A $\beta$ 42 peptides compared to WT APP transfected (Jonsson et al., 2012). These findings have since been replicated in mouse neuronal cultures and iPSC-derived human neurons expressing A673T APP. Decreased A $\beta$  production is therefore thought to explain the protective effects of this mutation against AD (Benilova et al., 2014; Maloney et al., 2014).

The occurrence of mutations in FAD that result in increased A $\beta$  load led to the development of the amyloid cascade hypothesis, proposed by Hardy and Higgins (Hardy et al., 1992). The theory suggests that A $\beta$  accumulation is the causative factor that drives AD pathogenesis. This hypothesis has since been modified to include that soluble A $\beta$ os are the toxic species driving synapse loss

rather than insoluble A $\beta$  fibrils and plaques (reviewed by Cline et al., 2018). A $\beta$ os are widely accepted as the pathogenic species that cause synaptic dysfunction and neuronal cell death by interacting with several postsynaptic receptors, including EphB2, PrPC and  $\alpha$ 7-nicotinic acetylcholine receptors ( $\alpha$ 7nAChR) (reviewed by Jarosz-Griffiths et al., 2016). Aberrant activation of these receptors have been associated with causing dysfunction of postsynaptic N-methyl-D-aspartate receptors (NMDARs), highlighting that NMDARs are a common denominator that may contribute to A $\beta$ o toxicity at postsynaptic sites. A $\beta$ os also interact with presynaptic receptors, including  $\alpha$ 7nAChR and the Na<sup>+</sup>/K<sup>+</sup>-ATPase  $\alpha$ 3 subunit (NaK $\alpha$ 3), which is associated with causing presynaptic dysfunction by altering presynaptic calcium levels (reviewed by Jarosz-Griffiths et al., 2016).

### 1.1.2 The role of tau in Alzheimer's disease

Another pathological hallmark of AD is the presence of neurofibrillary tangles (NFTs), which unlike A $\beta$ , accumulate intracellularly in neurons. NFTs show a stereotypical pattern of directional spreading between brain regions (referred to as Braak stages) that strongly correlates with the severity of cognitive decline (Bierer et al., 1995) (Braak et al., 1995). NFTs are composed of aggregated tau protein that is abnormally hyperphosphorylated. Tau is a microtubule-associated protein (MAP) that is abundant in axons and is involved in regulating microtubule stability, axonal transport, DNA maintenance and synaptic function (reviewed by (Kent et al., 2020).

In the adult human brain, expression of the single gene encoding tau (*MAPT*) results in the generation of six isoforms. This occurs as a result of alternative splicing (Figure 1.3) (Goedert et al., 1989). These isoforms depend on the number of N-terminal inserts of 29-amino acids (0N, 1N or 2N), and the presence or absence of exons 2, 3 and 10 to give rise to 3 or 4 C-terminal repeat domains (3R or 4R). In the adult human brain, there are roughly equal proportions of 3R and 4R isoforms (Goedert et al., 1989)(Trabzuni et al., 2012). In mice, the *MAPT* gene undergoes alternative splicing, however, unlike humans, only 4R tau isoforms are expressed in the adult mouse brain (Brion et al., 1993). The lack of 3R tau isoforms in mice could contribute to the absence of tau tangle pathology in AD mouse models with WT tau which may contribute to the lack of translation of findings from mice to humans (reviewed by Vargas-Caballero et al., 2016).

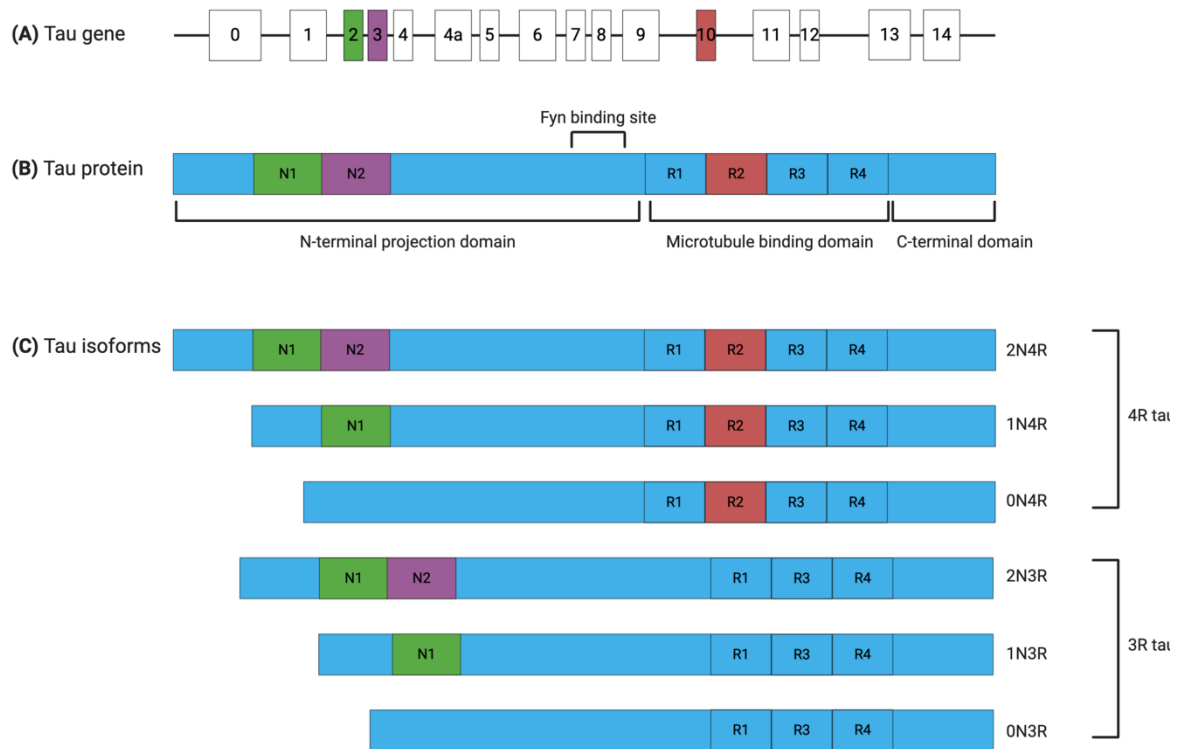


Figure 1.3 Tau gene and six isoforms in the human brain

**(A)** The *MAPT* gene, which encodes Tau protein. The *MAPT* gene is located on chromosome 17q21 in humans and comprises 16 exons. Alternative splicing of exons 2, 3 and 10 give rise to the six tau isoforms. **(B)** Tau protein can be divided into the N-terminal projection domain, the microtubule-binding domain and the C-terminal domain. N1 and N2 are present within the N-terminal projection domain and arise from exons 2 and 3 respectively. R2, which makes up the second repeat of the microtubule-binding domain, arises from exon 10. The binding site for Fyn is located on the N-terminal domain. **(C)** The six tau isoforms expressed in the adult human brain. These differ depending on the presence or absence of N1, N2 and R3. Adapted from Gao et al., 2018.

The phosphorylation state of tau is regulated by protein kinase and phosphatase activity. An imbalance in this activity is well recognised to play a role in AD pathogenesis, and is suggested to cause abnormal hyperphosphorylation of tau (Gong et al., 2008). The most common kinases involved in tau phosphorylation identified *in vitro* are members of the proline-directed protein kinases (PDPK), which include mitogen-activated protein kinase (MAPK), glycogen synthase kinase 3 (GSK3), tau-tubulin kinase and cyclin-dependent kinases (Buée et al., 2000). Other kinases such

as Fyn also contribute to tau phosphorylation (Lee et al., 2004), and the implication of this will be discussed in Section 1.9.

The precise mechanisms by which tau contributes to AD pathology are debated. Previous work has uncovered both loss- and toxic-gain- of function mechanisms. Under physiological conditions, tau regulates microtubule stability by existing in a dynamic equilibrium of bound and unbound to microtubules. The affinity of tau to bind microtubules is controlled primarily by phosphorylation of serine/threonine residues (Lindwall et al., 1984). However, other posttranslational modifications, including acetylation and ubiquitination, may also contribute (Morris et al., 2015). Hyperphosphorylation of tau in AD decreases the affinity of tau to microtubules. This loss-of-function of tau disrupts cytoskeletal integrity and axonal transport, and accumulation of unbound cytosolic tau promotes tau aggregation and NFT formation (reviewed by Wang et al., 2016). Toxic gain-of-functions of tau also occur via increased interaction of hyperphosphorylated tau with other targets, for example, hyperphosphorylation of tau is suggested to increase the interaction of tau with Fyn, and this may contribute to AD pathology (discussed in Section 1.9).

## 1.2 The Hippocampus

The hippocampus is vital for learning, memory and spatial navigation and is one of the earliest brain regions affected in AD. This is thought to underlie memory impairments seen in AD-diagnosed individuals (Andersen et al., 2009). The hippocampus comprises six regions: the dentate gyrus, hippocampus proper, subiculum, presubiculum, parasubiculum and the entorhinal cortex (Andersen et al., 2009). In rodents, the hippocampus proper, or *Cornu Ammonis* (CA), is composed of 3 subdivisions: CA1, CA2 and CA3 (Figure 1.5). The regions of the hippocampus are easily distinguishable, allowing specific areas and synaptic connections to be probed experimentally.

The overall hippocampal circuitry is complex with multiple pathways and, unlike the neocortex, many connections are unidirectional. The trisynaptic pathway forms a processing loop that begins with projections from layers II and III of the entorhinal cortex (EC) to the dentate gyrus. This is called the perforant pathway and forms the major cortical input to the hippocampus. Principal cells of the dentate gyrus (DG) called granule cells project to the CA3 region via the mossy fibre pathway, forming the second synapse of the trisynaptic circuit. Finally, CA3 pyramidal cells project

to the CA1 region via the Schaffer collateral pathway. The trisynaptic pathway can be simplified to  $EC \rightarrow DG \rightarrow CA3 \rightarrow CA1$ . CA1 pyramidal neurons project out of the hippocampus proper to layer V of the entorhinal cortex, either directly or via the subiculum (Andersen et al., 2009) (Figure 1.4).

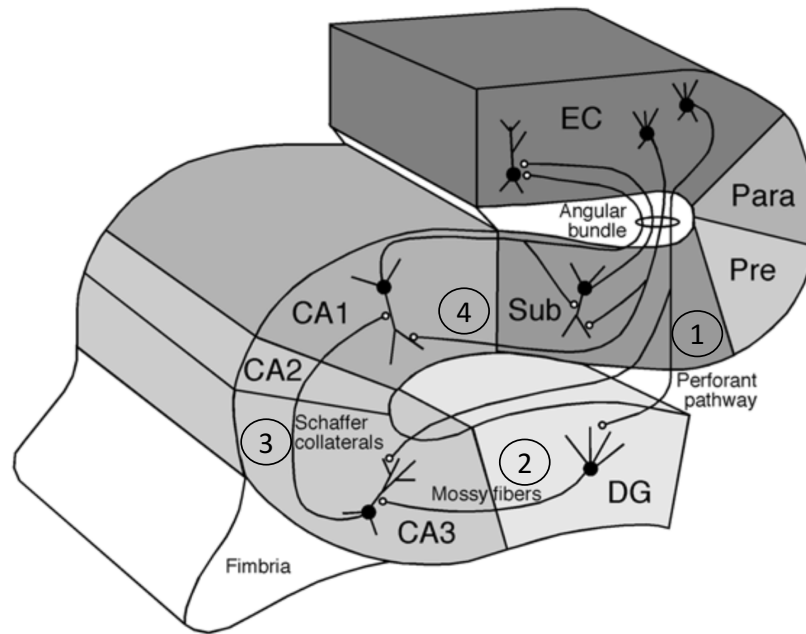


Figure 1.4 The hippocampal formation

**1.** Neurons from layer II and III of the entorhinal cortex (EC) project to the dentate gyrus (DG) and CA1 neurons via the perforant pathway. Neurons from layer III of the EC also project directly on CA1 neurons. **2.** Granule cells of the DG send synapse onto pyramidal cells in the CA3 pyramidal cells via mossy fibre projections. **3.** CA3 pyramidal cells send projections onto CA1 pyramidal neurons via Schaffer collaterals. **4.** Finally, CA1 pyramidal neurons send projections out of the hippocampus proper to layer V of the entorhinal cortex, either directly or via the subiculum. Adapted from (Andersen et al., 2009).

### 1.2.1 Hippocampal layers

The dentate gyrus is divided into three layers: stratum moleculare, stratum granulosum and hilus (also known as the polymorphic layer) (Figure 1.5). Granule cells of the dentate gyrus are located in the granule cell layer and project their dendrites into the molecular layer and axons into the polymorphic layer, which borders neurons in the CA3 region.

The hippocampus proper is also divided into layers: stratum oriens, stratum pyramidale, stratum radiatum, stratum lacunosum-moleculare and stratum lucidum. The stratum oriens contains the cell bodies of inhibitory basket cell neurons, basal dendrites of pyramidal neurons (which receive information from other pyramidal cells), septal fibres from the medial septum (MS) and commissural fibres from the contralateral hippocampus. The stratum pyramidale contains cell bodies of pyramidal cells and interneurons. Like the stratum oriens, the stratum radiatum contains septal fibres from the MS region and commissural fibres from the contralateral hippocampus. In addition, the stratum radiatum contains Schaffer collaterals (the projections from CA3 to CA1). The stratum lacunosum-moleculare contains perforant fibres from the entorhinal cortex. These fibres synapse onto the apical dendrites of pyramidal cells also located in this layer. CA3 also show an additional layer called the stratum lucidum, located between the stratum pyramidale and stratum radiatum and where the axons of mossy fibres terminate.

In this thesis, I take advantage of the highly defined pathways and visible layers of hippocampal slices to study synaptic function in mice using electrophysiology. Stimulating electrodes will be placed in the stratum pyramidale layer of the CA3 region to stimulate Schaffer collaterals extracellularly. At the same time, recording electrodes will be placed in the stratum pyramidale layer of the CA1 region to extracellularly record the response from CA1 pyramidal cells (Figure 2.3, step 4).



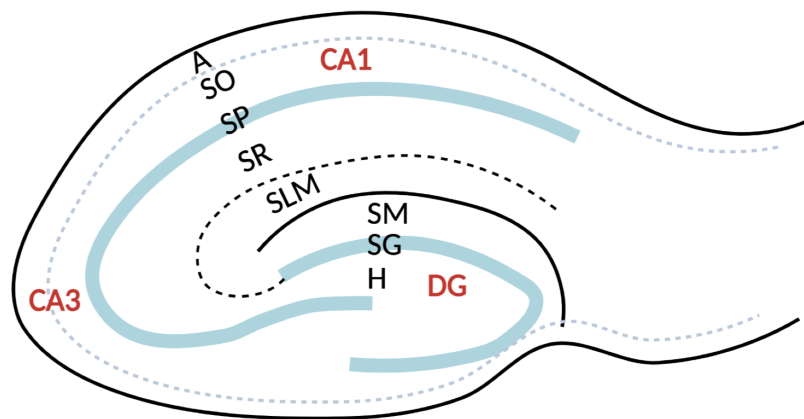
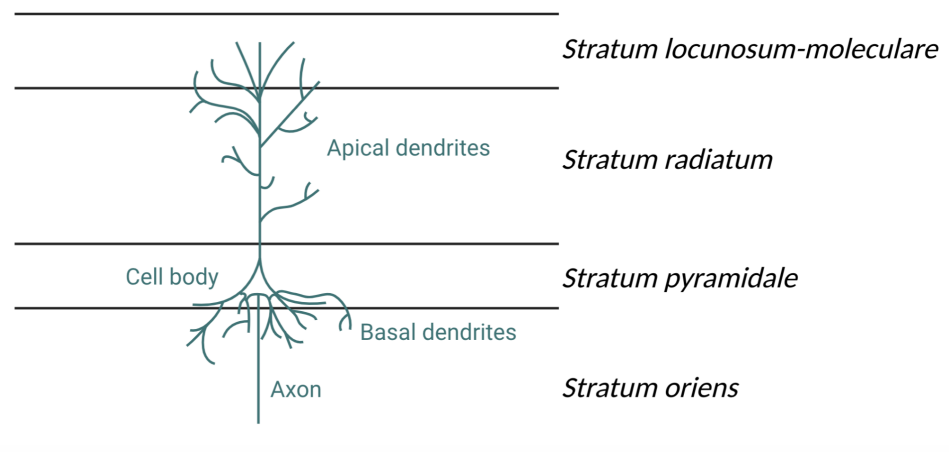
**A****B**

Figure 1.5 The rodent hippocampus

**(A)** Illustration of the layers in CA1 and the dentate gyrus (DG) of the hippocampus. The dentate gyrus has three layers: *stratum moleculare* (SM), *stratum granulosum* (SG) and *hilus* (H) (also known as the polymorphic layer). The CA1 region can also be further divided to give the *alveus* (A), *stratum oriens* (SO), *stratum pyramidale* (SP), *stratum radiatum* (SR), and *stratum lacunosum-moleculare* (SLM). CA3 also show an additional layer called the *stratum lucidum* which is located between the SP and SR. **(B)** Simplified illustration of the orientation of a CA1 pyramidal neuron through the layers of the hippocampus. Cell bodies of pyramidal cells are located in the SP and project their axons to the SO and apical dendrites to the SR and SLM. Created using Biorender.com.

## 1.3 Excitatory neurotransmission

L-glutamate is the major excitatory neurotransmitter in the mammalian CNS. When an action potential reaches the presynaptic terminal, voltage-gated  $\text{Ca}^{2+}$  channels open, and the influx of  $\text{Ca}^{2+}$  causes the release of glutamate from presynaptic vesicles. Glutamate then diffuses across the synaptic cleft and binds to receptors at the postsynaptic membrane to generate excitatory postsynaptic potentials (EPSPs). These include two categories of receptors: ionotropic and metabotropic glutamate receptors. Ionotropic glutamate receptors are cation-specific ion channels and include  $\alpha$ -amino-3-hydroxy-5-methyl-4-isoxazole propionic acid receptors (AMPA), N-methyl-D-aspartate receptors (NMDARs) and kainate receptors. Ionotropic glutamate receptors mediate fast excitatory transmission on the sub-millisecond timescale which permits high-precision propagation of neuronal signals (Andersen et al., 2009). In contrast, metabotropic glutamate receptors (mGluRs) are G-protein-coupled receptors (GPCRs) that operate on a relatively slower time scale from ten to several hundred milliseconds and transduce signals intracellularly via G-proteins (Silbering et al., 2010).

### 1.3.1 AMPA and NMDA receptors

#### 1.3.1.1 AMPA receptors

AMPA receptors are enriched at excitatory glutamatergic synapses. AMPARs are composed of four subunits, GluA1-4, that can arrange in different combinations to give rise to homo- or heterotetramers. This creates functional diversity amongst AMPARs since each subunit confers different channel kinetics, ion selectivity and receptor trafficking properties (Greger et al., 2017). For example,  $\text{Ca}^{2+}$  permeability is dependent on subunit composition such that GluA2-containing AMPARs, which form the majority of AMPARs, are impermeable to  $\text{Ca}^{2+}$ , whereas GluA2-lacking AMPARs are  $\text{Ca}^{2+}$  permeable (Cull-Candy et al., 2006)(Liu et al., 2007). In the rodent hippocampus, CA1 pyramidal neurons express mostly GluA1/2 and GluA2/3 heterotetrameric receptors, with GluA1/2 being the most prevalent (Wenthold et al., 1996) (Lu et al., 2009). AMPARs are located at both pre and postsynaptic sites and, whilst their role at the presynaptic sites remains poorly understood (reviewed by Zanetti et al., 2021), they play a vital role at the postsynapse in the normal function of neurons. For example, changes to the function properties or abundance of postsynaptic AMPARs contribute to changes in synaptic plasticity, which is a phenomenon thought to underpin the molecular mechanisms involved in learning and memory. This is discussed in Section 1.4.

Glutamate binding to the AMPAR induces a conformational change and opens the channel pore which, in GluA2-containing AMPARs, allows the influx of  $\text{Na}^+$  (as well as the efflux of  $\text{K}^+$ ). This causes depolarisation of the postsynaptic compartment. Compared NMDARs, AMPARs undergo faster activation and desensitisation, therefore allowing them to mediate fast excitatory synaptic transmission. The number of AMPARs expressed at the synapse is not fixed and is dependent on endocytosis and exocytosis at the cell surface membrane. Increased AMPAR exocytosis results in synaptic potentiation, whereas increased AMPAR endocytosis results in synaptic depression. This mechanism is one of the major ways that synaptic efficacy is altered and is essential for synaptic plasticity (discussed in Section 1.3). Kainate receptors show close structural homology with AMPAR but show a lower abundance compared to AMPAR (Bureau et al., 1999).

#### **1.3.1.2 NMDA receptor structure and properties**

Like AMPARs, NMDARs are also located on the pre and postsynapse. Here, we focus on postsynaptic NMDARs, which are found synaptically, perisynaptically and extrasynaptically. NMDARs are assembled as tetramers composed of two obligatory GluN1 subunits plus two GluN2 (GluN2A-D) or GluN3 (GluN3A-B) subunits. Together, these subunits form a cation permeable channel in the membrane that opens in response to the binding of glutamate and glycine. The subunits making up the NMDAR have a similar structure composed of 4 discrete domains: a large extracellular amino-terminal domain (ATD) which is involved in subunit assembly and allosteric modulation, the extracellular ligand-binding domain (LBD) which binds glycine in GluN1 and GluN3 subunits and glutamate in GluN2 subunits, the transmembrane domain (TMD) which is composed of 3 transmembrane helices (M1,3 and 4) and a re-entrance loop (M2), and an intracellular carboxyl-terminal domain (CTD) which is involved in receptor trafficking and anchoring to the cell surface membrane.

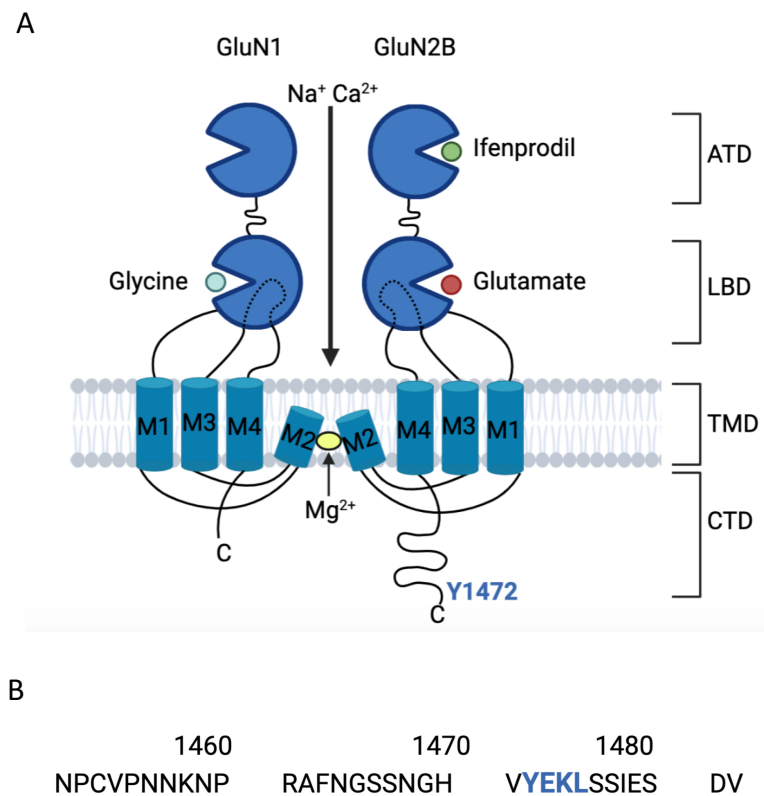


Figure 1.6 Structure of the GluN1/GluN2B NMDAR

**(A)** Schematic diagram of the GluN1/GluN2 NMDAR showing the functional domains and ligand binding domains (LBD). The NMDAR comprises two obligatory GluN1 subunits and 2 GluN2(A-D) and GluN3(A-B) subunits. Here, GluN2B is used as the example subunit. In the transmembrane domain (TMD), the M2 domains create the channel pore-forming loop which, under resting membrane conditions, is blocked by  $Mg^{2+}$ . GluN1 subunits contain the co-agonist glycine binding site, whereas GluN2 subunits contain the glutamate binding site. Binding sites for allosteric modulators are present in the amino terminal domain (ATD), for example, ifenprodil which selectively binds to GluN2B subunits. In the C-terminal domain (CTD), The C-terminal tail of GluN2B contains the Y1472 residue that is phosphorylated by Fyn to prevent clathrin-mediated endocytosis.

**(B)** The final 32 amino acids (1451-1482) of GluN2B. The Y1472 residue that forms part of the YEKL motif is highlighted in blue and is required for clathrin-mediated endocytosis. Created using Biorender.com and adapted from (Valdivielso et al., 2020).

NMDARs are voltage-dependent due to a  $Mg^{2+}$  ion block in the channel pore of the receptor. This means that, at resting membrane potentials, NMDARs are unable to flux current even if glutamate and glycine are bound to the receptor. However, upon depolarisation of the surrounding

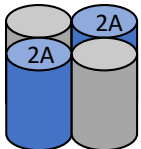
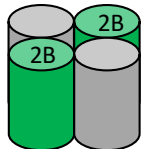
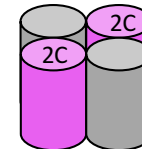
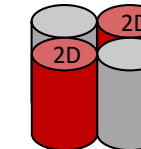


membrane, the  $Mg^{2+}$  is repelled from the channel pore to allow the flux of ions. This property gives NMDARs their function as coincidence detectors, whereby they detect the presence of both glutamate and depolarisation. This means that NMDARs will only permit current if the postsynaptic terminal is already partially depolarised whilst glutamate is bound. Unlike the majority of AMPARs, NMDARs are permeable to  $Ca^{2+}$  as well as  $Na^{+}$  and  $K^{+}$  (Traynelis et al., 2010). The ability of NMDARs to influx  $Ca^{2+}$  gives them an important role in synaptic plasticity as increased intracellular  $Ca^{2+}$  concentrations induce multiple downstream signalling cascades, including the insertion of new AMPAR and AMPAR phosphorylation (discussed in section 1.3). This enables NMDARs to regulate the excitability of the synapse and the efficiency of synaptic communication.

### 1.3.1.3 NMDA receptor subunits

NMDARs can exist as diheteromers composed of two GluN1 subunits and two identical GluN2 or GluN3 subunits (e.g. GluN1/2A/2A), or they can exist as triheteromers composed of two GluN1 subunits and two different GluN2 or GluN3 subunits (e.g. GluN1/2A/2B). The four GluN2 subunits determine the pharmacological and functional properties of the receptor which have been summarised by (Wyllie et al., 2013) and (Paoletti et al., 2013) and are shown in Table 1.

Table 1 GluN2 subunits alter the pharmacological and biophysical properties of NMDARs

Adapted from (Wyllie et al., 2013)

Subunit composition				
Properties				
Agonist potency				
Deactivation rate				
Sensitivity to Mg <sup>2+</sup> block	Higher		Lower	
Ca <sup>2+</sup> permeability	Higher		Lower	

NMDAR subunit expression changes during brain development. During forebrain development in mice, GluN2B expression is high and forms the predominant NMDAR subunit in the brain. After birth, GluN2A expression progressively increases to become the dominant subunit during postnatal weeks 2-5. This causes a switch from predominantly GluN2B to predominantly GluN2A which coincides with synapse maturation (Liu et al., 2004). GluN2C and GluN2D also undergo changes during early development. During the first 2 postnatal weeks, GluN2D expression decreases and becomes restricted mostly to mid-brain structures (diencephalon and mesencephalon). GluN2C expression begins during postnatal week 2 and is restricted to the cerebellum and olfactory bulb (Monyer et al., 1994). Therefore, in the mature adult forebrain, principal neurons express mainly GluN2A and GluN2B, with significantly less GluN2C and GluN2D.

The developmental GluN2B-to-GluN2A switch occurs in response to neuronal activity or sensory input. Mice that are reared in constant darkness from birth show significantly lower expression of GluN2A and higher GluN2B expression in cortical neurons of the visual cortex compared to mice reared under normal light-dark conditions (Philpot et al., 2001) (Quinlan et al., 1999). However, GluN2B expression decreases and GluN2A expression increases rapidly if the mice are exposed to visual stimuli. The molecular mechanisms responsible for the GluN2B-to-GluN2A switch are not fully understood but it is thought to occur via trafficking of GluN2A-containing NMDARs from the endoplasmic reticulum (ER) and endocytosis of existing GluN2B-containing NMDARs via clathrin-mediated endocytosis (Paoletti et al., 2013).

### **1.3.1.4 NMDA receptor allosteric modulation**

This thesis focusses on GluN2B-containing NMDARs and how they may play a role in early AD pathogenesis. Subunit-specific antagonists allow investigation into the contribution of different NMDAR compositions on synaptic function in physiology and disease. The large extracellular ATD of NMDARs contains binding sites for allosteric modulators.  $\text{Zn}^{2+}$  is one example which acts as an antagonist of NMDAR currents and binds to both GluN2A and GluN2B ATDs. However,  $\text{Zn}^{2+}$  displays a higher affinity for GluN2A such that, at low  $\text{Zn}^{2+}$  concentrations ( $<1 \mu\text{M}$ ) only GluN2A-containing NMDARs currents are reduced (Hatton et al., 2005)(Nozaki et al., 2011)

The synthetic compound ifenprodil and its derivative, Ro-256981, are antagonists that selectively inhibit GluN2B-containing NMDAR currents. Therefore, a comparison of  $Zn^{2+}$  and ifenprodil/Ro-256981 is used experimentally to compare currents carried by GluN2A and GluN2B-containing receptors. However, it is widely accepted that a significant proportion of NMDARs exist at triheteromers, containing both GluN2A and GluN2B. Both  $Zn^{2+}$  and ifenprodil/Ro-256981 bind to triheteromers with high affinity, however, they produce only partial inhibition (Hatton et al., 2005). Therefore, this method is not perfect for isolating the contribution of GluN2A and GluN2B-containing NMDARs. For example, a decrease in  $Zn^{2+}$  or ifenprodil/Ro-256981 sensitivity does not prove decreases in GluN2A or GluN2B expression conclusively as it could also indicate changes in di- versus tri-heteromeric assembly.

## 1.4 Synaptic plasticity

AMPA and NMDA receptors are crucial for hippocampal synaptic plasticity. Synaptic plasticity is defined as the ability to modulate the strength of their synaptic connections in response to neuronal activity. Synaptic plasticity was first postulated by Hebb who proposed that if a neuron repeatedly causes another neuron to fire, the synaptic strength between the two neurons increases (Hebb, 1949). This hypothesis was later proven experimentally in the perforant path in the hippocampus in rabbits (Bliss & Lømo, 1973), and has since been observed in multiple other regions (reviewed by Lynch, 2004).

This persistent (more than 30 minutes) activity-dependent increase in synaptic strength is known as long-term potentiation (LTP) and is widely accepted to be the closest model to the cellular mechanisms underlying learning and memory (Kumar, 2011). There are two requirements for LTP: firstly, it requires pre and postsynaptic coincident activity. This means the postsynaptic compartment must already be depolarised when glutamate is bound to the NMDA receptor. To achieve this experimentally, LTP can be induced using a wide variety of induction protocols, including high-frequency stimulation (HFS), theta burst stimulation (TBS), synaptic pairing and spike timing (reviewed by Shipton et al., 2013). These protocols induce different firing patterns which may engage distinctive downstream signalling pathways to induce plasticity changes. This means that experiments using different LTP induction protocols should be compared with caution. In this project, LTP is induced using a TBS induction protocol which is designed to mimic the 5Hz theta oscillations which occur spontaneously during voluntary movement and have been

implicated in spatial processing and navigation in both rodents and humans (Vanderwolf, 1969) (Buzsáki et al., 2013)(Figure 2.6).

How LTP is induced differs depending on the synapses being examined. With exception to the mossy fibre pathway, all other pathways in the hippocampus exhibit NMDA receptor-dependent LTP (Bortolotto et al., 2011). Collingridge et al. discovered that an NMDAR antagonist, APV, had no effect on synaptic transmission but blocked LTP at CA3-CA1 synapses, suggesting that NMDARs are required for CA3-CA1 LTP induction (Collingridge et al., 1983). This was explained by later patch-clamp experiments that showed that this was due to a voltage-gated  $Mg^{2+}$  block within the channel of the NMDAR, but following depolarisation during the induction phase the  $Mg^{2+}$  block was released, allowing NMDARs to influx ions and contribute to LTP induction (Nowak et al., 1984)(Mayer et al., 1984). The final piece of evidence that completed the idea of how NMDAR-dependent LTP is induced was through the discovery that NMDARs are permeable to  $Ca^{2+}$  (Ascher et al., 1988) (Macdermott et al., 1986). This explained why chelating postsynaptic  $Ca^{2+}$  also blocks LTP induction (Lynch et al., 1983). Together, these experiments showed that, at CA3-CA1 synapses, LTP is induced by voltage-dependent influx of  $Ca^{2+}$  via NMDARs. This is supported by behavioural studies showing that APV impairs spatial memory in mice in a dose-related manner (Inglis et al., 2013) and genetic ablation of GluN1 in CA1 or CA3 regions of adult mice also causes impaired spatial memory (Tsien et al., 1996) (Nakazawa et al., 2002).

Next, it was questioned how the influx of  $Ca^{2+}$  through NMDARs caused the expression of LTP, for example what changes occur at the synapse, and whether they occur pre- or postsynaptically. It is widely accepted that the majority of LTP is expressed postsynaptically but some LTP, mostly NMDAR independent forms (for example, mossy fibre-CA3 synapses) are expressed presynaptically (Nicoll, 2017; Nicoll et al., 2005). This project focusses on CA3-CA1 synapses which undergo NMDAR-dependent LTP that is expressed at the postsynapse.  $Ca^{2+}$  influx acts on various different biochemical pathways which may enhance synaptic strength. One  $Ca^{2+}$  binding protein is calmodulin (CaM) and together they form a  $Ca^{2+}$ /calmodulin ( $Ca^{2+}$ -CaM) complex. Of the many downstream targets of this complex is  $Ca^{2+}$ -CaM dependent kinases (CaMKII). Upon activation, CaMKII undergoes autophosphorylation at T286, resulting in CaM-independent activity that persists even when  $Ca^{2+}$  levels have returned to baseline. CaMKII plays a role in LTP and this is supported by the finding that introduction of a constitutively active form of CaMKII into postsynaptic CA1 neurons of rodent hippocampal slices enhanced synaptic transmission and prevented further potentiation by an LTP protocol-induction. This suggests that increased CaMKII



activity at the postsynapse is necessary and sufficient to express LTP (Pettit et al., 1994). In addition to LTP measurements, spatial learning and memory has also been assessed using the Morris Water Maze (MWM) which requires a mouse to use visual clues in order to swim to a hidden platform. Spatial learning is assessed by measuring the time taken for the mouse to reach the platform over a number of trials and these results correlate with hippocampal synaptic plasticity (Vorhees et al., 2006). Mutant mice which contain a point mutation to block autophosphorylation of CaMKII show no LTP in CA1 neurons and spatial learning in the MWM was completely abolished, suggesting that CaMKII autophosphorylation (required for persistent activity of CaMKII) is essential for hippocampal LTP and spatial learning (Giese et al., 1998).

One CaMKII target is the S831 GluA1 subunit of AMPARs. The importance of GluA1 for LTP is supported by evidence showing that adult GluA1 knockout (-/-) mice show no LTP in CA3-CA1 synapses, whereas GluA2<sup>-/-</sup> and GluA3<sup>-/-</sup> has no effect on LTP, suggesting a unique function of GluA1 subunits for LTP expression in CA3-CA1 synapses (Zamanillo et al., 1999)(Meng et al., 2003). GluA1 phosphorylation at S831 by CaMKII is increased following TBS-induced LTP in rodent hippocampal slices (Lee et al., 2000) and increases AMPAR single channel conductance (Barria et al., 1997) (Derkach et al., 1999)(Kristensen et al., 2011). Phosphorylation of GluA1 at another site, S845, by protein kinase A (PKA) is thought to act in combination with S831 phosphorylation to increase AMPAR cell-surface expression at the synapse for LTP. This is supported by evidence showing that phosphomutant mice with a serine-to-alanine mutation at S831 and S845 show reduced LTP in CA1 of the hippocampus and impairments in spatial learning and memory assessed using the MWM (Lee et al., 2000), however mice with single S831A or S845A mutations show normal LTP and learning (Lee et al., 2010).

Evidence supporting increased postsynaptic AMPAR expression following LTP is supported by experiments overexpressing GluA1 in CA1 neurons of cultured rat hippocampal slices and monitoring cell surface trafficking by measuring inward rectification (Hayashi et al., 2000). This is because most AMPARs in hippocampal pyramidal cells contain the GluA2 subunit which enables them to flux current equally in both inward and outward directions. However, AMPARs which lack GluA2 display inward rectification, such that current flux in the outward direction is minimal. Overexpression of GluA1 causes the formation of GluA1 homomeric AMPARs and therefore inward rectification is used as an electrophysiological tag. Under basal conditions in CA1 neurons, the overexpressed GluA1 homomeric AMPARs did not get incorporated into the synapse, as rectification was unchanged. However, insertion was initiated upon LTP induction or by

overexpression of active CaMKII (Hayashi et al., 2000). This provides evidence supporting AMPAR synaptic insertion following LTP induction.

In summary, at CA3-CA1 synapses, LTP induction requires postsynaptic NMDAR activation to increase intracellular  $\text{Ca}^{2+}$  concentrations.  $\text{Ca}^{2+}$  couples to multiple downstream pathways, for example activation of kinases like CaMKII and PKA. Ultimately this leads to increased conductance of individual AMPARs and insertion of new AMPARs at the postsynaptic membrane, and this is required for the expression of LTP. Other kinases are also implicated in the expression of LTP including the Src family kinase (SFK) members, Src and Fyn. The contribution of these kinases will be discussed in Section 1.10.5 and is highly relevant to this project since dysregulation of SFKs may contribute to plasticity impairments in AD (discussed in Section 1.10).

### **1.5 The NMDAR subunit composition may alter the type of plasticity induced**

How different patterns of neuronal activity confer LTP or LTD is not clear and is thought to be due to the NMDAR-mediated  $\text{Ca}^{2+}$  influx coupling to different intracellular signalling pathways.  $\text{Ca}^{2+}$  influx is greater during LTP induction compared to during LTD induction, leading to the hypothesis that the magnitude of  $\text{Ca}^{2+}$  influx may contribute to the form of plasticity expressed (reviewed by Shipton et al., 2013). Different subunit compositions give rise to different NMDAR kinetic properties that could cause distinct postsynaptic  $\text{Ca}^{2+}$  signalling (Table 1). This could allow NMDARs to influence plasticity to different extents. Single channel recordings in HEK293T cells showed that receptor opening probability in response to glutamate is higher for GluN2A- than GluN2B-containing NMDARs (Erreger et al., 2005). In addition, GluN2B-containing NMDARs display a slower deactivation rate compared to GluN2A-containing receptors (Table 1). A slower deactivation rate means there is a greater charge transfer across the membrane and, following the assumption that this equals the magnitude of the  $\text{Ca}^{2+}$  influx, this could allow GluN2B-containing NMDARs to have a greater contribution to plasticity with finer control. However, an over-elevated contribution of GluN2B-containing NMDARs could lead to pathological levels on intracellular  $\text{Ca}^{2+}$  and shift the balance of plasticity to promote LTD. Therefore, a fine balance of NMDAR signalling is required for normal  $\text{Ca}^{2+}$  signalling and plasticity, which may be more easily influenced by changes in synaptic surface expression of GluN2B-containing NMDARs.

In addition, the interaction of different intracellular proteins at the CTD of GluN2A and GluN2B could couple the receptor to different intracellular signalling cascades which could give rise to different effects on plasticity. For example, during induction of LTP, CaMKII is activated and this is sustained by autophosphorylation at T286 (see Section 1.4). The activation of CaMKII induces binding of CaMKII to the C-terminal tail of GluN2B, anchoring CaMKII at the synapse (Strack et al., 1998) (Bayer et al., 2001). GluN2B-CaMKII interaction is required for hippocampal LTP (Barria et al., 2005)(Zhou et al., 2007), possibly by capturing CaMKII in close proximity to synaptic substrates, such as AMPARs, whose phosphorylation is required for LTP (see Section 1.4). This supports the body of evidence suggesting that GluN2B subunits play an important role in hippocampal LTP, and provides one example as to how unique interactions with downstream signalling pathways may permit different NMDAR subunits to regulate plasticity. Finally, changes in quantity or postsynaptic localisation of NMDAR subunits could alter the plastic potential of synapses by modifying the basal synaptic state. At the postsynapse, NMDARs are found synaptically, perisynaptically and postsynaptically, and these distinct pools may play different roles in plasticity. However, how subunit composition and synaptic localisation relate continues to be debated.

Overall, activation of NMDARs with different subunit compositions could determine the type of plasticity induced by altering  $\text{Ca}^{2+}$  signalling dynamics or by engaging distinct downstream signalling pathways. The distinct properties of GluN2B-containing NMDARs mean that changes in synaptic surface levels of GluN2B-containing NMDARs may exert a greater influence on plasticity compared to GluN2A-containing NMDARs. Many studies have attempted to determine whether the type of plasticity induced depends on the subunit composition of the NMDAR activated, however results have been inconsistent, so this remains unclear.

## **1.6 Synapse loss and synaptic dysfunction in AD**

Synaptic dysfunction, for example a reduction in LTP or increase in LTD, may contribute the loss of synapses in AD. Synapse loss in AD is consistently observed in many brain regions in humans and has been reproduced in mouse models of AD. Synapses are key targets to study in AD because synapse loss is the strongest correlate of cognitive decline, even more so than NFT, plaque load, and neuron loss (Terry et al., 1991) (Marcello et al., 2012). A better understanding of the mechanisms that drive synapse loss could be useful in the discovery of new therapeutic targets to prevent or slow cognitive decline in AD.

Scheff et al. used stereology, an unbiased sampling method, paired with electron microscopy to quantify synapses in multiple brain regions of human post mortem tissue (Scheff et al., 2007) (Scheff et al., 2006)(Scheff et al., 2011). The post-mortem tissue used in these studies had a short post-mortem interval which is beneficial as it minimises protein denaturation and any enzyme activity that could destroy synapses shortly after death (Petit et al., 1990). These studies reported a consistent loss of synapses in individuals with mild-moderate AD (mean MMSE 18.6) compared to non-demented controls in the inferior temporal gyrus and in 2 hippocampal regions: the stratum radiatum of CA1 and molecular layer of the dentate gyrus (Scheff et al., 2007) (Scheff et al., 2006)(Scheff et al., 2011). Importantly, the decrease in synapses was recorded in the absence of any change in volume which indicates that neurons are maintained whilst synapses are lost and suggests that synapse loss may precede neuron loss in AD (Scheff et al., 2007) (Scheff et al., 2006). A significant decrease in the number of synapses was also reported in the inferior temporal gyrus of individuals with MCI (mean MMSE 26.8) compared to control (Scheff et al., 2011). The inferior temporal gyrus is thought to be one of the first neocortical sites affected in AD and so this suggests that synapse loss could begin before AD diagnosis in some brain regions (Convit et al., 2000). Other studies have used post-mortem tissue with longer post-mortem interval to measure synaptic markers. Post mortem frontal cortex brain tissue from MCI, moderate, and advanced AD individuals showed significant loss of the postsynaptic marker postsynaptic density-95 (PSD95), the presynaptic marker vesicle-associated membrane protein-2 (VAMP2), and postsynaptic scaffold proteins, Shank1 and Shank 3 (Pham et al., 2010). All markers show a negative correlation with levels of A $\beta$  dimers and cognitive decline recorded before death (Pham et al., 2010). This provides further evidence demonstrating progressive synapse loss in AD. Overall, observations from human post mortem tissue demonstrate a significant loss of synapses that occurs relatively early in AD and progresses as the disease advances.

Findings in mouse models of AD support observations from humans. Multiple A $\beta$ -accumulating mouse models of AD show synapse loss (reviewed by McKean et al., 2021). More specifically, observations from Tg2576 (APP<sub>Swe</sub>) mice support synapse loss as an early event in AD. These observations were recorded using a stereological approach to count dendritic spines in the dentate gyrus of Tg2576 mice. A significant decrease in spine density was recorded at 4 months old, which is well ahead of memory impairments, which do not arise until 7-10 months, and plaque deposition, which does not arise until 12-18 months of age (see Table 4). This provided evidence of early, plaque-independent synapse loss (Jacobsen et al., 2006). Overall, analysis of

post-mortem tissue from individuals with AD and tissue from AD mouse models provide clear evidence for extensive synapse loss that is driven early in AD pathology and strongly correlates with cognitive decline.

These data from A $\beta$ -accumulating mouse models of AD suggest that A $\beta$  can promote synapse loss in AD. However, non-inducible transgenic lines often begin accumulating A $\beta$  before birth, making it difficult to distinguish whether synapse loss occurs due to A $\beta$  in the mature brain or due to poor synaptic development. In addition, it does not clarify whether the effects are due to A $\beta$  or overexpression of APP or other by products of APP cleavage besides A $\beta$  (Figure 1.2). One method to overcome this is to apply A $\beta$ o directly to adult brain slices. Incubation of WT rodent organotypic hippocampal slices with A $\beta$ o purified from Chinese hamster ovary (CHO) cells expressing human APP<sub>715</sub> caused a progressive decrease in dendritic spine density in CA1 pyramidal neurons starting after 5 days of A $\beta$  exposure (Shankar et al., 2007). This provides direct evidence for A $\beta$ o as a species that can promote the loss of synapses and supports evidence from transgenic mice which accumulate A $\beta$ .

Since a decrease in spine density was not detected until after 5 days of A $\beta$ o exposure (Shankar et al., 2007), this could suggest that A $\beta$  causes more subtle disruptions in neuronal signalling pathways that, over time, drive the loss of synapses. For example, A $\beta$  could alter kinase activity to change phosphorylation states of synaptic proteins. One kinase that increases in activity in response to A $\beta$  is Fyn which phosphorylates GluN2B-NMDARs, amongst other targets (Section 1.7). Increased GluN2B phosphorylation by Fyn increases the contribution GluN2B-containing NMDARs at the plasma membrane and chronically elevated NMDAR signalling could cause initial synaptic dysfunction by promoting excitotoxicity. Over time, this could cause synaptic weakening which could drive the loss of synapses (discussed in Section 1.10). This hypothesis is supported by the usage of the NMDAR antagonist, CPP, which completely prevented the loss of dendritic spines upon A $\beta$  exposure in rodent organotypic slices (Shankar et al., 2007). This suggests that NMDARs are required for A $\beta$ -mediated synapse loss and that inhibition of NMDAR activity protects synapses from A $\beta$ -mediated synaptic breakdown (Shankar et al., 2007).

### 1.6.1 Synaptic dysfunction in the Line 102 mouse model

As well as utilising developmental onset AD mouse models or acute A $\beta$  application to slices, synaptic dysfunction in response to A $\beta$  has been investigated using a mouse model of inducible A $\beta$  accumulation (Line 102). This allows progressive A $\beta$  accumulation following normal brain development. Line 102 mice carry 2 transgenes: APP<sub>Swe/Ind</sub> and tTA. Experimental mice express both APP<sub>Swe/Ind</sub> and tTA (herein referred to as APPtTA mice). APP<sub>Swe/Ind</sub> is a chimera consisting of the mouse APP gene with a humanised A $\beta$  domain (mouse/human APP695) that contains the human Swedish (KM570/571NL) and Indiana (V617F) point mutations that cause FAD. The Swedish mutations are located at the  $\beta$ -secretase cleavage site and increase abnormal cleavage of APP by  $\beta$ -secretase whereas the Indiana mutation is located at the  $\gamma$ -secretase cleavage site, and increases abnormal cleavage of CTF $\beta$  by  $\gamma$ -secretase (Bi et al., 2019). Both result in increased A $\beta$  production. The tetracycline transactivator (tTA) gene controls the expression of APP<sub>Swe/Ind</sub>. The expression of tTA is controlled by the CaMKII $\alpha$  promoter which is expressed postnatally in principal neurons of the forebrain. The Line 102 model uses the tetracycline off system, whereby administration of tetracyclines, such as doxycycline (dox), suppresses APP<sub>Swe/Ind</sub> expression (Figure 1.7). This makes the line 102 mouse model advantageous over other mouse models because APP<sub>Swe/Ind</sub> expression can be delayed until brain development is complete. Delaying A $\beta$  accumulation until adulthood avoids potential confounds of transgenic expression during development that could permit compensatory mechanisms to oppose the effect of A $\beta$  and/or interfere with the normal development and/or maturation of brain circuits. This is unlike the majority of other mouse models of AD which express AD-related transgene(s) during development or shortly after birth.

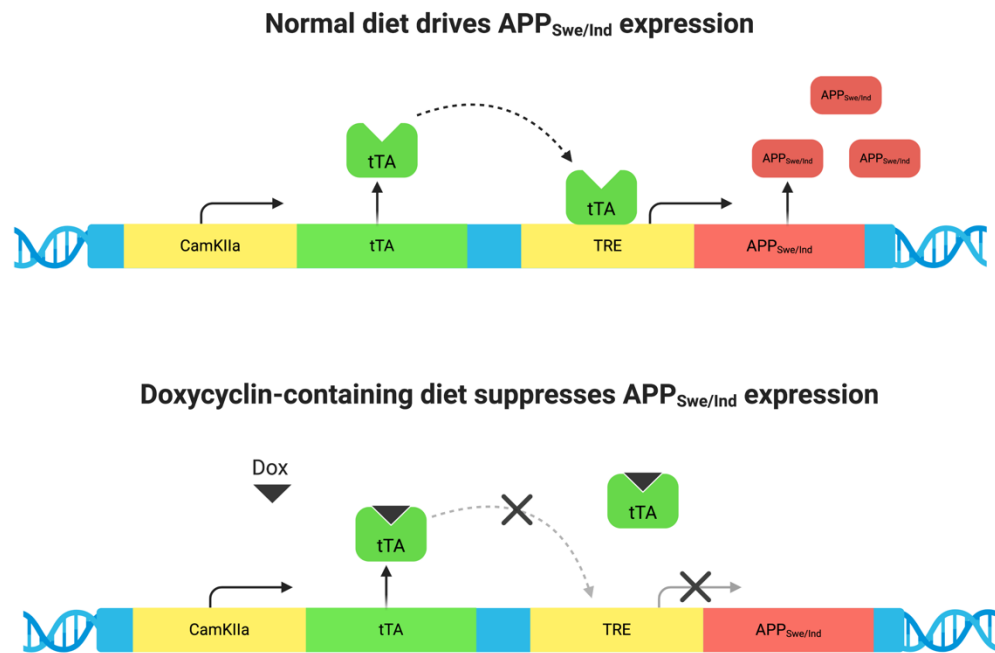


Figure 1.7 Doxycycline controls the expression of APP<sub>Swe/Ind</sub> in APPTA mice

APPTA mice carry the mouse APP gene with a humanised A $\beta$  domain (mouse/human APP695) that contains the human Swedish KM570/571NL and Indiana (V617F) mutations (APP<sub>Swe/Ind</sub>) under the tetracycline response element (TRE) promoter. Line 102 mice also carry a tetracycline transactivation (tTA) gene controlled by the CamKII $\alpha$  promoter. Without Doxycycline (Dox) in the diet (shown in the top panel) tTA binds to the TRE promoter and drives the expression of (APP<sub>Swe/Ind</sub>). When Dox is administered in the diet (bottom panel) it binds to tTA and prevents tTA from binding to TRE. This inhibits the expression of (APP<sub>Swe/Ind</sub>). Line 102 mice can be reared on a Dox-containing diet until (APP<sub>Swe/Ind</sub>) expression is required. Created using Biorender.com.

The relevance of delaying the onset of A $\beta$  accumulation is highlighted by data showing that LTP is impaired after 12 weeks of APP<sub>Swe/Ind</sub> expression in adult-onset but not developmental-onset Line 102 mice (Sri et al., 2019). This suggests that developmental APP expression allows neuronal circuits to withstand A $\beta$  toxic insults. This could occur due to the engagement of compensatory mechanisms which means that plasticity deficits are reversed by the time of recording. Alternatively, developmental APP expression could alter basal properties of neuronal circuits which allows them to be more resilient to A $\beta$  toxicity. For example, a reduction in surface expression of PrP<sup>C</sup> to decrease A $\beta$ -mediated PrP<sup>C</sup> activation could provide neuronal protection by limiting A $\beta$  signalling (Figure 1.9). In order to determine whether compensatory effects or altered

## Chapter 1

synaptic circuitry are responsible, LTP could be measured in developmental-onset Line 102 mice at earlier time points to gain a more comprehensive overview of plasticity over time. These findings highlight the advantages of delaying A $\beta$  accumulation to more closely model neuronal responses to A $\beta$  accumulation.

Delaying A $\beta$  accumulation provides an opportunity to investigate the progression from healthy synapses (before APP<sub>Swe/Ind</sub> expression begins) to the point at which synapses become compromised following the onset of APP<sub>Swe/Ind</sub> expression. Sri and colleagues delayed the onset of APP<sub>Swe/Ind</sub> expression until the mice reached sexual maturity at 6 weeks old and showed that synaptic dysfunction is first recorded after 3 weeks of APP<sub>Swe/Ind</sub> expression. This was revealed in the form of short-term memory deficits and a reduction in LTP in CA3-CA1 hippocampal synapses (Sri et al., 2019). Basal synaptic transmission, measured using input-output (IO) responses, remained unaffected suggesting that synapses are still viable and intact (Sri et al., 2019). Paired-pulse ratio, a measure of presynaptic function was also unaffected. However, by 12 weeks of APP<sub>Swe/Ind</sub> expression, IO responses are reduced suggesting a reduction in excitatory transmission. Paired-pulse ratio remained unaffected which indicates that the dysfunction is due to deficits at the postsynaptic (and not presynaptic) terminal. This implies that a loss of plasticity precedes the reduction in excitatory synaptic transmission in this model. Importantly, re-administering Dox after 3 weeks of APP<sub>Swe/Ind</sub> expression for 9-11 weeks reversed LTP deficits and prevented the subsequent reduction in basal synaptic transmission seen at 12 weeks (Sri et al., 2019). This suggests that reducing A $\beta$  can rescue impaired plasticity and later synaptic transmission deficits at this stage. Whether the earlier recorded loss of synaptic plasticity is causative of the later reduction in excitatory transmission requires further investigation, however, it suggests that preventing the early loss of synaptic plasticity may prevent later synaptic dysfunction. Understanding the mechanisms by which A $\beta$  causes the loss of synaptic plasticity is required to identify therapeutic targets to prevent it, and potentially protect synapses from future degeneration. Here, I use mature onset APP<sup>TtA</sup> mice to investigate whether SFK inhibition can rescue early synaptic plasticity impairments. Herein, mature onset Line 102 will be referred to as Line 102.

In support of synaptic dysfunction preceding synapse loss, a separate study using WT rat hippocampal slices showed that application of human A $\beta$ <sub>40</sub> (extracted from brain tissue from AD patients) inhibited LTP and enhanced LTD after 20 minutes (Shankar et al., 2008). This demonstrates a rapid impairment in synaptic function upon exposure to A $\beta$ <sub>40</sub> (Shankar et al.,



2008). Since acute slices remain viable for only 6-12 hours (Buskila et al., 2014), to study the longer-term effects of A $\beta$  the authors utilised organotypic slices which remain viable for weeks. In this system, a decrease in pyramidal dendritic spine density was detected after 10 days after A $\beta$  exposure. This suggests that A $\beta$  rapidly impairs synaptic function, which may be later followed by synapse loss (Shankar et al., 2008).

Understanding the mechanisms that drive early synaptic dysfunction in AD is important because it may represent one of the earliest pathological events that occur to synapses and could be causative of later synapse loss. Such understanding could contribute to the identification of new therapeutic targets for early AD treatment, where intervention may be more likely to be successful. This project explores the hypothesis that early synaptic dysfunction may be driven by A $\beta$ -mediated increase in Fyn activity. Evidence for increased Fyn activity in AD has been well-documented in studies using cell culture, AD mouse models and human brain tissue (discussed in Section 1.8). In the next Section, I will describe the structure and regulation of Fyn and other members of the SFKs. I will then discuss the evidence showing increased Fyn activity in AD and how this may contribute to early synaptic dysfunction and later loss of synaptic plasticity.

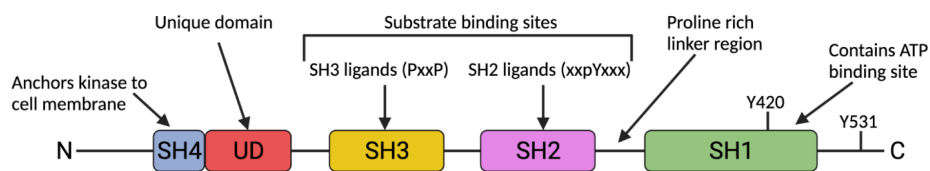
## 1.7 SFK structure and regulation

SFKs are non-receptor-type protein tyrosine kinases made up of 9 members, of which 5 (Src, Fyn, Yes, Lck and Lyn) are expressed in the mammalian CNS (Yagi, 1994). SFKs were first identified as proto-oncogene products but have since been implicated in the pathogenesis of AD and other neurodegenerative diseases such as multiple sclerosis and Parkinson's disease (Kalia et al., 2004) (Guglietti et al., 2021). Therefore, studying SFKs in the context of AD could increase our understanding of multiple neurodegenerative diseases.

SFKs share a conserved domain structure which consists of Src homology (SH) domains (SH1-4) and a unique domain that differs between family members (Figure 1.8). The activity of SFKs depends upon phosphorylation of both Y531 at the C-terminus and Y420 on the SH1 domain. In the basal state, Y531 is phosphorylated and forms an intramolecular interaction with the SH2 domain. This is maintained by kinases such as Csk and Cts (Salter et al., 2004). The inactive state is also supported by the proline-rich linker region between SH1 and SH2 interacting with the SH3 domain. This results in a closed conformation of the kinase that restricts the binding of substrate

molecules to SH2 and SH3 domains. The inactive conformation is also preserved by the unphosphorylated state of the Y420 residue. Dephosphorylation of the Y531 residue, for example by PTP $\alpha$ , disrupts this interaction and results in the open conformation of the kinase (Salter et al., 2004). Autophosphorylation of Y420 in the open conformation also enhances the activated state (Krämer-Albers et al., 2011). The open conformation exposes the SH3 and SH2 domains for substrates to interact. For example, PxxP motifs (where 'x' is any amino acid) in ligands such as tau, interact with the SH3 domain while ligands containing xypYxxx motifs interact with the SH2 domain (Boggon et al., 2004) (Figure 1.8). The active open conformation allows SFKs to transfer phosphate groups from the ATP binding site located in the SH1 domain onto tyrosine residues of target proteins, such as GluN2B subunits at Y1472.

**A**



**B**

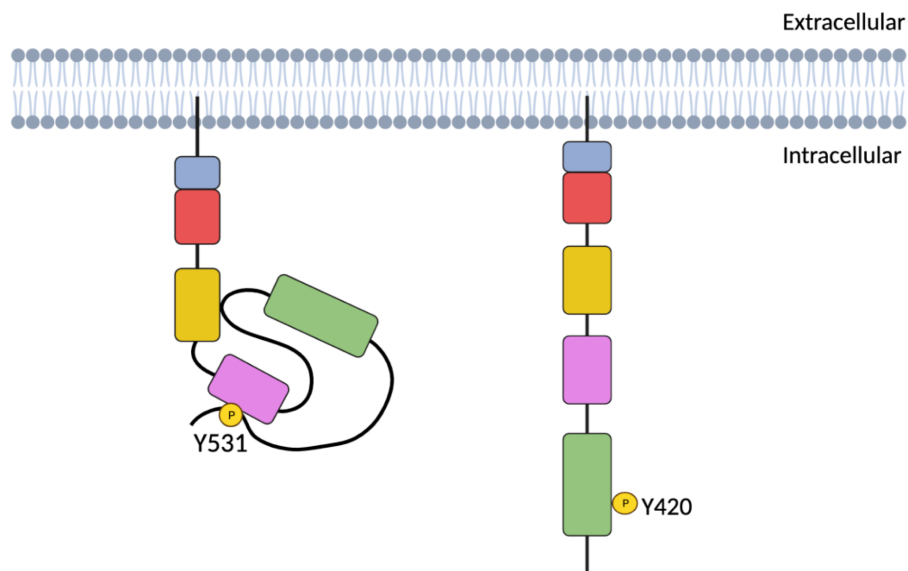


Figure 1.8 Structure and activation of SFKs

(A) Schematic diagram showing the Src homology (SH) domains (SH 1-4) and unique domain of SFKs. Y420 and Y531, residues that are important for regulating the activity of SFKs, Y420 and Y531, are labelled. (B) The inactive (left) and active (right) conformations

of Fyn. In the inactive state, Fyn is held in a close conformation due to intramolecular interactions of the SH2 domain with the phosphorylated C-terminal Y531 and the proline-rich linker region interacting with the SH3 domain. Dephosphorylation at Y531 disturbs the interaction and results in a conformation change to the open, active state. Autophosphorylation at Y420 in the SH1 domain stabilises the active state. Created using Biorender.com.

In this thesis I focus on the SFK, Fyn, and its potential role in AD pathogenesis. Fyn is involved in a variety of biological functions, both within and outside of the CNS. Outside of the CNS Fyn is involved in cell proliferation, migration and differentiation, platelet function and T-cell signalling (reviewed in Nygaard et al., 2014). Within the CNS Fyn is involved in regulating processes such as synaptic plasticity, synapse density and myelination (reviewed in Nygaard et al., 2014). The role of Fyn in synaptic function and plasticity is discussed in Section 1.10.5 and is of particular interest when studying AD as dysregulation of this role may contribute to the pathogenesis of AD (discussed in Section 1.6). In addition to the function of Fyn in the mature brain, Fyn is also important for both neurodevelopment. For example, Fyn contributes to neuronal migration by forming a component of the neural cell adhesion molecule that regulates neurite outgrowth (Beggs et al., 1994). This is supported by data showing that neurite outgrowth is inhibited in cerebellar and dorsal root ganglion neurons from Fyn<sup>-/-</sup> mice (Beggs et al., 1994). This function is suggested to be unique to Fyn and not all SFKs since neurite outgrowth was unaffected in Src<sup>-/-</sup> or Yes<sup>-/-</sup> neurons (Beggs et al., 1994). Fyn is also important for oligodendrocyte maturation and myelination and Fyn<sup>-/-</sup> mice show significantly reduced levels of myelin and oligodendrocytes (Sperber et al., 2001).

In the following Sections I review evidence suggesting that Fyn activity is increased in AD and that this may contribute to synaptic dysfunction in early AD by enhancing NMDAR activity. However, it must be noted that SFKs are involved in regulating many other ion channels. For example, Src increases inhibitory  $\gamma$ -aminobutyric acid (GABA)<sub>A</sub>-mediated currents in rodent primary hippocampal neurons (Wan et al., 1997) and suppresses voltage-gated potassium (Kv1.3) channel activity when co-expressed in HEK-293T cells (Fadool et al., 1997). SFKs may also be involved in AMPAR activity, but it is unclear whether their overall activity is increased or decreased and there may be opposing effects of different SFKs (Hayashi et al., 2004; Lu et al., 1998).

## **1.8 Fyn activity is increased in AD**

### **1.8.1 Evidence from humans**

The connection between Fyn and AD was first noted by Shirazi and Wood et al. who used immunohistochemistry to visualise Fyn in human post-mortem hippocampal slices from AD and control individuals (Shirazi et al., 1993). Total Fyn protein immunoreactivity, based on staining with an anti-Fyn antibody, was increased in a subset of neurons in AD patients. These neurons were also positive for abnormally phosphorylated tau, suggesting a possible link between Fyn and tau phosphorylation (Shirazi et al., 1993). Interestingly, the authors describe the subset of neurons as mostly normal in morphology, whereas the visually affected neurons showed normal levels of Fyn. This suggests that Fyn activity may be selectively elevated in neurons that are in the early stages of disease (Shirazi et al., 1993). This study used a small sample size of only 6 post-mortem samples, therefore further research has been carried out on a larger scale using 86 post-mortem tissue samples from the inferior temporal gyrus from individuals with moderately-severe AD (MMSE average 12.33), MCI (MMSE average 26.41) and control individuals (Larson et al., 2012). Western blotting showed that whilst total Fyn levels remained constant across groups, Fyn activity (pY420 Fyn) was significantly increased in individuals with AD compared with control individuals (Larson et al., 2012). A trend for increased Fyn activity was also seen in the MCI group compared to controls, though this was not statistically significant (Larson et al., 2012). This could reflect variation within the MCI cohort, as not all individuals with MCI progress to AD (Mitchell et al., 2008). The tissue samples used in this study had short post-mortem intervals and no correlation was found between all proteins measured (including total and pY420 Fyn) and the post-mortem interval, suggesting that significant degradation had not occurred within the tissues before processing. Fyn phosphorylates GluN2B subunits at Y1472, however whether phosphorylation at this residue is enhanced in human AD tissue has not been reported.

### **1.8.2 Evidence from model systems**

#### **1.8.2.1 Cell culture**

In WT mouse cortical neurons, application of 1-3  $\mu$ M synthetic A $\beta$  (estimated oligomeric concentration 10-30 nM) caused a dose-dependent increase in SFK pY416 (active form of SFKs) after 15 minutes (Um et al., 2012). This was replicated by application of homogenised extracts from the prefrontal cortex of individuals with AD (Um et al., 2012). This antibody does not differentiate between the different SFKs, however, immunoprecipitation of individual SFKs within

the same study demonstrated that the increase in SFK pY416 was specific to Fyn only. The increased SFK pY416 correlated with an increase in GluN2B Y1472 phosphorylation (pY1472), further supporting increased Fyn activity (Um et al., 2012). This suggests that A $\beta$  causes a rapid activation of Fyn and increase in GluN2B Y1472 phosphorylation. The increase was transient as after 60-180 minutes of A $\beta$  exposure, both Fyn activity and pY1472 GluN2B levels declined, with pY1472 GluN2B decreasing lower than basal levels (Um et al., 2012). This correlated with an increase in the activity of striatal-enriched protein tyrosine phosphatase (STEP), a phosphatase which opposes the activity of Fyn, which may explain the transient effects of GluN2B pY1472 (Nguyen et al., 2002).

Larson and colleagues also reported an increase in active Fyn (pY416) in WT mouse cortical neurons after 60 minutes of exposure to A $\beta$ o (estimated concentration of 5 nM) that was purified from human AD-brains (Larson et al., 2012). This disagrees with the transient measurement by Um et al., 2012 who saw Fyn activity decline by 60 minutes. This could be explained by differences between synthetic A $\beta$  preparations as during *in vitro* synthesis of A $\beta$ , the A $\beta$  monomers form a mixture of A $\beta$  conformations, which may affect their stability, toxicity and the ultimate aggregation pathway. This is thought to account for why the synthesis of the same peptide can produce differential effects on neuronal function (Benilova et al., 2012). Therefore, the different A $\beta$ o preparations by the two groups could contribute to the differences in their findings. In addition, A $\beta$  was not purified from the AD brain extracts used by Um et al., 2012, and so contamination by other proteins or lipids could contribute to the effects recorded. Measurements after longer exposure to A $\beta$ o were not reported by Larson and colleagues, but it is possible that Fyn activity could decrease over a longer exposure period. Nevertheless, overall observations from cell culture experiments demonstrate that A $\beta$  increases Fyn activity and increases phosphorylation of the Fyn target, GluN2B Y1472. Whether this is maintained over time remains unclear and will be addressed in this thesis by measuring the level of GluN2B pY1472 in the hippocampus and cortex of Line 102 mice at time points up to 16 weeks of A $\beta$  accumulation.

### 1.8.2.2 Mouse Models

Increased Fyn activity in AD has been implied in two mouse models of AD by measuring the phosphorylation of direct targets of Fyn, GluN2B pY1472 and Pyk2 pY402 (Ittner et al., 2010) (Kaufman et al., 2015). 4-month-old APP23 mice, which accumulate A $\beta$  (see Table 4), show increased levels of total Fyn and GluN2B pY1472 in synaptosome preparations compared to

## Chapter 1

controls (Ittner et al., 2010). APP23 mice show learning and memory defects starting at 3 months, but no plaque deposition until 6 months (see Table 4) (Van Dam et al., 2003). Therefore, findings by Ittner and colleagues in “pre-plaque” 4-month-old APP23 mice suggest that Fyn overactivity occurs independently of plaque deposition and could therefore be a relatively early event in disease progression. However, repeat experiments using other AD models, and at even earlier time points in AD pathology (for example before long-term memory deficits arise) are required to ascertain whether these observations can be generalised. In this project, I aim to address this by measuring the level of GluN2B pY1472 in the hippocampus and cortex of Line 102 mice when synaptic plasticity deficits first arise and later when long-term memory impairments begin.

Increased Fyn activity is also inferred in APP<sup>swe</sup>/PSEN1dE9 (APP/PS1) mice (see Table 4). The APP/PS1 model is a relatively aggressive model of AD in which A $\beta$  plaques first emerge in the cortex at 4 months old (Jackson et al., 2013). Western blotting of late-stage (11-12-month-old) APP/PS1 mice brain homogenate showed a 5-fold increase in Pyk2 (pY402) activity in the hippocampus compared to control (Kaufman et al., 2015). This was also significant, although less pronounced, in the cortex. Since Pyk2 is directly activated by Fyn, this implicates increased Fyn activity, although Fyn activity or other direct targets of Fyn, such as GluN2B pY1472, were not measured (Kaufman et al., 2015).

Overall, there is strong evidence from multiple different systems that points to increased Fyn activity in AD. Findings from human post-mortem tissue clearly demonstrate increased Fyn activity in AD and this is supported by increased Fyn activity by A $\beta$  neuronal cell culture and increased phosphorylation of Fyn targets in A $\beta$ -accumulating mouse models of AD. Further work has identified that A $\beta$ os activate Fyn by interacting with the cell surface receptor, PrPc. Activated PrPc then transduces the signal intracellularly via mGluR5 which leads to the activation (Um et al., 2013, 2012). This signalling pathway is illustrated in Figure 1.9. The role of Fyn in regulating synaptic function and how its increased activity in AD may contribute to synaptic dysfunction is discussed in Section 1.10.

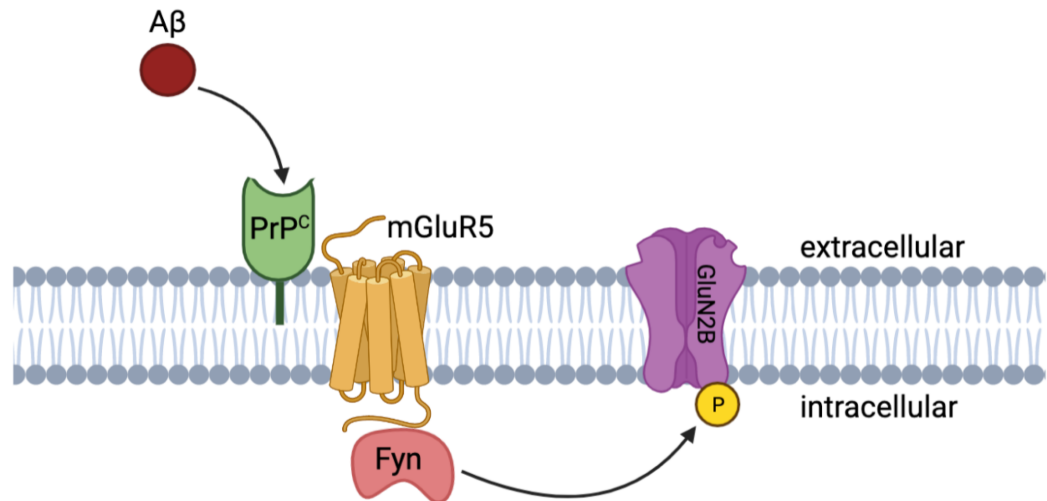


Figure 1.9 A $\beta$  mediates toxic effects via the PrP<sup>c</sup>-mGluR5-Fyn complex.

A $\beta$  binds to the PrP<sup>c</sup> receptor which is coupled to mGluR5 (GPCR). Activation of mGluR5 initiates multiple intracellular signalling pathways, including the activation of Fyn.

Activated Fyn phosphorylated GluN2B at Y1472 and this could contribute to synaptic dysfunction and ultimately lead to synapse loss and cell death (Um et al., 2013, 2012).

Created using Biorender.com.

## 1.9 A $\beta$ -Fyn-Tau interaction

Multiple experimental paradigms indicate that A $\beta$  and tau interact to drive AD pathology, and Fyn may permit such interaction. Evidence that A $\beta$ -tau interaction exacerbates pathology is supported by studies using P301L mice, which express mutant P301L 4R tau and develop NFT pathology by around 6 months old. However, P301L mice crossed with Tg2576 mice (which accumulate A $\beta$ , see Table 4) show enhanced NFT pathology compared to P301L single transgenic mice (Lewis et al., 2001). This demonstrates that transgenic expression of A $\beta$  increases tau aggregation in mutant tau-expressing mice. To ensure that the increased tau expression is due to A $\beta$  (and not APP overexpression or other APP cleavage products), 5-6-month-old P301L mice were injected with synthetic A $\beta$  or A $\beta$ -containing brain extract isolated from 24-month-old APP23 mice and, in both scenarios, there was an increase in NFT pathology (Götz et al., 2001)(Bolmont et al., 2007). These studies demonstrate that A $\beta$  can exacerbate existing tau pathology in P301L mice.

## Chapter 1

Endogenous tau is also required for the pathological effects of A $\beta$  in vitro, suggesting a synergistic relationship between tau and A $\beta$ . For example, application of synthetic A $\beta$  causes cell death in hippocampal cell cultures from WT and human-tau expressing mice, but not in cultures from tau<sup>-/-</sup> mice (Rapoport et al., 2002). This demonstrates an essential role of tau in A $\beta$ -induced cell death, which is conserved for both human and rodent tau isoforms. In vitro studies are supported by findings in vivo using 4-7-month-old J20 mice which accumulate A $\beta$  and show impairments in spatial learning assessed using the MWM, premature mortality and increased excitotoxin-induced seizure susceptibility (see Table 4) (Roberson et al., 2007). Reduction of endogenous tau in J20 mice rescued all of these phenotypes, suggesting that they are brought about by A $\beta$  acting via tau (Roberson et al., 2007). Importantly, immunostaining in the hippocampus showed that the high level of A $\beta$  plaque deposition in J20 mice was not altered by reducing endogenous tau expression, demonstrating that the protective effect without tau is not provided by reducing A $\beta$  plaque levels. Instead, it is more likely that protection without tau is provided by preventing the engagement of intracellular pathways mediated by A $\beta$ -tau interaction.

At the level of the synapse, acute application of human A $\beta$ 42 to hippocampal slices occludes LTP in WT mice but not tau<sup>-/-</sup> mice (Shipton et al., 2011). This demonstrates another protective effect without tau and suggests that A $\beta$  acts via tau to inhibit synaptic plasticity. Reintroduction of human tau in tau<sup>-/-</sup> mice restores the ability of A $\beta$  to inhibit LTP, showing that both human and rodent tau can facilitate A $\beta$ -induced synaptic dysfunction (Vargas-Caballero et al., 2017). Similar findings have been reported in an A $\beta$ -accumulating mouse model, J9 mice, where blunted LTP at 8-10-months-old was rescued by reduction of endogenous tau (Roberson et al., 2011). Taken together, the evidence strongly suggests an essential role of tau in A $\beta$ -induced synaptic dysfunction.

How tau and A $\beta$  interact to cause synaptic dysfunction at the molecular level is unclear. One potential candidate is Fyn kinase, which binds to tau via its SH3 domain (Lee et al., 1998). Under physiological conditions, tau is enriched in axons, where it binds to microtubules, however mislocalisation of tau to dendrites has been observed in human and mouse models of AD and other tauopathies, such as frontal temporal dementia (reviewed by Ittner et al., 2018). Ittner and colleagues suggested that tau-Fyn binding plays an essential role in targeting Fyn to dendritic regions, placing Fyn in close proximity to synaptic substrates, such as GluN2B (Ittner et al., 2010). By immunostaining for Fyn in hippocampal CA1 neurons from 2-3-month-old WT mice, they



showed that Fyn localises mainly in dendritic regions but in aged-matched  $\tau^{-/-}$  mice Fyn is reduced in the dendrites and accumulates in cell bodies (Ittner et al., 2010). This finding was replicated using mice that express a truncated form of tau ( $\Delta\tau 74$ ) throughout the brain. Truncated  $\Delta\tau 74$  contains the putative binding site for Fyn but does not contain the microtubule binding domain. This means that  $\Delta\tau 74$  outcompetes the interaction of endogenous tau with Fyn but remains in the soma because it fails to bind microtubules. Reduced dendritic localisation of tau in  $\tau^{-/-}$  and  $\Delta\tau 74$  mice suggest that tau is required for Fyn to reach the dendrites (Ittner et al., 2010). These findings support the hypothesis that mislocalisation of tau to dendritic compartments in AD may contribute to AD pathogenesis by increasing the amount of Fyn proteins at the dendrites, where Fyn is then in a prime position to be aberrantly activated by  $A\beta$  (illustrated in Figure 1.9).

Further evidence to support Tau-Fyn dendritic targeting comes from a study using single-molecule tracking to investigate the nanoscale distribution of Fyn in mouse hippocampal neuron cultures in dendritic shafts and spines (protrusions from shafts) (Padmanabhan et al., 2019). This showed that Fyn mobility is increased in dendritic shafts, but not spines of  $\tau^{-/-}$  mice. This suggests that Tau regulates the mobility of Fyn in dendritic shafts under physiological conditions. The mobility of Fyn was significantly decreased in spines containing Tau P301L (which models hyperphosphorylated tau) compared to WT tau, suggesting that tau hyperphosphorylation promotes the trapping of Fyn in dendritic spines (Padmanabhan et al., 2019). This complements findings from Ittner and colleagues and supports the hypothesis that Fyn requires tau to reach dendritic spines (Ittner et al., 2010) and suggests that this is enhanced when tau is hyperphosphorylated. This may contribute to increased Fyn activity in AD, as hyperphosphorylated tau may trap Fyn in dendritic spines, where it can be overactivated by  $A\beta$  signalling through postsynaptic receptors, such as  $PrP^C$  (Figure 1.9).

The decrease in levels of dendritic Fyn correlated with a decrease in GluN2B pY1472 in hippocampal extracts in  $\tau^{-/-}$  and  $\Delta\tau 74$  mice compared to WT, supporting the hypothesis that Fyn is less able to reach synaptic substrates without the translocation of tau to dendrites (Ittner et al., 2010). Phosphorylation of GluN2B at Y1472 stabilises GluN2B subunits in the plasma membrane (Discussed in section 1.10.1). Therefore, the authors hypothesised that the lack of tau ( $\tau^{-/-}$ ) or lack of functional tau ( $\Delta\tau 74$ ) could reduce the membrane stability of GluN2B-containing NMDARs by reducing GluN2B pY1472. Immunoprecipitation of PSD-95 showed a reduced interaction between NMDAR subunits and PSD95 in brain extracts  $\tau^{-/-}$  and  $\Delta\tau 74$  mice.

This supported their hypothesis and suggests reduced NMDAR stability at the postsynaptic density without tau (Ittner et al., 2010). Overall, findings from Ittner and colleagues showed that in the absence of tau, or in the absence of fully functioning tau (that cannot translocate to the dendrites), dendritic Fyn levels and GluN2B pY1472 are reduced, and the stability of GluN2B-containing NMDARs at the plasma membrane and synaptic expression is reduced.

The absence of tau may protect against the toxic effects of A $\beta$  by decreasing the level of Fyn and the dendrites and thereby reducing the capacity of A $\beta$  to increase dendritic Fyn activity (discussed in Section 1.9). This could prevent A $\beta$ -mediated increase in GluN2B pY1472 which may reduce A $\beta$ -mediated excitotoxicity. Expression of  $\Delta$ tau74 or reduction of endogenous tau in 4-month-old APP23 mice improved memory acquisition in the T-maze, prevented premature mortality and reduced the susceptibility to drug-induced seizures (Ittner et al., 2010). The elevated level of pY1472 GluN2B in APP23 mice was also rescued in APP23/ $\Delta$ tau74 mice and APP23/tau<sup>-/-</sup> mice whilst the level of A $\beta$  or plaque burden was unaffected (Ittner et al., 2010). This suggests a critical role of tau in enabling A $\beta$  to exert its toxicity, and that this may be driven by increased Fyn activity and phosphorylation of GluN2B pY1472.

### **1.10 Increased Fyn activity may contribute to AD pathology via GluN2B-containing NMDARs**

So far, I have described the evidence suggesting that A $\beta$  increases Fyn activity and GluN2B pY1472, and that this requires tau-Fyn interaction and subsequent shuttling of Fyn to the dendrites. Increased Fyn activity and GluN2B pY1472 may contribute to AD pathology by impairing synaptic function and driving synapse loss. This is supported by data showing that overexpression of Fyn in an A $\beta$ -overexpressing mouse model (J9 mice) accelerated the onset of synapse loss and cognitive impairment, whilst genetic ablation of Fyn rescued synapse loss and reduced premature mortality in a similar A $\beta$  overexpressing model (J20 mice) (Chin et al., 2004) (Chin et al., 2005). This suggests that increased Fyn activity exacerbates A $\beta$ -induced toxicity and suggests a protective effect against A $\beta$  without Fyn, however, the precise mechanism by which increased Fyn activity enhances A $\beta$  toxicity remains unknown. In the following Sections, I will review the evidence suggesting that increased Fyn activity contributes to A $\beta$ -mediated synaptic dysfunction by enhancing GluN2B pY1472.

### 1.10.1 Fyn-mediated GluN2B phosphorylation increases cell-surface expression of GluN2B-containing NMDARs

The GluN2B residues phosphorylated by Fyn were identified in HEK-293T cells using multiple GluN2B mutants where each C-terminal tyrosine was mutated to phenylalanine. These mutants were co-expressed with constitutively active (Y531F) Fyn (CA-Fyn) and the level of tyrosine phosphorylation was quantified. This identified Y1252, Y1336 and Y1472 as sites phosphorylated by Fyn, with Y1472 as the primary phosphorylated site *in vitro* (Nakazawa et al., 2001). In mouse models, GluN2B pY1472 is enhanced in CA-Fyn expressing mice, demonstrating that increased Fyn activity increases GluN2B Y1472 phosphorylation *in vivo* (Xia et al., 2014). In the brain of Fyn<sup>-/-</sup> mice, tyrosine phosphorylation of GluN2B subunits is markedly reduced which suggests a decrease in Y1472 phosphorylation, however overall tyrosine phosphorylation and not Y1472 was probed (Dunah et al., 2004). Future work to quantify GluN2B pY1472 in Fyn<sup>-/-</sup> mice would determine whether Fyn is the only kinase to contribute to GluN2B Y1472 phosphorylation.

The Y1472 residue of GluN2B forms part of the YEKL motif on the distal C-terminal cytoplasmic tail of GluN2B (Figure 1.6). The YEKL sequence fits the motif: tyrosine-XX-Φ (where X is a polar or charged amino acid and Φ is a hydrophobic amino acid). This is present on many cell surface receptors and forms the binding site for the μ2 subunit of the clathrin adaptor protein, AP2, which is required for clathrin-mediated endocytosis (Owen et al., 1998). The AP2 complex is thought to initiate endocytic events in mammalian cells and bind to the plasma membrane at the pinching site and recruit scaffold proteins. This is followed by the recruitment of clathrin and other proteins to form the clathrin coat required for clathrin-mediated endocytosis (reviewed by Kaksonen et al., 2018).

The role of Y1472 in clathrin-mediated endocytosis is supported by studies using a Tac-GluN2B chimera. This chimera consists of the distal C-terminus of GluN2B (amino acids 1315-1482) bound to a cell surface-expressed interleukin 2 receptor alpha chain (Tac). Antibodies against Tac are then used to visualise cell-surface expression. When expressed in HeLa cells, Tac-GluN2B was readily internalised, suggesting that the distal C-terminal tail of GluN2B (where Y1472 is located) is sufficient to induce internalisation (Roche et al., 2001). Truncation of the C-terminal tail by deletion of 11 amino acids removes the YEKL motif and significantly inhibited internalisation of

the Tac-GluN2B chimera, which is consistent with the requirement of the YEKL motif for internalisation (Roche et al., 2001). Finally, point mutations of Y1472 to alanine or phenylalanine prevented internalisation in HeLa cells and primary hippocampal neurons (Lavezzari et al., 2003). These findings support the role of Y1472 in regulating GluN2B-containing NMDAR cell-surface expression via interaction with AP2 to promote clathrin-mediated endocytosis.

Following endocytosis, NMDARs are trafficked to either recycling endosomes where they can be returned to the synaptic plasma membrane or to late endosomes for degradation. The route taken after endocytosis is dependent on subunit composition. This has been studied in HeLa cells, where GluN2A proteins show increased localisation with the late endosomal marker, Rab-9, whereas GluN2B proteins show co-localisation with the recycling endosomal marker, Rab-11 (Lavezzari et al., 2004). These findings have been replicated in WT rodent hippocampal cultures which also show internalisation and recycling following GluN1/GluN2B co-expression (Scott et al., 2004). This suggests that the majority of GluN2A subunits are sorted into late endosomes to be sent for degradation whilst GluN2B-containing NMDARs are recycled ready to be reinserted into the plasma membrane. GluN2B also has a dominant effect in that GluN2A/GluN2B triheteromers are sorted into recycling endosomes and not late endosomes (Tang et al., 2010). This suggests that regulation of GluN2B-containing NMDARs may be a more efficient way to alter NMDAR cell surface expression and synaptic function compared to GluN2A-containing NMDARs.

Structural analysis showed that phosphorylation of GluN2B at Y1472 prevents the interaction with AP2 because tyrosine phosphorylation renders the binding pocket too small for AP2 interaction (Owen et al., 1998). This is supported by findings using a yeast-2-hybrid assay where co-expression of the C-terminus of GluN2B and  $\mu 2$  subunit of AP2 resulted in a strong interaction, however this was significantly reduced by point mutations of Y1472 (Y1472A or Y1472F) (Lavezzari et al., 2003). Therefore, Fyn activity may regulate GluN2B-NMDAR expression via phosphorylation of GluN2B at Y1472 and so enhanced Fyn activity and subsequent GluN2B pY1472 in AD could increase surface expression of GluN2B-NMDARs at the synapse through lack of internalisation. In line with this, applying A $\beta$  to WT cortical cultures increased Fyn activity, GluN2B pY1472 and cell-surface expression of GluN2B-containing NMDARs (Um et al., 2012). However, in cortical cultures from Fyn<sup>-/-</sup> mice, A $\beta$  did not affect cell-surface expression or phosphorylation state of GluN2B Y1472 (Um et al., 2012). This suggests that Fyn is required for A $\beta$  to increase GluN2B pY1472 and GluN2B cell-surface expression. Abnormally high Fyn activity in AD could increase surface

expression of GluN2B-NMDARs and cause overactivation of NMDARs during glutamatergic transmission, thus increasing vulnerability to excitotoxic damage (Forner et al., 2017).

### **1.10.2 Fyn-mediated GluN2B phosphorylation increases synaptic contribution of GluN2B-containing NMDARs**

It is clear that increased Fyn activity promotes cell-surface expression of GluN2B-containing NMDARs by preventing clathrin-mediated endocytosis. Electrophysiological recordings complement these findings and show that increased Fyn activity enhances synaptic NMDAR contribution. This comes from studies showing that expression of CA-Fyn in rodent cerebellar granule cell cultures increased the amplitude of NMDA-miniature excitatory postsynaptic currents (mEPSCs) but caused no change in NMDAR single-channel currents (Prybylowski et al., 2005). This suggests that Fyn enhances the number of synaptic NMDARs whilst not affecting individual channel conductance. The increased NMDAR currents are mediated specifically by GluN2B-containing NMDAR and this is supported by evidence showing that application of recombinant Fyn to isolated rodent CA1 neurons potentiated NMDAR currents that could be inhibited the GluN2B-selective antagonist, Ro-256981, but not GluN2A-selective antagonists, NVP-AAM007,  $Zn^{2+}$ , or GluN2A<sup>-/-</sup> cultures (Yang et al., 2012). Together, these findings show that recombinant Fyn increases the amplitude of mEPSCs carried by GluN2B-containing NMDARs.

To test whether endogenous Fyn produces the same effects, Fyn can be activated pharmacologically. SKF81297 is a dopamine 1 (D1) receptor agonist that results in the engagement of multiple downstream signalling cascades including activation of CaMKII, Protein Kinase C (PKC) and Protein Kinase A (PKA) (Figure 1.10). One downstream target of PKA is Fyn activation. PKA also phosphorylates STEP to decrease STEP activity (Paul et al., 2000). This reduces the ability of STEP to dephosphorylate Fyn which preserves Fyn in its active state and therefore maintains GluN2B Y1472 phosphorylation. As illustrated in Figure 1.10, SKF81297 is not a drug specific to Fyn, however, it provides the advantage of enhancing Fyn activity via an endogenous pathway without the confounds of developmental transgenic expression.

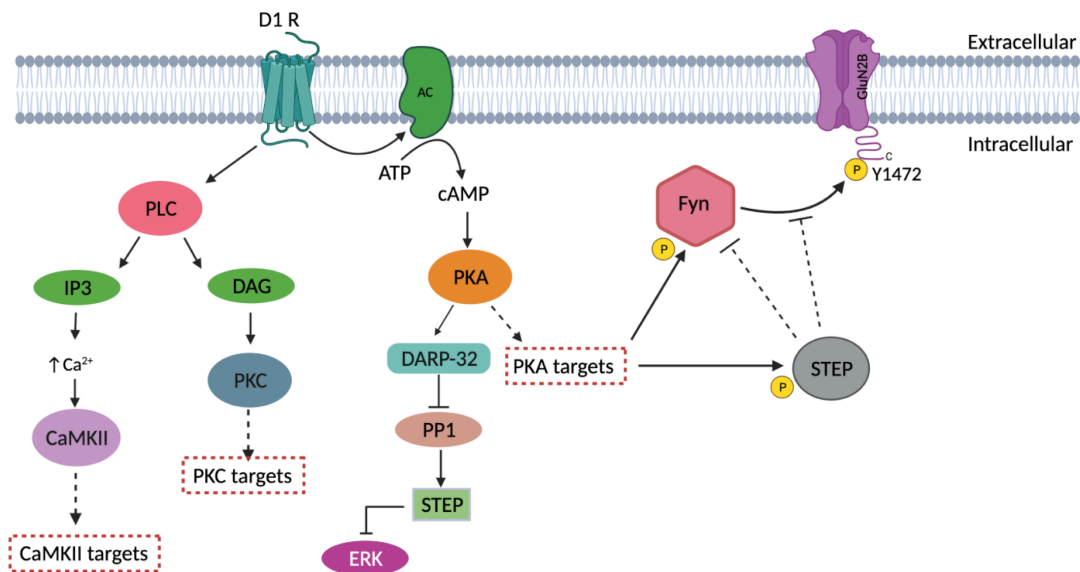


Figure 1.10 D1 receptor activation by SKF81297

SKF81297 is a D1 R agonist. Activation of D1 R results in the engagement of multiple intracellular signalling pathways. This diagram illustrates the major kinases activated by D1 R stimulation, CaMKII, PKC and PKA, and their various target proteins. One PKA target is Fyn which is phosphorylated by PKA at Y420, resulting in Fyn activation. Activated Fyn subsequently phosphorylates GluN2B subunits at Y1472. PKA also phosphorylates STEP which decreases STEP activity. This inhibits STEP-mediated dephosphorylation of Fyn at Y420, maintaining Fyn in its active state. Decreased STEP activity also reduces dephosphorylation of GluN2B Y1472, maintaining GluN2B pY1472. Adapted from (Klein et al., 2019) & (Nishi et al., 2011). Created using Biorender.com.

Whole-cell patch clamp of CA1 neurons from isolated CA1 neuron cultures or acute hippocampal slices from WT rats showed that SKF81297 enhanced NMDAR currents evoked by NMDA or stimulation of the CA3 field respectively (Yang et al., 2012). Based on previous findings described earlier in this section and in Section 1.10.1, it is assumed that this is due to an increase in the overall number of NMDARs and not due to changes in single NMDAR conductance, however this was not measured. The increase in NMDA-induced currents by SKF81297 was mediated by Fyn specifically because co-application of a Fyn-specific interfering peptide, Fyn(39-57), prevented the increase in NMDAR currents. Fyn(39-57) is a synthetic peptide based on the unique domain of Fyn (amino acids 39-57) which acts to outcompete the function of endogenous Fyn. This is hypothesised to occur by preventing Fyn from binding to an unknown scaffold protein in the

NMDAR complex that is required for Fyn to potentiate NMDAR currents (Figure 1.11) (Yang et al., 2012).

A Src interfering peptide, Src(40-58), had no effect on the SKF81297-mediated increase in NMDAR currents suggesting that, although SKF81297 is a broad-spectrum drug, the SKF81297-mediated increase in NMDAR current is driven specifically by Fyn. The effect was also prevented by application of Ro-256981 but not NVP- AAM007 or  $Zn^{2+}$ , suggesting that SKF81297 potentiates NMDAR currents by acting on GluN2B-containing NMDARs specifically, potentially by increasing the number of synaptically expressed GluN2B-containing NMDARs. Immunoprecipitation followed by western blotting showed that application of SKF81297 to WT rat hippocampal slices increased the activity of Fyn but not Src. SKF81297 also increased GluN2B Y1472 phosphorylation in hippocampal slices from WT but not Fyn<sup>-/-</sup> mice (Yang et al., 2012). This provides further evidence that SKF81297 is specific to Fyn and not Src, and implies that increased Fyn activity potentiates GluN2B-containing NMDAR currents. Finally, SKF81297 did not affect NMDAR currents in hippocampal slices from GluN2B Y1472F (non phosphorylatable) knock-in mice, suggesting that phosphorylation of GluN2B subunits at Y1472 is essential for SKF81297 to increase NMDAR currents (Yang et al., 2012).

Together, these findings suggest that increased endogenous Fyn activity by SKF81297 promotes GluN2B pY1472 which enhances GluN2B-containing NMDAR currents. This agrees with findings using CA-Fyn mice and recombinant Fyn application and is in line with other studies showing increased surface expression of GluN2B-containing NMDARs with increased Fyn activity (discussed in Section 1.10.1). Following these findings, increased Fyn and GluN2B pY1472 in AD could enhance synaptic expression of GluN2B-containing NMDARs and increase NMDAR currents in response to glutamate release from presynaptic terminals. Chronically elevated  $Ca^{2+}$  as a result of excessive NMDAR activation could contribute to excitotoxicity (discussed in Section 1.10.4) and alter synaptic plasticity (discussed in Section 1.10.5), which could ultimately lead to synapse loss (Forner et al., 2017). Via this mechanism, increased Fyn activity could contribute to the pathogenesis of AD.

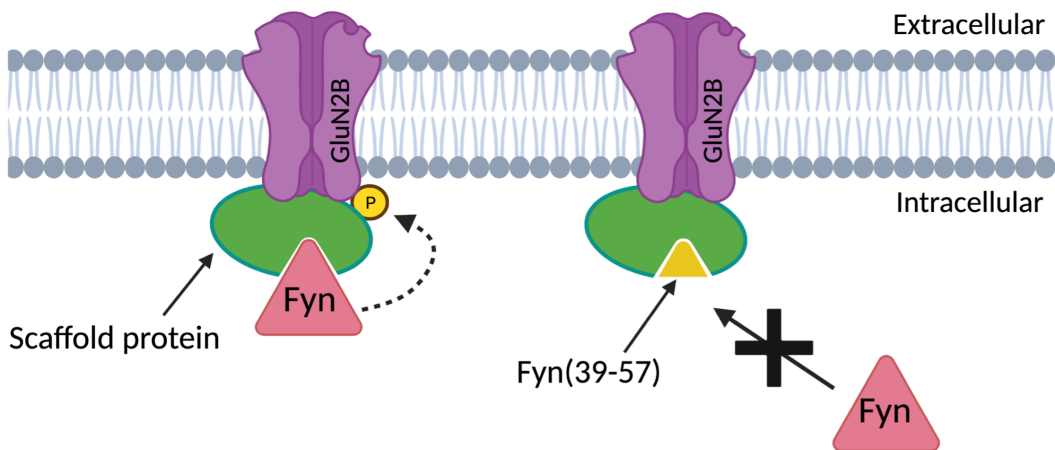


Figure 1.11 Mechanism of action of Fyn(39-57)

Fyn(39-57) is a Fyn interfering peptide based on the unique domain of Fyn. Fyn(39-57) is hypothesized to prevent the localization of Fyn to the NMDAR complex by preventing endogenous Fyn from interacting with an unknown scaffold protein (green). Fyn(39-57) prevents endogenous Fyn from docking to the NMDAR complex and therefore reduces Fyn-mediated GluN2B Y1472 phosphorylation. Src(40-58) acts via a similar mechanism by preventing endogenous Src-ND2 binding therefore preventing Src from localising to and phosphorylating NMDARs. Created using Biorender.com.

### 1.10.3 Src enhances NMDAR-mediated currents

Due to structural similarities between SFKs, there are currently no drugs approved for use in humans that inhibit Fyn specifically. Therefore, the function of other SFKs in the CNS must be considered. Of the other SFKs expressed in the mammalian CNS, Src has also been implicated in regulating NMDAR activity. However, whether Src activity is altered in AD and therefore whether it contributes to AD pathogenesis remains unknown. Inhibition of endogenous Src using an antibody inhibitor (anti-src1) or a Src-specific interfering peptide, Src(40-58), significantly reduces basal synaptic NMDAR currents in cultured dorsal horn (Yu et al., 1997) and CA1 neurons (Yang et al., 2012). In contrast, recombinant Src potentiates NMDAR currents in cultured dorsal horn neurons (Yu et al., 1997) and in isolated rodent CA1 neuronal cultures (Yang et al., 2012). Activation of endogenous Src can be achieved using a Src-activating phosphopeptide (EPQ(pY)EEIPIA). This peptide binds to the SH2 domain of Src which inhibits the formation of the inactive conformation by preventing interaction between the SH2 domain and the



phosphorylated C-terminal tail (Figure 1.8). Consistent with findings using recombinant Src, application of EPQ(pY)EEIPIA in the patch pipette increased NMDAR currents in cultured dorsal horn neurons and CA1 pyramidal neurons from hippocampal slices (Yu et al., 1997) (Lu et al., 1998). Single-channel conductance was unaffected, suggesting an increased number of NMDARs rather than changes in conductance of individual receptors (Yu et al., 1997). The effect of EPQ(pY)EEIPIA on NMDAR currents is Src specific because its ability to increase NMDAR currents was prevented by anti-src1 or Src(40-58). Finally, Src can be activated using pituitary adenylate cyclase activating peptide (PACAP38) which acts through G-coupled protein receptors to activate multiple intracellular proteins, one of which is Src. Application of PACAP38 potentiated NMDA-induced currents in isolated CA1 neurons via activation of Protein kinase C. Again, this is Src specific because it was prevented by co-application of Src (40-58) (Yang et al., 2012). Together, these findings suggest that inhibition of Src decreases, and activation increases, NMDAR currents.

Unlike Fyn which upregulates NMDARs via GluN2B phosphorylation, Src is thought to act via GluN2A phosphorylation. This is supported by evidence showing that increased NMDAR currents by recombinant Src were not affected by co-application of a GluN2B inhibitor, Ro-256981, but were prevented by a GluN2A competitive antagonist, NVP-AAM007 and  $Zn^{2+}$  at a low concentration which preferentially blocks GluN2A rather than GluN2B receptors (Yang et al., 2012). In addition, application of recombinant Src did not affect NMDAR currents when applied to CA1 neurons from GluN2A<sup>-/-</sup> mice. These findings suggest that Src potentiates NMDAR currents by acting on GluN2A subunits of NMDAR, whereas Fyn potentiates NMDAR currents by acting upon GluN2B-containing NMDARs (Section 1.10.2). A summary of evidence that supports this statement is illustrated in Figure 1.12. Increased GluN2B-containing NMDAR currents by Fyn may have a more significant impact on increasing intracellular  $Ca^{2+}$  levels compared to GluN2A-containing NMDARs. This is because GluN2B-containing NMDARs have slower deactivation kinetics and therefore may permit a larger  $Ca^{2+}$  influx upon activation (discussed in Section 1.5). Excessive  $Ca^{2+}$  influx causes cellular damage by promoting excitotoxicity (discussed in Section 1.10.4). Therefore, increased Fyn activity could have a greater influence on promoting excitotoxicity than increased GluN2A-containing NMDAR currents by Src.

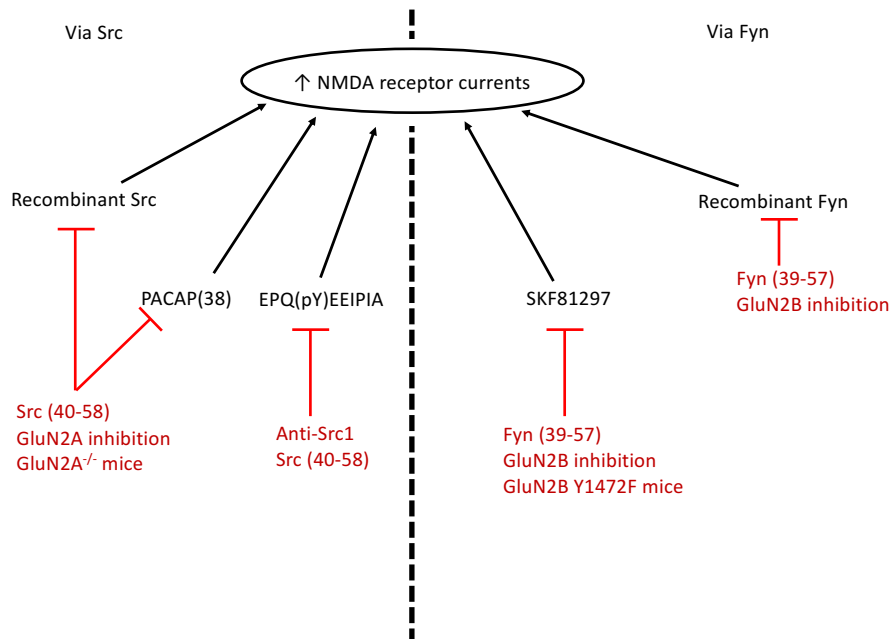


Figure 1.12 Src and Fyn activity enhance NMDAR currents

Src is activated using recombinant Src, PACAP(38) (which activates Src via protein kinase C) or EPQ(pY)EEIPIA (which activates Src by binding to the SH2 domain and preventing the formation of the inactive conformation). These drugs increased NMDAR currents in hippocampal cultures and slices and their effects could be prevented by GluN2A, but not GluN2B, inhibition (using NVP-AAM007 or  $Zn^{2+}$ ) or in  $GluN2A^{-/-}$  mice. Conversely Fyn is activated using recombinant Fyn or SKF81297 (which activates Fyn via dopamine 1 receptors). These drugs also increased NMDAR currents in hippocampal cultures and slices, however their effects could be prevented by GluN2B, but not GluN2A, inhibition using Ro-256981 or GluN2B Y1472F mice.

#### 1.10.4 Increased Fyn activity may promote excitotoxicity

An enhanced contribution of GluN2B-containing NMDARs following increased Fyn activity could drive excitotoxicity. This could contribute to synaptic dysfunction and loss in AD. Excitotoxicity is thought to be a common pathological mechanism contributing to many neurological diseases such as ischemia, epilepsy, AD and other neurodegenerative diseases such as Huntington's disease and Parkinson's disease (Armada-Moreira et al., 2020). Excitotoxicity is triggered by increased glutamate concentration causing excessive  $Ca^{2+}$  influx which is predominantly mediated by NMDARs (Choi, 1992). In agreement with this, glutamate-induced intracellular  $Ca^{2+}$  accumulation and cell death can be almost completely prevented by NMDAR-selective inhibitors (Hartley et al., 1989). This is in contrast to the L-type  $Ca^{2+}$  channel antagonist, nifedipine, which

minimally reduced intracellular  $\text{Ca}^{2+}$  accumulation (Choi, 1992). Excessive  $\text{Ca}^{2+}$  influx through NMDAR disrupts ionic gradients to cause the release of further  $\text{Ca}^{2+}$  from intracellular stores, such as from the mitochondria and ER (reviewed by Mehta et al., 2013). Together this causes a dramatic increase in  $\text{Ca}^{2+}$  that triggers a cascade of events leading to cellular damage and ultimately cell death. This includes mitochondrial impairment causing impaired ATP synthesis and the release of reactive oxygen species and proapoptotic mitochondrial proteins, and ER impairment leading to attenuation of protein translation and aberrant activation of proteases and protein kinases (reviewed by Yan Wang et al., 2010). This ultimately causes synapse loss and neuronal death, which both correlate closely with cognitive decline seen in individuals with AD. (Terry et al., 1991)(Gómez-Isla et al., 1997)

It is possible that  $\text{A}\beta$ -mediated increased Fyn activity in AD promotes excitotoxicity by enhancing NMDAR-mediated excitatory currents (Sections 1.10.1 to 1.10.3). Evidence suggesting that Fyn promotes excitotoxicity is supported by studies that have inferred  $\text{A}\beta$ -mediated excitotoxicity through examining neuronal cell viability and cell death, for example via quantification of lactate dehydrogenase release (LDH). LDH release is used as a readout of cell viability where increased LDH release is indicative of plasma membrane damage and therefore reduced cell viability. Application of  $\text{A}\beta_0$  to WT mouse cortical neuron cultures caused a dose-dependent increase in LDH release over 1-3 hours, however this was absent in  $\text{Fyn}^{-/-}$  cells (Um et al., 2012). This is in line with previous findings which quantified plasma membrane integrity and metabolic activity and showed that cells of the DG and CA3 region in hippocampal slices from  $\text{Fyn}^{-/-}$  are protected from  $\text{A}\beta_0$ -induced cell death (Lambert et al., 1998). Similarly, application of  $\text{A}\beta_0$  to WT hippocampal neurons induced dendritic spine loss after 5 hours, however this is also absent in  $\text{Fyn}^{-/-}$  cells (Um et al., 2012). Together, the evidence shows a neuroprotective effect without Fyn and suggests that  $\text{A}\beta$  exerts its toxicity via Fyn to drive neuronal damage and death. However, these experiments do not ascertain whether this is caused by NMDAR overactivation.

Therefore, further experiments examined the effect of co-application of NMDAR antagonists, ifenprodil and APV with  $\text{A}\beta$ . This revealed that NMDAR inhibition partially rescued LDH release after 1 hour and fully rescued dendritic spine loss after 5 hours of  $\text{A}\beta_0$  exposure in WT cortical and hippocampal neuron cultures (Um et al., 2012). Together with previous findings described here, this suggests that  $\text{A}\beta$ -mediated cell death can be prevented by inhibiting Fyn activity and reduced by inhibiting NMDAR activity. However, since NMDAR antagonists did not fully rescue the phenotype, it suggests that Fyn acting on other targets may contribute to  $\text{A}\beta_0$ -driven cell damage.

## Chapter 1

Whether GluN2B Y1472 phosphorylation is required for A $\beta$  toxicity would be interesting experiment to determine whether the protective effect in Fyn<sup>-/-</sup> mice is provided by reducing GluN2B pY1472. This could be investigated by applying A $\beta$ o to slices from GluN2B Y1472F mice and quantifying cell death.

Excitotoxicity can also be inferred by measuring seizure activity in animal models because seizures results from neuronal hyperexcitability, and glutamate-induced excitotoxicity is suggested to play a key role in the molecular mechanism causing epilepsy (Green et al., 2021). Seizures are observed in several A $\beta$ -accumulating mouse models of AD, suggesting a hyperexcitability of circuits (Bezzina et al., 2015). (Maltera, 2011)(Born et al., 2014). Seizure activity could be explained by extensive neuronal loss and subsequent loss of excitatory/inhibitory balance. However, APP<sub>Swe/Ind</sub> (CRND8) mice demonstrate increased sensitivity to seizures induced by a GABA antagonist, pentylenetetrazol, at both 6-8-weeks-old (before neuronal loss) and 18-24-weeks-old (after neuronal loss onset), implying that increased network excitability may be caused directly by A $\beta$ -signalling rather than neuron loss and subsequent loss of excitatory/inhibitory balance (Jolas et al., 2002)(Del Vecchio et al., 2004).

Increased spontaneous seizure activity in J9 mice is worsened by overexpression of Fyn (Roberson et al., 2011). This suggests that increased Fyn activity in AD may contribute to increasing cell hyperexcitability and therefore exacerbate excitotoxic damage. This is further supported by work using CA-Fyn and Fyn<sup>-/-</sup> mouse models. CA-Fyn expressing mice show increased seizure activity compared to controls induced by pentylenetetrazol or via electric stimulation of the amygdala which is linked to the onset of seizures (Kojima et al., 1998). This suggests that increased Fyn activity may increase network excitability which therefore renders circuits more susceptible to seizure induction. Similarly, Fyn<sup>-/-</sup> mice show decreased susceptibility to seizures induced by pentylenetetrazol and other GABA receptor antagonists: picrotoxin and bicuculline, and glutamate receptor agonists: kainic acid and NMDA (Miyakawa et al., 1996). Together, these findings suggest that A $\beta$  accumulation contributes to network hyperexcitability, which is exacerbated by Fyn activity. Decreasing Fyn activity lowers the susceptibility of seizures in mice, suggesting that inhibition of Fyn may reduce A $\beta$ -mediated hyperexcitability.

Excitotoxicity could drive synaptic dysfunction, and this may lead to synapse loss. We hypothesise that excessive Ca<sup>2+</sup> influx through GluN2B-containing NMDARs contributes to network

hyperexcitability and therefore excitotoxicity. This could occur via increased Fyn-mediated GluN2B Y1472 phosphorylation and increased GluN2B-NMDAR surface expression. However, a direct link between GluN2B Y1472 phosphorylation and seizure susceptibility has not been shown. This could be investigated by measuring seizure susceptibility in mice expressing GluN2B Y1472F (non-phosphorylatable) or GluN2B Y1472E (phosphomimetic).

#### 1.10.5 Src and Fyn modulate synaptic plasticity

In addition to driving excitotoxicity, increased Fyn-mediated GluN2B Y1472 phosphorylation may drive synaptic dysfunction via alterations in synaptic plasticity. This could underlie memory deficits seen in individuals with AD and may contribute to later synapse loss. The role of SFKs in hippocampal synaptic plasticity was first speculated when various broad protein tyrosine kinase (PTK) inhibitors were found to prevent HFS-induced LTP in CA1 neurons from guinea pig hippocampal slices (O'Dell et al., 1991). Later evidence using transgenic mice indicated that Fyn activity modulates synaptic plasticity. This was shown in hippocampal slices from CA-Fyn expressing mice, where a weak TBS induction protocol that is subthreshold for inducing LTP in control slices produced LTP in CA1 synapses (Lu et al., 1999). This suggests that increased Fyn activity reduced the threshold for LTP, and therefore increased plasticity. Fyn<sup>-/-</sup> mice show impaired HFS-induced LTP in CA3-CA1 synapses which suggests a decrease in plasticity with decreased Fyn activity (Grant et al., 1992). Fyn<sup>-/-</sup> mice also show impaired learning in the MWM, which complements the electrophysiological findings and suggests that Fyn may contribute to spatial learning (Grant et al., 1992). Therefore, experiments using transgenic mice suggest that Fyn modulates the threshold for LTP induction such that increasing Fyn activity increases plasticity whereas decreasing Fyn decreases plasticity. Interestingly, Src<sup>-/-</sup> and Yes<sup>-/-</sup> mice show normal LTP in CA1 synapses, suggesting a unique role for Fyn in synaptic plasticity that may not be shared by all SFKs (Grant et al., 1992).

SFKs play a key role in the CNS during development by regulating the development of neurons and glia (reviewed by Guglietti et al., 2021). Therefore, the alterations in Fyn activity in Fyn<sup>-/-</sup> mice and constitutively active Fyn expressing mice could impair normal brain development and contribute to the altered plasticity. Abnormal brain development with altered Fyn activity is reported in Fyn<sup>-/-</sup> mice which display abnormal brain architecture in the form of aberrant undulation of the pyramidal cell layers in the posterior CA3 and anterior dentate gyrus (Kojima et al., 1997). These morphological defects could be responsible for the lack of LTP recorded in Fyn<sup>-/-</sup>

## Chapter 1

mice, rather than the lack of Fyn in the adult brain. However, postnatal reintroduction of Fyn in Fyn<sup>-/-</sup> mice under the CaMKII $\alpha$  promoter rescued HFS-induced LTP, even though the same degree of morphology abnormality was present in the hippocampus (Kojima et al., 1997). This suggests that the inhibition of LTP in Fyn<sup>-/-</sup> mice is not due to the morphological defects reported, although, it is possible that other unknown defects caused by the lack of Fyn during development could be responsible for the changes observed.

Studies have modulated Src and Fyn activity pharmacologically to overcome the issue of altering Fyn activity during development. Inhibition of Src using Src(40-58) or anti-src1 in the patch pipette prevented the induction of HFS-induced LTP in CA1 neurons of rodent hippocampal slices during whole-cell patch clamp (Lu et al., 1998). This disagrees with findings from Src<sup>-/-</sup> mice but could be due to acute pharmacological inhibition compared to chronic inhibition (as in transgenic mice). It is possible that, like Fyn<sup>-/-</sup> mice, Src<sup>-/-</sup> mice could show abnormal brain development, however this has not been reported. The effect of pharmacological Fyn inhibition on synaptic function and plasticity in WT mice or in a mouse model of AD has not been reported. In this project, I aim to address this by recording synaptic transmission and plasticity following SFK inhibition in hippocampal slices from adult WT and Line 102 mice.

In contrast to pharmacologically decreasing Src and Fyn activity, there has been relatively more research into the effect of increasing Src and Fyn activity on synaptic plasticity. These studies are highly relevant to AD and may indicate how increased Fyn activity in AD could affect synaptic plasticity. Following the basis that SKF81297 increases Fyn activity and PACAP38 increases Src (Section 1.10.2 & 1.10.3), these drugs were used to investigate whether increasing endogenous Src or Fyn activity pharmacologically alters synaptic plasticity. Using electrophysiological field recordings, different degrees of plasticity can be induced in hippocampal slices by altering the frequency of pulses during the induction phase. High-frequency pulses induce LTP, whereas low-frequency pulses induce LTD. The authors applied 600 pulses of various frequencies to WT rat hippocampal slices to determine how increasing Fyn or Src activity alters synaptic strengthening and weakening (Yang et al., 2012). At a low frequency of 10Hz (to induce LTD), application of SKF81297 enhanced LTD in CA3-CA1 synapses from 3-4-week-old WT rat hippocampal slices compared to untreated slices. At a neutral 20Hz induction paradigm that induces neither LTP or LTD in control slices, LTD occurred in SKF81297-treated slices. This means that SKF81297 treatment promotes LTD at frequencies that usually would not affect synaptic strength, suggesting that the overall balance of plasticity is shifted towards synaptic weakening. At higher

frequencies (50Hz and 100Hz) to induce LTP, there was no significant difference in LTP in control and SKF81297-treated slices. This suggests that increased Fyn activity by SKF81297 does not affect the ability for synapses to strengthen with high frequency inputs, but favours LTD at lower frequencies. Other targets of SKF81297 (illustrated in Figure 1.10) must be acknowledged as these could also contribute to altering plasticity. However, the preference for LTD at low induction frequencies following SKF81297 application was absent in GluN2B Y1472F transgenic mice, implying that GluN2B Y1472 phosphorylation (likely by Fyn) is required for SKF81297 to alter plasticity. Overall, findings by Yang and colleagues support the body of evidence to suggest that Fyn activity modulates synaptic plasticity by phosphorylating GluN2B Y1472 (Yang et al., 2012).

The lack of effect of SKF81297 on high induction frequencies to induce LTP reported by Yang and colleagues disagrees with the previously described findings showing enhanced TBS-induced LTP in CA-Fyn expressing mice (Lu et al., 1999). This could be due to a number of reasons. Firstly, disparities in findings could arise due to different effects of chronic compared to acute increases in Fyn activity in SKF81297 and CA-Fyn mice respectively. Secondly, activation of other D1 R signalling pathways outside of enhancing NMDAR currents may contribute to the effect of SKF81297 on LTP (Figure 1.10). Thirdly, transgenic manipulation of Fyn in constitutive active Fyn expressing mice could give rise to improper CNS development which may impact LTP. Finally, differences in the LTP protocols used may engage distinct mechanisms to express LTP.

Prior work disagrees with findings from Yang and colleagues as pre-treatment of 6-13-weeks-old WT rat hippocampal slices with 30  $\mu$ M SKF81297 enhanced HFS-induced LTP (Stramiello et al., 2008). This was prevented by co-application of a GluN2B-antagonist (Ro-256981). This is in line with previous findings showing that Ro-256981 prevents SKF81297-mediated increase in NMDAR currents (Yang et al., 2012) and suggests that GluN2B-containing NMDARs are required for SKF81297 to potentiate NMDAR currents and to enhance LTP. This finding also agrees with results showing increased synaptic plasticity in CA-Fyn expressing mice (Lu et al., 1999) but is in opposition to Yang et al. who report a decreased threshold for LTD in the presence of SKF81297 (Yang et al., 2012). This could be due to a number of factors, for example, Stramiello et al induced LTP using standard HFS protocol (100 pulses at 100Hz at repeated 3 times at 20s intertrain intervals) whereas Yang et al induced LTP using 1 train of 600 pulses at 100Hz. Another consideration is that Stramiello et al used SKF81297 at a 3x higher dose than Yang et al and it is possible that SKF81297 may have off target effects at higher concentrations, and if so, engagement with these off-target effects could have caused the increase in LTP.

The effect of increasing Src activity on plasticity has also been investigated. Increasing endogenous Src activity via application of PACAP38 lowered the threshold for LTP induction at CA1 synapses as LTP was observed at low frequencies that would otherwise cause LTD (10Hz) or no change (20Hz). This suggests that increased Src activity by PACAP38 increases synaptic plasticity by favouring LTP at lower frequencies. This is in opposition to Fyn which decreased plasticity following Fyn activation by SKF81297 in the same experimental set-up. The effect of PACAP38 was abolished in GluN2A Y1325F mice, suggesting that Y1325 phosphorylation (a site phosphorylated by Src) is required for PACAP38 to increase plasticity (Yang et al., 2012).

Overall, the effect of increasing Src and Fyn activity on synaptic plasticity has been reported in both transgenic mice expressing CA-Fyn and pharmacologically using PACAP38 to activate Src and SKF81297 to activate Fyn. These studies agree that increasing Fyn and Src activity promotes GluN2B Y1472 and GluN2A Y1325 phosphorylation, respectively, and increase NMDAR currents (Yang et al., 2012). Pharmacological increase of Src suggests that Src activity increases plasticity. However, this has not been investigated in transgenic constitutively active mouse models that could provide information about how chronically elevated Src activity affects plasticity. There are opposing conclusions about how increased Fyn activity affects synaptic plasticity. Increased Fyn activity in CA-Fyn mice increases synaptic plasticity (Lu et al., 1999), however two independent studies to pharmacologically increase Fyn activity have opposing conclusions (Yang et al., 2012) (Stramiello et al., 2008). Therefore, the effect of increased Fyn activity on synaptic plasticity remains unclear, so whether the increase in Fyn activity contributes to the loss of plasticity in AD cannot be inferred.

In terms of reducing SFK activity, Fyn<sup>-/-</sup> but not Src<sup>-/-</sup> mice showed impaired LTP (Grant et al., 1992), suggesting that reducing Fyn activity reduces plasticity. Pharmacologically decreasing Src activity, however, prevented LTP and so disagrees with findings in Src<sup>-/-</sup> mice (Lu et al., 1998). The effect of pharmacological Fyn inhibition on synaptic plasticity remains unknown. I aim to address this in this thesis by recording LTP in WT mouse hippocampal slices following acute inhibition of SFKs using Saracatinib. Details of Saracatinib and prior work using this drug relative to this project will be described in Section 1.11. Moreover, I aim to determine whether increased Fyn (and other SFK) activity contributes to the onset of reduced plasticity by testing whether acute treatment with Saracatinib rescues impaired LTP in Line 102 mice which model early AD.



To summarise Section 1.10, the evidence suggests that increased Fyn activity by A $\beta$  increases GluN2B pY1472 and thereby increases cell-surface expression of GluN2B-containing NMDAR expression. Consistent with this, increasing Fyn activity (by recombinant Fyn or by drugs to activate endogenous Fyn activity) enhances GluN2B-NMDAR mediated currents, which requires GluN2B Y1472 phosphorylation. Src, on the other hand, increases GluN2A-mediated NMDAR currents. Fyn is also required for A $\beta$ -induced cell death and this may be at least in part, via increased activation of GluN2B-containing NMDARs to drive excitotoxicity. Finally, the effect of increased Src and Fyn activity on synaptic plasticity remains controversial and findings using transgenic mice and pharmacological manipulation disagree. Overall, the literature suggests that Fyn is a key player in A $\beta$ -induced synaptotoxicity and that this may be via Fyn-mediated phosphorylation of GluN2B at Y1472. This could underlie cognitive impairments seen in AD, and therefore, inhibition of Fyn is a promising therapeutic target for the treatment of AD.

### 1.11 Inhibiting Fyn in AD: Saracatinib

The ability of Fyn to regulate the pathogenic potential of A $\beta$ , possibly via phosphorylation of GluN2B-containing NMDARs, makes it an attractive target for the treatment of AD. Saracatinib is a drug developed by AstraZeneca that inhibits Fyn and other SFKs (see Table 2) and was initially developed for the treatment of multiple cancers but was unsuccessful (Baselga et al., 2010). Repurposing Saracatinib to inhibit Fyn for the treatment of AD has since been investigated in mice and humans, and has shown some promising results. Preincubation of hippocampal slices for 30-120 minutes with 2  $\mu$ M Saracatinib prevented the A $\beta$ -induced increase in phosphorylation Fyn and Pyk2 at residues required for activity (pY416 and pY402 respectively). This suggests that Saracatinib prevents the A $\beta$ -mediated activation of Fyn and Pyk2. Consistent with this, increased GluN2B Y1472 phosphorylation by A $\beta$  was also prevented by Saracatinib in the same experiment (Kaufman et al., 2015). This suggests that acute inhibition of SFKs by Saracatinib is protective against A $\beta$ -induced activation of Fyn and Pyk2 and phosphorylation of GluN2B-NMDARs. Whether Saracatinib can reverse deficits in synaptic function and plasticity is unknown and will be investigated in this project.

Table 2 SFKs inhibited by 2  $\mu$ M Saracatinib

Adapted from Green et al., 2009

Kinase	Description	Adult mouse brain expression	Mean IC <sub>50</sub> (nM)
Src	SFK	Yes	2.7
Lck	SFK	Yes	<4
Yes	SFK	Yes	4
Lyn	SFK	Yes	5
Fyn	SFK	Yes	10
Fgr	SFK	No	10
Blk	SFK	No	11

Behavioural studies investigating spatial learning and memory in APP/PS1 mice suggest that Saracatinib rescues A $\beta$ -induced memory deficits. APP/PS1 mice present with a progressive loss of spatial and learning memory deficits in the MWM that begins between 6 and 10 months old (see Table 4) (Minkeviciene et al., 2008). 11-12 month-old APP/PS1 mice show elevated active Pyk2 (pY402) levels in the hippocampus and cortex (Kaufman et al., 2015). Increased Fyn activity was inferred from this measurement based on Pyk2 Y402 being a direct target of Fyn and because of previous findings showing A $\beta$ -induced increased Fyn activity in acute hippocampal slices (Kaufman et al., 2015). Following this hypothesis, it is likely that GluN2B pY1472 may also be increased, but this was not reported. Oral administration of Saracatinib (5mg/kg/day) to 11-12-month-old APP/PS1 mice for 2 weeks restored the elevated Pyk2 activity to WT levels (Kaufman et al., 2015). Whether chronic administration of Saracatinib altered the level of GluN2B pY1472 was also not reported. Spatial and learning memory deficits in APP/PS1 mice, measured in the MWM, were not improved by 2 weeks of Saracatinib treatment, However, after 3-5 weeks of treatment APP/PS1 mice performed as well as WT (Kaufman et al., 2015). Further benefits were recorded after 6 weeks of Saracatinib treatment, where APP/PS1 mice performed equally to controls in the novel object recognition task (Kaufman et al., 2015). This correlated with the full recovery of pre and postsynaptic markers, SV2a and PSD95 respectively, in the dentate gyrus (Kaufman et al., 2015). This suggests that chronic SFK inhibition may permit the recovery of memory impairments and lost synapses, but the exact mechanism by which Saracatinib permits this is still to be determined.

Synaptic function and plasticity following Saracatinib treatment has not been reported, and this would be invaluable to understand the mechanisms behind how Saracatinib can rescue memory impairments in an AD mouse model. Findings by Kaufman and colleagues suggest that Saracatinib treatment can rescue synapse loss and memory deficits. LTP is impaired in APP/PS1 mice starting at 3-4 months of age (Trinchese et al., 2004) and therefore we hypothesise that Saracatinib-mediated rescue in memory deficits in 11-12-month-old APP/PS1 mice may correlate with a rescue in LTP, however this was not reported. Similarly, whether Saracatinib is able to rescue A $\beta$ -induced basal synaptic transmission deficits is unknown. I aim to address this here by investigating whether Saracatinib can rescue impairments in basal synaptic transmission and plasticity in CA3-CA1 synapses of hippocampal slices from Line 102 mice. This will increase our understanding as to how Saracatinib confers its benefits in improving memory in APP/PS1 mice.

Importantly, the beneficial effects of Saracatinib in mice persist even after treatment is stopped. Deficits in spatial memory (measured by the MWM and novel object recognition) and synaptic density (measured by quantification of PSD-95 immunoreactivity) in 12-month-old APP/PS1 mice is rescued by Saracatinib treatment for 5 weeks (Smith et al., 2018). These benefits are sustained for at least one month after therapy cessation (Smith et al., 2018). This implies disease-modifying potential of Saracatinib for the treatment of AD. This is in opposition to the symptomatic relief therapy by Memantine (an NMDAR antagonist) which improved spatial memory after 5 weeks of treatment, but the effect was fully reversed after therapy cessation (Smith et al., 2018). This makes SFK inhibition all the more attractive as a potential therapeutic target for AD because the findings suggest that Saracatinib corrects, rather than masks, A $\beta$ -induced deficits.

Further support for the use of Saracatinib in AD is that the drug already has approval for use in humans. A phase Ib clinical trial demonstrated the safety, tolerability and CNS availability of oral administration of Saracatinib for 4 weeks (Nygaard et al., 2015). A phase IIa randomised clinical trial treated 152 patients with mild-moderate AD (MMSE 18-26) with a daily administration of 100-125mg Saracatinib for 52 weeks. This did not slow the rate of decline in cognition compared to placebo. However, MRI analysis revealed non-statistically significant trends for slowing the decrease in hippocampal volume and entorhinal thickness after Saracatinib treatment in AD. This prompted post hoc exploratory analyses that showed a significant slowing in the decline of cerebral metabolism in the entorhinal cortex of the Saracatinib-treated cohort (Van Dyck et al.,

2019)(Alexander et al., 2002). It is possible that Saracatinib did not slow cognitive decline because it was administered to individuals too late in disease progression. Saracatinib has not been tested earlier in AD. Here, I test whether Saracatinib can rescue early synaptic dysfunction in Line 102 mice that model the initial stages of AD before long-term memory impairments, A $\beta$  accumulation and synapse loss. These findings may give an insight into whether Saracatinib could be beneficial for much earlier intervention in humans.

The authors report that a small pharmacokinetic substudy alongside the clinical trial found that CSF levels of Saracatinib fell below the targets set by findings from findings in mice (Kaufman et al., 2015) and the phase 1b trial (Nygaard et al., 2015), however, these data were not made available (Van Dyck et al., 2019). This finding is important since Kaufman and colleagues reported that a dose reduction from 5mg/kg/d to 2mg/kg/day eliminated the beneficial effects of Saracatinib, suggesting a very narrow therapeutic window that may not have been reached in the clinical trial. This could explain the lack of translation from findings in transgenic mice. The adverse effects of Saracatinib, which most frequently include gastrointestinal disorders including diarrhoea, restrict the possibility to increase the dose in humans. Therefore, although these findings show the limits of Saracatinib treatment in humans, it does not exclude Fyn inhibition as a potential therapeutic strategy, and perhaps a more Fyn-specific drug with fewer adverse effects is required.

Inhibition of Fyn (using Saracatinib or other potential future Fyn inhibitors) may be a beneficial therapeutic intervention for AD. Here, I have reviewed evidence that suggests that Fyn inhibition may provide protection against A $\beta$  by reducing phosphorylation of GluN2B-containing NMDARs, thereby reducing NMDAR currents. However, I acknowledge that any beneficial effects Saracatinib could occur via other Fyn or SFK targets. It is clear that SFKs have a broad role in the CNS and therefore SFK inhibition by Saracatinib could alter basal synaptic properties of neurons, and could consequently have unknown effects on normal brain function. Current evidence to inhibit Fyn activity using knockout mice and pharmacological manipulations give an insight into how Saracatinib may affect synaptic plasticity under physiological conditions (summarised in Table 3). However, the effect of pharmacological Fyn (or SFK) inhibition on synaptic plasticity has not been reported under either physiological or pathological conditions. Therefore, the effect of modulating Fyn activity on synaptic plasticity remains unclear and so Saracatinib could have unknown effects on synaptic plasticity.



Table 3 Decreasing Fyn activity alters NMDAR phosphorylation, plasticity, cell viability and behaviour in mice.

Fyn Manipulation	NMDAR phosphorylation	Plasticity	Cell viability	Learning and Memory
Fyn <sup>-/-</sup> mice	<p>Tyrosine phosphorylation of GluN2B subunits is significantly reduced in the brain of Fyn<sup>-/-</sup> mice (Dunah et al., 2004).</p> <p>Aβ-mediated increase in GluN2B pY1472 and cell-surface expression is prevented in cortical cultures from Fyn<sup>-/-</sup> mice (Um et al., 2012).</p>	LTP is inhibited in CA3-CA1 synapses of hippocampal slices (Grant et al., 1992)	<p>Cortical cultures and hippocampal slices from Fyn<sup>-/-</sup> mice are protected against Aβo-induced cell death and dendritic spine loss (Lambert et al 1998)(Um et al., 2012).</p> <p>Ablation of Fyn in J20 mice rescues synapse loss and reduced premature mortality (Chin et al., 2004).</p>	Impaired spatial learning and memory in the Morris water maze (Grant et al., 1992)
Pharmacological decrease	Acute Saracatinib application decreases GluN2B pY1472 and prevents Aβo-induced increase in GluN2B pY1472 in WT hippocampal slices (Kaufman et al., 2015)	?	<i>In vivo</i> administration of Saracatinib to APP/PS1 mice completely rescues synaptic markers (PSD-95 and SV2A) in the dentate gyrus(Kaufman et al., 2015)	<i>In vivo</i> administration of Saracatinib in APP/PS1 mice recovers deficits in the Morris Water Maze and novel object recognition (Kaufman et al., 2015)

Table 4 Mouse models of AD relevant to this project

Mouse model	Mutation	Promoter	Start of expression	Deficits in hippocampal plasticity	Appearance of spatial learning memory defects	Appearance of A $\beta$ plaques
J20	APP <sub>Swe/Ind</sub>	PDGF- $\beta$	E15 <sup>1</sup>	TBS-LTP impaired by 3-6 months <sup>5</sup>	Deficits in radial arm maze and MWM by 4 months <sup>3,4</sup>	5-7 months <sup>2,3</sup>
Tg2576	APP <sub>Swe</sub>	PrP	E12.5 <sup>6</sup>	TBS-LTP impaired by 4-5 months <sup>7</sup>	MWM deficits by 10 months <sup>8</sup>	11-13 months <sup>9</sup>
APP/PS1	APP <sub>Swe</sub> /PS1 $\Delta$ E9	PrP	E12.5 <sup>6</sup>	HFS- LTP normal up to 12-months (HFS) <sup>10</sup>	MWM deficits by 6-10 months <sup>11,12</sup>	4 months <sup>13</sup>
APP23	APP <sub>Swe</sub>	Thy1 <sup>11</sup>	p7 <sup>11</sup>	TBS- LTP is normal up to 24 months <sup>15</sup>	MWM deficits by 3 months <sup>16</sup>	6 months <sup>14</sup>
Line 102 mature onset	APP <sub>Swe/Ind</sub>	CaMKII $\alpha$ <sup>17</sup>	P5 (if not suppressed with Dox) <sup>18</sup>	TBS-LTP impaired after 3 weeks of APP <sub>Swe/Ind</sub> expression <sup>19</sup>	T-maze (short-term spatial working memory) and Y-water maze (long-term spatial reference memory) deficits after 3 and 12weeks of APP <sub>Swe/Ind</sub> expression respectively <sup>19</sup>	7 months <sup>19</sup>

<sup>1</sup>(Sasahara et al., 1991)<sup>2</sup>(Mucke et al., 2000)<sup>3</sup>(Wright et al., 2013)<sup>4</sup>(Cheng et al., 2007)<sup>5</sup>(Saganich et al., 2006)<sup>6</sup>(Asante et al., 2002)<sup>7</sup>(Jacobsen et al., 2006)<sup>8</sup>(Kishimoto et al., 2013)<sup>9</sup>(Irizarry et al., 1997)<sup>10</sup>(Volianskis et al., 2010)<sup>11</sup>(Minkeviciene et al., 2008)<sup>12</sup>(Lalonde et al., 2005)<sup>13</sup>(Garcia-Alloza et al., 2006)<sup>14</sup>(Sturchler-Pierrat et al., 1997)<sup>15</sup>(Roder et al., 2003)<sup>16</sup>(Van Dam et al., 2003)<sup>17</sup>(Jankowsky et al., 2005)<sup>18</sup>(Bayer et al., 1999)<sup>19</sup>(Sri et al., 2019)

## 1.12 Aims and Objectives

The project aims to uncover the effect of SFK inhibition on normal synaptic function and plasticity and to determine whether inhibiting SFKs in a mouse model of early AD can rescue synaptic dysfunctions inflicted by A $\beta$ . To investigate these points, I employ WT mice, Line 102 mice and Saracatinib to complete the following aims:

1. To investigate the effect of acute SFK inhibition on basal synaptic function and plasticity in CA3-CA1 synapses from adult WT mouse hippocampal slices.
2. To compare the level of a direct Fyn target, GluN2B pY1472, in Line 102 mice when synaptic dysfunction first occurs and later when there is evidence of synapse loss.
3. To investigate whether Saracatinib can rescue early synaptic dysfunctions in CA3-CA1 synapses from hippocampal slices of Line 102 mice.



## Chapter 2 Methods

### 2.1 Animals

#### 2.1.1 Animal husbandry

Animal care and experimental procedures were conducted in accordance with UK Home Office regulations under the Animals (Scientific Procedures) Act of 1986. C57Bl/6 WT mice and Line 102 mice were housed in groups at 21° under a 12hr/12hr light dark cycle, with food and water *ad libitum*. Ages of mice are detailed in main text.

#### 2.1.2 Line 102

APP and tTA transgenic mice from the Line 102 model were generously provided by Joanna Jankowsky, Baylor School of Medicine. Transgenic APP mice carry the mouse APP gene with a humanised A $\beta$  domain (mouse/human APP695) that contains the human Swedish (KM570/571NL) and Indiana (V617F) mutations (APP<sub>Swe/Ind</sub>). APP<sub>Swe/Ind</sub> expression is controlled by the tetracycline responsive element (TRE) (see Figure 1.7). Transgenic tTA mice carry the tetracycline transactivator (tTA) gene, controlled by the CamKII $\alpha$  promoter which is expressed postnatally in neurons of the forebrain. Single transgenic APP and tTA mice were crossed to give the four possible offspring genotypes: wild type (WT), single transgenic APP or tTA mice, or double transgenic APP/tTA mice. Mice were reared on 625mg/kg doxycycline (dox) which was incorporated into the food pellets. This prevented expression of APP (Figure 2.1 A). Upon removal of the dox diet, APP expression was induced in mice expressing both APP and tTA (Figure 2.1 B).

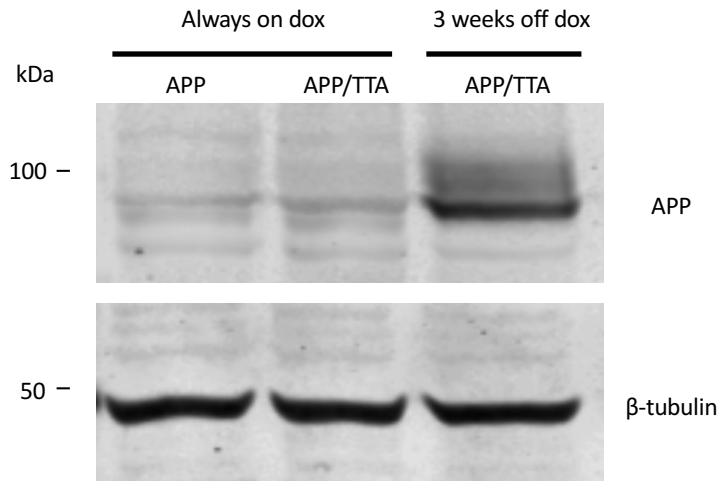
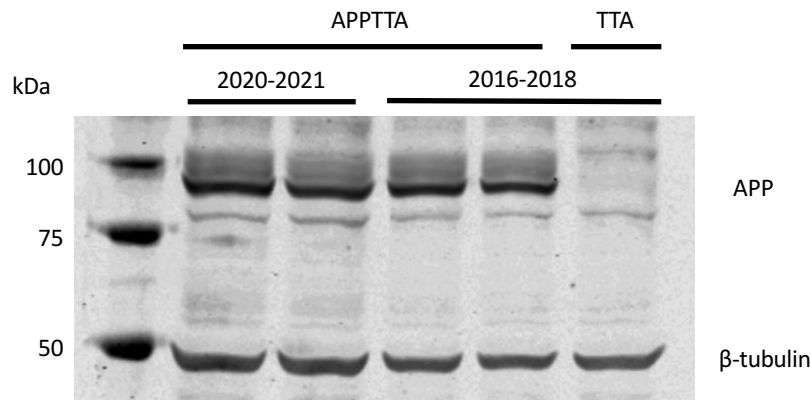
**A****B**

Figure 2.1. APP expression upon dox diet removal in Line 102 mice.

**(A)** Western blot image of cortical tissue from age-matched Line 102 mice that have always been on dox (lane 1-2) or have been off dox for 3 weeks starting at 6-weeks old (lane 3). Blots were probed for APP and  $\beta$ -tubulin. **(B)** Sample blot of freshly-frozen cortical homogenate from Line 102 mice expressing both APP and TTA transgenes or only the TTA transgene. The samples were collected during the 2016-2018 period (by Dr Sarmi Sri) or 2020-2021 period.

## 2.2 Genotyping

Mice were genotyped at 6 weeks old by taking an ear clipping. Clips were taken specifically such that the position of the ear clipping gave each mouse an identifying number. On the day of the experiment, a mouse was chosen from the cage at random. Following brain extraction and slicing the ear clipping number was identified and its genotype was documented. This means that brain

extraction and slicing was performed blindly. However, electrophysiological recordings were performed with the knowledge of the genotype.

### 2.2.1 DNA extraction

Mice ear clippings were used for genotyping. All centrifugation steps in DNA extraction were performed at room temperature. DNA lysis buffer containing 10 mM TRIS, 10 mM EDTA, 100 mM NaCl, 20% SDS and 0.4 mg/ml Proteinase K in RNA-ase free water was prepared and 100  $\mu$ l was added to each ear clipping in an Eppendorf. Lysis buffer containing ear clippings were heated at 54 degrees for 30 minutes or until the ear clipping had fully dissolved. Unwanted hair and material were pelleted by centrifuging the samples for 10 minutes at 13,000 RPM. The supernatant was removed and an equal volume of isopropanol was added and mixed by gently flicking the Eppendorf until the DNA precipitated as a thin white strand. Then the samples were centrifuged for 5 minutes at 10,000 RPM to pellet the DNA. The DNA pellet was washed by adding 100  $\mu$ l of 70% ethanol. The samples were centrifuged again 5 minutes at 10,000 RPM and ethanol carefully removed and discarded. Any remaining ethanol was left to evaporate by leaving Eppendorf upside down with the lids open for around 30 minutes. Once dry, the DNA was re-suspended in 25  $\mu$ l of RNA-ase free water. The amount of DNA extracted was estimated using the spectrophotometer (NanoDrop).

### 2.2.2 PCR

Following the protocol by (Jankowsky et al., 2005), the same PCR reaction was used to genotype for APP and tTA transgenes. This used five different primers listed in Table 5. Primers to amplify endogenous mouse prion protein was used as a positive control. The PCR reaction was run on GeneAmp PCR system 9700 (Applied Biosciences, UK), under the conditions listed in Table 6.

Table 5 PCR components for genotyping Line 102 mice

	Volume ( $\mu$ l)	Primer sequence
S36 (2 $\mu$ M)	1	CCG AGA TCT CTG AAG TGA AGA TGG ATG
PrP-AS-J (2 $\mu$ M)	1	CCA AGC CTA GAC CAC GAG AAT GC

## Chapter 2

Tn10 (2 $\mu$ M)	2	CGC TGT GGG GCA TTT TAC TTT AG
VP16 (2 $\mu$ M)	2	CAT GTC CAG ATC GAA ATC GTC
PrP-S-J (2 $\mu$ M)	1	GGG ACT ATG TGG ACT GAT GTC GG
REDTaq	12.5	
Water	4.5	

Table 6 PCR reaction conditions

	Temp (°C)	Time (min)	Number of cycles
Initial	94	5	1
Denaturing	94	0.5	37
Annealing	64	1	
Extension	72	1	
Final extension	72	10	1
Hold	4	$\infty$	1

### 2.2.3 Agarose gel electrophoresis

A 1% agarose gel was prepared by dissolving agarose in 1x TBE. The solution was warmed in a microwave until all agarose has dissolved. After leaving to cool for a few minutes, GelRed was added at 1:10,000 and the solution was poured into the casting mould. The gel was allowed to set for 30 minutes and was then transferred into an electrophoresis tank filled with 1x TBE. 4  $\mu$ l of DNA ladder (hyperladder, Bioline) was added into the first well followed by 10-12  $\mu$ l of the PCR products into the subsequent wells. The gel was run at 120V for 35-50 minutes. Finally, the gel was imaged using the trans illuminator and the genotype was determined by the presence or absence of bands at the known PCR product base pair (bp) size: APP 400bp, tTA 480bp, PrP 750bp. Figure 2.2 shows an example image of the gel showing all four possible genotypes arising from Line 102 breeding.

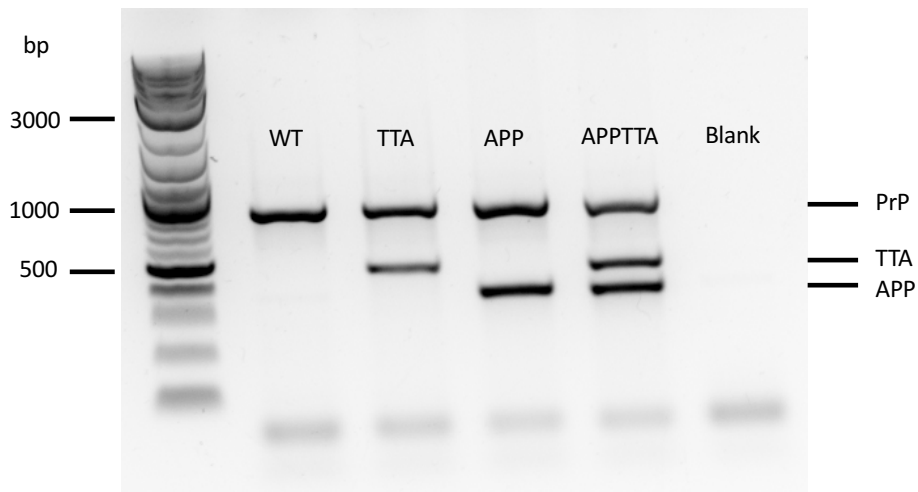


Figure 2.2 Genotyping Line 102 mice

Sample gel image of PCR products from ear clippings of the 4 possible genotypes from breeding Line 102 mice. From left to right: WT, TTA, APP, APPTTA, water control (blank).

## 2.3 Electrophysiology

### 2.3.1 Solutions

Artificial cerebral spinal fluid (aCSF) consisting of NaCl 126 mM, CaCl<sub>2</sub> 2 mM, glucose 10 mM, MgSO<sub>4</sub> 2 mM, KCl 3 mM, NaH<sub>2</sub>PO<sub>4</sub> 1.25 mM, NaHCO<sub>3</sub> 26.4 mM (pH 7.2-7.4) was prepared on the day of the experiment by diluting 10x stocks (stock I: NaCl, CaCl<sub>2</sub>, glucose, MgSO<sub>4</sub>, KCl, NaH<sub>2</sub>PO<sub>4</sub>, stock II: NaHCO<sub>3</sub>) and was oxygenated with 95% O<sub>2</sub>/5% CO<sub>2</sub> for at least 10 minutes before use.

### 2.3.2 Brain extraction

Mice were anaesthetised using inhalation of isoflurane using a vaporiser and then immediately culled by cervical dislocation followed by decapitation. The head was instantly submerged in cold aCSF (~4°C). Whilst keeping the head submerged, small scissors were used to cut open the skin and skull across the midline. The skull bone plates were broken off using tweezers and single transverse cut behind the olfactory bulbs was made using scissors. The brain was carefully removed using a spatula. The entire process of dissecting out the brain was completed as quickly as possible in less than 2 minutes.

### 2.3.3 Preparation of hippocampal slices

Figure 2.3 summarises the steps taken to prepare hippocampal slices for field recordings. Following brain extraction, the hemispheres were separated by cutting down the midline with a scalpel. The hemispheres were then glued midline-down onto a metal cutting stage using superglue. The metal cutting stage was then transferred to a slice chamber filled with ice-cold aCSF and surrounded by ice. The aCSF was continuously bubbling with carbogen during slicing. 350  $\mu$ M thick sagittal slices were prepared using the vibrating microtome at 1.0Hz. Slices were trimmed of midbrain using a scalpel and then transferred to a resting chamber containing room temperature aCSF continuously bubbling with carbogen for at least one hour. Hippocampal slices from both the left and right hemisphere were used at random.

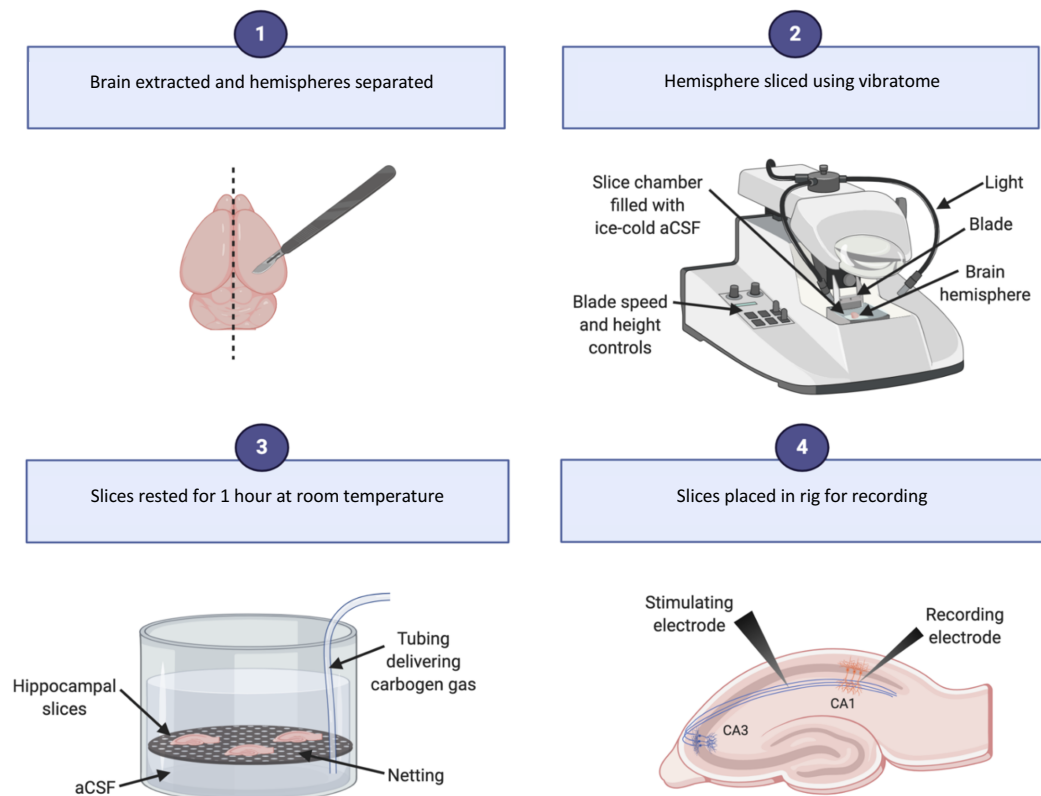


Figure 2.3 Preparation of hippocampal slices for field recordings

The brain was extracted quickly in ice-cold aCSF and cut in half along the midline. 350  $\mu$ M thick sagittal hippocampal slices were prepared in ice-cold aCSF using a vibratome. The slices were then rested in an incubation chamber at room temperature for 1 hour. The chamber was made from a beaker with a layer of thin netting which the slices rested on. Following the rest period, the slices were transferred into the rig for

electrode placement. At all stages the aCSF was continuously bubbled with carbogen (95% O<sub>2</sub>/5% CO<sub>2</sub>). Created using Biorender.com.

### 2.3.4 Field recordings rig setup

The rig was positioned on an antivibration table surrounded by a Faraday cage. The rig was made up of 4 smaller inner (recording) chambers positioned on top of one large outer chamber. Separate recording chambers meant that multiple slices could be recorded in different conditions at the same time. The outer chamber was filled with warmed H<sub>2</sub>O and was bubbled with carbogen to create a humid, oxygen rich environment. Brain slices rested on the inner chambers made from removable plastic rings with thin netting tightly secured over. The recording chambers were constantly perfused with bubbling aCSF that was maintained at 28-32°C and recycled using a peristaltic pump. Using the peristaltic pump, the aCSF travelled in tubing from a beaker through the warm outer chamber and into the inner chambers before recycling back to the beaker. Some experiments were recorded in submerged style (brain slice complete submerged in aCSF) and others were recorded in interface style set-up (where the level of aCSF is lowered to form a meniscus on top of the slice). Some experiments were also recorded in the presence of 3 mM Gabazine. Where experimental set up differs is indicated in the figure legends.

A transfer pipette was used to move brain slices to the recording chambers. To ensure a stable baseline could be achieved, the slices were left to rest for at least 1 hour in the recording chamber before any electrodes were placed. Stimulating and recording electrodes were lowered into the slice under the visual guidance of overhead cameras so that they penetrated very slightly into the tissue. The stimulating electrode was placed in the stratum radiatum of CA1 to stimulate the Schaffer collateral projections, whilst the recording electrode was placed in the stratum radiatum of CA3 to record the dendritic region of CA3 pyramidal cells.

Recording electrodes were made from Borosilicate glass capillaries (1 µM) (World Precision Instruments) using a P-97 Flaming/Brown micropipette puller (Sutter Instrument). The electrode was filled with aCSF and a silver chloride wire was placed inside. Silver chloride wires were produced by placing silver wire in bleach overnight. Stimulating electrodes were made from stainless steel (Diameter 0.010 in., Length 3in, AM-Systems). Recording and stimulating electrodes were mounted onto micromanipulators (NMN-25 micromanipulator, Narishige) which were



controlled by hand to lower the electrodes into the slice. Thin cotton was wrapped around both the recording and stimulating electrodes to prevent any condensation droplets accumulating.

### 2.3.5 Eliciting field excitatory postsynaptic potentials (fEPSPs)

An electrical impulse was delivered via the stimulating electrode using custom-written MATLAB functions. The intensity of the stimulus was controlled using an A.M.P.I. ISO-Flex stimulator and recording were made using an Axoclamp 2B amplifier (Molecular Devices, Sunnyvale, U.S.A). Recordings were converted from analogue to digital via a National Instruments card PCIe-6343 and later loaded within MATLAB R2020a.

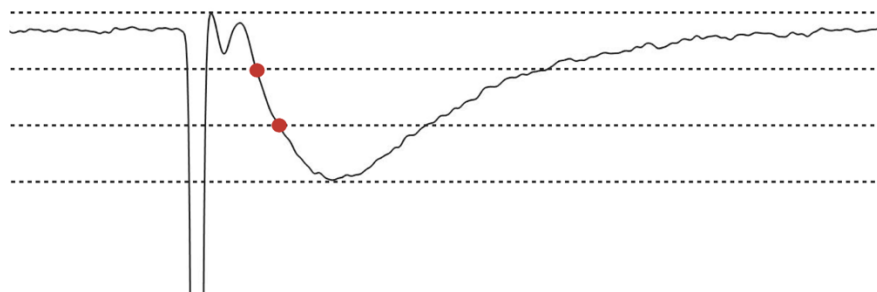


Figure 2.4 Measuring the postsynaptic response

Sample fEPSP trace measured in the stratum radiatum of CA1 following electrical stimulation of Schaffer collateral. Two points within the middle third of the EPSP were chosen and the corresponding change in voltage (y axis) was divided over change in time (x axis) to calculate the fEPSP slope.

### 2.3.6 Input-Output response

Synaptic strength in CA3-CA1 synapses was measured using input-output response. The input-output relationship was recorded for the CA3-CA1 pathway by stimulating at increasing intensities (in  $\mu\text{A}$ ): 20, 30, 40, 50, 60, 70, 100 and 200. Each stimulus intensity was applied for 0.1 ms. Synaptic strength was determined by measuring the fEPSP slope. This was calculated by choosing two time points within the middle third of the fEPSP (Figure 2.4). The slope was calculated by dividing the voltage by the time interval. For each stimulus, the slice was stimulated three times and an average fEPSP slope was calculated. This was then averaged across slices so that the final output was the average fEPSP slope per slice. The values were imported into GraphPad Prism and the mean  $\pm$ SEM was plotted for each condition.

The maximum response during the input-output response was visually determined by the shape of the fEPSP and the stimulus intensity which resulted in a fEPSP that was ~40% of the maximum response was used for paired-pulse facilitation and for the baseline of LTP protocols. This was chosen to prevent action potential spiking during experiments.

### 2.3.7 Paired-pulse ratio

Paired-pulse ratio (PPR) at CA3-CA1 synapses was assessed by delivering two 50  $\mu$ s stimuli at increasing interstimulus intervals of (in ms): 10, 20, 40, 80, 160, 320 and 640 (Kimura et al., 2014). This was repeated 4 times at 0.1Hz (Figure 2.5). Paired-pulse ratios were calculated for each interstimulus interval by dividing the amplitude of the second fEPSP slope by the amplitude of the first.

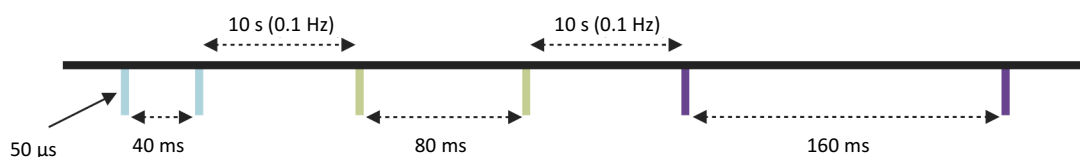


Figure 2.5 Paired-pulse ratio

Illustration of the first three inter-stimulus intervals used to assess paired-pulse ratio.

Each pulse is delivered for 50  $\mu$ s and each pair of pulses is separated by 10 s (0.1 Hz).

The timing between the pair of pulses increases, shown here using 40, 80 and 160 ms as examples.

### 2.3.8 Theta-burst induced LTP

Schaffer collaterals were stimulated once every 20s and the resulting slope of the fEPSP was recorded and an average was plotted every minute. This was recorded for a minimum of 15 minutes or until a stable baseline was achieved. A baseline was considered stable if it did not drift more than 15%. LTP was then induced using a theta-burst stimulation (TBS) of the Schaffer collateral outlined in Figure 2.6. This consisted of 3 trains of stimulation separated by 15s. Each train consisted of 10 bursts at 5Hz (0.2s apart), with each burst containing four pulses at 100Hz

(10 ms apart). Immediately following the induction protocol, the Schaffer collateral were stimulated every 20s (the same as the baseline) and the fEPSP slopes were recorded and an average plotted every minute for 45 minutes. For quality control, the pre and post LTP fibre volleys had to overlay within 2 standard deviations, else they were discarded. LTP plots were created in MATLAB by normalising the baseline slopes to 1 and plotting the average fEPSP slopes per minute for the recording. The mean  $\pm$ SEM per slice was plotted for each condition. An end LTP value was determined by averaging the fEPSP slopes in the final 5 minutes of after TBS (40-45 minutes).

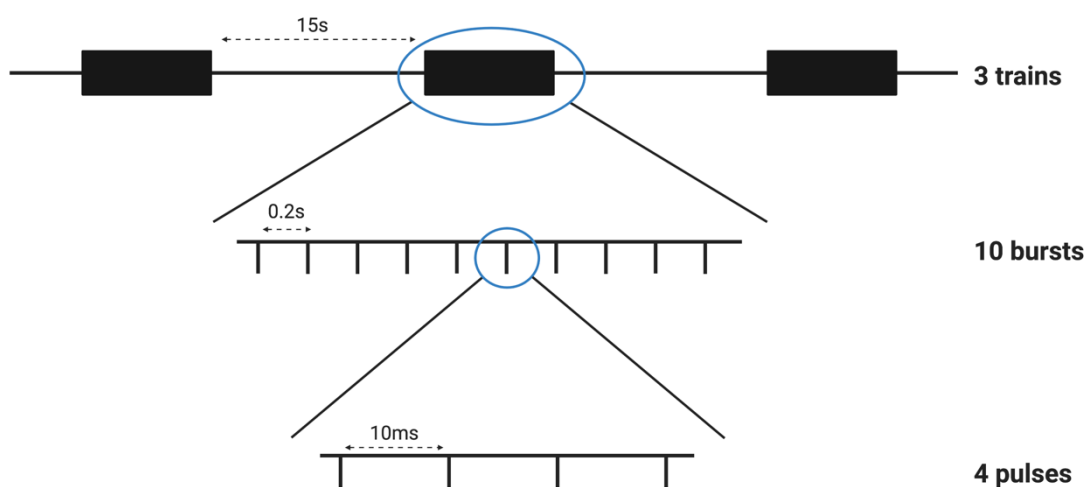


Figure 2.6 Theta burst stimulation protocol

The Theta burst stimulation protocol was used to induce LTP in CA3-CA1 synapses. This was achieved by stimulating the CA3 region with 3 trains of stimulation, each separated by 15s. Each train consisted of 10 bursts at 5Hz (0.2s apart), with each burst containing four pulses at 100Hz (10 ms apart).

## 2.4 Drug application

No blinding procedures were used with drug applications, both *ex vivo* and *in vivo* experiments.

### 2.4.1 Saracatinib for *ex vivo* application

Saracatinib was obtained from Selleckchem (catalogue no. S1006). 60 mM Saracatinib dilution was prepared in DMSO and warmed with 50°C water bath as per manufacturer instructions and

was frozen in 5  $\mu$ L aliquots. Saracatinib was added to aCSF on the day of the experiment to give a 2  $\mu$ M Saracatinib concentration. For field recordings, slices were rested in the rig (with aCSF containing 2  $\mu$ M Saracatinib) for 2 hours prior to recordings.

### 2.4.2 Saracatinib for *in vivo* administration

The vehicle for oral gavage was made from 0.5% HPMC and 0.1% Polysorbate 80. Due to solubility issues, Saracatinib was first dissolved in DMSO (35 mg/mL) and warmed with a 50°C water bath as per manufacturer instructions. The final DMSO dose was well below toxic levels in mice (Gad et al., 2006). This was then added to the HMPC/Polysorbate 80 solution immediately before dosing the mouse. The total volume for gavage was 100  $\mu$ L and the concentration of Saracatinib was 5mg/kg/day or 10mg/kg/day. The volume of Saracatinib and HMPC/Polysorbate 80 was adjusted to give this final volume based on the weight of the mouse. The volume was measured using a pipette before being drawn up into a syringe and a stainless-steel feeding tube was attached.

Lorraine House (BRF technician) dosed the mice by oral gavage by restraining the mouse in a scruff in the upright position. Then, the stainless-steel feeding tube was inserted into the mouse to the left or right of the midline and down the oesophagus. The contents of the syringe were then carefully expelled into the stomach. Mice were dosed with either 5mg/kg, 10mg/kg or vehicle. Following (Kaufman et al., 2015), the dose was split into 2 equal amounts and were administered to the mice in the morning and afternoon for 3 days. On the final day of the experiment, the mice were sacrificed after 30 minutes of the final dose and the brains were extracted and stored on dry ice.

### 2.4.3 DHPG

DHPG was used to induce chemical LTD. Following (Kumar et al., 2014), recordings were made in the presence of 3 mM Gabazine and the CA3 region of the slice was removed using a scalpel before being placed into the rig. Schaffer collaterals were stimulated once every 20s and the resulting slope of the fEPSP was recorded and an average was plotted every minute. This was recorded for a minimum of 15 minutes or until a stable baseline was achieved. 100  $\mu$ M DHPG was added to the aCSF and allowed to circulate the rig for 10 mins. This was then replaced with standard aCSF that circulated the rig for the remainder of the experiment.

#### 2.4.4 TAT-Fyn(39-47)

TAT-Fyn(39-47) inhibitor peptide and its corresponding control, TAT-Fyn(Scram), were gifted by Professor Michael Salter. The peptides were dissolved directly into aCSF to give a final concentration of 10  $\mu$ M. Hippocampal slices were incubated in 10  $\mu$ M TAT-Fyn(39-47) or TAT-Fyn(Scram)-containing aCSF for 30 mins and then immediately removed and frozen on dry ice. Samples were stored at -80°C before being homogenised for Western blotting.

## 2.5 Western blotting

### 2.5.1 Protein extraction

Un sliced cortical and hippocampal samples were collected for Western blotting. Following brain extraction described in Section 2.3.2, the brain was cut down the midline and a hemisphere was randomly selected for tissue collection. Using curved fine forceps, the midbrain was removed and discarded. The cerebellum was also removed and discarded using a scalpel. The hippocampus was visually identified and removed using curved fine forceps and immediately frozen in an Eppendorf on dry ice. The frontal portion of the cortex was cut away using a scalpel and also immediately frozen in a separate Eppendorf on dry ice.

Frozen brain samples were weighed and homogenised in RIPA buffer (1X PBS, 0.5% sodium deoxycholate, 0.5% Triton-X, 2.5 mM EDTA, 0.1% SDS, titrated to pH 7.6) containing Halt protease and phosphatase inhibitor cocktail (1:100) at a volume that is 5 times the weight of the sample. Samples were homogenised using Kontes pellet pestle motor for at least 30 seconds. The resulting homogenate was then centrifuged at 13,000 rpm for 10 min at 4°C. The pellet was discarded and the supernatant transferred to a new tube. Protein concentration was measured using the Bio-Rad protein assay kit using manufacturer's instructions. The standard curve for the assay was prepared by diluting BSA stock in RIPA buffer. Protein concentration was measured by measuring absorbance using FLOUstar OPTIMA and OPTIMA data analysis software. The standard curve  $R^2$  value must be >0.95 to interpret results. All samples were diluted to 2.5  $\mu$ g/ $\mu$ L using RIPA buffer containing Halt protease and phosphatase inhibitor cocktail and stored at -80°C.

### 2.5.2 Sample preparation

On the day of running the Western blot, the samples were diluted 1:3 in 4x sample buffer (8% SDS, 20% 2-mercaptoethanol, 40% glycerol, 0.008% bromophenol blue and 0.250M Tris-HCl at pH 6.8) to give a final concentration of 1.875  $\mu\text{g}/\mu\text{l}$ . The samples were then boiled at 90°C for 5 minutes before centrifuging at 13,000 rpm for 60 seconds.

### 2.5.3 SDS-polyacrylamide gel electrophoresis (PAGE)

7% SDS-PAGE gels were made from resolving and stacking solutions, see Table 7 for reagents and volumes used. Glass plates were cleaned with 70% ethanol before being assembled into the plate holder. The resolving solution was poured into the assembled plates up to ~80% of the height of the plate. Isopropanol was added to remove any bubbles and the solution was allowed to set into a gel for ~10 min. The isopropanol was removed and rinsed with water. The stacking solution was then poured on top of the resolving gel and a 10 well comb was inserted before leaving it to set to a gel (~10 mins).

Table 7 Reagents and their volumes to make one 7% gel for Western blot

Reagent	Resolving gel (7%) (mL)	Stacking Gel (mL)
30% acrylamide	2.33	0.65
1.5M Tris-HCl 10% SDS (pH 8.8)	2.5	-
0.5M Tris-HCl 0.4% SDS (pH 6.8)	-	1.25
10% Ammonium persulphate	0.1	0.05
Tetramethylenediamine	0.01	0.005
Water	5.06	3.05

The plates containing the formed gel were then placed in an electrophoresis holder and transferred to a tank (Bio-Rad) containing 1X Laemmli buffer (25 mM tris, 192 mM glycine and 1% SDS) and the comb was carefully removed. 4 $\mu\text{l}$  of Biorad precision blue protein ladder was added to the first well followed by 16 $\mu\text{l}$  (30 $\mu\text{g}$ ) of protein into subsequent wells. The gels were run at 100V for ~100 minutes until the ladder was separated.

#### 2.5.4 Electroblotting of protein to nitrocellulose membrane

Transfer buffer was prepared containing 1X Transfer buffer (5.8g Tris and 2.9g glycine) 20% methanol and distilled water. Sponges, nitrocellulose membranes and filter papers were pre-soaked in transfer buffer to make the transfer 'sandwich'. This was arranged as illustrated in Figure 2.7 and contained a polyacrylamide gel against a nitrocellulose membrane with 2 pieces of filter paper either side to ensure good contact between the gel and the membrane. A roller was moved over the surface of the filter papers to remove any bubbles between the gel and the membrane before sponges were placed either side and the sandwich was sealed. This was then placed in a transfer cassette in a tank (BioRad) so that the membrane is orientated nearest to the positive electrode and the gel is orientated nearest the negative electrode. Therefore, the negatively charged proteins will migrate out of the gel and on to the membrane. The tank was surrounded by ice to ensure optimal transfer. Proteins were transferred to the nitrocellulose membranes at 100V for 1.5hr.

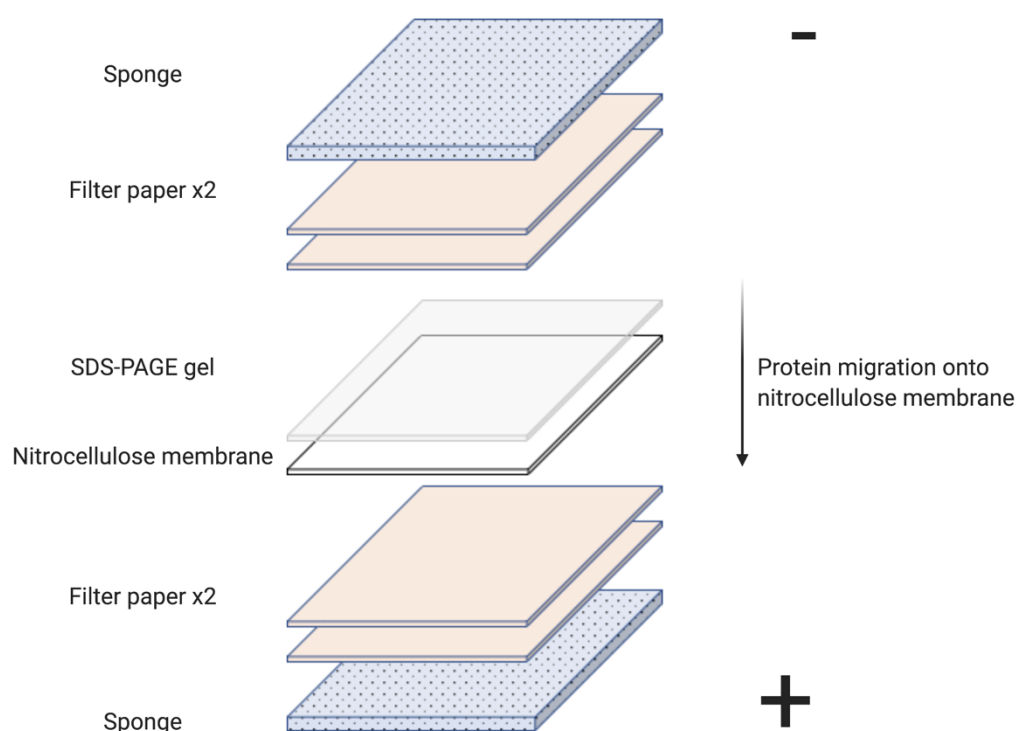


Figure 2.7 Arrangement of materials for SDS-PAGE protein transfer

The SDS-PAGE gel is arranged in a 'transfer sandwich' where the nitrocellulose membrane is in direct contact with the gel. 2 Filter papers are placed either side to ensure good contact between the gel and the membrane and to prevent movement during transfer. Sponges are placed either side and the sandwich is inserted into a transfer cassette. This is then placed into a tank in an orientation such that the nitrocellulose membrane is closest to the anode (+). This results in the movement of the negatively charged proteins from the SDS-PAGE gel towards to the anode (+) and onto the nitrocellulose membrane. Created using Biorender.com.

### 2.5.5 Antibody labelling

Following protein transfer, the nitrocellulose membrane was removed and blocked with TBS-T (1x TBS, 0.1% Tween) containing 5% BSA for one hour on a rocker at room temperature. Then the membrane was incubated with primary antibody containing TBS-T, 5% BSA, 0.1% sodium azide. Concentrations and timings for antibody incubations are shown in Table 8. The primary antibody was removed and stored for re-use and the membrane was washed for 5 mins with TBS-T on a rocker 3 times. Then, secondary antibody diluted 1:10,000 with TBS-T containing 5% BSA was added to the membrane and left to incubate for one hour at room temperature on a rocker. Secondary antibodies were not re-used. Finally, the membrane was washed again for 5 mins with TBS-T on a rocker 3 times before scanning with an Odyssey Infrared Imaging Scanner at the 700/800 nm wavelength. The image of the scan was obtained using the Image Studio Scanner software. The band quantified following labelling with the anti-GluN2B antibody was positioned at 180kDa which is the expected molecular weight for full-length GluN2B. Therefore, GluN2B refers to full-length GluN2B throughout this thesis.

Table 8 Primary antibodies used for Western blotting

MW: molecular weight, O/N: overnight

Antibody	Supplier	Source	Immunogen	Dilution	MW (kDa)	Incubation
GluN2B	BD Bioscience (610416)	Monoclonal Mouse	NMDAR amino acids 892-1051	1:1000	180	O/N at 4°C



pY1472 GluN2B	R&D Systems (PPSO14)	Polyclonal Rabbit	Phosphopeptide corresponding to amino acids surrounding the pY1472	1:1000	180	O/N at 4°C
$\beta$ -tubulin	Cell Signalling (5568)	Monoclonal Rabbit	Carboxy terminus of $\beta$ 3 tubulin	1:1000	55	1 hour at RT

### 2.5.6 Quantification and data analysis

Blots were quantified using Image Studio Lite software. A rectangle of the same size was drawn around each fluorescent band of interest and signal intensity was recorded considering top/bottom background noise. The same standard control brain sample was run in each blot and quantification all of all bands was expressed relative to the standard control. This minimised changes that could arise due to differences in transfer efficiency and antibody efficiency (i.e. the number of times it had been re-used) from one blot to another.  $\beta$ -tubulin was used as a loading control throughout.

## 2.6 Statistics

The data are presented and analysed as n=mouse for analysis between genotypes and n=slice for analysis of pharmacological manipulations. The data were analysed using parametric tests for normally distributed data (Analysis of Variance, ANOVA) and non-parametric tests for data that are not normal (Kruskal-Wallis test). Multiple comparison t-tests were used to compare variables following a statistically significant finding between all the variables used in the experiment. As indicated in the figure legend, multiple comparisons were conducted two-way unless prior evidence was available to provide a hypothesis and, in such cases, a one-way t-test was used. Power analysis was not conducted prior to data collection.



## Chapter 3 The effect of SFK inhibition on synaptic function and plasticity in WT mice

Fyn activity is increased in AD and this may contribute to pathology by driving excitotoxicity and synaptic dysfunction (See Section 1.10.4). Therefore, Fyn inhibition is a promising therapeutic intervention for AD. However, when modulating the activity of a target protein(s) for the treatment of disease it is important to consider its physiological role in the healthy system. SFKs may be required for normal plasticity, and this is supported by evidence showing impaired LTP and spatial learning and memory in Fyn<sup>-/-</sup> mice (See Section 1.10.5). Despite the fact that Saracatinib entered human clinical trials, the effect of pharmacologically decreasing SFK activity on synaptic function and plasticity has not been reported. This is important since Fyn<sup>-/-</sup> mice develop morphological brain defects and so may not properly model Fyn inhibition in the healthy brain (Kojima et al., 1997). Therefore, it is unknown whether Saracatinib (or other potential future SFK inhibitors) will affect these fundamental properties which could affect normal brain function. To address this, I aimed to determine the effect of Saracatinib on normal synaptic function and plasticity in adult WT mice.

Behavioural readouts following Fyn inhibition give an insight into the function of memory circuits in the brain. Kaufman and colleagues showed that *in vivo* administration of 5mg/kg/day Saracatinib for 6 weeks rescues learning and memory deficits in APP/PS1 mice but did not affect the performance of control littermates in control mice (see Section 1.11) (Kaufman et al., 2015). This suggests that 6 weeks of Saracatinib exposure does not alter spatial learning and memory in healthy mice, which may imply that it also does not alter synaptic plasticity within this treatment time window, however this was not reported. A direct measurement of synaptic plasticity following Saracatinib exposure in WT mice is needed to complement behavioural data and to understand the effect of pharmacological Fyn inhibition at the cellular level in the hippocampus.

### 3.1 Chapter aims

1. To determine whether acute Saracatinib application inhibits Fyn in hippocampal slices from adult WT mice by measuring GluN2B pY1472.
2. To investigate whether Saracatinib affects basal synaptic function and plasticity using input-output, paired pulse and LTP/LTD measurements.

3. To complete a pilot study to determine whether Saracatinib administration *in vivo* to adult WT mice reduces GluN2B pY1472

## 3.2 Results

### 3.2.1 Antibody validation

Before analysing the level of GluN2B pY1472 in Western blot experiments, I first sought to validate the anti-GluN2B pY1472 antibody. The ideal experiment to test antibody specificity is to compare the fluorescent signal produced from probing WT and knockout tissue of the protein of interest. The band of interest should be absent in the knockout tissue, providing confidence in antibody specificity and confirming that the quantified band is the protein of interest and not a non-specific target. However, since I did not have access to such tissue, I tested the antibody using pharmacological manipulations to increase or decrease tyrosine phosphorylation in hippocampal slices. To do this I used two drugs: Sodium orthovanadate ( $\text{Na}_3\text{VO}_4$ ) and Saracatinib. Sodium orthovanadate is a general inhibitor of phosphotyrosine phosphatases and so its application increases tyrosine phosphorylation. Conversely, Saracatinib inhibits SFKs thereby decreasing GluN2B pY1472. I found that  $\text{Na}_3\text{VO}_4$  increased and Saracatinib decreased the signal intensity produced by the anti-pY1472 GluN2B antibody at the molecular weight expected for GluN2B (~190kDa) (Figure 3.1). This provides confidence that the band quantified in my Western blot experiments following incubation with the anti-GluN2B pY1472 antibody is a true measure of the level of GluN2B pY1472.

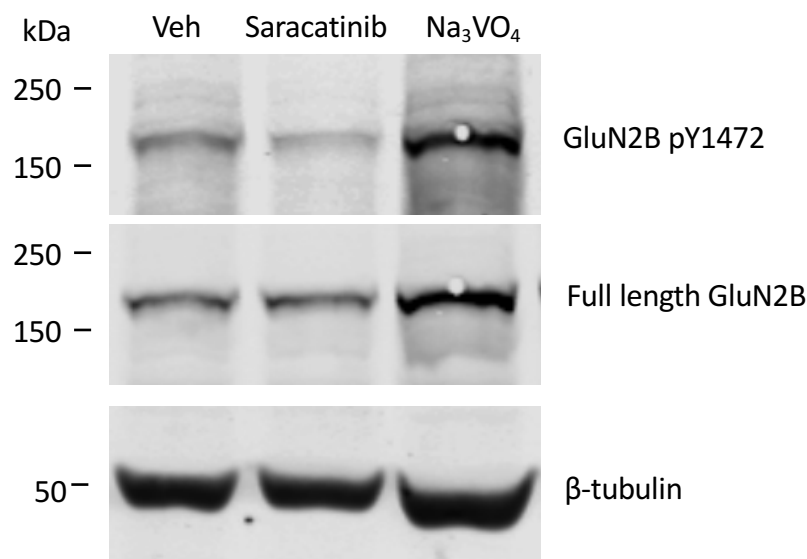


Figure 3.1 Western blot image of hippocampal slices from adult WT mice following incubation in aCSF (veh), 2  $\mu$ M Saracatinib (2 hours) or 0.1 mM Na<sub>3</sub>VO<sub>4</sub> (10 minutes).

### 3.2.2 Acute application of Saracatinib reduces GluN2B pY1472 in adult WT hippocampal slices

I first established whether acute inhibition with Saracatinib reduces GluN2B pY1472 in adult mice. Following Kaufman et al, I incubated hippocampal slices from adult WT mice with 2  $\mu$ M Saracatinib or vehicle for 2 hrs. This concentration and timing previously reduced GluN2B pY1472 in hippocampal slices from young (3-4-week-old) WT mice (Kaufman et al 2015). It is unknown whether Saracatinib will be as effective in reducing GluN2B pY1472 in adult WT mice which express a lower GluN2B content than 3-4-week-old mice (Liu et al., 2004). This is relevant to this project as adult Line 102 mice that model AD pathology will be used for future experiments using Saracatinib, and therefore it is important to determine whether Saracatinib produces similar effects in adult mice.

To measure GluN2B pY1472 I performed Western blotting using specific antibodies against GluN2B, GluN2B pY1472 and  $\beta$ -tubulin and quantified immunoreactivity (Figure 3.2). As expected, I found a reduction in the proportion of GluN2B subunits phosphorylated at Y1472 in Saracatinib-treated slices compared to vehicle-treated slices (Figure 3.2. B; t-test:  $p=0.018$ , vehicle  $n=7$ , Saracatinib  $n=7$ ). This was not due to a reduction in overall GluN2B levels because I did not detect

a change in GluN2B immunoreactivity between Saracatinib and vehicle treated samples (Figure 3.2. C; t-test:  $p=0.105$ ).

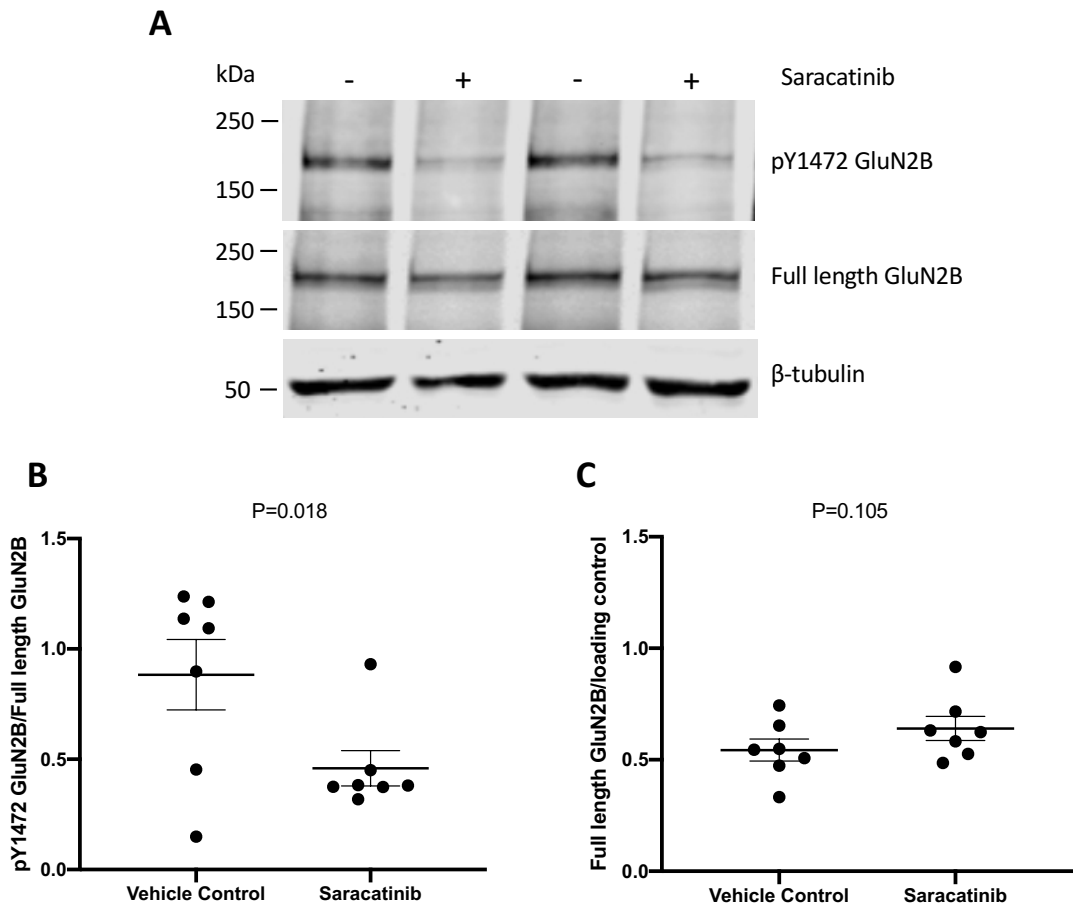


Figure 3.2 Saracatinib reduces GluN2B phosphorylation at Y1472 in WT adult hippocampal slices

**(A)** Sample blots of sliced hippocampal homogenate from WT mice treated with either 2  $\mu$ M Saracatinib or Vehicle control for 2 hrs. Blots were probed for pY1472 GluN2B, GluN2B and  $\beta$ -tubulin. **(B, C)** Quantification of the proportion of GluN2B subunits phosphorylated at Y1472 **(B)** and quantification of GluN2B/ $\beta$ -tubulin **(C)** in acute hippocampal slices following 2-hour incubation with 2  $\mu$ M Saracatinib or vehicle control. All data are presented as  $n$ =mouse, mean  $\pm$  SEM. Data were analysed using one-tailed, unpaired t-test.

These data show that acute inhibition of SFKs with Saracatinib significantly reduces GluN2B pY1472 after 2 hrs in hippocampal slices from adult WT mice. This agrees with findings from 3-4-

week-old mice and is indicative of Fyn inhibition since Y1472 is the primary residue of GluN2B phosphorylated by Fyn (Dunah et al., 2004; Nakazawa et al., 2001). Therefore, Saracatinib can be used to acutely inhibit SFKs to test whether this affects synaptic function and plasticity in the hippocampus of adult mice.

In addition to broad SFK inhibition by Saracatinib, I wanted to analyse the effect of Fyn inhibition in isolation. This would allow future experiments to determine the effects of Fyn inhibition on synaptic function and plasticity whilst leaving the activity of other SFKs unaltered. To do this, I utilised TAT-Fyn(39-57) which is a peptide based on the unique domain of Fyn that acts to outcompete the function of endogenous Fyn and prevents the localisation of Fyn to the NMDAR complex (see Figure 1.11). Transactivating transcriptional activator (TAT) is isolated from human immunodeficient virus-1 and permits translocation of the peptide across the cell membrane. TAT-Fyn(scram), which contains the same amino acids in a scrambled (scram) order, was used as a control. We hypothesised that TAT-Fyn(39-57) would inhibit Fyn kinase activity and therefore reduce GluN2B pY1472. To test this I followed (Yang et al., 2012) and incubated hippocampal slices from adult WT mice in aCSF containing 10  $\mu$ M TAT-Fyn(39-57) or TAT-Fyn(scram) for 2 hrs and performed western blotting and probes for GluN2B pY1472, GluN2B and  $\beta$ -tubulin.

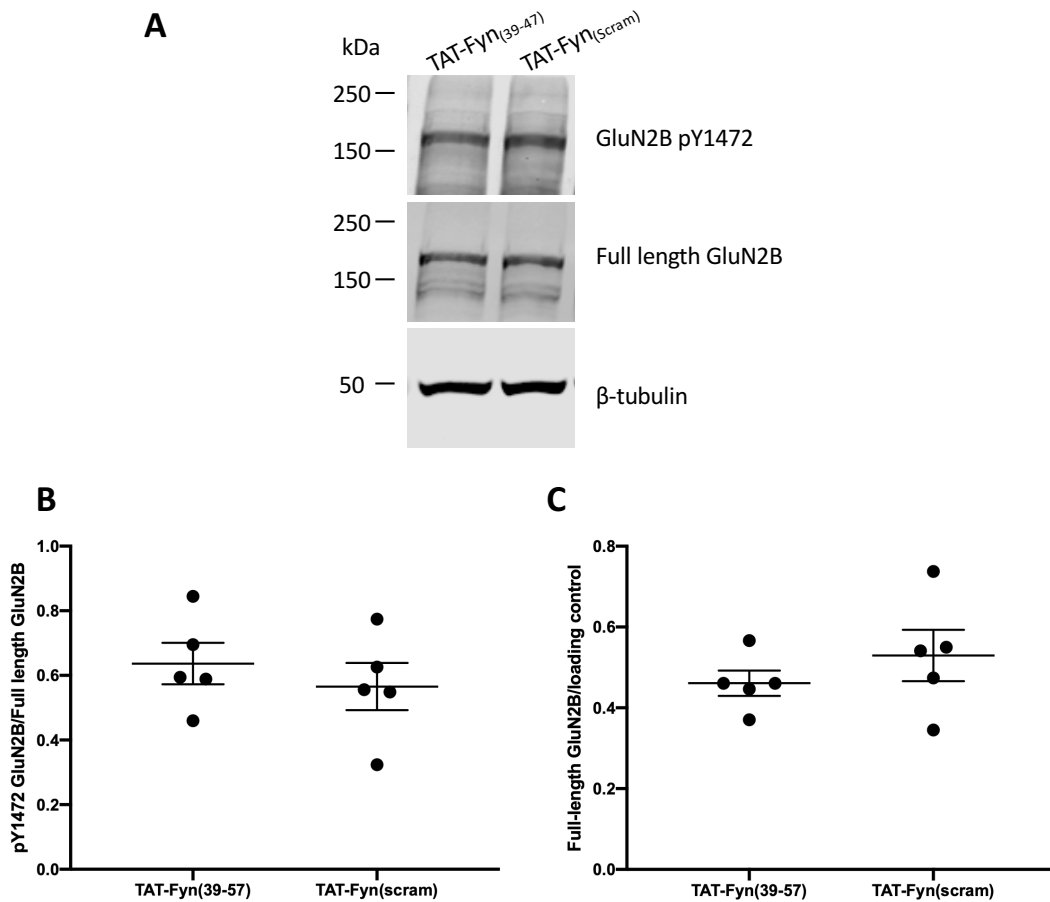


Figure 3.3 The level of GluN2B and pY1472 GluN2B in hippocampal slices from adult WT mice following acute application of TAT-Fyn(39-57) peptide inhibitor

**(A)** Sample blots of sliced hippocampal homogenate from adult WT mice incubated in 10  $\mu$ M TAT-Fyn<sub>(39-57)</sub> or TAT-Fyn<sub>(Scrambled)</sub> for 2 hours. Blots were probed for pY1472 GluN2B, GluN2B and  $\beta$ -tubulin. **(B,C)** Quantification of the proportion of GluN2B subunits phosphorylated at Y1472 **(B)** and of GluN2B/ $\beta$ -tubulin **(C)**. Data presented as N=slice, mean  $\pm$  SEM.

Using a paired t-test, I found that TAT-Fyn(39-57) had no significant effect on the proportion of GluN2B phosphorylated at Y1472 (Figure 3.3 B,  $p=0.267$ , TAT-Fyn(39-57)  $n=5$ , TAT-Fyn(Scram)  $n=5$ ) or of total GluN2B (Figure 3.3 C,  $p=0.461$ , TAT-Fyn(39-57)  $n=5$ , TAT-Fyn(Scram)  $n=5$ ). This suggests that TAT-Fyn(39-57) did not successfully inhibit Fyn in these slices. It is also possible that there was no significant Fyn activity to inhibit, since the control GluN2B pY1472/GluN2B ratio reported in these experiments (Figure 3.3) is smaller than those in Figure 3.2. Since I found no significant effect of TAT-Fyn(39-57), I was unable to test Fyn inhibition specifically on synaptic function and plasticity, and instead focused the remainder of my experiments on using Saracatinib.



### 3.2.3 Acute application of Saracatinib does not alter basal synaptic transmission in adult WT hippocampal slices

Since *Fyn*<sup>-/-</sup> show impaired LTP and spatial learning and memory, it is possible that inhibition of *Fyn* by Saracatinib could impair synaptic function in WT mice (Kojima et al., 1997). To investigate whether Saracatinib alters synaptic function, I performed field recordings at CA3-CA1 synapses in adult WT hippocampal slices that have been incubated with 2  $\mu$ M Saracatinib or vehicle for 2 hrs. Synaptic function was then assessed by measuring input-output (IO) and paired-pulse ratio (PPR) (Figure 3.4)

IO responses are a measure of fast synaptic transmission mediated principally by postsynaptic AMPARs. IO responses are obtained by increasing the stimulus intensity applied to the CA3 region and measuring the slope of the resulting fEPSP from the CA1 region at each stimulus amplitude. Analysis of IO responses showed a significant effect of stimulus amplitude but no effect upon treatment with Saracatinib compared to vehicle (*Figure 3.4. A, B; 2-way RM ANOVA: treatment*  $F_{1,179}=0.588$ ,  $p=0.453$ , *stimulation*  $F_{7,119}=74.95$ ,  $p<0.0001$ , *treatment x stimulation*  $F_{7,119}=0.289$ ,  $p=0.957$ , *Saracatinib*  $n=9$ , *vehicle control*  $n=10$ .) This shows that acute application of Saracatinib does not alter AMPAR contribution at CA3-CA1 synapses and therefore suggests that SFKs do not play a vital role in basal AMPAR regulation.

PPR allows the investigation of short-term (millisecond) modulation of synaptic strength. PPR responses are obtained by applying 2 rapidly evoked stimuli at increasing interstimulus interval (see Figure 2.5). PPR is then measured by dividing the amplitude of the second response by the slope of the first. Most excitatory synapses in the hippocampus, including CA3-CA1 synapses, show facilitation (PPF) at short interstimulus intervals (Bortolotto et al., 2011). I measured PPR at inter-pulse intervals of 10-640 ms (Figure 3.4. B). I extracted and analysed PPR data from the 40 ms inter-pulse interval because this interval causes robust facilitation with minimal interference from early depression and is therefore most likely to reveal any changes caused by Saracatinib (Stevens et al., 1995) (Thomson et al., 1999) (Figure 3.4. C). I was readily able to induce PPF in my slice preparations and this was not affected by Saracatinib (*Figure 3.4. B,C, p=0.253, Saracatinib*  $n=9$ , *vehicle*  $n=11$ ). This shows that acute application of Saracatinib does not alter this aspect of

presynaptic function in CA3-CA1 synapses from adult WT hippocampal slices, however whether longer-term SKF inhibition may reveal an effect is still to be determined.

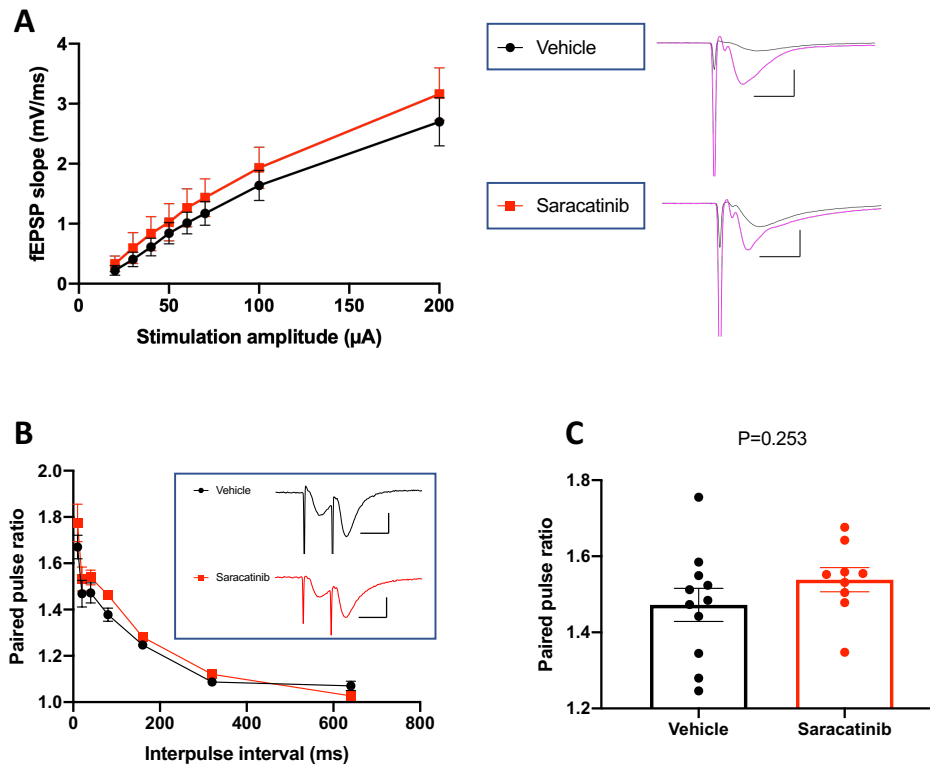


Figure 3.4 Acute application of Saracatinib does not alter basal synaptic transmission in WT adult hippocampal slices

**(A)** Input-output responses from WT hippocampal slices treated with 2  $\mu$ M Saracatinib (n=9) or vehicle control (n=10) for 2 hrs. Example traces showing the fEPSP in response to 40  $\mu$ A (black) and 200  $\mu$ A (magenta) stimulus input for Saracatinib and vehicle treated conditions. Scale bar calibration: 2 mV, 5 ms. Data analysed using a two-way RM ANOVA. **(B)** Paired pulse response from WT hippocampal slices treated with 2  $\mu$ M Saracatinib (n=9) or vehicle control (n=11) for 2 hrs. Example traces showing the fEPSP in response to a pair of pulses delivered with 40 ms interstimulus interval for Saracatinib and vehicle treated conditions. Scale bar calibration: 5 ms, 5 mV. Data analysed using a two-way RM ANOVA. **(C)** Quantification of paired pulse ratio at 40 ms inter-pulse interval. Data analysed using an unpaired two-tailed t-test. All data are represented as n=slice, mean  $\pm$  SEM.

### 3.2.4 Acute application of Saracatinib does not alter basal synaptic plasticity in adult WT hippocampal slices

Previous work suggests that SFK inhibition may reduce synaptic plasticity (Yang et al., 2012) (Grant et al., 1992) and therefore I aimed to determine whether acute inhibition by Saracatinib alters plasticity in CA3-CA1 circuits of adult WT mice. To do this I tested the ability of CA3-CA1 synapses to both strengthen (LTP) and weaken (LTD). To test synaptic strengthening I induced LTP using a TBS induction protocol in hippocampal slices from WT mice that had been incubated in either 2  $\mu$ M Saracatinib or vehicle for 2 hrs (Figure 3.5) Similar levels of TBS-induced LTP were observed between Saracatinib and vehicle treated slices (Figure 3.5 . C; *t*-test:  $p=0.840$ , Saracatinib  $n=11$ , vehicle  $n=17$ ). This means that acute incubation with Saracatinib does not affect CA3-CA1 LTP in the hippocampus of adult WT mice.

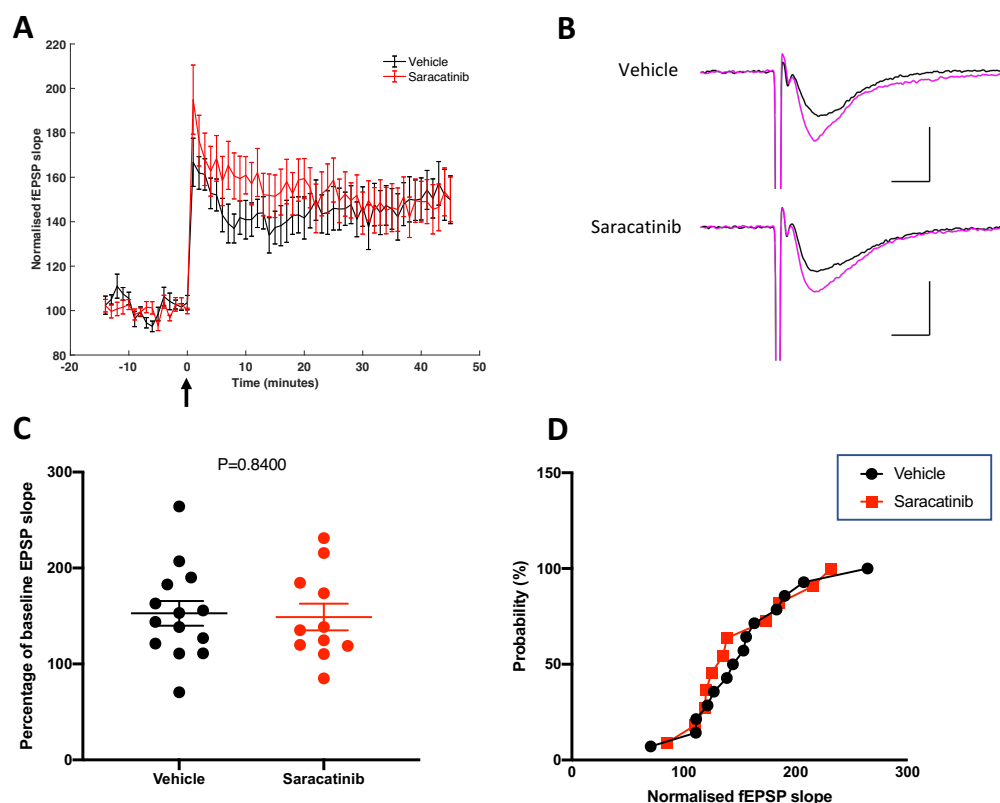


Figure 3.5 Acute application of Saracatinib does not alter LTP in WT adult hippocampal slices

**(A)** TBS-induced LTP (arrowhead) in WT hippocampal slices treated with 2  $\mu$ M Saracatinib ( $n=11$ ) or vehicle control ( $n=17$ ) for 2 hrs. Experiments recorded in submerged style chambers **(B)** Example LTP traces showing the fEPSP before (black) and

after LTP induction (magenta) for Saracatinib and control treated slices. Scale bar calibration: 10 ms, 0.5 mV. **(C,D)** Percentage change in the fEPSP slope in the final 5 minutes after LTP-induction represented in a cumulative frequency plot **(C)** and bar graph **(D)**. Data are represented as n=slice, mean  $\pm$  SEM. Data analysed using unpaired, two-tailed t-test.

To investigate synaptic weakening, I induced LTD using ,5-dihydroxyphenyl-glycine (DHPG). DHPG-LTD is NMDAR independent and induces LTD by activating mGluR1 receptors to reduce postsynaptic AMPAR expression (Xiao et al., 2001). To determine whether Saracatinib alters the ability for synapses to weaken, I induced DHPG-LTD in WT hippocampal slices following incubation with Saracatinib or vehicle. I found that DHPG induced LTD in both vehicle and Saracatinib treated slices (Figure 3.6) and there was no significant difference between the two groups (*Figure 3.6. C, t-test:  $p=0.881$ , vehicle  $n=11$ , Saracatinib  $n=8$* ). This suggests that acute inhibition of SFKs does not affect the ability of CA3-CA1 synapses to weaken in slices from WT mice.

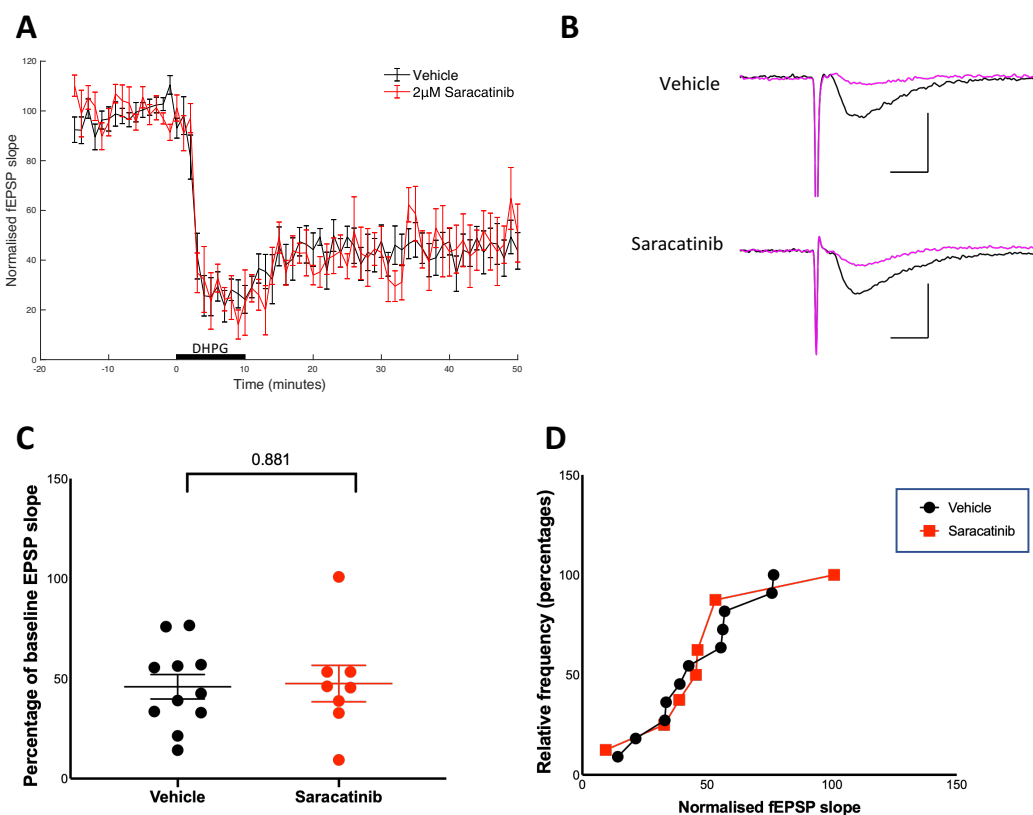


Figure 3.6 Acute application of Saracatinib does not alter DHPG-induced LTD in WT adult hippocampal slices

**(A)** Application of 100  $\mu$ M DHPG for 10 minutes to induce LTD in hippocampal slices from WT mice incubated in 2  $\mu$ M Saracatinib or vehicle control for 2 hrs. Experiments recorded in submerged style chambers. **(B)** Example traces showing the fEPSP before (black) and after (magenta) application of DHPG. Scale bar calibration: 10 ms, 0.5 mV. **(C,D)** Percentage change in the fEPSP slope average from the last 10 minutes of the recording represented as a bar graph **(C)** and cumulative frequency plot **(D)**. Data represented as n=slice, mean  $\pm$  SEM and analysed using an unpaired, two-tailed t-test.

Together, Figure 3.5 and Figure 3.6 demonstrate that acute application of Saracatinib does not affect two key forms of plasticity in CA3-CA1 synapses in the normally-developed adult mouse brain. Following on from this, I wanted to investigate whether my findings are sustained when SFKs are inhibited chronically (i.e. administration of Saracatinib *in vivo*).

### 3.2.5 In vivo administration of Saracatinib in adult WT mice

My primary aim is to measure synaptic function and plasticity following chronic Saracatinib administration in adult WT mice, however, I first needed to establish whether I can replicate previous findings showing that *in vivo* administration of Saracatinib in adult mice successfully inhibits SFKs in the brain (Kaufman et al., 2015). Therefore, I completed a short pilot study to administer Saracatinib to 13-week-old WT mice. Following Kaufman and colleagues, I administered two doses; the clinically relevant 5mg/kg/day dose and a higher dosage of 20mg/kg/day and compared these to vehicle treated mice for 3 days. At the end of the experiment the mice were sacrificed, and I collected the hippocampus and portion of the frontal cortex (described in Section 2.5.1). Samples were analysed using Western blotting and then probed for GluN2B pY1472, GluN2B and  $\beta$ -tubulin (Figure 3.7).

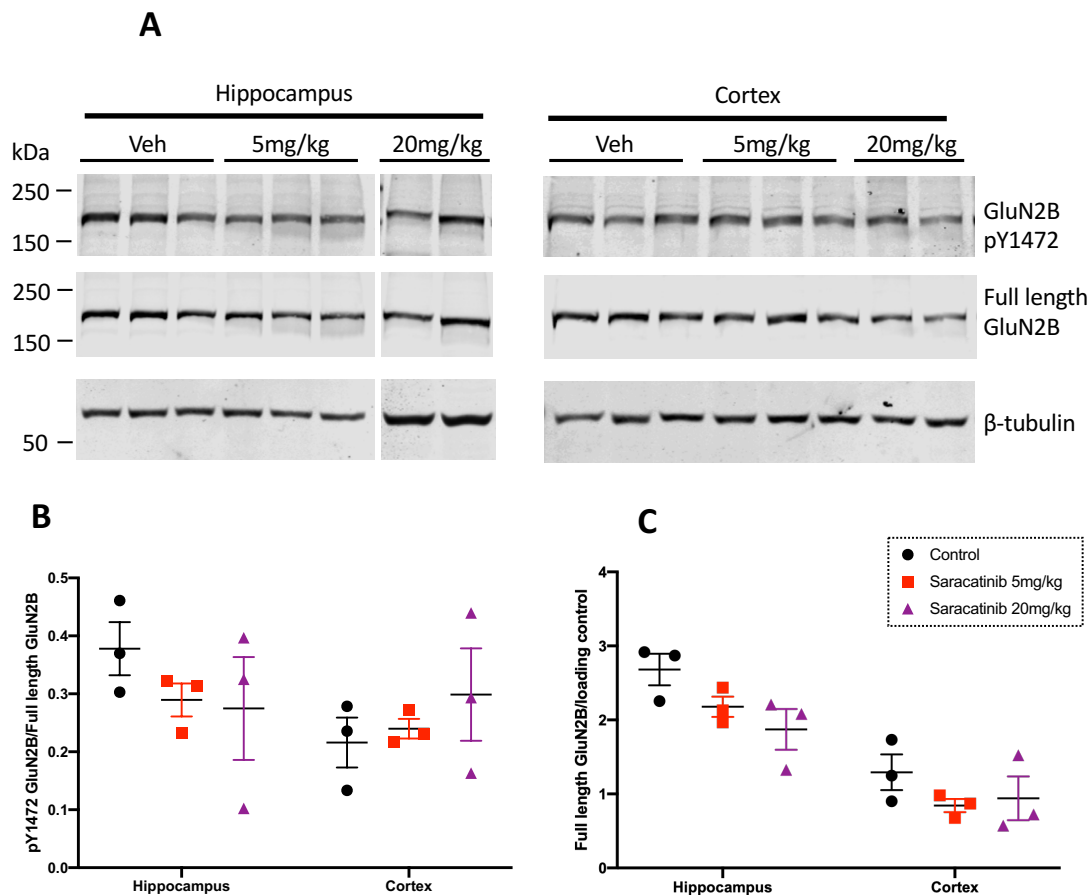


Figure 3.7 The level of GluN2B and pY1472 GluN2B in the hippocampus and cortex from adult WT mice following *in vivo* treatment with 5mg/kg/day or 20mg/kg/day Saracatinib for 3 days

**(A)** Sample blots of hippocampal and cortical homogenate from adult (13-week-old) WT mice following 3 days of administration of 5mg/kg/day or 20mg/kg/day Saracatinib for 3 days. Blots were probed for pY1472 GluN2B, GluN2B and  $\beta$ -tubulin. **(B,C)** Quantification of the proportion of GluN2B subunits phosphorylated at Y1472 **(B)** and of GluN2B/ $\beta$ -tubulin **(C)**. Data presented as N=mouse, mean  $\pm$  SEM. The data were analysed using a two-way ANOVA followed by Tukey's multiple comparisons.

Following my acute Saracatinib incubation experiments, I analysed the proportion of GluN2B subunits phosphorylated at Y1472 and the total level of GluN2B following Saracatinib administration *in vivo*. I noticed trend for a decrease in the proportion of GluN2B phosphorylated at Y1472 in the hippocampus, but not the cortex, of 5mg/kg/day Saracatinib treated mice compared to vehicle (Figure 3.7 B). Unlike the 5mg/kg/day dose, I found a high variability in the proportion of GluN2B phosphorylated at Y1472 at the 20mg/kg/day dose.

Using a two-way ANOVA, I analysed the ratio of GluN2B pY1472 to GluN2B which revealed no significant effect of Saracatinib treatment ( $F(2,12)=0.1$ ,  $p=0.846$ , control  $n=6$ , 5mg/kg/day  $n=6$ , 20mg/kg/day  $n=6$ ) or brain region ( $F(2,12)=1.8$ ,  $p=0.202$  hippocampus  $n=9$ , cortex  $n=9$ ) (Figure 3.7 B). Therefore, even though a subtle difference was seen in the hippocampus of the 5mg/kg/day group, it is not statically significant compared to vehicle.

The level of GluN2B showed little variability between groups and I consistently saw a trend for a decrease in the level of GluN2B in Saracatinib treated mice compared to controls, and it seemed as though it could be dose-dependent in the hippocampus (Figure 3.7 C). I analysed the data using a two-way ANOVA which revealed that the level of GluN2B was significantly altered by Saracatinib ( $F(2,12)=3.92$ ,  $p=0.049$ , control  $n=6$ , 5mg/kg/day  $n=6$ , 20mg/kg/day  $n=6$ ,) and brain region ( $F(1,12)=45.51$ ,  $p<0.0001$  hippocampus  $n=9$ , cortex  $n=9$ ,) although, there was no interaction between brain region and treatment ( $F(2,12)=0.637$ ,  $p=0.546$ ) (Figure 3.7 C). However, post hoc analysis using Tukey's multiple comparisons showed no significant difference in the level of GluN2B in the hippocampus between vehicle and Saracatinib treated mice at either the low ( $p=0.609$ , control hippocampus  $n=3$ , 5mg/kg/day hippocampus  $n=3$ ) or high ( $p=0.174$ , control hippocampus  $n=3$ , 20mg/kg/day hippocampus  $n=3$ ) Saracatinib dose. I also saw no significant difference in the cortex between vehicle and Saracatinib treated mice at either the low ( $p=0.704$ , control cortex  $n=3$ , 5mg/kg/day cortex  $n=3$ ) or high ( $p=0.861$ , control cortex  $n=3$ , 20mg/kg/day cortex  $n=3$ ) Saracatinib dose. Therefore, this pilot study suggests that the production or degradation of GluN2B protein in the hippocampus and cortex is not altered by 3-days of Saracatinib administration *in vivo*. My data also show that there is a significantly higher basal level of GluN2B in hippocampus compared to the cortex in adult WT mice (Figure 3.7 C);  $p=0.008$ , control hippocampus  $n=3$ , control cortex  $n=3$ ). This explains why the ANOVA reported a significant effect of Saracatinib, however the significance is attributed to treatment across brain regions rather than treatment within the same brain region.

The lack of significance in the data could be due to a small sample size. I was particularly interested in the 5mg/kg/day dose because the data showed less variability than the 20mg/kg/day dose and also showed a trend (yet non-significant) to decrease with Saracatinib in both the level GluN2B and the ratio of GluN2B to GluN2B pY1472. I wanted to determine whether this trend would persist at a higher sample size and therefore I repeated the experiment

comparing 5mg/kg/day to vehicle. For this repeated experiment I used slightly older (22-week-old) WT mice, however, I did not expect this to alter the effect of Saracatinib. Information from this age group may also be more relevant for any potential future work to repeat this experiment in later-stage Line 102 mice.

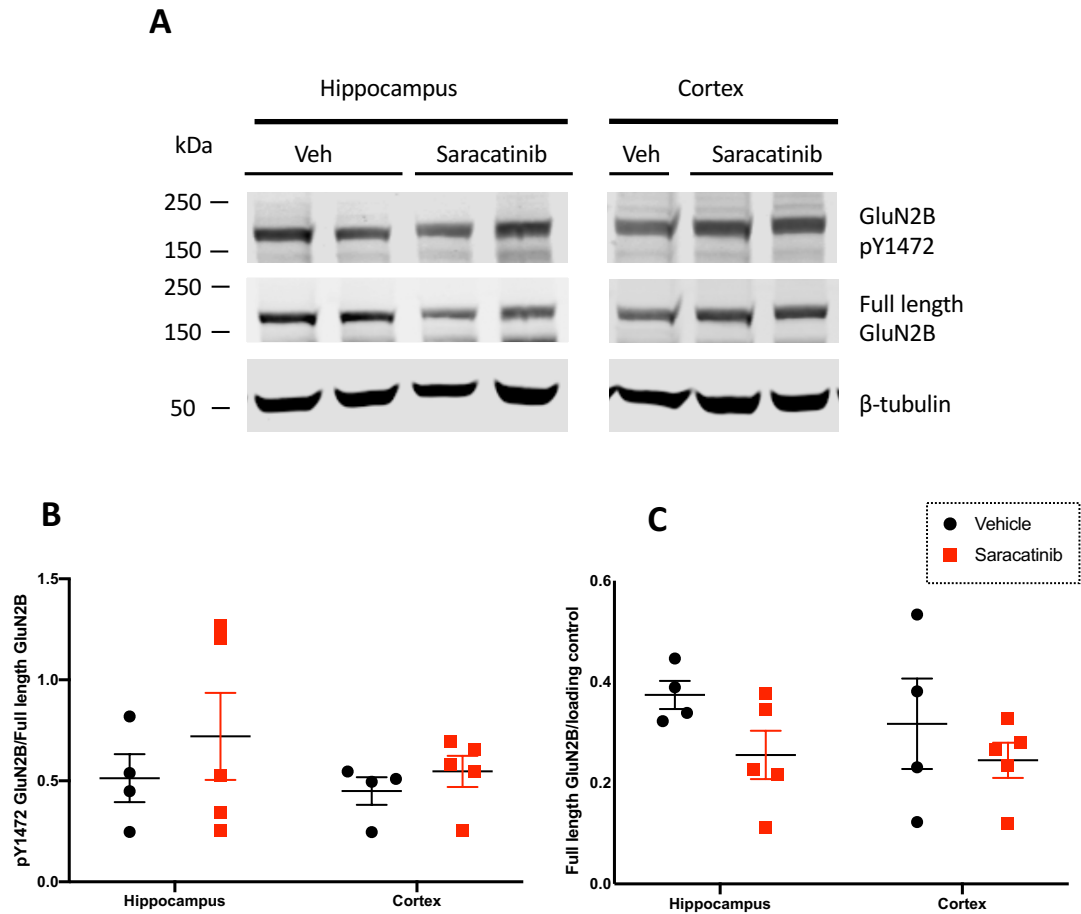


Figure 3.8 The level of GluN2B and pY1472 GluN2B in the hippocampus and cortex from adult WT mice following in vivo treatment with 5mg/kg/day Saracatinib for 3 days

**(A)** Sample blots of hippocampal and cortical homogenate from adult (22-weeks-old) WT mice following 3 days of administration of 5mg/kg/day Saracatinib for 3 days. Blots were probed for pY1472 GluN2B, GluN2B and  $\beta$ -tubulin. **(B,C)** Quantification of the proportion of GluN2B subunits phosphorylated at Y1472 **(B)** and of GluN2B/ $\beta$ -tubulin **(C)**. Data presented as N=mouse, mean +/- SEM. The data were analysed using a two-way ANOVA.

The data were much more variable than in the first experimental repeat and analysis of the proportion of GluN2B subunits phosphorylated at Y1472 using a two-way ANOVA showed that



there was no effect of Saracatinib treatment ( $F(1, 14)=1.129$ ,  $p=0.306$ , control  $n=8$ , 5mg/day/day  $n=10$ ) or brain region ( $F(1, 14)=0.688$ ,  $p=0.421$ , hippocampus  $n=9$ , cortex  $n=9$ ) (Figure 3.8, B).

Analysis of the level of GluN2B using a two-way ANOVA also showed no effect of Saracatinib treatment ( $F(1, 14)=3.24$ ,  $p=0.094$ , control  $n=8$ , 5mg/day/day  $n=10$ ) or brain region ( $F(1, 14)=0.408$ ,  $p=0.533$ , hippocampus  $n=9$ , cortex  $n=9$ ) (Figure 3.8, C). Overall, neither experimental repeats revealed a significant effect of Saracatinib administration on the level of GluN2B pY1472 or GluN2B in the hippocampus or cortex of WT mice *in vivo*.

### 3.3 Discussion

In this Chapter I set out to determine whether Saracatinib reduces GluN2B pY1472 in adult WT mice (both in slices and *in vivo*) and whether acute application of Saracatinib affects synaptic function and plasticity of CA3-CA1 synapses in hippocampal slices from WT mice. First, I applied Saracatinib to hippocampal slices from adult WT mice and, using Western blotting, showed that this significantly decreases GluN2B pY1472, suggesting successful Fyn inhibition (Figure 3.2).

In order to understand whether Saracatinib alters synaptic function and plasticity, I performed electrophysiological field recordings to assess synaptic function and plasticity within the hippocampal CA3-CA1 pathway of adult WT mice. I showed that acute application of Saracatinib does not alter IO responses or PPR, suggesting that SFK inhibition does not alter baseline synaptic transmission acutely (Figure 3.4 A, B). I also showed that TBS-induced LTP and DHPG-induced LTD are not affected by acute Saracatinib application, suggesting that acute SFK inhibition also does not alter synaptic plasticity at CA3-CA1 synapses. Finally, I completed a short pilot study to determine whether administration of Saracatinib *in vivo* would produce similar effects seen in my slice experiments, however I detected no significant effect of Saracatinib administration by oral gavage for 3 days (Figure 3.7 and Figure 3.8). The findings in this chapter show that acute Saracatinib application to slices significantly reduces GluN2B pY1472 but does not alter basal synaptic transmission or two key forms of synaptic plasticity in CA3-CA1 synapses. Further work is required to optimise *in vivo* administration in order to test whether these readouts are altered following longer-term Saracatinib application.

### **3.3.1 Acute Saracatinib application reduces GluN2B phosphorylation**

Reduced GluN2B pY1472 in slices treated with Saracatinib is consistent with previous experiments using 3-4-week-old WT mice (Kaufman et al., 2015) and suggests that acute Saracatinib treatment successfully inhibits Fyn activity in slices from adult mice. The synthesis of most proteins takes between 20 seconds and several minutes (Alberts et al., 2001) and calpain-mediated degradation of GluN2B is detected in rodent hippocampal slices after 30 mins of NMDA application (Hawasli et al., 2014). Therefore, it is possible that production and degradation of GluN2B could occur within the 2hr Saracatinib incubation period, which could underline changes in GluN2B pY1472.

However, my results showed that there is no statistically significant difference in the level of GluN2B in vehicle and Saracatinib treated slices. This suggests that acute Saracatinib exposure does not affect the production or degradation of GluN2B subunits and that the decrease in GluN2B pY1472 is due to a decrease in phosphorylation and not changes in protein expression.

Although my results detected no significant difference in the level of GluN2B following Saracatinib application, the Western blotting technique does not distinguish between the localisation of GluN2B subunits, for example synaptic versus extrasynaptic or cell-surface membrane versus internalised. It is possible that Saracatinib could alter this subcellular distribution and/or plasma membrane association of GluN2B-NMDARs. This could alter the number of synaptic NMDARs available for signalling and negatively affect normal synaptic function and plasticity.

The Y1472 residue of GluN2B is required for clathrin-mediated endocytosis of GluN2B-containing NMDARs. Phosphorylation at Y1472 prevents clathrin-mediated endocytosis and therefore inhibits the internalisation of GluN2B-containing NMDARs (See Section 1.10.1). Following this rationale, we hypothesised that decreased GluN2B pY1472 by Saracatinib will permit clathrin-mediated endocytosis and thereby decrease the number of synaptic GluN2B-containing NMDARs. However, since the majority of endocytosed GluN2B-containing NMDARs enter recycling endosomes, this means that they will not be degraded and will therefore still be detected by the anti-GluN2B antibody. Future experiments could use WT slices incubated in Saracatinib or vehicle and utilise surface biotinylation assays to quantitatively measure surface versus total GluN2B protein. Alternatively, patch clamp electrophysiology could be used to record synaptic NMDAR and the GluN2B-specific inhibitor, Ro 25-6981, would provide information regarding whether the contribution of synaptic GluN2B-containing NMDARs specifically is altered by Saracatinib.

NMDARs can laterally diffuse between synaptic and extrasynaptic sites (Tovar et al., 2002). The Saracatinib-induced reduction of GluN2B pY1472 could alter the synaptic and extrasynaptic expression levels of GluN2B-containing NMDARs. The physiological role of extrasynaptic NMDARs is not fully understood, but their activation following glutamate spillover may decrease synaptic plasticity by promoting cell death (Hardingham et al., 2002). This may be less relevant in a WT context where synapses show controlled glutamate release and reuptake, however, activation of extrasynaptic NMDARs has been implicated in many neurodegenerative diseases, including AD (reviewed by Hardingham et al., 2010). Whole-cell recordings in WT hippocampal slices showed that A $\beta$  enhances extrasynaptic GluN2B-containing NMDAR currents and inhibits HFS-induced LTP in CA3-CA1 synapses (Li et al., 2011). The impaired LTP was rescued by decreasing extracellular glutamate levels using glutamic-pyruvic transaminase or with a GluN2B-selective antagonist, Ro-256981 or ifenprodil, suggesting that A $\beta$  impairs LTP by increased activation of GluN2B-containing NMDARs. This is supported by other studies showing that applying TBOA to induce glutamate spillover reduced HFS-induced LTP in CA3-CA1 synapses of hippocampal slices (Delgado et al., 2018). However, this was prevented by blocking GluN2B-containing NMDARs using ifenprodil (Delgado et al., 2018). Therefore, it is possible that expression of A $\beta$  in Line 102 could increase NMDAR currents carried by extrasynaptic GluN2B-containing NMDARs and this could underlie the impaired LTP reported in this thesis, however, this has not been tested. To investigate whether extrasynaptic GluN2B-containing NMDARs mediate the LTP impairment by A $\beta$ , the authors inhibited p38 mitogen-activated protein kinase (MAPK), which is activated following stimulation of extrasynaptic GluN2B-containing NMDARs (Waxman et al., 2005). Inhibition of p38 MAPK rescued the LTP deficit induced by A $\beta$ , suggesting that A $\beta$  impairs LTP by activating extrasynaptic GluN2B-containing NMDARs and engaging their downstream signalling pathways (Li et al., 2011).

It is unknown whether SFKs regulate the balance of GluN2B expression at synaptic and extrasynaptic sites. Whether Saracatinib alters synaptic localisation of NMDARs could be investigated using synaptosomal preparations to separate synaptic and extrasynaptic compartments in hippocampal slices. The level of GluN2B protein in each compartment can be quantified using Western blotting and probing for GluN2B. Alternatively, an antibody which targets an extracellular portion of GluN2B could be used to stain plasma membrane expressed GluN2B subunits which could then be stained and quantified as synaptic or extrasynaptic based on location. Finally, another approach could use patch-clamp electrophysiology whereby synaptic NMDAR are blocked using a use-dependent, irreversible NMDAR antagonist (for example, MK-801). Extrasynaptic NMDAR currents can then be recorded in isolation to determine whether Saracatinib alters extrasynaptic or synaptic NMDAR-mediated currents.

Hypothetically, if SFKs regulate synaptic and extrasynaptic GluN2B-containing NMDAR expression, inhibition of SFKs with Saracatinib could change the synaptic localisation of GluN2B-containing NMDARs and alter the vulnerability of synapses to A $\beta$ . For example, if Saracatinib increases the expression of GluN2B-containing NMDARs at extrasynaptic sites, this could make synapses more vulnerable to A $\beta$  and exacerbate LTP impairments. Conversely, if the balance shifts towards more GluN2B-containing NMDARs at synaptic sites, this could provide a protective effect against A $\beta$ . Under physiological conditions where glutamate release and uptake are highly controlled, changes in extrasynaptic NMDAR expression may have little to no effect on synaptic plasticity. This could explain why Saracatinib did not alter synaptic plasticity in WT slices. However, an effect may be revealed in the presence of A $\beta$  in Line 102 mice, which will be investigated later in Chapter 5.

### **3.3.2 Acute Saracatinib application does not alter basal synaptic transmission**

Even though acute Saracatinib application caused a significant decrease in GluN2B pY1472 in WT hippocampal slices, the electrophysiological data presented here show for the first time that this does not alter IO responses at CA3-CA1 synapses (Figure 3.4 A, B). This suggests that acute SFK inhibition causes no detectable change in postsynaptic cell-surface expression of AMPARs. Lyn is a member of the SFKs and phosphorylates the GluR2 subunit of AMPARs at Y876. This is relevant to the experiments in this chapter because Saracatinib inhibits Lyn with an IC<sub>50</sub> of 5 nM. Phosphorylation at this residue disrupts the interaction of GluR2 with GRIP1/2 scaffold proteins and allows internalisation of GluR2-containing AMPARs (Hayashi et al., 2004). Therefore, the addition of 2  $\mu$ M Saracatinib will inhibit Lyn and, based on the study by Hayashi and colleagues, may decrease GluR2 Y876 phosphorylation and reduce GluR2-AMPA internalisation. I have not tested phosphorylation levels at this site, however, my IO data shows no significant difference between control and vehicle treated slices, which suggests that 2 hrs of SFK inhibition by Saracatinib causes no detectable change in postsynaptic cell-surface expression of AMPARs, irrespective of any changes in GluR2 Y876 phosphorylation. I planned to use TAT-Fyn(39-57) inhibitor peptide to avoid such confounds of inhibiting other SFK members and to inhibit Fyn in isolation. However, I saw no significant effect of TAT-Fyn(39-57) on GluN2B pY1472 compared to TAT-Fyn(scram) control peptide after 2 hr incubation in aCSF (Figure 3.3). In this experiment I followed previous findings by (Yang et al., 2012) which showed that 10  $\mu$ M TAT-Fyn(39-57) prevented SKF81297-mediated increase in GluN2B pY1472 in WT hippocampal slices. The authors

did not show the effect of TAT-Fyn(39-57) on basal levels of GluN2B pY1472 levels (without prior treatment) so it is possible that the effect size on basal GluN2B pY1472 is too small to be detected within the noise. Yang et al. also used slices from young (4-6 week-old) mice and so it is possible that the peptide does not have the same effect when applied to slices from adult mice which express a lower GluN2B content than young mice (Liu et al., 2004). Finally, it is possible that the drug may not be able to effectively penetrate through the slice. This could be overcome by applying the drug to cell cultures or by intracellular application (i.e. if the peptide is included in the intracellular solution of the patch pipette). However, for the purpose of my experiments using field recordings in slices, I focussed my future experiments on Saracatinib.

As well as measuring IO responses, it was important to measure PPR following Saracatinib treatment because SFKs are expressed both pre- and post synaptically (Kalia et al., 2003) (Figure 3.4 C, D). However, there is very limited research into the function of SFKs at the pre-synapse and so the function of SFKs at this site remains unknown. My data showed that PPR was unaffected by acute Saracatinib application, suggesting that acute SFK inhibition does not alter presynaptic function at CA3-CA1 synapses.

### **3.3.3 Acute Saracatinib application does not alter synaptic plasticity**

It was previously unknown whether Saracatinib would alter hippocampal synaptic plasticity in WT mice. Here I show that there is no effect when Saracatinib is applied acutely in CA3-CA1 synapses. This is true for two key forms of plasticity in CA3-CA1 synapses: LTP (Figure 3.5) and LTD (Figure 3.6). LTP in CA3-CA1 synapses is well characterised and is expressed postsynaptically by increasing AMPAR contribution and requires NMDAR activation (discussed in Section 1.4). However, it would be interesting to see if Saracatinib affects plasticity in other hippocampal synapses where LTP is presynaptically driven and is NMDAR independent, for example the mossy fiber pathway (dentate gyrus-CA3) (reviewed by Nicoll & Schmitz, 2005).

My findings complement prior behavioural studies showing no changes in learning and memory after 3-5-weeks of Saracatinib administration in control mice (Kaufman et al., 2015). It is also in line with data from GluN2B Y1472F knock-in mice that show no deficits in hippocampal LTP, further supporting the rationale that phosphorylation of GluN2B at Y1472 is not required for hippocampal CA3-CA1 synaptic plasticity (Nakazawa et al., 2006). However, *Fyn*<sup>-/-</sup> mice show

impaired LTP which suggests a decrease in plasticity without Fyn and disagrees with my findings (Grant et al., 1992). However, this could highlight the key differences between inhibition of Fyn during development versus inhibition of Fyn in the adult brain, or the difference between chronic and acute Fyn inhibition.

### 3.3.4 *In vivo* administration of Saracatinib

It is possible that chronic inhibition of Fyn may expose plasticity deficits. I aimed to test this, however I was unable to replicate previous findings (Kaufman et al., 2015) and saw no significant effect of Saracatinib administration by oral gavage for 3 days (Figure 3.7 and Figure 3.8). Kaufman and colleagues showed that administration of 5mg/kg/day Saracatinib by oral gavage for 3 days resulted in successful BBB penetration and an average of 50 nM Saracatinib was detected in the CSF after 1 hour of the final dose (Kaufman et al., 2015). The Saracatinib used in their study was prepared as the salt form (Saracatinib difumarate). I was unable to source the same Saracatinib formulation and instead used a free base form of Saracatinib. I used the same vehicle (0.5% w/v HPMC/0.1% w/v Polysorbate 80) as Kaufman and colleagues, however I first had to dissolve the Saracatinib in DMSO due to decreased solubility of the free base form. This is the same Saracatinib formulation that I have used in slice experiments which consistently showed a robust decrease in GluN2B pY1472 (Figure 3.2 and Figure 4.4), therefore I am confident that this formulation inhibits SFKs effectively. It is possible that the formulation I used did not produce the same effects *in vivo* because of reduced blood-brain-barrier (BBB) penetration. Future work is required to validate Saracatinib administration *in vivo* in our lab. For example, CSF sampling to determine whether the free-base Saracatinib effectively crosses the BBB in mice, or generation of Saracatinib difumarate to mirror experiments by Kaufman and colleagues. These validation steps are vital before testing effect of the drug on synaptic function and plasticity. Alternatively, low statistical power due to the small number of animals used in the experiments could explain why an effect of Saracatinib was not detected. Findings from both experiments shown in Figure 3.7 and Figure 3.8 could not be grouped as the samples were analysed in separate blots and an internal control was not used. This means the arbitrary units could not be normalised and so the data were analysed separately (described in Methods Section 2.5.6).

### 3.3.5 Conclusions

In this Chapter, I show that acute application of Saracatinib reduces GluN2B pY1472 in adult WT hippocampal slices, and I show for the first time that this does not impact synaptic function and plasticity in CA3-CA1 synapses. This suggests that decreasing Fyn, and other SFK, activity and GluN2B pY1472 does not impact basal synaptic transmission or hippocampal synaptic plasticity within 2 hrs, both in terms of potentiating and depressing synapses. This is an important step that supports the potential future use of Saracatinib (or other potential future SFK inhibitors) as a treatment for AD because it doesn't affect basic functional properties of CA3-CA1 circuits in the hippocampus. However, more research is required to see if this is upheld when Saracatinib is administered chronically. The results from this Chapter added confidence to my subsequent experiments where I test whether acute Saracatinib incubation can rescue synaptic impairments in the Line 102 mouse model of AD.





## Chapter 4 GluN2B phosphorylation in a mouse model of early Alzheimer's Disease

Evidence from human post-mortem tissue, cell culture and AD mouse models suggests increased Fyn activity in AD. Human post-mortem tissue from the inferior temporal gyrus of individuals with moderately-severe AD shows an increase in Fyn phosphorylation at the site required for Fyn activation (pY420), suggesting increased Fyn activity in AD (Larson et al., 2012). Increased Fyn phosphorylation at the activation site is also enhanced in WT cortical neurons following application of A $\beta$  (synthetic or derived from AD brains) (Um et al., 2012)(Larson et al., 2012). Finally, enhanced Fyn activity is inferred in two AD mouse models via increased phosphorylation of direct Fyn targets. 4-month-old APP23 mice show increased GluN2B pY1472, and 11-12-month old APP/PS1 mice show increased Pyk2 pY402 (Ittner et al., 2010) (Kaufman et al., 2015).

The level of active Fyn in the inferior temporal gyrus of individuals with MCI showed a non-significant trend for increasing. The lack of significance could be due to variation within the cohort because not all individuals with MCI progress to AD (Mitchell et al., 2008). The level of active Fyn or phosphorylation of Fyn targets has not been reported in mice that model the earlier stages of AD. 4-month-old APP23 mice and 11-12-month old APP/PS1 mice already demonstrate severe spatial memory defects in the MWM (Serneels et al., 2009)(Van Dam et al., 2003), and APP/PS1 also show synapse loss and plaques deposition (Bittner et al., 2012). Therefore, the findings from these mice infer increased Fyn activity in later stage AD, and Fyn activity earlier in AD remains unknown.

Saracatinib did not slow the rate of cognitive decline when tested on a cohort with mild-moderate AD (Van Dyck et al., 2019). The lack of effect could be because the group may have progressed too far in AD pathology for Saracatinib to be beneficial. Therefore, it is important to test whether the level of active Fyn or phosphorylation state of Fyn targets is increased earlier in AD and, if so, whether reducing this with Saracatinib has a beneficial effect on early deficits in AD, such as synaptic dysfunction.

## Chapter 4

To address this, I used Line 102 mice to model early AD after a short period (3-16 weeks) of A $\beta$  accumulation and measured GluN2B pY1472 to infer Fyn activity. I tested two time points in this model: when synaptic dysfunction first arises (3 weeks) and later when long-term memory impairments arise and basal synaptic transmission is impaired (12-16 weeks) (Sri et al., 2019). Findings from this Chapter will form the foundations for future experiments in this project where I test whether Saracatinib can rescue early synaptic dysfunction.

### 4.1 Chapter aims

I set out to determine whether Fyn activity is increased in a mouse model of early AD, and if so, whether the increase can be rescued by Saracatinib. To address this, my aims are:

1. To compare the level of GluN2B Y1472 phosphorylation in Line 102 mice when synaptic plasticity impairments first arise and later after when basal synaptic transmission is compromised.
2. To determine whether any increases in GluN2B Y1472 phosphorylation can be rescued by acute Saracatinib application.

### 4.2 Results

#### 4.2.1 GluN2B Y1742 phosphorylation is increased after 3 weeks, but not 12 or 16 weeks, off dox in adult onset Line 102 mice

I measured the phosphorylation level of a Fyn target, GluN2B pY1472, in Line 102 mice after 3-weeks of APP<sub>Swe/Ind</sub> expression (or weeks off dox) when synaptic dysfunction first arises, and later after 12-16 weeks off dox when long-term memory impairments arise (Sri et al., 2019). To do this I collected the brains from Line 102 mice following 3, 12 and 16 weeks off dox and analysed the samples using Western blotting and probed for GluN2B, GluN2B pY1472 and  $\beta$ -tubulin (Figure 4.1, Figure 4.2 & Figure 4.3).

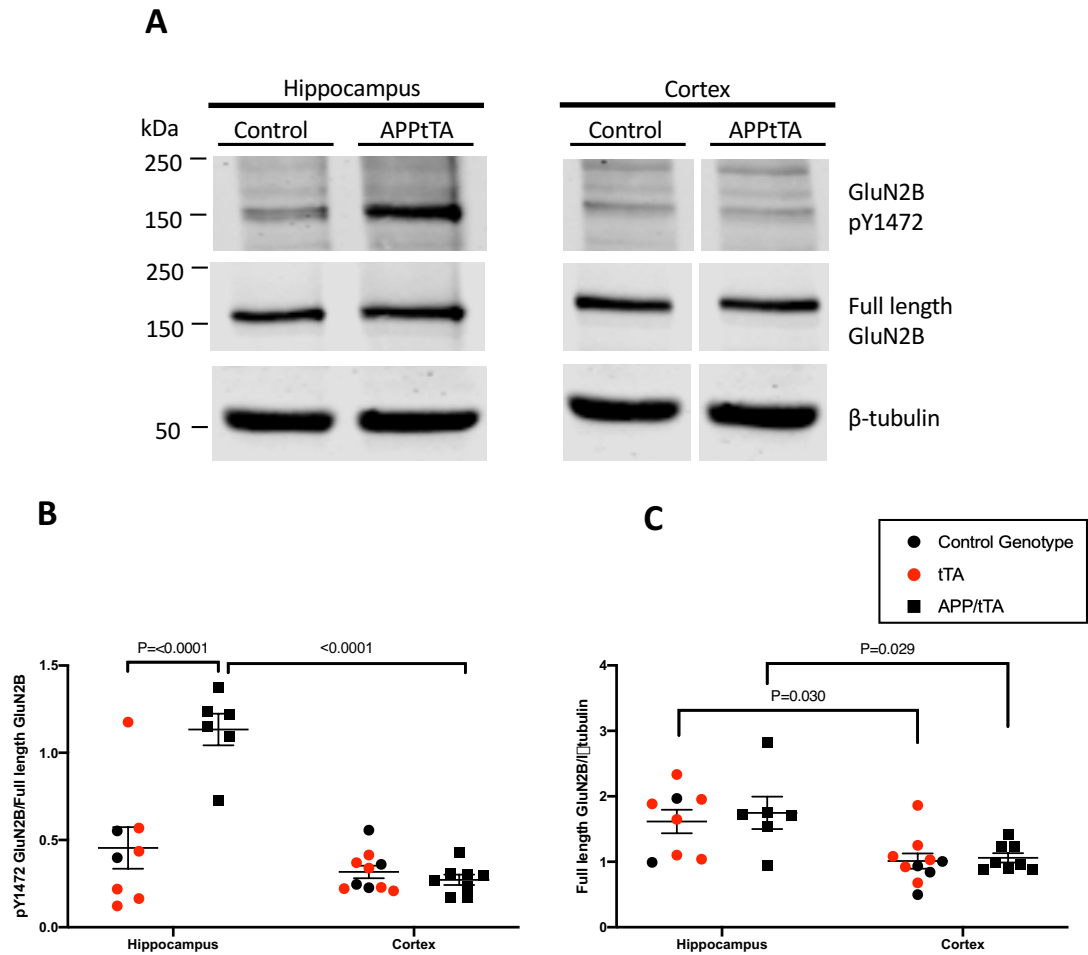


Figure 4.1 The level of GluN2B and pY1472 GluN2B in the hippocampus and cortex of Line 102 mice after 3 weeks of Dox removal.

**(A)** Sample blots of freshly-frozen hippocampal and cortical homogenate from Line 102 APPtTA and control littermates. Blots were probed for pY1472 GluN2B, GluN2B and  $\beta$ -tubulin. **(B, C)** Quantification of the proportion of GluN2B subunits phosphorylated at Y1472 **(B)** and quantification of GluN2B/ $\beta$ -tubulin **(C)** in the hippocampus and cortex of Line 102 and control littermates. All data are presented as N=mouse, mean  $\pm$  SEM. Control mice hippocampus n=8, APP/tTA mice hippocampus n=6, control mice cortex n=10, APP/tTA mice cortex n=8. Red circles indicate TTA control mice, black circles indicate APP and WT control mice. Data were analysed using a two-way ANOVA and Tukey's multiple comparisons. Tissue was collected by Dr Sarmita Sri.

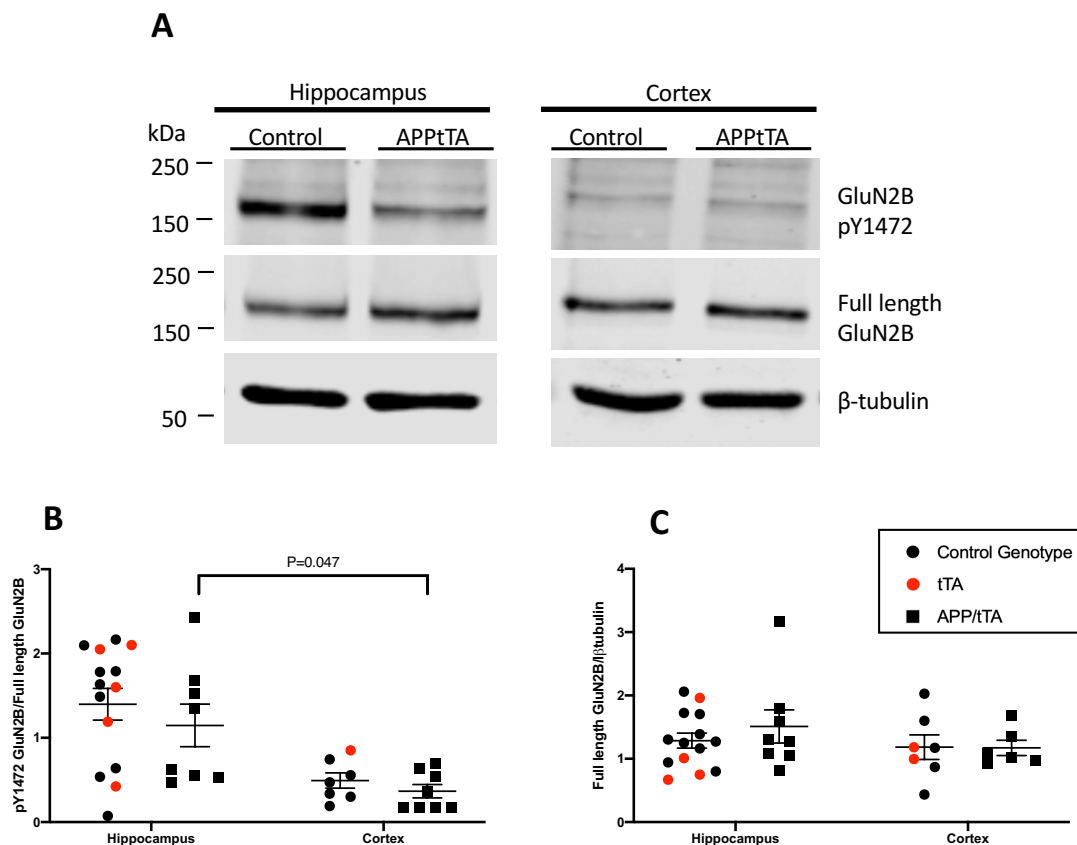


Figure 4.2 The level of GluN2B and pY1472 GluN2B in the hippocampus and cortex of Line 102 mice after 12 weeks of Dox removal.

**(A)** Sample blots of freshly-frozen hippocampal and cortical homogenate from Line 102 APPtTA and control littermates. Blots were probed for pY1472 GluN2B, GluN2B and  $\beta$ -tubulin. **(B, C)** Quantification of the proportion of GluN2B subunits phosphorylated at Y1472 **(B)** and quantification of GluN2B/ $\beta$ -tubulin **(C)** in the hippocampus and cortex of Line 102 and control littermates. All data are presented as N=mouse, mean  $\pm$  SEM. Control mice hippocampus n=14, APP/tTA mice hippocampus n=8, control mice cortex n= 7, APP/tTA mice cortex n= 8. Red circles indicate TTA control mice, black circles indicate APP and WT control mice. Data were analysed using a two-way ANOVA and Tukey's multiple comparisons. Tissue was collected by Dr Sarmi Sri.

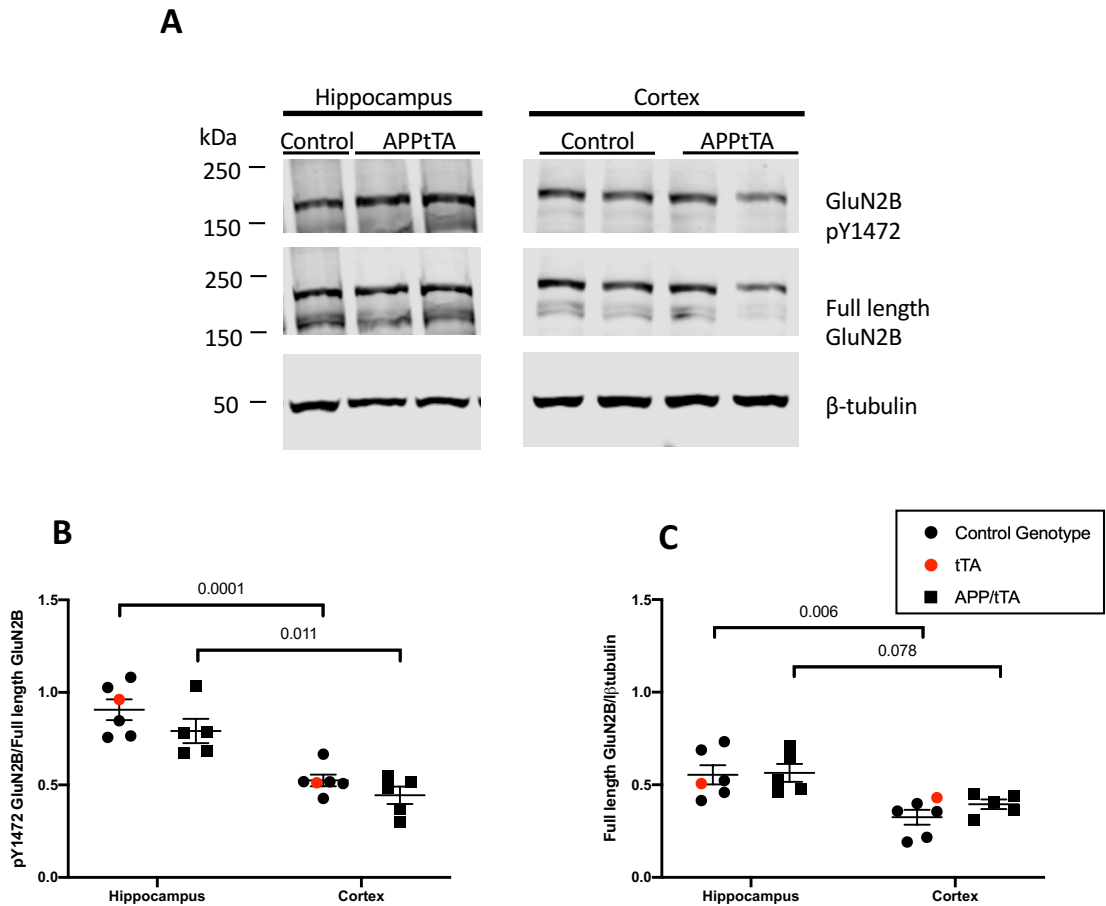


Figure 4.3 The level of GluN2B and pY1472 GluN2B in the hippocampus and cortex of Line 102 mice after 16 weeks of Dox removal.

**(A)** Sample blots of freshly-frozen hippocampal and cortical homogenate from Line 102 APptTA and control littermates. Blots were probed for pY1472 GluN2B, GluN2B and  $\beta$ -tubulin. **(B, C)** Quantification of the proportion of GluN2B subunits phosphorylated at Y1472 **(B)** and quantification of GluN2B/ $\beta$ -tubulin **(C)** in the hippocampus and cortex of Line 102 and control littermates. All data are presented as N=mouse, mean  $\pm$  SEM. Control mice hippocampus n=6, APP/tTA mice hippocampus n=5, control mice cortex n=6, APP/tTA mice cortex n=5. Red circles indicate TTA control mice, black circles indicate APP and WT control mice. Data were analysed using a two-way ANOVA and Tukey's multiple comparisons

Here, I quantify GluN2B and GluN2B pY1472 in hippocampal and cortical tissue from Line 102 mice separately. Before comparing APptTA mice and controls, I first aimed to determine whether there are any differences in these readouts between brain regions. First, I analysed the level of

## Chapter 4

GluN2B in the cortex and hippocampus of 3, 12 and 16-week off dox mice. I analysed the data using a two-way ANOVA and found a significant effect of brain region within 3-week off dox mice (Figure 4.1. C:  $F(1,28)=17.56$ ,  $p=0.0003$ , Control mice hippocampus  $n=8$ , APP/tTA mice hippocampus  $n=6$ , control mice cortex  $n=10$ , APP/tTA mice cortex  $n=8$ .) and 16-week off dox mice (Figure 4.3. C:  $F(1,18)=20.45$ ,  $p=0.0003$ , Control mice hippocampus  $n=6$ , APP/tTA mice hippocampus  $n=5$ , control mice cortex  $n=6$ , APP/tTA mice cortex  $n=5$ ) but not in 12-week off dox mice (Figure 4.2. C:  $F(1,31)=1.425$ ,  $p=0.2417$ , Control mice hippocampus  $n=14$ , APP/tTA mice hippocampus  $n=8$ , control mice cortex  $n=7$ , APP/tTA mice cortex  $n=8$ ).

Post hoc analysis of 3 and 16 week off dox mice using Tukey's multiple comparisons revealed that the level of GluN2B is significantly higher in the hippocampus compared to the cortex in control mice after 3 weeks (Figure 4.1. C,  $p=0.029$ , control hippocampus  $n=8$ , control cortex  $n=10$ ) and 16 weeks off dox (Figure 4.3. C,  $p=0.006$ , control hippocampus  $n=6$ , control cortex  $n=6$ ). When comparing brain regions within APpTtA mice, I found significantly more GluN2B in the hippocampus compared to the cortex in 3-week off dox mice (Figure 4.1. C,  $p=0.030$ , APpTtA hippocampus  $n=6$ , APpTtA cortex  $n=8$ ) and a trend for significance was seen in APpTtA mice after 16-weeks off dox (Figure 4.3. C,  $p=0.078$ , APpTtA hippocampus  $n=5$ , APpTtA cortex  $n=5$ ).

Increased GluN2B in the hippocampus compared to the cortex in 3 and 16 weeks off dox mice are consistent with my previous findings in WT mice (Figure 3.7), however it is not clear why the effect was not consistent across groups. The significant effect size in 3- and 16- week off dox mice was small and therefore it is possible that the effect could be lost by biological variability or small sample size. Further investigation is required to understand differences in NMDAR subunit expression across brain regions, however this is not the focus of this project.

Following on from this, I compared the proportion of GluN2B subunits phosphorylated at Y1472 between brain regions by calculating the ratio of GluN2B pY1472 to GluN2B in the cortex and the hippocampus. A two-way ANOVA returned a significant effect of brain region in all groups: 3 weeks off dox (Figure 4.1. B:  $F(1,28)=44.93$ ,  $p<0.0001$ , Control mice hippocampus  $n=8$ , APP/tTA mice hippocampus  $n=6$ , control mice cortex  $n=10$ , APP/tTA mice cortex  $n=8$ .), 12 weeks of dox (Figure 4.2. B:  $F(1,33)=18.77$ ,  $p=0.001$ , Control mice hippocampus  $n=14$ , APP/tTA mice hippocampus  $n=8$ , control mice cortex  $n=7$ , APP/tTA mice cortex  $n=8$ ), 16 weeks off dox (Figure 4.3. B:  $F(1,18)=51.39$ ,  $p<0.001$ , Control mice hippocampus  $n=6$ , APP/tTA mice hippocampus  $n=5$ ,

*control mice cortex n= 6, APP/tTA mice cortex n= 5*). Tukey's multiple comparisons showed that there is a significant increase in the proportion of GluN2B subunits phosphorylated at Y1472 in the hippocampus compared to the cortex of control mice after 12 weeks off dox (*Figure 4.2. B, p=0.009, control hippocampus n=14, control cortex n=7*) and 16 weeks off dox (*Figure 4.3. B, p=0.001, control hippocampus n=6, control cortex n=6*). The same effect was also revealed in APptTA mice, where the proportion of GluN2B subunits phosphorylated at Y1472 is also significantly increased in the hippocampus after 12 weeks off dox (*Figure 4.2. B, p=0.047, APptTA hippocampus n=8, APptTA cortex n=8*) and 16 weeks off dox (*Figure 4.3. B, p=0.0011, APptTA hippocampus n=5, APptTA cortex n=5*). In 3 week off dox mice, I found a significant increase in the proportion of GluN2B subunits phosphorylated at Y1472 in the hippocampus compared to the cortex of APptTA mice (*Figure 4.1. B, p= <0.0001, APptTA hippocampus n=6, APptTA cortex n=8*) but not control mice (*Figure 4.1. B, p= 0.511, control hippocampus n=8, control cortex n=10*).

Next, I aimed to determine whether the level of GluN2B is altered by genotype. I analysed the level of GluN2B using a two-way ANOVA which revealed no significant effect of genotype on the level of GluN2B in all groups: 3 weeks off dox: (*Figure 4.1. C: F (1,28)=0.351, p=0.5584, Control mice hippocampus n=8, APP/tTA mice hippocampus n=6, control mice cortex n= 10, APP/tTA mice cortex n= 8*), 12 weeks off dox: (*Figure 4.2.C: F (1, 31) =0.334, p=0.568, Control mice hippocampus n=14, APP/tTA mice hippocampus n=8, control mice cortex n= 7, APP/tTA mice cortex n= 8*), 16 weeks off dox: (*Figure 4.3. C: F (1,18)=0.836, p=0.3725, Control mice hippocampus n=6, APP/tTA mice hippocampus n=5, control mice cortex n= 6, APP/tTA mice cortex n= 5*). This suggests that A $\beta$  accumulation in this model does not alter the production or degradation of GluN2B subunits up to 16 weeks of APP<sub>Swe/Ind</sub> expression in this model. However, this analysis does not inform on plasma membrane or synaptic localisation.

Finally, I compared the proportion of GluN2B subunits phosphorylated at Y1472 between control and APptTA mice. A two-way ANOVA revealed a significant effect of genotype in 3-week off dox mice (*Figure 4.1. B: F (1,28)=18.09, p=0.0002, Control mice hippocampus n=8, APP/tTA mice hippocampus n=6, control mice cortex n= 10, APP/tTA mice cortex n= 8*). Post hoc analysis using Tukey's multiple comparisons revealed a significant increase in the proportion of GluN2B subunits phosphorylated at Y1472 in the hippocampus of APptTA mice compared to controls (*Figure 4.1. B; p=<0.0001, control hippocampus n=8, APptTA hippocampus n=6*). This effect was unique to the hippocampus as no significant difference was found when comparing the cortex of APptTA and control mice (*Figure 4.1. B; p=0.686, control cortex n=10, APptTA cortex n=8*). Since I detected no

effect of genotype on the level of GluN2B, the increase in GluN2B pY1472 is not due to changes in expression or degradation of the GluN2B protein. My findings agree with other AD mouse models (Ittner et al., 2010) (Kaufman et al., 2015) and suggest that Fyn activity is increased in the hippocampus of APPtTA mice when synaptic dysfunction first arises. However, analysis of 12 and 16-week off dox mice using a two-way ANOVA found no significant effect of genotype on the proportion of GluN2B subunits phosphorylated at Y1472 in 12-week off dox mice (*Figure 4.2.B: F* (1, 33) = 0.940, *p* = 0.3395, *Control mice hippocampus n* = 14, *APP/tTA mice hippocampus n* = 8, *control mice cortex n* = 7, *APP/tTA mice cortex n* = 8), or 16-week off dox mice (*Figure 4.3. B: F* (1, 18) = 3.661, *p* = 0.072, *Control mice hippocampus n* = 6, *APP/tTA mice hippocampus n* = 5, *control mice cortex n* = 6, *APP/tTA mice cortex n* = 5). This means that the initial increase in GluN2B pY1472 is lost as A $\beta$  continues to accumulate in the model, suggesting a transient increase in Fyn activity.

### 4.2.2 Acute treatment of Line 102 hippocampal slices with Saracatinib

Next, I aimed to determine whether the increase in GluN2B pY1472 in 3-week off dox Line 102 mice could be rescued by acute application of Saracatinib. I have already established that acute application of Saracatinib reduces GluN2B pY1472 in adult WT mice, however I wanted to test whether Saracatinib would partially or fully rescue the elevated GluN2B pY1472, or if levels would be decreased below baseline control levels. To investigate this, I incubated hippocampal slices from 3-week off dox Line 102 mice with 2  $\mu$ M Saracatinib or vehicle for 2 hrs and performed Western blotting then probed for GluN2B, GluN2B pY1472 and  $\beta$ -tubulin (*Figure 4.4*).



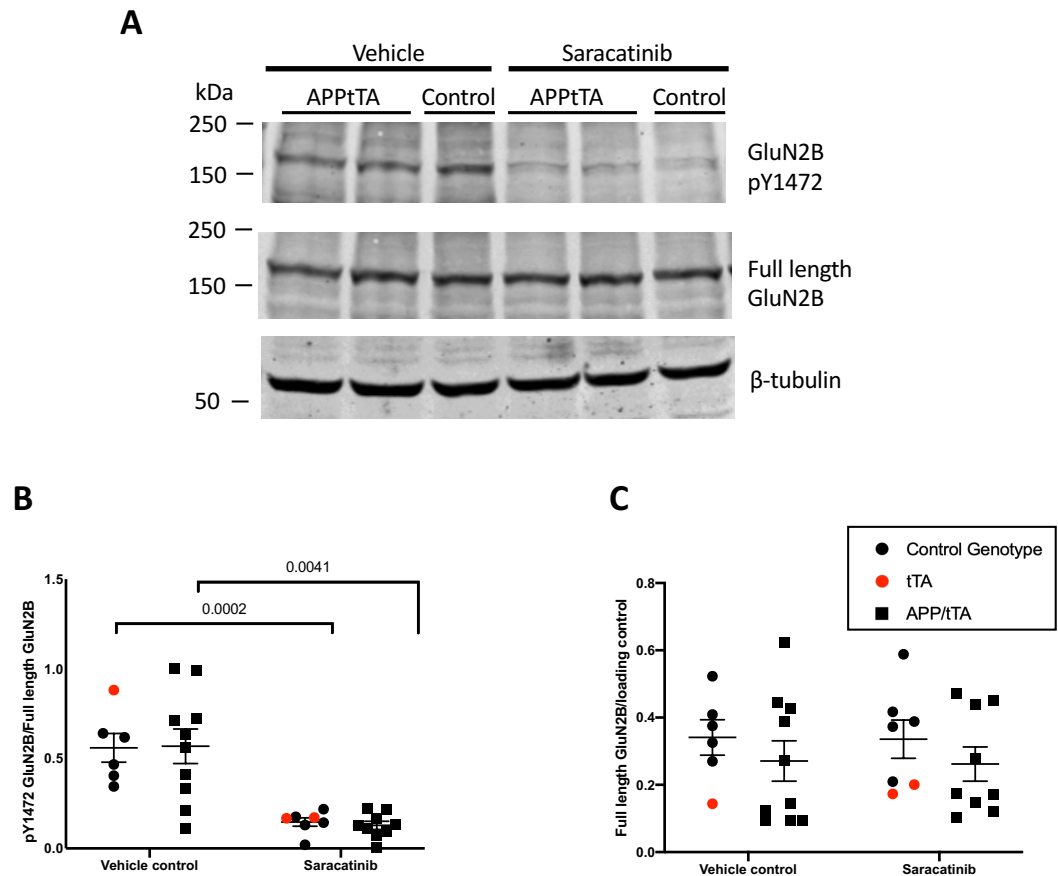


Figure 4.4 The levels of GluN2B and pY1472 GluN2B in hippocampal slices from Line 102 mice following acute application of Saracatinib

**(A)** Sample blots of sliced hippocampal homogenate from Line 102 mice and control littermates after 3-4 weeks off dox. Slices were incubated with 2  $\mu$ M Saracatinib or vehicle control for 2 hours at 30 degrees. Blots were probed for pY1472 GluN2B, GluN2B and  $\beta$ -tubulin. **(B,C)** Quantification of the proportion of GluN2B subunits phosphorylated at Y1472 **(B)** and of GluN2B/ $\beta$ -tubulin **(C)**. Data presented as N=mouse, mean  $\pm$  SEM. Red circles indicate TTA control mice. Control genotype vehicle n=6, control genotype Saracatinib n=7, APPtTA vehicle n=10, APPtTA Saracatinib n=9. Data were analysed using a two-way ANOVA and Tukey's multiple comparisons.

I used a two-way ANOVA to analyse the effect of treatment and genotype on level of GluN2B (Figure 4.4. C). A two-way ANOVA revealed no effect of either treatment ( $F(1,28)=0.015$ ,  $p=0.90$ , Control genotype vehicle n=6, control genotype Saracatinib n=7, APPtTA vehicle n=10, APPtTA Saracatinib n=9) or genotype ( $F(1,28)=1.54$ ,  $p=0.226$ , Control genotype vehicle n=6, control genotype Saracatinib n=7, APPtTA vehicle n=10, APPtTA Saracatinib n=9). This agrees with my

previous findings in adult WT mice (Figure 3.2) and demonstrates that acute application of Saracatinib does not alter GluN2B production or degradation in slices from Line 102 mice in this time frame.

Next, I analysed the ratio of GluN2B pY1472 to GluN2B using a two-way ANOVA (Figure 4.4. B). As expected, I found a significant effect of Saracatinib treatment ( $F(1,28)=36.11$ ,  $p<0.0001$ , Control genotype vehicle  $n=6$ , control genotype Saracatinib  $n=7$ , APPTTA vehicle  $n=10$ , APPTTA Saracatinib  $n=9$ ), however I was surprised to find no effect of genotype ( $F(1, 28)= 0.004$ ,  $p=0.94$ , Control genotype vehicle  $n=6$ , control genotype Saracatinib  $n=7$ , APPTTA vehicle  $n=10$ , APPTTA Saracatinib  $n=9$ ). In line with my findings from adult WT slices (Figure 3.2), Tukey's multiple comparisons test confirmed that Saracatinib significantly decreased the proportion of GluN2B subunits phosphorylated at Y1472 in slices from both APPTTA mice ( $p=0.0002$ , APPTTA vehicle  $n=10$ , APPTTA Saracatinib  $n=9$ ) and control littermates ( $p=0.0041$ , control vehicle  $n=6$ , control Saracatinib  $n=7$ ) compared to vehicle treated slices. This demonstrates the Saracatinib effectively reduces GluN2B pY1472 in hippocampal slices. However, the lack of effect between genotypes indicates that there is no significant difference between slices from APPTTA mice compared to control mice after 3-weeks off dox. This disagrees with my previous findings which showed an increase in GluN2B pY1472 in unsliced tissue from 3-week off dox mice (Figure 4.1 B).

### 4.2.3 The effect of slicing on GluN2B Y1472 phosphorylation

We questioned whether the slicing technique could alter GluN2B Y1472 phosphorylation and therefore mask the changes seen in unsliced tissue from 3-week off dox mice. To investigate the effect of slicing on GluN2B Y1472 phosphorylation, I scarified adult WT mice and collected the hippocampus from one (randomly selected) hemisphere and sliced the other hemisphere. Following a 1hr rest period, the hippocampus was dissected out of the slices and frozen. Unsliced and sliced samples were then analysed using Western blotting and probed for GluN2B pY1472, GluN2B and  $\beta$ -tubulin (Figure 4.5).

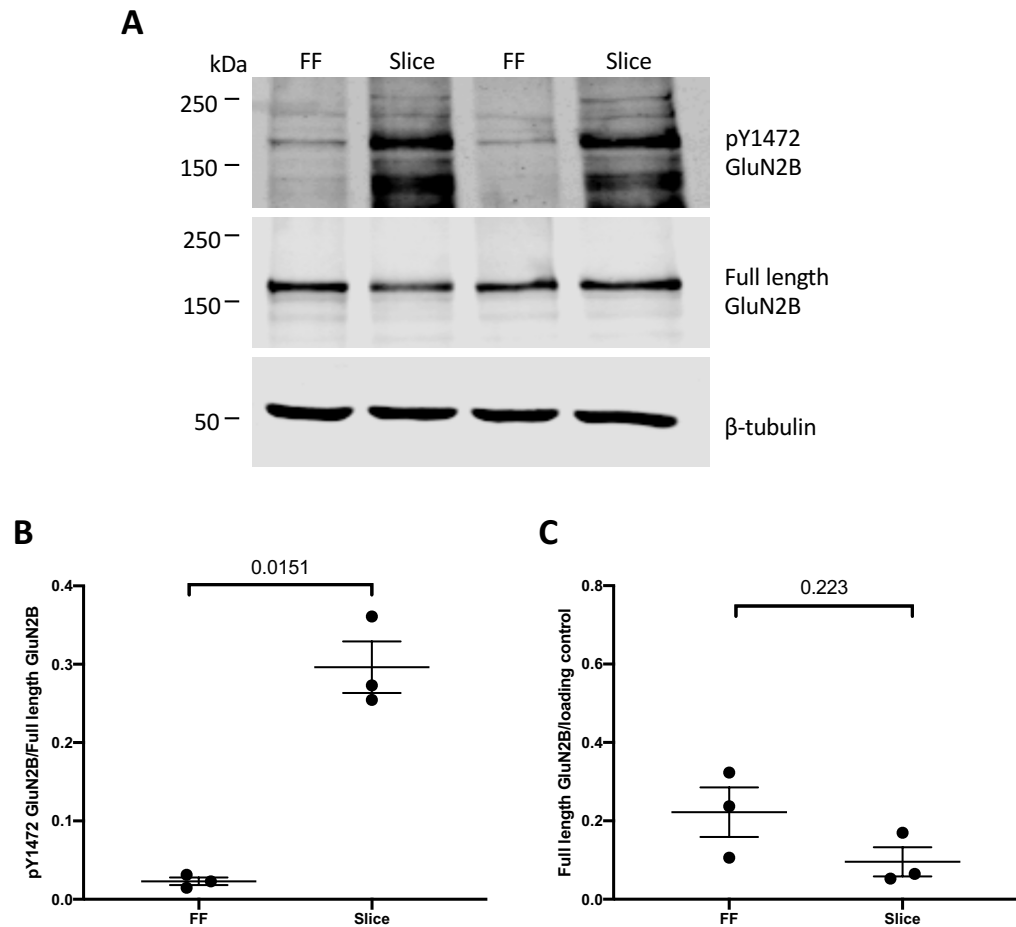


Figure 4.5 The effect of slicing on GluN2B Y1472 phosphorylation

**(A)** Sample blots of unsliced, freshly-frozen (FF) hippocampi and hippocampal slices prepared in standard aCSF from adult C57Bl/6 mice. Blots were probed for pY1472 GluN2B, GluN2B and β-tubulin. **(B,C)** Quantification of the proportion of GluN2B subunits phosphorylated at Y1472 **(B)** and of GluN2B/β-tubulin **(C)**. Data presented as N=slice, mean +/- SEM. FF n=3, Slice n=3. Data analysed using a two-tailed paired t-test.

I found that the proportion of GluN2B subunits phosphorylated at Y1472 was increased in sliced hippocampal tissue compared to unsliced hippocampal tissue. (*Figure 4.5 B, two-tailed, paired t-test; P=0.0151, FF n=3, slice n=3*). This was not due to changes in GluN2B expression because I detected no significant difference between the level of GluN2B in sliced compared to unsliced hippocampal (*Figure 4.5.C, two-tailed, paired t-test; P=0.223, FF n=3, slice n=3*). However, due to the small sample size of the dataset, repeat experiments would be useful to determine whether these findings are reproducible.

We questioned whether the enhanced GluN2B pY1472 in sliced versus unsliced hippocampal tissue is due to glutamate induced toxicity during slicing. Therefore, I considered incorporation of the broad glutamate receptor antagonist, Kynurenic acid (KA), during slicing. Application of 1 mM KA to the aCSF (KA-aCSF) during slicing and in the initial recovery phase greatly improves slice viability (Fitzjohn et al., 2010). Following methodology by Fitzjohn et al., I used adult WT mice and collected the hippocampus from one (randomly selected) hemisphere and prepared hippocampal slices in aCSF containing 1 mM KA from the other hemisphere. Slices were then left to recover in room temperature KA-aCSF for 30 minutes before resting in standard aCSF for 30 minutes. The hippocampus was then dissected out of the slices and frozen. Unsliced and sliced samples were analysed using Western blotting and probes for GluN2B pY1472, GluN2B and  $\beta$ -tubulin (Figure 4.6)

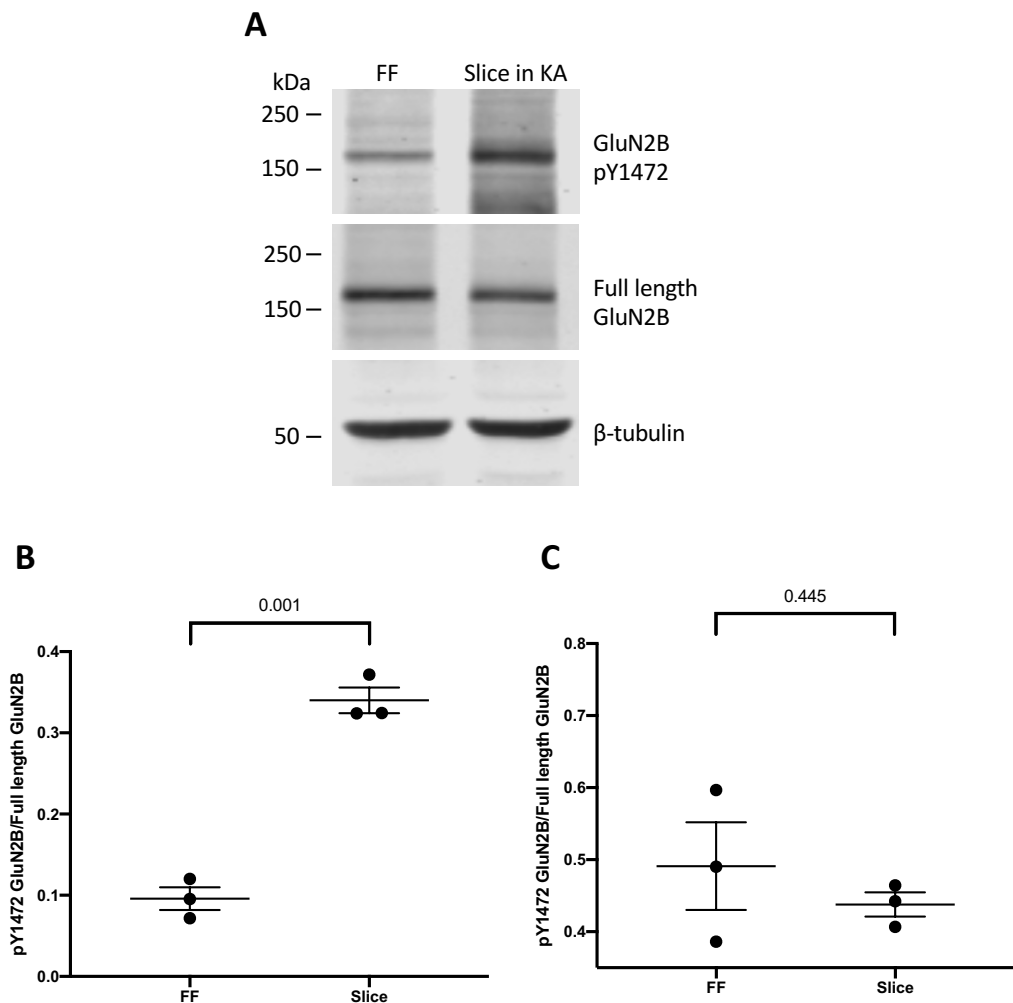


Figure 4.6 The effect of slicing in aCSF containing kynurenic acid on GluN2B Y1472 phosphorylation

**(A)** Sample blots of freshly-frozen (FF) hippocampus and hippocampal sliced prepared in aCSF-containing kynurenic acid from adult C57Bl/6 mice. Blots were probed for pY1472 GluN2B, GluN2B and  $\beta$ -tubulin. **(B,C)** Quantification of the proportion of GluN2B subunits phosphorylated at Y1472 (**B**) and of GluN2B/ $\beta$ -tubulin (**C**). Data presented as N=mouse, mean  $\pm$  SEM. FF n=3, slice n=3. Data analysed using a two-tailed paired t-test.

I found that the proportion of GluN2B subunits phosphorylated at Y1472 was significantly increased in slices prepared in KA-containing aCSF compared to unsliced hippocampi (Figure 4.6. B; two-tailed paired t-test,  $p=0.001$ , FF n=3, slice n=3). I measured an increase of  $0.24 \pm 0.014$  which is comparable to the increase recorded in standard aCSF where I measured an increase of  $0.27 \pm 0.034$  (Figure 4.5. B). The level of GluN2B also remained unaltered in sliced vs unsliced

hippocampal tissue (*Figure 4.6. C; two-tailed paired t-test,  $p=0.445$ ,  $FF\ n=3$ , slice  $n=3$* ). Therefore, the addition of 1 mM KA during slicing and in the initial recovery phase was not useful in preventing the increase in GluN2B Y1472 phosphorylation and suggests that the slicing-induced increase in GluN2B Y1472 phosphorylation is not mediated by excessive glutamate receptor activation.

### 4.3 Discussion

In this Chapter I utilised Line 102 mice that model early AD and showed that GluN2B pY1472 is increased following 3 weeks off APP<sub>Swe/Ind</sub> expression, when synaptic plasticity dysfunctions first arise. However, this increase was not sustained by 12 and 16 weeks off APP<sub>Swe/Ind</sub> expression. In order to determine whether Saracatinib could rescue the increased GluN2B pY1472 observed in Line 102 mice after APP<sub>Swe/Ind</sub> expression, I incubated slices in Saracatinib and performed Western blotting to quantify the level of GluN2B pY1472. I found that the increased GluN2B pY1472 was lost following slicing and so I was unable to conclude this question using this technique.

#### 4.3.1 GluN2B Y1472 phosphorylation in Line 102 mice following 3 and 12 weeks of APP<sub>Swe/Ind</sub> expression

I found a significant increase in GluN2B pY1472 in Line 102 mice after 3-weeks of APP<sub>Swe/Ind</sub> expression (*Figure 4.1*). This suggests an increase in Fyn activity in response to A $\beta$  and is in line with findings from human AD post mortem tissue, A $\beta$  application to cell cultures and other mouse models of AD (Larson et al., 2012) (Um et al., 2012)(Ittner et al., 2010) (Kaufman et al., 2015). However, unique to other studies, my data show for the first time that GluN2B pY1472 is increased in mice that model early AD pathology, before detectable synapse loss and the presence of plaques. At the same time point measured in this project (3 weeks of APP<sub>Swe/Ind</sub> expression) APP<sub>TA</sub> mice first show signs of synaptic dysfunction in the form of reduced LTP (Sri et al., 2019). We hypothesise that the increased GluN2B pY1472 reported here may contribute to the reduced LTP reported previously. I aim to address this hypothesis in the next chapter by applying Saracatinib acutely to hippocampal slices from Line 102 mice following 3 weeks of APP<sub>Swe/Ind</sub> expression and measuring LTP.

I found that the increase in GluN2B pY1472 following 3 weeks of APP<sub>Swe/Ind</sub> expression is not sustained after 12 and 16 weeks of APP<sub>Swe/Ind</sub> expression (Figure 4.2 & Figure 4.3). This transient effect could be due to homeostatic mechanisms to rebalance the GluN2B Y1472 phosphorylation levels and regain normal NMDAR synaptic expression and neuronal excitability. GluN2B pY1472 is regulated by STEP in two ways: direct dephosphorylation of GluN2B Y1472 and inactivation of Fyn by dephosphorylation at Y420 (see Figure 1.8) (Snyder et al., 2005). An increase in STEP activity is therefore associated with a reduction in GluN2B Y1472 phosphorylation which permits clathrin-mediated internalisation of GluN2B-containing NMDARs (Roche et al., 2001)(Lavezzari et al., 2003). In agreement with this, STEP<sup>-/-</sup> mice show increased GluN2B pY1472 and surface expression of GluN2B-containing NMDARs in hippocampal synaptosomal fractions (Venkitaramani et al., 2011). The level of STEP protein is increased in Tg2576 mice starting from 6-months old, however, 3-month-old Tg2576 mice that model earlier stages of pathology, for example before synapse loss (Lanz et al., 2003), show no statistical difference in STEP levels compared to control mice (Kurup et al., 2010). Increased STEP activity is also documented in AD post-mortem cortical tissue; however, the authors do not specify whether the samples are from mild, moderate or severe cases of AD (Kurup et al., 2010). Findings from Tg2576 mice indicate that STEP levels may increase and contribute to later A $\beta$ -mediated pathologies. More work is required to determine whether this finding is extended to other mouse models and human AD tissue at progressive stages of AD.

A $\beta$  causes a rapid increase in GluN2B pY1472 and this is supported by findings showing that application of 1-3 mM synthetic A $\beta$  to WT cortical cultures increased GluN2B pY1472 after 15 mins, however this increase was lost by 60 mins and was correlated with an increase in STEP activity (Um et al., 2012). The authors hypothesise that increased STEP activity could explain why increased phosphorylation is seen acutely but not at the later time point (Um et al., 2012). It is possible that a similar effect is occurring in the Line 102 mouse model and I theorise that the transient increase in GluN2B pY1472 seen at 3 weeks of APP<sub>Swe/Ind</sub> expression may be lost by 12 and 16 weeks due to increased STEP activity. Here, I compare GluN2B pY1472 from 3 to 16 weeks of APP<sub>Swe/Ind</sub> expression in a mouse model that accumulates endogenously produced A $\beta$  progressively and in the picomolar range (Sri, 2018). This is within the same unit range as individuals with AD (Murphy et al., 2007) but is vastly different to *in vitro* studies by Um et al 2012 where the application of A $\beta$  onto neuronal cultures is sudden, for a much shorter time period and at a much higher (micromolar) concentration. This makes it difficult to draw a comparison between these *in vitro* and *in vivo* studies on Y1472 phosphorylation, however quantification of the level of active STEP in hippocampal homogenate from 3, 12 and 16 weeks off dox Line 102 mice could determine if this theory is true.

Even though the level of GluN2B pY1472 is no longer enhanced by 12 and 16 weeks of APP<sub>Swe/Ind</sub> accumulation, any synaptic damage that the earlier elevated GluN2B pY1472 may have caused could persist. Furthermore, other SFK or Fyn targets, for example Pyk2, may not undergo homeostatic rebalancing and so their phosphorylation state remains elevated which could contribute to synaptic function and plasticity deficits. Therefore, Fyn inhibition at this later time point may still be useful to rescue synaptic deficits even though GluN2B pY1472 residue is no longer increased.

We questioned whether the way I grouped the data could impact my findings. For example, the effect of individual control genotypes (WT, APP and TTA mice) or the effect of sex. Differences arising from these factors could explain why the increase in GluN2B pY1472 following 3 weeks of APP<sub>Swe/Ind</sub> expression was not detected by 12 or 16 weeks of expression. This could also explain the lack of consistency in the level of GluN2B across brain regions. To control for individual transgenes, I used all three genotypes from the littermates of APPTTA mice: WT, APP and TTA. APP mice display very low levels of APP expression, however they perform as well as WT and TTA controls in the MWM and do not show impairments in synaptic function or plasticity (Sri et al., 2019). However, TTA mice show decreased brain weight at 12-16-week-old and thinning of the dentate gyrus at 48-weeks-old compared to non-transgenic mice (Helboe et al., 2017) (Pitera et al., 2019). CHOP is a transcription factor involved in unfolded protein response-induced cell death and its expression is increased in 3-month-old TTA mice compared to age-matched controls (Pitera et al., 2019). This suggests that neurons are not indifferent to the presence of TTA and therefore, it was important to test whether the expression of TTA could alter GluN2B pY1472 and/or GluN2B levels. Therefore, I isolated data from TTA mice (shown in red in Figure 4.1- Figure 4.4 B,C) and found that the data fall within the range measured from WT and APP mice, therefore these readouts are unaffected by TTA expression and so TTA mice were grouped with WT and APP controls for analysis in these experiments.

Next, I considered whether sex could influence my results. Many sex differences in the mammalian brain have been reported (Jazin et al., 2010). For example, expression of GluN1 and GluN2B subunits in the hippocampus are higher in female rats than male rats (Wang et al., 2015). To test whether sex has an effect on my experiments, I split the data to isolate males and females (Appendix A). This significantly reduced my sample size but revealed no effect of sex on the level



of GluN2B or GluN2B pY1472, therefore I did not further consider this factor in my subsequent experiments.

#### **4.3.2 Application of Saracatinib to slices from Line 102 mice following 3 weeks of APP<sub>Swe/Ind</sub> expression**

Following the discovery that GluN2B pY1472 is increased in APP<sub>Tg</sub> mice following 3-weeks of APP<sub>Swe/Ind</sub> expression compared to controls (Figure 4.1), I set out to determine whether acute application of Saracatinib to hippocampal slices from these mice rescued the phenotype. However, I was unable to detect a change in GluN2B pY1472 between genotypes in slices. This meant that I was unable to determine whether the increase in GluN2B pY1472 was rescued fully, partially or below baseline levels using this technique.

It is possible that acute injury caused by slicing increases Fyn activity, resulting in an increase in GluN2B Y1472 phosphorylation in sliced hippocampal tissue compared to unsliced. This agrees with reports from Ho and colleagues who showed a significant increase in the activity of SFKs (pY416) and Pyk2 (pY402) immediately after slicing compared to unsliced hippocampi (Ho et al., 2004). This suggests that slicing increases the activity of Fyn, and potentially other SFKs, and therefore it is likely that the slices in this project show hyperphosphorylation of multiple SFK targets as well as GluN2B. Ho and colleagues showed that the increased activity of Pyk2 and SFKs was maintained even 8 hours after slice recovery and regardless of whether the slices were maintained in a submerged or interface-style chamber (Ho et al., 2004). This suggests that allowing a longer recovery time in my experiment, or changing the experimental setup to an interface-style chamber, would not be useful to permit recovery of elevated pY1472 GluN2B levels post slicing.

We hypothesise that slicing may increase GluN2B pY1472 such that the level of phosphorylation is equally high in both APP<sub>Tg</sub> mice and control mice, meaning that a difference in GluN2B pY1472 between genotypes can no longer be detected. It is well established that LTP can be induced in adult WT rodent hippocampal slices. Therefore, this suggests that the acute increase in GluN2B pY1472 following slicing does not affect synaptic plasticity. This may suggest that GluN2B Y1472 phosphorylation state does not contribute to plasticity. Alternatively, plasticity may remain unaffected because the increase in phosphorylation is acute, whereas a chronic increase in

GluN2B pY1472 *in vivo* (as may be the case of 3-week off dox APPTTA mice) may cause synaptic damage and alter synaptic plasticity. Therefore, it is possible that chronically elevated GluN2B pY1472 detected in unsliced tissue from APPTTA expressing APP<sub>Swe/Ind</sub> for 3 weeks may induce long lasting effects that are not altered by acutely elevating the GluN2B pY1472 levels by slicing.

In this project, I trialled kynurenic acid to inhibit glutamate receptors during slicing and initial recovery; however, this did not prevent the slicing-induced increase in GluN2B pY1472, suggesting that activation of glutamate is not responsible for this effect. I followed the conventional technique of preparing slices in ice-cold aCSF to reduce metabolic activity and minimise neuronal damage during slicing (Andersen, 1981). An alternative approach is to prepare slices in warm (physiological temperate) aCSF which may produce better quality slices and prevent slice-induced increase in GluN2B pY1472. In support of this, slicing in ice-cold aCSF causes architectural changes to the slice, for example exposure to cold temperate during the preparation of adult rodent hippocampal slices caused the loss of dendritic spines in CA1 pyramidal cells (Kirov et al., 2004). This also occurs following the ice-cold preparation of cerebellar slices from adult rodents (Eguchi et al., 2020). Upon re-warming to physiological temperatures (~37°C), the spines are rapidly reformed, however the excessive proliferation results in synaptic densities beyond that found in perfused-fixed tissue (Kirov et al., 2004) (Bourne et al., 2012). However, if the slices are prepared at room temperature (~25°C) using a tissue chopper, the resulting number of spines following the recovery period is comparable to perfusion-fixed tissue (Bourne et al., 2012). This suggests that a warmer preparation of hippocampal slices prevents synapse proliferation and may result in slices that better model the brain *in vivo*.

Western blotting of recovered slices following preparation at cold temperatures also reduces the protein level of GluA1 and GluA3 AMPAR subunits in hippocampal slices of young adult rats (Taubenfeld et al., 2002). This has also been shown by immunogold labelling of GluA1-3 in fixed adult rodent cerebellar slices (Eguchi et al., 2020). However, preparation of cerebellar slices at 35-37°C prevented the decrease in AMPAR protein expression, suggesting an advantage of warm slice preparation in preserving physiological AMPAR expression (Eguchi et al., 2020). The effect of cold versus warm slice preparation on the phosphorylation state of synaptic proteins, including GluN2B, has not been reported. Future work could assess whether preparation of slices at physiological temperature prevents the slicing-induced increase in GluN2B pY1472, and if so, this could provide a better technique to model physiological levels of GluN2B pY1472 for slice

electrophysiology and may enable the maintenance of the elevated GluN2B pY1472 seen in unsliced tissue from Line 102 mice after 3 weeks of APP<sub>Swe/Ind</sub> expression.

As with all techniques, brain slicing has its disadvantages, however my results do not invalidate the use of acute slice preparations, rather it highlights the limitations of the technique which must be considered when measuring GluN2B phosphorylation from acute slices. It also highlights the need for others to test phosphorylation states of proteins of interest when using brain slices. Alternative experimental approaches that bypass the need for slicing, such as *in vivo* manipulations, could be used. I explored this idea with a pilot study in Chapter 3 to administer Saracatinib *in vivo*, however further investigation is required to determine the optimum dose and administration length of Saracatinib to cause a significant reduction in GluN2B Y1472 phosphorylation.

#### 4.3.3 Conclusions

The key findings in this Chapter show that GluN2B pY1472 is increased in fresh-frozen hippocampus of 3-week off dox APPTA mice compared to controls, suggesting increased Fyn activity. Following on from this finding, I aim to test whether acute Saracatinib application can rescue previously established synaptic dysfunctions at this time point (Sri et al., 2019), which could occur by reducing GluN2B pY1472 or other Fyn or SFK targets. I show that the increase in GluN2B pY1472 is not sustained by 12- or 16-weeks of APP<sub>Swe/Ind</sub> expression. This could suggest a homeostatic mechanism to regain normal levels of phosphorylation in the system. However, it remains possible that Saracatinib may still have a beneficial effect in rescuing synaptic dysfunction seen at this time point since Saracatinib acts to inhibit broad SFKs which have multiple targets outside of GluN2B pY1472. Therefore, the following Chapter also aims to test whether acute Saracatinib can rescue synaptic dysfunctions at this later time point.



## Chapter 5 The effect of SFK inhibition in Line 102 mice

In the previous Chapter I showed that GluN2B pY1472 is enhanced in fresh-frozen hippocampal tissue of Line 102 mice after 3 weeks of APP<sub>Swe/Ind</sub> expression, suggesting increased Fyn activity. Previous work in our lab showed decreased synaptic plasticity in Line 102 mice at the same time point. Therefore, it is possible that increased Fyn activity may contribute to the decrease synaptic plasticity (Sri et al., 2019). This hypothesis is supported by experiments showing that transgenic modulation of Fyn alters synaptic plasticity (Lu et al., 1999, Grant et al., 1992). In addition, other experiments have shown that pharmacologically increasing Fyn activity using SKF81297 decreases synaptic plasticity (Yang et al. 2012) (discussed in Section 1.10.5). Following this rationale, we hypothesise that inhibition of Fyn may rescue synaptic plasticity defects in Line 102 mice after 3 weeks of APP<sub>Swe/Ind</sub> expression.

It is possible that increased Fyn activity could disrupt synaptic plasticity via increased GluN2B Y1472 phosphorylation. Increased plasma membrane expression of GluN2B-containing NMDARs following enhanced Y1472 phosphorylation by Fyn could impair LTP by disrupting normal GluN2B downstream signalling. However, hyperphosphorylation of other Fyn targets could also contribute to synaptic dysfunction at this stage and even later in AD progression. This thesis aims to determine whether a broad SFK inhibitor, Saracatinib, can rescue synaptic dysfunction in hippocampal slices from Line 102 mice. Whilst GluN2B Y1472 phosphorylation is used as a proxy for SFK activity, it is not possible to determine from the following experiments whether any beneficial effects of Saracatinib are due to Fyn or GluN2B Y1472 phosphorylation specifically, and it remains possible that other SFKs and/or their downstream targets may be responsible.

Synaptic dysfunction is hypothesised to precede synapse loss (Sri et al., 2019), which is the strongest correlate of cognitive decline and may potentially be irreversible (see Section 1.6). Therefore, whether Saracatinib is able to rescue early dysfunctions in AD could advise future clinical trials as to whether re-testing Saracatinib on individuals in the earlier stages of AD would be worthy of investigation. Furthermore, understanding the key components that drive synaptic dysfunction may be useful to identify new therapeutic targets that could ultimately prevent or slow synaptic loss by preventing synaptic dysfunction.

## 5.1 Chapter aims

To determine whether acute Saracatinib treatment rescues early synaptic transmission and plasticity impairments in CA3-CA1 synapses from hippocampal slices of Line 102 mice:

1. Early when LTP is first impaired (3 weeks of APP<sub>Swe/Ind</sub> expression) (Sri et al., 2019).
2. Later when IO responses are first impaired (12 weeks of APP<sub>Swe/Ind</sub> expression) (Sri et al., 2019).

## 5.2 Saracatinib rescues plasticity deficits in Line 102 mice following 3 weeks of A $\beta$ accumulation

I began by focussing on Line 102 mice following 3 weeks of APP<sub>Swe/Ind</sub> expression for two reasons. Firstly, I found that these mice showed increased GluN2B pY1472, implying increased Fyn activity (Figure 4.1). Secondly, I wanted to determine whether broad inhibition by SFKs would be beneficial at the time point when synaptic dysfunction first arises but before long-term memory loss (Sri et al., 2019). Saracatinib could provide beneficial effects by modulating GluN2B pY1472 or phosphorylation of other target proteins. To test the effect of Saracatinib, I performed field recordings at CA3-CA1 synapses in hippocampal slices from Line 102 mice after 3-weeks off dox that had been incubated with 2  $\mu$ M Saracatinib or vehicle for 2 hours. Following Sri et al 2019 and my previous work in WT mice in Chapter 3, I induced LTP using a TBS induction protocol in CA3-CA1 synapses of hippocampal slices from APPtTA and control mice after 3-weeks off dox (Figure 5.1).

To analyse the data, I averaged the normalised fEPSP slope from 40-45 mins after induction for each slice recording. The data were non-normal and therefore I analysed the data using a non-parametric Kruskal-Wallis test which does not assume a normal distribution and is less sensitive to outliers. Using this test, I found a statistically significant difference between groups (*Figure 5.1 C*,  $p=0.0158$ , control vehicle  $n=25$ , control Saracatinib  $n=15$ , APPtTA vehicle  $n=21$ , APPtTA Saracatinib  $n=20$ ). Further analysis using an uncorrected Dunn's test showed a significant decrease in LTP in slices from APPtTA mice compared to controls ( $p=0.0367$ , control vehicle  $n=25$ , APPtTA vehicle  $n=21$ ). Therefore, although the effect size was smaller than in Sri et al (Sri et al:  $-53.70 \pm 5.047$ , Figure 5.1:  $28.58 \pm 12.45$ ), I was able to detect a significant decrease in LTP in APPtTA mice after 3 weeks of APP<sub>Swe/Ind</sub> expression. However, to compare between control and APPtTA

genotypes the statistical  $n$  should equal mouse, rather than  $n$ =slice, which is used in this thesis to compare pharmacological manipulations. Analysis of the data when the statistical  $n$ =mouse revealed no significant difference in LTP between control and APPtTA mice (*Figure 5.1 E*,  $p=0.178$ , control vehicle  $n=15$ , APPtTA vehicle  $n=9$ ). This disagrees with findings reported per slice in (*Figure 5.1 C*). However, the cumulative frequency plot (*Figure 5.1 F*) shows that the level of potentiation following LTP induction is consistently lower in slices from APPtTA mice compared to controls. It is possible that reducing the statistical  $n$  by averaging per mouse resulted in less power to detect significance. Repeat experiments are required to determine whether there is an impairment in LTP that can be detected per mouse to add confidence to the significant finding reported by analysing per slice.

To analyse the effect of Saracatinib, the data were compared with the statistical  $n$ =per slice. Therefore, this assumes an impairment in LTP in slices from APPtTA mice compared to controls. Comparing Saracatinib and vehicle treated slices, I found that Saracatinib had no effect on LTP in control mice (*Figure 5.1 C*  $p=0.195$ , control vehicle  $n=25$ , control Saracatinib  $n=15$ ). This agrees with my findings in WT mice (*Figure 3.5*). Analysis of recordings from APPtTA mice showed a significant increase in potentiation in Saracatinib treated slices compared to vehicle treated slices ( $p=0.008$ , APPtTA vehicle  $n=21$ , APPtTA Saracatinib  $n=20$ ). Furthermore, vehicle treated slices from APPtTA mice were not significantly different compared to vehicle-treated slices from control mice ( $p=0.074$  APPtTA vehicle  $n=21$ , control vehicle  $n=25$ ). This suggests that acute Saracatinib treatment rescued LTP impairments back to control levels in CA3-CA1 synapses from APPtTA mice following 3 weeks of APP<sub>Swe/Ind</sub> expression. Whether the beneficial effect of Saracatinib occurs via altering GluN2B pY1472 or phosphorylation of other SFK targets requires further investigation and will be discussed in Section 5.6.

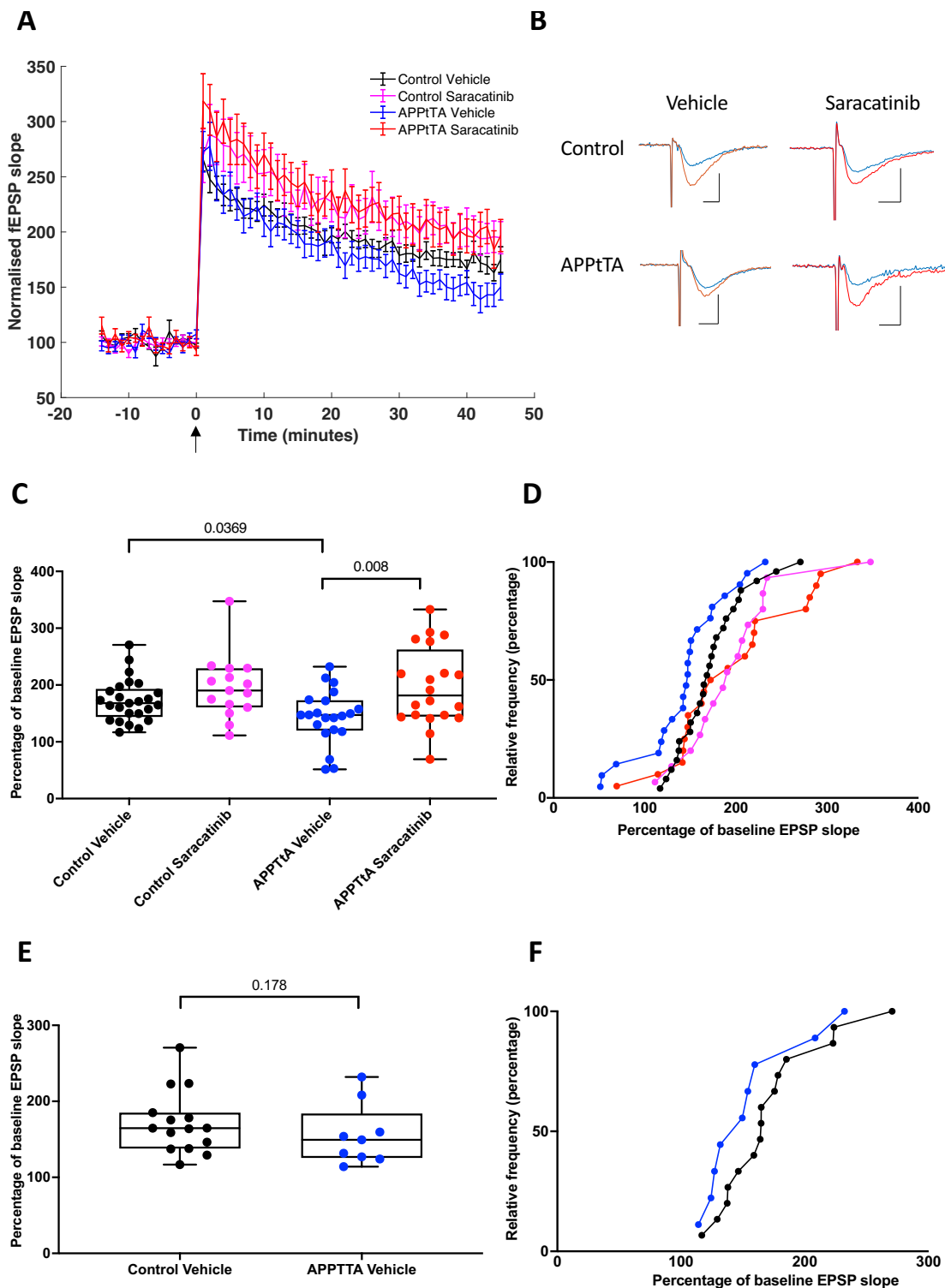


Figure 5.1 The effect of acute Saracatinib treatment on LTP in hippocampal slices from Line 102 mice after 3 weeks of dox removal

**(A)** TBS-induced LTP (arrowhead) in WT hippocampal slices from APPTTA mice and control littermates treated with 2  $\mu$ M Saracatinib or vehicle control for 2 hours. **(B)** Example LTP traces showing the fEPSP before (blue) and after LTP induction (red) for each condition. Scale bar calibration: 5 ms, 0.5 mV. **(C-F)** Percentage change in the fEPSP



slope in the final 5 minutes after LTP-induction represented in a box and whisker plot (**C and E**), and cumulative frequency plot (**D and F**). Data are represented as n=slice, mean  $\pm$  SEM in **C and D**. Control vehicle n=25, Control Saracatinib n=15, APptTA vehicle n=21, APptTA Saracatinib n=20. Data are represented as n=mouse in **E and F** where control vehicle n=15, APptTA vehicle n=9. The data in (**C**) were analysed using a Kruskal-Wallis test followed by uncorrected Dunn's multiple comparisons. Multiple comparisons were two-tailed with exception to control vehicle vs APptTA vehicle which was analysed one-tailed. The data in (**E**) were analysed using a one-tailed t-test. All experiments were performed in an interface-style rig and the aCSF contained 1  $\mu$ M Gabazine.

### 5.3 Saracatinib does not alter basal synaptic transmission in Line 102 mice following 3 and 12 weeks of A $\beta$ accumulation

Next, I investigated the effect of acute Saracatinib treatment on basal synaptic function in Line 102 mice after 3 weeks of APP<sub>Swe/Ind</sub> expression. To do this I measured IO and PPR of CA3-CA1 synapses from hippocampal slices of APptTA mice and control littermates following incubation with 2  $\mu$ M Saracatinib or vehicle. We hypothesised that, following Sri et al 2019., I would find no significant difference of IO or PPR in APptTA mice compared to controls following 3 weeks of A $\beta$  accumulation, suggesting that synapses are still viable and intact. Following my previous findings in WT mice (see Chapter 3), we also hypothesised that acute treatment with Saracatinib would not alter these readouts.

Analysis of IO responses using a repeated measures three-way ANOVA showed a significant effect of stimulus amplitude ( $F(7, 161)=57.86$ ,  $p<0.0001$ , Control vehicle n=12, control Saracatinib n=4, APptTA vehicle n=6, APptTA Saracatinib n=5) but no effect of Saracatinib treatment  $F(1,23)=$ ,  $p=0.993$  or of genotype ( $F(1,23)=0.6701$ ,  $p=0.421$ , Control vehicle n=12, control Saracatinib n=4, APptTA vehicle n=6, APptTA Saracatinib n=5) (Figure 5.2, A,B). This demonstrates that IO responses at CA3-CA1 synapses are not altered by A $\beta$  accumulation in the mouse model, which agrees with previous reports from Sri et al 2019. I also found no significant effect of Saracatinib treatment on IO responses in either control or APptTA mice, which is in line with findings from WT mice (Figure 3.4) and adds further confidence that acute SFK inhibition does not alter synaptic AMPAR contribution at CA3-CA1 synapses.

Analysis of PPR at the 40 ms interstimulus interval using a two-way ANOVA revealed a significant effect of interpulse interval ( $F(18, 126)=41.65$ ,  $p<0.0001$ , Control vehicle  $n=8$ , control Saracatinib  $n=5$ , APPTA vehicle  $n=7$ , APPTA Saracatinib  $n=5$ ), but no effect of Saracatinib treatment ( $F(3,21)=1.091$ ,  $p=0.375$ , Control vehicle  $n=8$ , control Saracatinib  $n=5$ , APPTA vehicle  $n=7$ , APPTA Saracatinib  $n=5$ ), or stimulus treatment interaction ( $F(18,126)=0.723$ ,  $p=0.783$ ), Control vehicle  $n=8$ , control Saracatinib  $n=5$ , APPTA vehicle  $n=7$ , APPTA Saracatinib  $n=5$ ) (Figure 5.2, C,D). This suggests that there is no change in presynaptic function after 3 weeks of APP<sub>Swe/Ind</sub> expression which, again, agrees with previous findings by Sri et al 2019. I also recorded no effect of Saracatinib on this readout in both APPTA and control mice which is in line with WT data presented earlier in this project (Chapter 3) and shows that acute Saracatinib treatment does not alter this readout of presynaptic function in CA3-CA1 synapses.

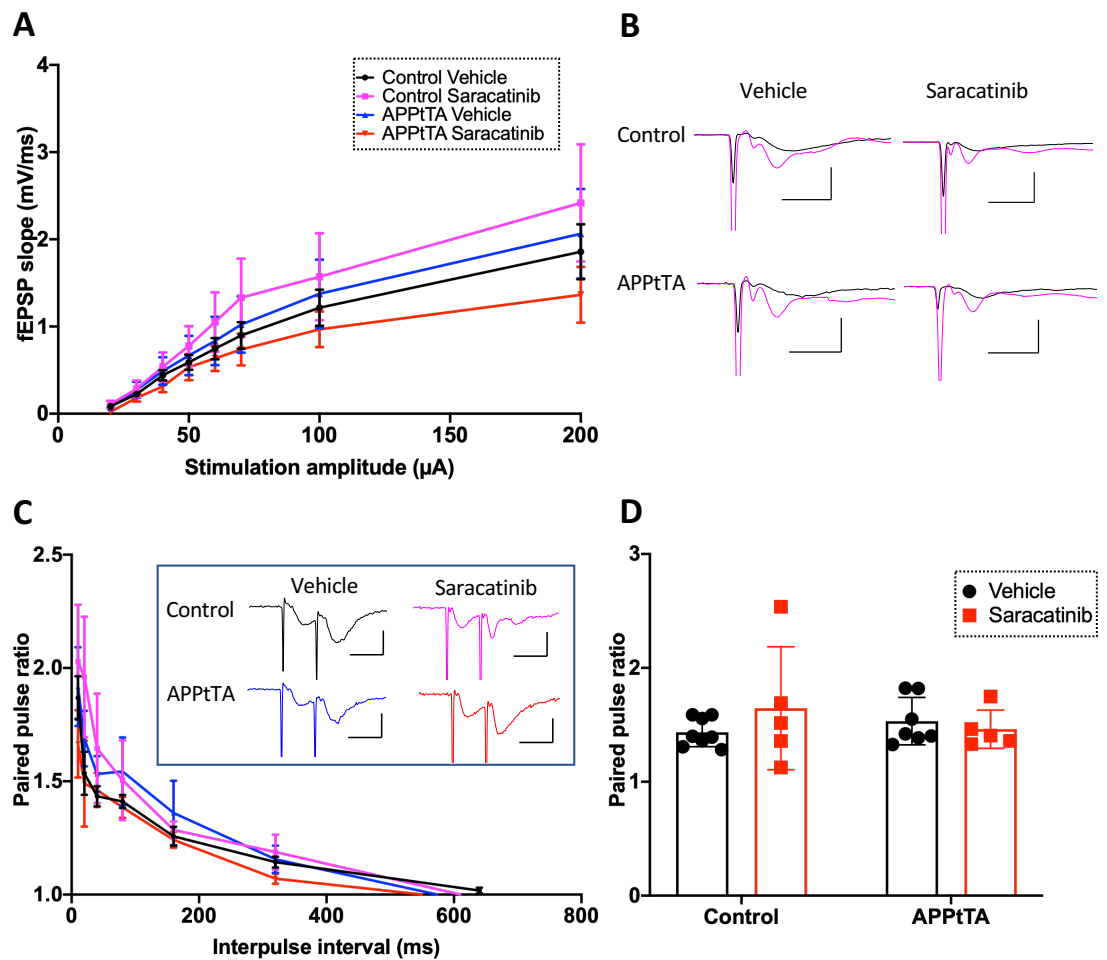


Figure 5.2 The effect of acute Saracatinib treatment on basal synaptic transmission in hippocampal slices from Line 102 mice after 3 weeks of dox removal

**(A)** Input-output responses from hippocampal slices from APPTTA mice treated with 2  $\mu$ M Saracatinib or vehicle control and slices from control littermates treated with 2  $\mu$ M Saracatinib or vehicle control for 2 hours. Data presented as n=slice. Control vehicle n=12, control Saracatinib n=4, APPTTA vehicle n=6, APPTTA Saracatinib n=5. **(B)** Example traces showing the fEPSP in response to 40  $\mu$ A (black) and 200  $\mu$ A (magenta) stimulus input for each condition. Scale bar calibration: 5 ms, 2 mV. **(C)** Paired pulse response from hippocampal slices from APPTTA mice treated with 2  $\mu$ M Saracatinib or vehicle and slices from control littermates treated with 2  $\mu$ M Saracatinib or vehicle. Example traces showing the fEPSPs in response to a pair of pulses delivered with 40 ms interstimulus interval for Saracatinib and vehicle treated conditions. Scale bar calibration: 10 ms, 0.5 mV. Data presented as n=slice. Control vehicle n=8, control Saracatinib n=5, APPTTA vehicle n=7, APPTTA Saracatinib n=5. **(D)** Analysis of the paired pulse ratio at 40 ms interpulse interval extracted from **(C)**. Experiments were performed in an interface-style

rig and the aCSF contained 1  $\mu$ M Gabazine. Data are represented as n=slice, mean  $\pm$  SEM. All data were analysed using a 3-way RM ANOVA.

Next, I aimed to investigate whether Saracatinib was beneficial at later time points when A $\beta$  is allowed to accumulate for 12 weeks. Previous work showed that 12 weeks of APP<sub>Swe/Ind</sub> expression in APPTTA mice reduced LTP in CA3-CA1 synapses and impaired IO responses (Sri et al., 2019). This suggests that, as well as synaptic plasticity deficits, CA3-CA1 synapses also show impaired glutamatergic synaptic transmission. Given my previous observation of a smaller effect size in LTP impairment, I chose to express APP<sub>Swe/Ind</sub> for a slightly longer (to 16 weeks) to maximise the LTP impairment. Using a time point where IO are impaired also provides the opportunity to test whether Saracatinib rescues deficits in basal synaptic transmission. We hypothesised that an acute reduction in GluN2B pY1472 is unlikely to rescue IO deficits because basal synaptic transmission is mediated primarily by AMPARs since NMDAR remained inactive due the Mg<sup>2+</sup> block. However, it is possible that Saracatinib acting on other SFKs, or Fyn broader targets, may rescue the IO deficits.

## 5.4 Replicating LTP impairments in 16-week off dox Line 102 mice

Before applying Saracatinib, I first aimed to determine whether I could reproduce a significant impairment in LTP in this later time point in Line 102 mice. To test this, I recorded TBS-induced LTP in CA3-CA1 synapses from hippocampal slices of 16-week off dox Line 102 mice. Analysis of the fEPSP slope from 40-45 mins after induction revealed no significant difference in LTP between APPTTA and control mice (*Figure 5.3, unpaired t-test p=0.311, control n=4 and APPTTA n= 5*). This suggests that the synaptic mechanism for LTP induction and expression is intact in CA3-CA1 synapses of these mice, indicating a recovery of synaptic plasticity as A $\beta$  continues to accumulate. Recovery in synaptic plasticity is reported in the A $\beta$ -accumulating PDAPP model (expressing APP<sub>Ind</sub>), where TBS-induced LTP in CA3-CA1 synapses is impaired in 4-5-month-old mice but not in 27-29-month-old mice (J. Larson et al., 1999). However, the mechanisms engaged to permit this remain unknown. Prolonged exposure to A $\beta$  could initiate compensatory mechanisms which could induce synaptic changes that permit normal plasticity in Line 102 mice after 16 weeks of APP<sub>Swe/Ind</sub> expression. However, LTP deficits have been observed up to 29 weeks of APP<sub>Swe/Ind</sub> expression in this model. Alternative explanations for the lack of reproducibility between my recordings and Sri et al 2019 will be explored in Section 5.6. Nevertheless, since I did not detect a

deficit in plasticity, I did not continue with this experiment to test the effect of Saracatinib on this readout.

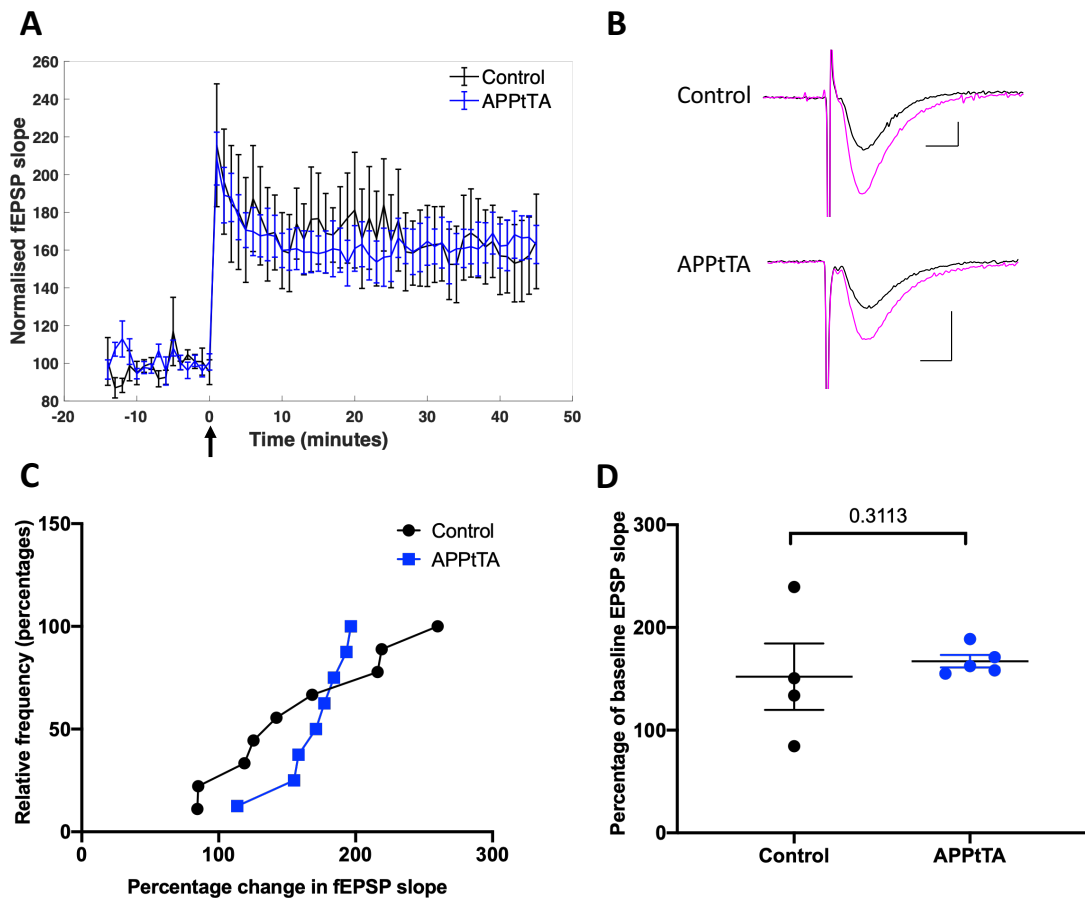


Figure 5.3 The level of LTP in hippocampal slices from Line 102 mice after 16 weeks of dox removal

**(A)** TBS-induced LTP (arrowhead) in hippocampal slices from APtTA mice (n=8 slices, 5 mice) and control littermates (n=9 slices, 4 mice). **(B)** Example LTP traces showing the fEPSP before (black) and after LTP induction (magenta) for APtTA and control littermate slices. Scale bar calibration: 10 ms, 0.5 mV. **(C,D)** Percentage change in the fEPSP slope in the final 5 minutes after LTP-induction represented in a cumulative frequency plot **(C)** and bar graph **(D)**. Experiments were formed in a interface-style rig in standard aCSF solution. Data are presented as mean  $\pm$  SEM, n=slice in (C) where control n= 9 and APtTA n= 8, and n=mouse in (D) where control n=4 and APtTA n= 5. Data were analysed using one-tailed unpaired t-test.

## 5.5 Acute application of Saracatinib does not rescue impaired basal synaptic transmission in 16-week off dox Line 102 mice

Signs of impaired synaptic transmission in CA3-CA1 synapses become evident after 12 weeks of APP<sub>Swe/Ind</sub> expression in APPtTA mice, which is detected in the form of reduced IO responses (Sri et al., 2019). The effect is even more pronounced by 29 weeks of APP<sub>Swe/Ind</sub> expression, suggesting a progressive decline in glutamatergic transmission as A $\beta$  accumulates. I aimed to replicate these impairments following 16 weeks of APP<sub>Swe/Ind</sub> expression to test whether the deficit could be rescued by Saracatinib.

Analysis of IO responses using a repeated measures three-way ANOVA showed a significant effect of stimulus amplitude ( $F(7, 567)=280.7, p<0.0001$ , Control vehicle  $n=20$ , control Saracatinib  $n=14$ , APPtTA vehicle  $n=17$ , APPtTA Saracatinib  $n=12$ ) and of genotype ( $F(1, 81)=32.21, p<0.001$ , Control vehicle  $n=20$ , control Saracatinib  $n=14$ , APPtTA vehicle  $n=17$ , APPtTA Saracatinib  $n=12$ ). (Figure 5.4. A,B). Dunnett's multiple comparisons revealed a significant reduction in IO responses in slices from APPtTA mice compared to controls at all inputs from 50  $\mu$ A to 200  $\mu$ A inclusive. This demonstrates that synaptic transmission in CA3-CA1 synapses is impaired in APPtTA after 16 weeks of APP<sub>Swe/Ind</sub> expression, which agrees with previous reports from Sri et al 2019. The three-way ANOVA also revealed no significant effect of Saracatinib treatment ( $F(1,81)=1.065, p=0.3052$ , Control vehicle  $n=20$ , control Saracatinib  $n=14$ , APPtTA vehicle  $n=17$ , APPtTA Saracatinib  $n=12$ ) suggesting that acute Saracatinib does not rescue impaired IO in Line 102 mice after 16 weeks of APP<sub>Swe/Ind</sub> expression. PPR was similar across all four groups (Figure 5.4. C). Analysis of the 40 ms interstimulus interval using a two-way ANOVA revealed no significant effect of genotype ( $F(1,62)=0.292, p=0.591$  or treatment  $F(1,62)=3.014, p=0.088$  or of genotype  $\times$  treatment interaction  $F(1,62)=0.252, p=0.617$ , Control vehicle  $n=21$ , control Saracatinib  $n=15$ , APPtTA vehicle  $n=17$ , APPtTA Saracatinib  $n=13$ ). This shows that PPR is not affected by 16 weeks of APP<sub>Swe/Ind</sub> expression nor by acute Saracatinib application at CA3-CA1 synapses.

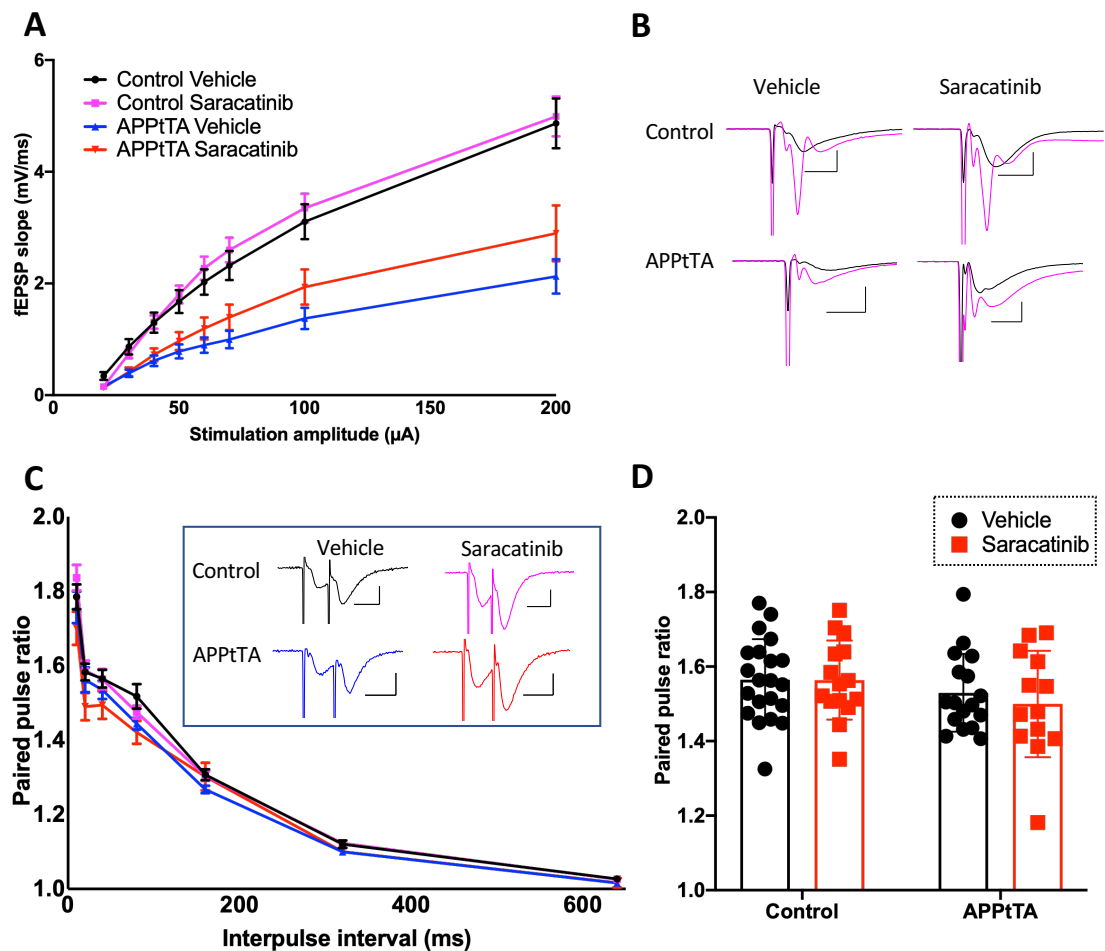


Figure 5.4 The effect of acute Saracatinib treatment on basal synaptic transmission in hippocampal slices from Line 102 mice after 16 weeks of dox removal

**(A)** Input-output responses from hippocampal slices from APPTTA mice treated with 2 μM Saracatinib or vehicle and slices from control littermates treated with 2 μM Saracatinib or vehicle for 2 hours. Data are represented as n=slice. Control vehicle n=20, control Saracatinib n=14, APPTTA vehicle n=17, APPTTA Saracatinib n=12. **(B)** Example traces showing the fEPSP in response to 40 μA (black) and 200 μA (magenta) stimulus input for each condition. Scale bar calibration: 5 ms, 2 mV. **(C)** Paired pulse response from hippocampal slices from APPTTA mice treated with 2 μM Saracatinib or vehicle and slices from control littermates treated with 2 μM Saracatinib or vehicle. Example traces showing the fEPSPs in response to a pair of pulses delivered with 40 ms interstimulus interval for Saracatinib and vehicle treated conditions. Scale bar calibration: 10 ms, 0.5 mV. Data are represented as n=slice. Control vehicle n=21, control Saracatinib n=15, APPTTA vehicle n=17, APPTTA Saracatinib n=13. **(D)** Analysis of the paired pulse ratio at 40 ms interstimulus interval extracted from **(C)**. Experiments were performed in an interface-style rig in standard aCSF solution. All data are represented as n=slice, mean

+/- SEM. Data were analysed using a 3-way RM ANOVA and Dunnett multiple comparisons

## 5.6 Discussion

In this chapter I aimed to determine whether acute Saracatinib treatment rescues early synaptic transmission and plasticity impairments in CA3-CA1 synapses from hippocampal slices of Line 102 mice after 3 and 16 weeks of APP<sub>Swe/Ind</sub> expression. I performed electrophysiological field recordings of CA3-CA1 synapses from hippocampal slices of Line 102 mice and showed that acute Saracatinib application rescues TBS-induced LTP impairments in Line 102 mice following 3 weeks of APP<sub>Swe/Ind</sub> expression, whilst LTP of control mice remain unaffected. I also show that basal synaptic transmission in CA3-CA1 synapses of APP<sub>PtTA</sub> mice after 3 weeks of APP<sub>Swe/Ind</sub> expression is comparable to control mice and, similarly to findings in WT mice, this is not altered by acute Saracatinib application. Line 102 mice that have expressed APP<sub>Swe/Ind</sub> for 16 weeks showed normal TBS-induced LTP but impaired basal synaptic transmission in the form of impaired IO responses. However, this was not rescued by Saracatinib. Overall, the findings in this chapter show that early synaptic plasticity impairments in Line 102 mice following 3 weeks of APP<sub>Swe/Ind</sub> expression is rescued by acute application of Saracatinib. However, later deficits in basal synaptic transmission following 16 weeks of APP<sub>Swe/Ind</sub> are not rescued.

### 5.6.1 The effect of acute Saracatinib application to CA3-CA1 synapses of Line 102 mice following 3 weeks of APP<sub>Swe/Ind</sub> expression

The Saracatinib-mediated rescue of LTP recorded in this project (Figure 5.1) supports behavioural findings showing that administration of Saracatinib *in vivo* rescues learning and memory deficits in APP/ mice (Kaufman et al., 2015)(see Section 1.11). Therefore, my findings support the suggestion that Saracatinib may be useful for the treatment of AD. In addition, since synaptic dysfunction is first detected after 3-weeks of APP<sub>Swe/Ind</sub> expression in the line 102 model, my findings also suggest that Saracatinib may be useful specifically in the early stages of AD pathology.



It is not clear whether Saracatinib rescues plasticity deficits (described here) and memory deficits (previously described by Kaufman et al., 2015) as a result of reducing Fyn or other SFK activity. More work is needed to define the mechanism by which Saracatinib lends its beneficial effects, for example testing whether Fyn- or Src- specific inhibitors produce a similar rescue as Saracatinib. This could lead to the generation of new drug(s) to target the specific kinase responsible. I planned to use TAT-Fyn(39-47) to test Fyn inhibition in isolation, however since I did not see an effect of this drug in WT mice (Figure 3.3), I did not carry it forward into experiments with Line 102 mice. Alternative approaches to define how acute Saracatinib rescued LTP impairments in Line 102 mice could include incorporating conditional knockout mouse models of individual SFKs into the Line 102 model, however this line would need to be designed and engineered. For example, mice with a drug-inducible knockout of each SFK can be generated using the Cre/loxP system. This is a powerful tool for mammalian gene editing and works by expressing Cre recombinase (Cre) which recognises two specific DNA sequences called loxP sites. The DNA sequence between the two loxP sites is excised by Cre, causing a knockout of the gene of interest (Kim et al., 2018). In inducible Cre lines, Cre activity is controlled pharmacologically, for example by tamoxifen, allowing adult-induced knockouts and therefore avoiding potentially developmental confounds.

Wfs1-Tg3-CreERT2 mice express tamoxifen-inducible Cre recombinase under the control of the mouse Wolfram Syndrome 1 (*Wfs1*) promoter where *cre* activity is observed in the cortex, hippocampus, striatum, thalamus and cerebellum following tamoxifen administration (Madisen et al., 2010). This line could be used as the driver line. Mutant mice with loxP sites flanking part of each SFK need to be generated and crossed with the driver line to create Cre/loxP mice. Cre/loxP mice for each SFK can then be crossed with Line 102 mice to generate a mouse model in which APP<sub>Swe/Ind</sub> expression can be induced by dox and specific SFK knockout can be induced using tamoxifen. Electrophysiological experiments can be performed on slices from these mice to determine whether ablation of specific SFK activity prevents the LTP after 3 weeks and/or the IO deficit after 16 weeks. This would avoid the confounds of disrupting SFK expression during development and allow inhibition of specific SFKs chronically and without off target effects. This will help determine which of the SFKs contribute to early synaptic dysfunction in Line 102 mice. However, this experiment would be expensive and time consuming. This technique could be bypassed if specific SFK inhibitors are generated which can be administered to mice *in vivo*.

### 5.6.2 The effect of acute Saracatinib application to CA3-CA1 synapses of Line 102 mice following 16 weeks of APP<sub>Swe/Ind</sub> expression

Here, I observed impaired IO responses in APPTA mice following 16 weeks of APP<sub>Swe/Ind</sub> expression compared to controls (Figure 5.4). This has been previously reported in Line 102 mice and other A $\beta$ -accumulating mouse models (reviewed by Dietrich et al., 2018) and suggests that A $\beta$  decreases glutamatergic synaptic transmission. IO responses do not distinguish whether the deficit is due to pre or postsynaptic changes, and therefore PPR is used to examine the presynaptic component. Since I observed no significant difference in PPRs between genotypes, the impaired IO response suggests a deficit in the postsynaptic compartment.

Application of A $\beta$ 42 to WT primary hippocampal neurons reduced endogenous cell-surface GluA2 expression (Liu et al., 2010) (Almeida et al., 2005). Similarly, co-expression of APP and fluorescently-tagged GluA2 in organotypic hippocampal slices significantly reduced surface expressed GluA2 and depressed both AMPA and NMDAR-mediated synaptic transmission (Hsieh et al., 2006). The GluA2-AMPA endocytosis following A $\beta$  application required GluA2 Ser880 phosphorylation, which promotes GluA2 internalisation from the surface (Liu et al., 2010). Together, these studies agree that A $\beta$  drives the internalisation of AMPARs via phosphorylation of GluA2 subunits at S880. Therefore, it is possible that a similar mechanism may be occurring in Line 102 mice following 16 weeks of APP<sub>Swe/Ind</sub> expression where A $\beta$  accumulation causes GluA2 Ser880 phosphorylation and drives AMPAR internalisation. This could explain the reduced IO responses reported here and in Sri et al 2019. Future experiments could investigate whether this is the underlying cause of the reduced IO responses by using biotinylation to measure surface levels of AMPARs in acute slices from APPTA mice and controls.

It is also possible that the decreased synaptic responses are due to synapse loss. A decrease in pre- and postsynaptic markers, synapsin and PSD-95 are detected in cortical extracts APPTA mice following 49 weeks of APP<sub>Swe/Ind</sub> expression mice compared to controls (Fowler et al., 2014). However, data by S. Sri showed no significant difference in the level of PSD-95 and synaptophysin in the hippocampus of APPTA mice up to 29 weeks of APP<sub>Swe/Ind</sub> expression (Sri, 2018, page 138). This suggests that the impaired IO recorded is not due to loss of these synaptic proteins and suggests that CA3-CA1 synapse loss may not be occurring but the synapses may be non-functional.

I found that acute Saracatinib application was not effective in rescuing the impaired IO responses (Figure 5.4). This suggests that decreasing SFK activity acutely is not sufficient to rescue this phenotype. Previous work quantified pre- and post-synaptic markers and showed that administration of Saracatinib for 7 weeks *in vivo* rescued synapse loss in 12-month-old APP/PS1 mice (Kaufman et al., 2015). Therefore, we questioned whether chronic administration of Saracatinib *in vivo* is required to rescue the impaired IO responses recorded in this project. However, since previous work by Dr Sarmi Sri detected no difference in pre- and post-synaptic markers, it is unclear whether longer term application of Saracatinib *in vivo* will be effective. A better understanding of the mechanisms underlying the impaired IO recorded in this project and by Sri et al 2019 (for example whether it is due to decreased AMPAR expression at the postsynaptic site) will be useful in identifying alternative approaches to rescue this impairment.

Here, I detected no significant difference in LTP between genotypes but impaired IO following 16 weeks of APP<sub>Swe/Ind</sub> expression. This means that although glutamatergic transmission is weakened, the synapses are still plastic and can strengthen in response to LTP induction by TBS (Figure 5.3). It is not clear why the impaired LTP observed after 3 weeks of APP<sub>Swe/Ind</sub> expression is recovered by 16 weeks of expression. This correlates with GluN2B pY1472, which is enhanced after 3 weeks but not after 16 weeks of APP<sub>Swe/Ind</sub> expression. However, this increase was seen in fresh-frozen tissue and not sliced hippocampus where I recorded the LTP deficit. Therefore, whether enhanced GluN2B pY1472 contributes to LTP deficits in slice remains unclear. Recovery in LTP has not been reported before in Line 102 and previous work showed that TBS-induced LTP in CA3-CA1 synapses is evident up to 29 weeks of APP<sub>Swe/Ind</sub> expression (Sri et al., 2019). We hypothesise that the disparity in findings could arise due to subtle difference in technique. For example, the time taken to extract and slice the brain, the speed of the vibratome and how the slices are handled once they are freed will all affect the quality of the slices (Papouin et al., 2018). A $\beta$  load in the brain increases vulnerability to external stressors *in vivo*, for example injection of A $\beta$  peptide into the rodent brain exacerbates memory impairments and cell death caused by ischaemia (Song et al., 2013). Therefore, slices from APP<sub>TtTA</sub> mice which contain high levels of A $\beta$  may be more susceptible to *ex vivo* manipulations during brain extraction and slicing. It is possible that differences in brain extraction or slice acquisition and maintenance in this project means that electrophysiological differences between genotypes are less pronounced. This could also explain why the decrease in LTP recorded in APP<sub>TtTA</sub> following 3 weeks of APP<sub>Swe/Ind</sub> expression had a much smaller effect size compared to data reported by Sri et al 2019.

Another possibility to explain why I was unable to reproduce findings by Sri et al could be due to genetic drift in the colony. The COVID-19 pandemic caused many groups to reduce the size of their mouse colony and this has highlighted how maintaining mouse colonies with reduced numbers speeds up genetic drift (Moncaut et al., 2021). The majority of mutations that occur are undetectable but some can cause phenotypic variation and this could compromise reproducibility of research with that line. As a small lab group, our Line 102 colony was small in size and this was worsened during the pandemic. Therefore, this prompted us to check the basic properties of the line.

Western blotting confirmed that the level of APP<sub>Swe/Ind</sub> expression upon dox removal in the mice used in this project is comparable to the mice used in the Sri et al 2019 publication (Figure 2.1 B). I also tested whether the dox diet was working to suppress APP<sub>Swe/Ind</sub> expression (Figure 2.1 A). This was important to test because compensatory effects occur if APP<sub>Swe/Ind</sub> is expressed during development (See Section 1.6.1). Therefore, if the dox was not working effectively, this could counteract LTP deficits. However, my results showed that the dox diet was working effectively to suppress APP<sub>Swe/Ind</sub> expression. Together, these findings suggest that there have been no detectable changes in APP<sub>Swe/Ind</sub> expression levels or in the ability of the TetOff system to suppress APP<sub>Swe/Ind</sub> expression in the presence of dox. However, it is possible that other mutations could have occurred to the line but unfortunately, there are currently no reliable and affordable technologies to check for genetic drift.

## 5.7 Conclusions

In this Chapter, I show that acute application of Saracatinib rescues TBS-induced LTP in CA3-CA1 synapses from APP<sup>Ta</sup>TA hippocampal slices mice following 3 weeks off APP<sub>Swe/Ind</sub> expression. This suggests that acute inhibition of SFKs rescues A $\beta$ -induced synaptic plasticity deficits when they first arise in this model. Whether this occurs via Fyn or GluN2B pY1472 requires further investigation and detailed future experiments to test this are discussed in Section 6.2. I also show that, following a longer period of A $\beta$  accumulation to 16 weeks, acute application of Saracatinib does not rescue deficits in basal synaptic transmission in the model. However, impairments in synaptic transmission may be caused by the loss of plasticity (discussed in Section 1.6.1) (Sri et al., 2019). Therefore, Saracatinib may successfully prevent, rather than reverse, synaptic transmission deficits if administered before its onset. An experimental designed to test this is proposed in Chapter 6. Overall, this work builds on the evidence supporting Fyn inhibition for the treatment of

AD, and we suggest that it may be useful specifically in earlier stages of pathology before the onset of memory loss and correlating synapse loss. This could explain why Saracatinib did not slow cognitive decline when administered to individuals with mild-to-moderate AD (Nygaard et al., 2015) (Section 1.11). Future identification of biomarkers to detect AD in individuals prior to symptom onset will be required to test whether Saracatinib is beneficial in the earlier stages of AD in humans.



## Chapter 6 Overall conclusions and future work

### 6.1 Research question and main findings

The molecular mechanisms underlying the onset of synaptic dysfunction and plasticity in Alzheimer's disease are not clear. One candidate is Fyn, since its activity is increased in AD (Larson et al., 2012), and phosphorylation of Fyn targets (GluN2B and Pyk2) are increased in AD mouse models (Ittner et al., 2010; Kaufman et al., 2015) and following A $\beta$  application in neuronal cell cultures (Larson et al., 2012; Um et al., 2012). Whether Fyn activity is increased in the early stages of AD pathology (and if so, whether it contributes to synaptic defects) is poorly understood. One reason for this is a lack of experimental models that allow investigation into early AD. Even human tissue from individuals with MCI gives limited insight into early AD mechanisms because not all individuals in the cohort continue to develop dementia, and this correlates with the high variability in the level of active Fyn (Fyn pY416) in this cohort (Larson et al., 2012).

The Line 102 mouse model is a powerful tool to model aspects of early AD because A $\beta$  expression can be induced on demand, allowing the onset of A $\beta$  accumulation and pathology after brain development has occurred. This means that the transition from healthy to dysfunctional synapses can be followed more closely, which allows the investigation into whether Fyn contributes to this. I used previously mapped time points following APP<sub>Swe/Ind</sub> expression: when CA3-CA1 synapses first show reduced plasticity (after 3 weeks) and reduced basal synaptic transmission (after 12 weeks) (Sri et al., 2019). I quantified the level of GluN2B pY1472 in freshly-frozen hippocampus and cortex as a method to infer Fyn activity. Next, I prepared hippocampal slices from these mice and WT mice and measured basal synaptic transmission and TBS-induced LTP with and without acute Saracatinib incubation. From this, I was able to determine whether acute inhibition of Fyn and other SFKs by Saracatinib rescues the early loss of LTP in this model whilst also assessing the impact on normal synaptic function and plasticity in slices from WT mice.

The key findings of this thesis are:

1. Saracatinib reduces GluN2B pY1472 but does not alter basal synaptic function and plasticity in CA3-CA1 synapses when applied acutely to hippocampal slices from adult WT mice.

2. Acute application of Saracatinib to hippocampal slices from Line 102 mice rescues early LTP impairments in CA3-CA1 synapses that occur after 3 weeks of APP<sub>Swe/Ind</sub> expression
3. Later impairments in basal synaptic transmission in CA3-CA1 synapses of Line 102 mice following 16 weeks of APP<sub>Swe/Ind</sub> expression are not rescued by acute application of Saracatinib to hippocampal slices.

## 6.2 Limitations of this study and recommendations for future research

### 6.2.1 Using mouse models to study Alzheimer's Disease

Mouse models are valuable tools for understanding human disease mechanisms in a complex mammalian organism. They are especially important for understanding the mechanistic onset and development of disease, for example the preclinical stages of AD. This is because current medicine is not able to identify people with preclinical AD and so mouse models provide a means to understand disease onset mechanisms. This thesis utilises the Line 102 mouse line which provides the unique advantage of controlling the onset of APP expression and therefore A $\beta$  accumulation. In this thesis, the mice were able to develop normally and then begin A $\beta$  accumulation once the mice had reached sexual maturity at 6 weeks old (Figure 1.7). This is advantageous because it avoids compensatory mechanisms and/or abnormal development to occur, and this has been shown previously in Line 102 mice (discussed in Section 1.6.1, Sri et al., 2019).

Although powerful, there are disadvantages to using mouse models to study AD. There are multiple transgenic mouse lines that recapitulate different aspects of AD, such as A $\beta$  or tau accumulation. These models can differ further depending on the mouse strain, transgene constructs and promotor used to express the transgene. For example, the chosen promotor impacts where the protein accumulates and to what extent. This makes it difficult to compare between mouse lines and may explain why some findings are not reproducible between mouse models. In addition, A $\beta$  accumulation in transgenic models is achieved by overexpression of APP. Therefore, it is difficult to determine whether any effects recorded are due to A $\beta$  accumulation or accumulation of APP or other APP cleavage fragments shown in Figure 1.2. Finally, like other mouse models of A $\beta$  accumulation, Line 102 mice do not present with neurofibrillary tau pathology. This is important to highlight as the pathology caused by neurofibrillary tangles and



the interplay between A $\beta$  and tau will not be modelled in these mice, and therefore the mice do not perfectly mimic AD pathology. The lack of success of AD clinical trials could be partly due to translation of findings from transgenic mice that model only aspects of AD pathology to humans (reviewed by Drummond et al., 2017). To avoid this, the ideal experiment should use human tissue wherever possible. Resected human brain tissue from neurosurgeries can be thinly sliced and used for electrophysiological recordings to understand synaptic transmission and plasticity. However, it is not possible to use human tissue from AD patients because the tissue is only available post-mortem and this is not suitable for electrophysiological recordings. Therefore, AD mouse models are a good option to study intact, functioning synapses and gain a better understanding synaptic transmission and plasticity whilst mimicking aspects of AD pathology.

### **6.2.2 Measuring GluN2B Y1472 phosphorylation as a readout of Fyn activity**

In this thesis I measured the level of GluN2B Y1472 to infer Fyn activity in samples from APPTA vs control mice and vehicle vs Saracatinib treated samples. This residue was chosen because it is a known site phosphorylated by Fyn and is suggested to contribute to AD pathology and regulation of synaptic plasticity (discussed in Section 1.8 and 1.10.5). Phosphorylation status of other targets could also have been measured, for example Pyk2. This would have provided further evidence to show that Saracatinib inhibited broad SFKs when applied to adult mouse hippocampal slices. In addition, assessing the phosphorylation status of other SFK targets would be useful to determine whether only Fyn or also other SFKs are increased in Line 102 mice. The ideal experiment would be to measure the activity of each SFK individually by measuring the phosphorylation status of the active site (Y420). However, this is not possible since there are currently no available active-SFK specific antibodies. One solution to this problem would be to isolate Fyn by performing an immunoprecipitation assay using a Fyn-specific antibody before probing the with a non-specific antibody of active SFKs. This experiment could be repeated for other SFKs to get a clearer indication of changes in individual SFK activity.

A further reason for measuring GluN2B Y1472 phosphorylation was because GluN2B Y1472 phosphorylation and subsequent increases in NMDAR currents is specific to Fyn and not other SFKs, for example increased NMDAR currents following intracellular application of recombinant Fyn could be prevented by GluN2B but not GluN2A inhibition and by GluN2B Y1472F transgenic mice (Yang et al., 2012). However, the findings from this thesis do not determine whether enhanced GluN2B Y1472 phosphorylation is causative of the LTP dysfunction measured in CA3-

CA1 synapses of 3-week off dox APPtTA mice. Instead, GluN2B Y1472 phosphorylation is utilised to infer Fyn activity. Phosphorylation at Y1472 by other, currently unknown, kinases is likely and therefore must also be taken into consideration when interpreting the findings from this thesis.

### 6.2.3 Which kinase is responsible for the rescue of LTP by Saracatinib

It remains unknown how Saracatinib yields its beneficial effects both in this project, where its acute application rescues CA3-CA1 plasticity defects in APPtTA mice and in another study, where its chronic administration rescues spatial memory deficits and synaptic depletion in APP/PS1 mice (Kaufman et al., 2015). Saracatinib is a broad SFK inhibitor, meaning that the inhibition of other SFKs, besides Fyn, may contribute to the beneficial effects of Saracatinib recorded here and by others.

Of the SFKs, Src, Lck, Yes, Lyn and Fyn are expressed in the mammalian brain (Yagi, 1994). From these, most studies have focussed on the role of Src and Fyn in synaptic function, with Fyn receiving the most attention in the study of AD pathology, likely due to the fact that its activity is increased in post-mortem tissue from individuals with mild-moderate AD (Larson et al., 2012). Identification of the SFK(s) responsible for the beneficial effect of Saracatinib reported here and by others (Kaufman et al., 2015; Smith et al., 2018) would be a useful avenue for further research. This could suggest which particular SFK(s) contribute early pathological mechanisms driven by A $\beta$  and may aid the generation of future more specific drugs that could be tested for the treatment of early AD.

In this project, I found that Saracatinib rescued LTP deficits in CA3-CA1 synapses in hippocampal slices from Line 102 mice after 3 weeks of APP<sub>Swe/Ind</sub> expression. One way to determine which SFK(s) must be inhibited to produce this rescue in plasticity is to use SFK-specific inhibitors. I planned to complete this by applying membrane-permeable TAT-Fyn(39-47) to hippocampal slices from Line 102 mice after weeks of APP<sub>Swe/Ind</sub> expression to test whether Fyn inhibition specifically rescues LTP in CA3-CA1 synapses. However, the application of TAT-Fyn(39-47) to adult WT hippocampal slices did not alter GluN2B pY1472, suggesting unsuccessful Fyn inhibition (Chapter 3). We hypothesise that this could be due to a number of reasons such as ineffective drug penetration through the slice and into cells, low basal Fyn activity in the slices prior to treatment, or that another kinase could also phosphorylate Y1472 of GluN2B.

An alternative approach is to use whole-cell patch clamp electrophysiology and include the Fyn(39-47) peptide in the recording pipette solution. This allows dialysis of Fyn(39-47) into the cell and bypasses the need for the TAT peptide, whilst Fyn(Scram) peptide is used as a control. Taking hippocampal slices from APP<sup>Ta</sup> and control mice after 3 weeks of APP<sup>Swe/Ind</sup> expression, Fyn can be inhibited in individual CA1 pyramidal cells using whole-cell patch clamp. Similar to field recording experiments conducted in this project, a stimulation electrode can be placed in the CA3 field to extracellularly stimulate Schaffer collaterals. Whilst holding the patched CA1 neuron at -70 mV, evoked excitatory postsynaptic currents (EPSCs) can be recorded in response to Schaffer collateral stimulation. After obtaining a stable EPSC baseline, LTP can be induced by a TBS or pre- and postsynaptic pairing protocols (Zhao et al., 2005). Under physiological conditions, the EPSC amplitude increases following TBS. In line with my field LTP experiments, I hypothesise that this potentiation will be significantly impaired in CA1 cells in Line 102 mice after 3 weeks of APP<sup>Swe/Ind</sup> expression. Whether this is rescued by Fyn(39-47) will provide mechanistic insight into whether Fyn inhibition is sufficient to rescue plasticity deficits in CA3-CA1 synapses in this model. This experiment can be repeated using the Src(40-58) inhibitor peptide to determine whether Src inhibition is able to rescue plasticity deficits. Specific inhibitors of Lck, Yes and Lyn are not available, and so their contribution cannot be tested using this method.

#### **6.2.4 Which SFK target protein(s) is responsible for the rescue of LTP by Saracatinib?**

SFK inhibition by Saracatinib reduces SFK-mediated phosphorylation of target proteins. We hypothesised that Saracatinib rescued LTP deficits in CA3-CA1 synapses in hippocampal slices from Line 102 mice after 3 weeks of APP<sup>Swe/Ind</sup> expression by reducing GluN2B pY1472. I found that the slicing procedure increased GluN2B pY1472 in hippocampal slices from adult WT mice. This may explain why enhanced GluN2B pY1472 when comparing APP<sup>Ta</sup> and control mice after 3 weeks of APP<sup>Swe/Ind</sup> expression is seen in freshly-frozen hippocampal tissue but not in hippocampal slices. Even though GluN2B pY1472 was similar in slices between genotypes, acute Saracatinib application could still rescue LTP impairments in CA3-CA1 synapses from APP<sup>Ta</sup> mice. It is therefore possible that enhanced GluN2B pY1472 observed in fresh-frozen tissue does not contribute to the LTP deficit recorded in slices in APP<sup>Ta</sup> mice, and therefore reduced phosphorylation of other SFK targets, besides GluN2B pY1472 should be considered.

It is difficult to test whether the reduction of GluN2B pY1472 is solely responsible for the rescued plasticity deficits by Saracatinib in this model because there are currently no drugs to inhibit phosphorylation at this site without also reducing the phosphorylation of other proteins. Instead, transgenic mice could be employed, for example, GluN2B Y1472F (non-phosphorylatable) mutant mice. Previous work using this model showed that these mice display impaired fear learning and amygdaloid LTP and, although the data were not available, the authors also stated that hippocampal LTP was comparable between Y1472F and control mice (Nakazawa et al., 2006). A relatively simple experiment would be to apply A $\beta$  to hippocampal slices from WT and GluN2B Y1472F and record TBS-induced LTP to determine whether GluN2B pY1472 is required for A $\beta$  to impair LTP. Cortical cultures and hippocampal slices from Fyn<sup>-/-</sup> mice are protected by A $\beta$ -induced cell death and dendritic spine loss (Um et al., 2012) (Lambert et al., 1998), and NMDAR antagonists fully rescue dendritic spine loss after 5 hours (Um et al., 2012). This suggests that Fyn and NMDARs contribute to synapse loss and neuronal cell death. Electrophysiological recordings following the application of A $\beta$  to slices from GluN2B Y1472F mice would complement these studies and suggest whether GluN2B pY1472 is required for A $\beta$  to impair LTP. Similarly, GluN2B Y1472E phosphomimetic mice could be utilised to model increased GluN2B Y1472 phosphorylation. To date, there are no findings published using this mouse model. Whether CA3-CA1 LTP is affected in slices from these mice would determine whether enhanced Y1472 phosphorylation is sufficient to impair LTP at these synapses. If LTP is reduced, whether application of A $\beta$  impairs LTP further would give further information to suggest whether GluN2B pY1472 is required for A $\beta$  to impair LTP.

### **6.2.5 Pyk2 may contribute to the beneficial effects of Saracatinib**

An alternative target of Fyn is the AD risk gene product, Pyk2 (Lambert et al., 2013). Pyk2 is a non-receptor tyrosine kinase that belongs to the focal adhesion kinase (FAK) non-receptor tyrosine kinase family. Application of 2  $\mu$ M Saracatinib to WT hippocampal slices from 3-4-week-old mice decreased Pyk2 phosphorylation at the site required for Pyk2 activation (pY402), suggesting reduced Pyk2 activity following acute SFK inhibition (Kaufman et al., 2015). Here, I applied Saracatinib to hippocampal slices at the same concentration and timings as Kaufman et al., and so I hypothesise that Pyk2 pY402 is also decreased in Saracatinib treated slices in this project and the potential implications of this on synaptic plasticity are discussed in Section 6.2.5.2. Future work to quantify the level of Pyk2 pY402 is required to support this and could be addressed using Western blotting of hippocampal slice lysates following the incubation with Saracatinib or vehicle. Based on previous findings showing that acute Saracatinib treatment decreases Pyk2 activity, it is

therefore possible that reduced Pyk2 activity could contribute to how Saracatinib rescued LTP in slices from APPTA mice after 3 weeks of APP<sub>Swe/Ind</sub> expression.

#### **6.2.5.1 The synergistic relationship between Fyn and Pyk2**

Pyk2 is activated in two steps: initial priming occurs via phosphorylation at Y402, which is a prerequisite for full activation by phosphorylation at Y579. Pyk2 Y402 and Y579 phosphorylation were significantly reduced in HeLa cells by SFK inhibitors (SU11333 and PP2), suggesting a role of SFKs in activating Pyk2 (Zhao et al., 2016). Further supporting this, overexpression of Src significantly increased Pyk2 pY402 whilst a kinase-dead form of Src reduced pY402 (Zhao et al., 2016). Fyn<sup>-/-</sup> mice display reduced Pyk2 pY402, whilst CA-Fyn expressing mice show increased Pyk2 pY402 (Li et al., 2018). Together, these findings suggest that Src and Fyn contribute to the activation of Pyk2.

As well as Fyn and Src-mediated phosphorylation of Pyk2, Pyk2 also phosphorylates Src and Fyn, suggesting a synergistic relationship between the kinases. This is supported by evidence from Pyk2<sup>-/-</sup> mice which show decreased SFK pY420, suggesting decreased SFK activity without Pyk2 (Giralt et al., 2017). GluN2B pY1472 is also decreased in Pyk2<sup>-/-</sup> mice, however it is not known whether Pyk2 phosphorylates GluN2B directly or whether the decrease in GluN2B pY1472 is attributed only to decreased Fyn activity. Therefore, it is possible that Pyk2 and Fyn have similar effects on LTP by acting on converging pathways leading to GluN2B pY1472.

#### **6.2.5.2 Pyk2 and synaptic plasticity**

Pyk2 activity is suggested to play a role in plasticity, and this is supported by whole-cell patch clamp data showing that LTP is blocked when Pyk2 is inhibited in isolated CA1 cells from 2-3-week-old rats (Bartos et al., 2010). Pyk2 inhibition was achieved by including the SH3 domain of PSD-95 or the SH3 binding site on Pyk2 in the patch pipette. Pyk2 interaction with SH3-PSD-95 is required for full Pyk2 activation, therefore preventing this interaction inhibits Pyk2 (Bartos et al., 2010). LTP is also prevented by intracellular administration of kinase-dead Pyk2 in CA1 cells from hippocampal slices of 4-6-week old WT rats (Huang et al., 2001).

CA3-CA1 synapses show reduced HFS-induced LTP in hippocampal slices from 3-4-month-old *Pyk2*<sup>-/-</sup> mice (Giralt et al., 2017). This was not due to developmental confounds since the results were replicated in 3-month-old mice bearing floxed *Pyk2* alleles to allow reduced *Pyk2* expression after development (starting at 4-weeks) (Giralt et al., 2017). In line with these findings, *Pyk2*<sup>-/-</sup> mice also show impairments in spatial learning and memory (Giralt et al., 2017). However, Salazar and colleagues showed normal TBS-induced LTP in CA3-CA1 synapses from 2-6-month-old *Pyk2*<sup>-/-</sup> mice (Salazar et al., 2019). The different induction protocols used could explain the different conclusions drawn from these studies. To address this, CA3-CA1 LTP was induced in hippocampal slices from *Pyk2*<sup>-/-</sup> mice by either HFS or TBS (Mastrolia et al., 2021). The data showed that *Pyk2*<sup>-/-</sup> slices display reduced LTP induced by HFS but not by TBS. Therefore, the absence of *Pyk2* impairs CA3-CA1 LTP in a protocol-dependent manner.

In this project I showed that acute application of Saracatinib causes no detectable change in TBS-induced LTP at CA3-CA1 synapses. Therefore, if my hypothesis that *Pyk2* activity is decreased by Saracatinib in adult hippocampal slices, my data would suggest that acute inhibition of *Pyk2* does not alter synaptic plasticity at CA3-CA1 synapses. However, repeat experiments to induce LTP using HFS-induction protocols would be useful to determine whether acute application of Saracatinib alters LTP in a protocol-dependent manner.

### 6.2.5.3 AD relevance

*Pyk2* activity is implicated in the pathogenesis of AD by evidence showing increased *Pyk2* activity in hippocampal and cortical lysates from 11-month-old APP/PS1 mice (Kaufman et al., 2015) and following application of A $\beta$  to WT hippocampal slices (Haas et al., 2016; Kaufman et al., 2015). *Pyk2* activity in post-mortem AD tissue has not been reported but may help determine whether this finding translates from rodent models to human AD. Overexpression of *Pyk2* in mouse hippocampal neuron cultures increased *Pyk2* pY402 and decreased spine density (Lee et al., 2019), suggesting that increased *Pyk2* activity contributes to synapse loss.

Reducing *Pyk2* in AD models is protective against AD-related phenotypes. For example, acute application of 2  $\mu$ M Saracatinib prevents A $\beta$ -induced increase in *Pyk2* activity in WT hippocampal slices (Kaufman et al., 2015). Genetic deletion of *Pyk2* prevents A $\beta$ -induced memory impairments, synapse loss, astrogliosis and synaptic plasticity in APP/PS1 mice (Salazar et al., 2019). These

findings suggest that A $\beta$  increase Pyk2 activity, and decreasing Pyk2 activity (pharmacologically or via genetic manipulation) provides protection against A $\beta$ -induced toxicity. Whether Pyk2 inhibition also protects against A $\beta$ -induced deficit in synaptic plasticity is not known. Since reducing Pyk2 activity in a physiological background impairs HFS-induced LTP and spatial learning and memory (Giralt et al., 2017; Mastrolia et al., 2021), it suggests that a fine balance of Pyk2 activity is required for normal synaptic plasticity and memory. This highlights the importance of measuring the effect of Saracatinib on synaptic plasticity in hippocampal slices from WT mice.

In this project, I did not measure the level of Pyk2 pY402 in brain lysates or slices from APPtTA mice. I found that GluN2B pY1472 is increased following 3 weeks of APP<sub>Swe/Ind</sub> expression, suggesting increased Fyn activity. Given that Fyn also phosphorylates Pyk2 to lead to Pyk2 activation, I hypothesise that Pyk2 activity may also be increased in brain lysates at this time point however this remains to be determined. Like GluN2B pY1472, Pyk2 pY402 is increased in response to slicing (Ho et al., 2004), therefore whether increased Pyk2 activity contributes to the loss of LTP recorded in slices from APPtTA mice following 3 weeks of APP<sub>Swe/Ind</sub> expression is not clear. To overcome slicing-induced increases in phosphorylation in GluN2B, Pyk2 and potentially other proteins, *in vivo* LTP could be used. This would allow experimentation without slicing artefacts, however this would require optimisation of *in vivo* administration of Saracatinib to mice.

The mechanism by which Pyk2 contributes to AD-related phenotypes is not clear. Modulating Pyk2 activity alters GluN2B pY1472, suggesting that Pyk2 has a role in the phosphorylation of GluN2B pY1472 (Giralt et al., 2017). Whether this occurs directly by Pyk2 or via Fyn through synergistic SFK activation is not clear, but decreased GluN2B pY1472 following Pyk2 inhibition could explain why reducing Pyk2 activity is protective against A $\beta$ . This may explain the beneficial effects of Saracatinib reported here and by others (Kaufman et al., 2015).

#### 6.2.5.4 Experimental proposal

Here I report that acute Saracatinib application to slices from APPtTA mice following 3 weeks of APP<sub>Swe/Ind</sub> expression rescues TBS-induced LTP. If Pyk2 inhibition contributes to how Saracatinib rescues the early loss of LTP in this model, then Pyk2 inhibition alone should yield similar results. PF-719 is a Pyk2-selective inhibitor that prevented dendritic spine loss caused by overexpression of Pyk2 in hippocampal neuronal cultures (S. Lee et al., 2019) and PF-719 (500 nM) pre-treatment

for 30 mins prevented the loss of TBS-induced LTP by application of synthetic A $\beta$  in hippocampal slices from 2-6-month-old WT mice (Salazar et al., 2019). This suggests that Pyk2 is essential for A $\beta$ -mediated synaptic plasticity deficits. To complement this work and to test whether increased Pyk2 activity contributes to the impairment in LTP in Line 102 mice recorded in Chapter 5, TBS-induced LTP can be recorded in hippocampal slices from control and APPtTA mice following 3 weeks of APP<sub>Swe/Ind</sub> expression with or without the application of 500 nM PF-719 for 30mins. This experiment would contribute to the understanding of why synaptic plasticity deficits first arise in CA3-CA1 synapses of APPtTA mice and whether they can be rescued by Pyk2 inhibition. However, this approach would not conclude whether Saracatinib acts solely via Pyk2 to rescue the phenotype and, given the synergistic relationship between Fyn and Pyk2, this may not be possible. It is possible that the benefits of Pyk2 inhibition reported by others (Lee et al., 2019; Salazar et al., 2019) occur by reducing phosphorylation of GluN2B Y1472, either directly by inhibiting Pyk2 from phosphorylating GluN2B, or indirectly by disrupting Pyk2 activation of Fyn.

### 6.2.6 Does chronic Saracatinib prevent synapse loss in Line 102

In this project, I showed that acute application of Saracatinib does not rescue IO impairments in hippocampal slices from APPtTA mice following 16 weeks of APP<sub>Swe/Ind</sub> expression. Acute application of Saracatinib was unable to rescue the IO impairment, however we hypothesise that it may be able to prevent it if Saracatinib is administered before the onset of synaptic dysfunction. In APPtTA mice that have been off dox for 3 weeks, re-administering dox for 9-11 weeks rescued A $\beta$ <sub>40</sub> and A $\beta$ <sub>42</sub> levels back to levels of littermate controls and rescued the impairment in TBS-induced LTP in CA3-CA1 synapses (Sri et al., 2019). This also prevented the progressive reduction in basal synaptic transmission, since deficits in IO responses were prevented (Sri et al., 2019). This suggests that preventing the loss of synaptic plasticity may prevent the subsequent reduction in synaptic transmission. Therefore, since Saracatinib prevents the loss of LTP after 3 weeks of APP<sub>Swe/Ind</sub> expression, its chronic administration may also prevent later impairments in IO responses.

#### 6.2.6.1 Experimental proposal

Since acute hippocampal slices are not viable for more than 6-12 hours (Buskila et al., 2014), a chronic experiment would require *in vivo* administration of Saracatinib. This could be performed by removing the dox diet from Line 102 mice at 6 weeks old and then, after 3 weeks off dox,



Saracatinib is administered at 5mg/kg/day, as previously described by (Kaufman et al., 2015). After 13 weeks of Saracatinib administration (and 16-weeks of APP<sub>Swe/Ind</sub> expression) the mice are sacrificed for slice preparation and electrophysiological experiments to measure LTP and IO responses in CA3-CA1 synapses. This experimental design is illustrated in Figure 6.1.

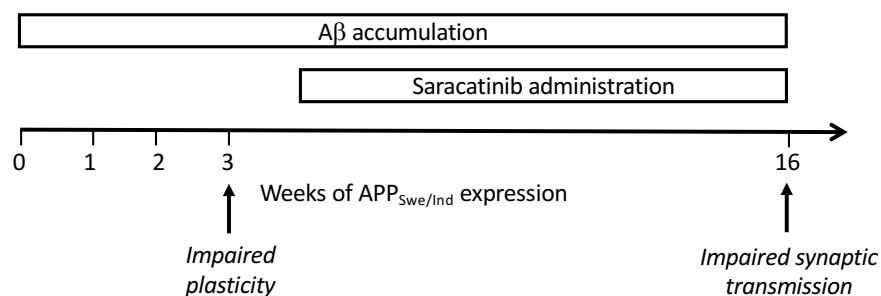


Figure 6.1 Experiment design for administration of Saracatinib in vivo using Line 102 mice

Experimental design to determine whether Saracatinib is able to rescue TBS-induced LTP deficits and the later reduction in basal synaptic transmission in CA3-CA1 synapses. At 6 weeks old (0 weeks of APP<sub>Swe/Ind</sub> expression, the dox diet is removed from Line 102 mice to cause Aβ accumulation in APPtTA mice. After 3 weeks off dox (when LTP is first impaired), Saracatinib administration begins 5mg/kg/day, as previously described by (Kaufman et al., 2015). After 13 weeks of Saracatinib administration (and 16 weeks of APP<sub>Swe/Ind</sub> expression) the mice are sacrificed and TBS-induced LTP and IO responses are measured in APPtTA mice and control litter mates. Equal numbers of APPtTA and control mice will be administered vehicle to control for Saracatinib.

For this experiment to be completed successfully, two factors to be addressed: firstly, *in vivo* administration of Saracatinib needs to be optimised. I was unable to reproduce findings by Kaufman et al., 2015 as I did not detect an effect of *in vivo* Saracatinib application after 3 days in WT mice. As discussed in Section 3.2.5, the difumarate form of Saracatinib used by Kaufman and colleagues may be required to ensure efficient BBB penetration. Secondly, this experiment relies on the hypothesis that *in vivo* application of Saracatinib to APPtTA mice will rescue LTP after 3 weeks of APP<sub>Swe/Ind</sub> expression in the same way that I found acute application can rescue LTP in Chapter 5. If the early reduction in LTP recorded after 3 weeks of APP<sub>Swe/Ind</sub> expression is responsible for the subsequent reduction in IO responses recorded after 16 weeks of APP<sub>Swe/Ind</sub> expression, then I would expect that, if *in vivo* application of Saracatinib prevents the loss of LTP

at 3 weeks, then extended administration will prevent the later reduction in IO responses. This would mean early treatment with SFK inhibitor can prevent later loss of synapses in Line 102 mice.

This work will contribute to our understanding of the early disease mechanisms driven by A $\beta$ . If in vivo administration of Saracatinib is effective in preventing both LTP and IO deficits in this model, this would add further evidence to support the use of Saracatinib and SFK inhibitors as a preventative treatment to be trialled in humans at the very early stages of AD. This may also explain why Saracatinib did not slow the rate of decline of cognition when trialled in patients with mild-moderate AD (Nygaard et al., 2015), since early synaptic changes would already be in place. Effective treatment with SFK inhibitors may therefore require the development of early diagnostic tools or biomarkers to identify individuals at these very early stages where Saracatinib could prove to be effective.

### 6.3 Conclusions and perspective

Despite the growing burden of AD, there are currently no disease-modifying treatments available to help those currently suffering from AD. There is growing evidence supporting the role of Fyn in the pathophysiology of AD. Fyn is an attractive target given its essential role in A $\beta$  signal transduction but also interacts with Tau, bridging the gap between the two major pathological hallmarks of AD.

Using an inducible mouse model of AD, my findings support the body of evidence suggesting that Fyn activity is increased in AD. My results suggest that this increase may occur early in disease progression, possibly before symptom onset. My findings also support studies in suggesting that Saracatinib or other SFK inhibitors remain a promising therapeutic target for the treatment of AD. Potential future discoveries of biomarkers to identify AD before symptom onset would be required to test whether Saracatinib can prevent or slow symptom onset in humans.

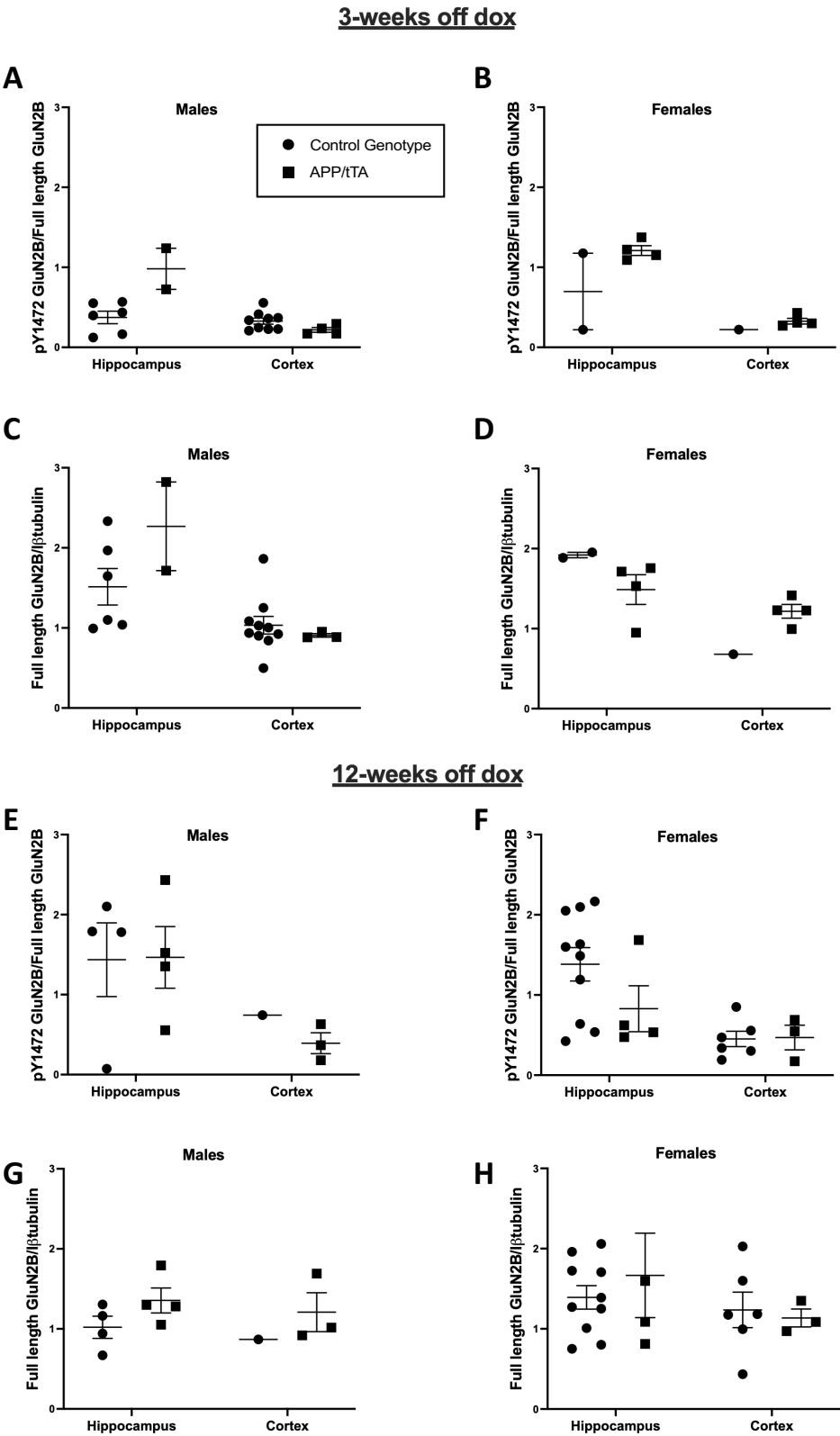
One of the major questions left following this work is to determine which SFK and downstream signalling pathway is responsible for the ability of Saracatinib to rescue AD-related phenotypes in mice and whether these downstream pathways are also engaged in human disease. Identification

of these pathways may enable the generation of more specific drugs which may have limited side effects and prove to be effective for the treatment of early AD. The identification of a drug that is able to prevent onset or slow symptom progression in AD would benefit the lives of millions of individuals with AD, and reduce the economic burden of AD.



## **Appendix A      The effect of sex on GluN2B pY1472 in Line 102 mice**

Data shown in Figure 4.1 and Figure 4.2 were reanalysed to compare the level of GluN2B and the ratio of GluN2B pY1472 to GluN2B in male and female Line 102 mice following 3 and 12-weeks off dox. The hippocampus and cortex were analysed separately. We found that grouping the data by sex did not reveal any effects on the level of GluN2B or GluN2B pY1472 (Appendix A.1). However, this analysis reduced the size of the dataset considerably and therefore repeat experiments may be required to determine whether any effects are revealed.



Appendix A.1: Reanalysis of data to compare the level of GluN2B and pY1472 GluN2B in the hippocampus and cortex of Line 102 mice within sex.

**(A-D)** Quantification of the proportion of GluN2B subunits phosphorylated at Y1472 (A-B) and quantification of GluN2B/ $\beta$ -tubulin (C-D) in the hippocampus and cortex of APPtTA mice and control littermates after 3 weeks off dox. **(E-H)** Quantification of the proportion of GluN2B subunits phosphorylated at Y1472 (E-F) and quantification of GluN2B/ $\beta$ -tubulin (G-H) in the hippocampus and cortex of APPtTA mice and control littermates after 12 weeks off dox. **(A, C, E and G)** show data collected from male mice and **(B, D, F and H)** show data collected from female mice. All data are presented as N=mouse, mean  $\pm$  SEM. Data were analysed using a two-way ANOVA.





## List of References

- Alberts, B., Johnson, A., Lewis, J., Raff, M., Roberts, K., & Walter, P. (2001). *Molecular Biology of the Cell. 4th edition*. New York: Garland Science/Taylor & Francis LLC.
- Alexander, G. E., Chen, K., Pietrini, P., Rapoport, S. I., & Reiman, E. M. (2002). Longitudinal PET evaluation of cerebral metabolic decline in dementia: A potential outcome measure in Alzheimer's disease treatment studies. *American Journal of Psychiatry*, 159(5), 738–745.
- Almeida, C. G., Tampellini, D., Takahashi, R. H., Greengard, P., Lin, M. T., Snyder, E. M., & Gouras, G. K. (2005). Beta-amyloid accumulation in APP mutant neurons reduces PSD-95 and GluR1 in synapses. *Neurobiology of Disease*, 20(2), 187–198.
- Andersen, P. (1981). Brain slices- a neurobiological tool of increasing usefulness. *Trends in Neurosciences*, 4(C), 53–56.
- Andersen, P., Morris, R., Amaral, D., Bliss, T., & O'Keefe, J. (2009). The Hippocampus Book. In *The Hippocampus Book*.
- Armada-Moreira, A., Gomes, J. I., Pina, C. P., Savchak, O. K., Gonçalves-Ribeiro, J., Rei, N., ... Vac, S. H. (2020). Going the Extra (Synaptic) Mile: Excitotoxicity as the Road Toward Neurodegenerative Diseases. *Frontiers in Cellular Neuroscience*, 14, 90.
- Asante, E. A., Gowland, I., Linehan, J. M., Mahal, S. P., & Collinge, J. (2002). Expression pattern of a mini human PrP gene promoter in transgenic mice. *Neurobiology of Disease*, 10(1), 1–7.
- Ascher, P., & Nowak, L. (1988). The role of divalent cations in the N-methyl-D-aspartate responses of mouse central neurones in culture. *The Journal of Physiology*, 399, 247–266.
- Barria, A., Derkach, V., & Soderling, T. R. (1997). Identification of the Ca<sup>2+</sup>/Calmodulin-dependent Protein Kinase II Regulatory Phosphorylation Site in the  $\alpha$ -Amino-3-hydroxyl-5-methyl-4-isoxazole-propionate-type Glutamate Receptor. *Journal of Biological Chemistry*, 272(52), 32727–32730.
- Barria, A., & Malinow, R. (2005). NMDA Receptor Subunit Composition Controls Synaptic Plasticity by Regulating Binding to CaMKII. *Neuron*, 48(2), 289–301.
- Bartos, J. A., Ulrich, J. D., Li, H., Beazely, M. A., Chen, Y., MacDonald, J. F., & Hell, J. W. (2010). Postsynaptic Clustering and Activation of Pyk2 by PSD-95. *Journal of Neuroscience*, 30(2), 449–463.

## List of References

- Baselga, J., Cervantes, A., Martinelli, E., Chirivella, I., Hoekman, K., Hurwitz, H. I., ... Tabernero, J. (2010). Phase I safety, pharmacokinetics, and inhibition of src activity study of saracatinib in patients with solid tumors. *Clinical Cancer Research*, 16(19), 4876–4883.
- Bayer, K. U., De Koninck, P., Leonard, A. S., Hell, J. W., & Schulman, H. (2001). Interaction with the NMDA receptor locks CaMKII in an active conformation. *Nature* 2001 411:6839, 411(6839), 801–805.
- Bayer, K. U., Löhler, J., Schulman, H., & Harbers, K. (1999). Developmental expression of the CaM kinase II isoforms: Ubiquitous  $\gamma$ - and  $\delta$ -CaM kinase II are the early isoforms and most abundant in the developing nervous system. *Molecular Brain Research*, 70(1), 147–154.
- Beggs, H. E., Soriano, P., & Maness, P. F. (1994). NCAM-dependent neurite outgrowth is inhibited in neurons from Fyn-minus mice. *The Journal of Cell Biology*, 127(3), 825–833.
- Belyaev, N. D., Kellett, K. A. B., Beckett, C., Makova, N. Z., Revett, T. J., Nalivaeva, N. N., ... Turner, A. J. (2010). The transcriptionally active amyloid precursor protein (APP) intracellular domain is preferentially produced from the 695 isoform of APP in a  $\beta$ -secretase-dependent pathway. *Journal of Biological Chemistry*, 285(53), 41443–41454.
- Benilova, I., Gallardo, R., Ungureanu, A. A., Cano, V. C., Snellinx, A., Ramakers, M., ... De Strooper, B. (2014). The Alzheimer Disease Protective Mutation A2T Modulates Kinetic and Thermodynamic Properties of Amyloid- $\beta$  (A $\beta$ ) Aggregation. *The Journal of Biological Chemistry*, 289(45), 30977.
- Benilova, I., Karran, E., & De Strooper, B. (2012, March 29). The toxic A $\beta$  oligomer and Alzheimer's disease: An emperor in need of clothes. *Nature Neuroscience*, Vol. 15, pp. 349–357.
- Bezzina, C., Verret, L., Juan, C., Remaud, J., Halley, H., Rampon, C., & Dahan, L. (2015). Early onset of hypersynchronous network activity and expression of a marker of chronic seizures in the Tg2576 mouse model of Alzheimer's disease. *PLoS ONE*, 10(3), e0119910.
- Bi, C., Bi, S., & Li, B. (2019). Processing of Mutant  $\beta$ -Amyloid Precursor Protein and the Clinicopathological Features of Familial Alzheimer's Disease. *Aging and Disease*, 10(2), 383.
- Bierer, L. M., Hof, P. R., Purohit, D. P., Carlin, L., Schmeidler, J., Davis, K. L., & Perl, D. P. (1995). Neocortical Neurofibrillary Tangles Correlate With Dementia Severity in Alzheimer's Disease. *Archives of Neurology*, 52(1), 81–88.
- Bittner, T., Burgold, S., Dorostkar, M. M., Fuhrmann, M., Wegenast-Braun, B. M., Schmidt, B., ... Herms, J. (2012). Amyloid plaque formation precedes dendritic spine loss. *Acta*

- Neuropathologica*, 124(6), 797–807.
- Bliss, T. V. P., & Lømo, T. (1973). Long-lasting potentiation of synaptic transmission in the dentate area of the anaesthetized rabbit following stimulation of the perforant path. *The Journal of Physiology*, 232(2), 331–356.
- Boggon, T. J., & Eck, M. J. (2004, October 18). Structure and regulation of Src family kinases. *Oncogene*, Vol. 23, pp. 7918–7927.
- Bolmont, T., Clavaguera, F., Meyer-Luehmann, M., Herzig, M. C., Radde, R., Staufenbiel, M., ... Jucker, M. (2007). Induction of tau pathology by intracerebral infusion of amyloid- $\beta$ -containing brain extract and by amyloid- $\beta$  deposition in APP x tau transgenic mice. *American Journal of Pathology*, 171(6), 2012–2020.
- Born, H. A., Kim, J. Y., Savjani, R. R., Das, P., Dabaghian, Y. A., Guo, Q., ... Jankowsky, J. L. (2014). Genetic suppression of transgenic APP rescues hypersynchronous network activity in a mouse model of alzheimer's disease. *Journal of Neuroscience*, 34(11), 3826–3840.
- Bortolotto, Z. A., Amici, M., Anderson, W. W., Isaac, J. T. R., & Collingridge, G. L. (2011). Synaptic plasticity in the hippocampal slice preparation. *Current Protocols in Neuroscience*, Chapter 6(Unit 6.13).
- Bourne, J. N., & Harris, K. M. (2012). Nanoscale analysis of structural synaptic plasticity. *Current Opinion in Neurobiology*, 22(3), 372–382.
- Braak, H., & Braak, E. (1995). Staging of alzheimer's disease-related neurofibrillary changes. *Neurobiology of Aging*, 16(3), 271–278.
- Brion, J. P., Smith, C., Couck, A. M., Gallo, J. M. M., & Anderton, B. H. (1993). Developmental Changes in  $\tau$  Phosphorylation: Fetal  $\tau$  Is Transiently Phosphorylated in a Manner Similar to Paired Helical Filament- $\tau$  Characteristic of Alzheimer's Disease. *Journal of Neurochemistry*, 61(6), 2071–2080.
- Brothers, H. M., Gosztyla, M. L., & Robinson, S. R. (2018, April 25). The physiological roles of amyloid- $\beta$  peptide hint at new ways to treat Alzheimer's disease. *Frontiers in Aging Neuroscience*, Vol. 10, p. 118.
- Buée, L., Bussière, T., Buée-Scherrer, V., Delacourte, A., & Hof, P. R. (2000, August 1). Tau protein isoforms, phosphorylation and role in neurodegenerative disorders. *Brain Research Reviews*, Vol. 33, pp. 95–130.

## List of References

- Bureau, I., Bischoff, S., Heinemann, S. F., & Mulle, C. (1999). Kainate Receptor-Mediated Responses in the CA1 Field of Wild-Type and GluR6-Deficient Mice. *The Journal of Neuroscience*, 19(2), 653.
- Buskila, Y., Breen, P. P., Tapson, J., Van Schaik, A., Barton, M., & Morley, J. W. (2014). Extending the viability of acute brain slices. *Scientific Reports* 2014 4:1, 4(1), 1–7.
- Buzsáki, G., & Moser, E. I. (2013). Memory, navigation and theta rhythm in the hippocampal-entorhinal system. *Nature Neuroscience*, 16(2), 130–138.
- Chen, G. F., Xu, T. H., Yan, Y., Zhou, Y. R., Jiang, Y., Melcher, K., & Xu, H. E. (2017, September 1). Amyloid beta: Structure, biology and structure-based therapeutic development. *Acta Pharmacologica Sinica*, Vol. 38, pp. 1205–1235.
- Cheng, I. H., Searce-Levie, K., Legleiter, J., Palop, J. J., Gerstein, H., Bien-Ly, N., ... Mucke, L. (2007). Accelerating amyloid- $\beta$  fibrillization reduces oligomer levels and functional deficits in Alzheimer disease mouse models. *Journal of Biological Chemistry*, 282(33), 23818–23828.
- Chin, J., Palop, J. J., Puoliväli, J., Massaro, C., Bien-Ly, N., Gerstein, H., ... Mucke, L. (2005). Fyn kinase induces synaptic and cognitive impairments in a transgenic mouse model of Alzheimer's disease. *Journal of Neuroscience*, 25(42), 9694–9703.
- Chin, J., Palop, J. J., Yu, G. Q., Kojima, N., Masliah, E., & Mucke, L. (2004). Fyn kinase modulates synaptotoxicity, but not aberrant sprouting, in human amyloid precursor protein transgenic mice. *Journal of Neuroscience*, 24(19), 4692–4697.
- Choi, D. W. (1992). Excitotoxic cell death. *Journal of Neurobiology*, 23(9), 1261–1276.
- Cline, E. N., Bicca, M. A., Viola, K. L., & Klein, W. L. (2018). The Amyloid- $\beta$  Oligomer Hypothesis: Beginning of the Third Decade. *Journal of Alzheimer's Disease*, Vol. 64, pp. S567–S610.
- Collingridge, G. L., Kehl, S. J., & McLennan, H. (1983). Excitatory amino acids in synaptic transmission in the Schaffer collateral-commissural pathway of the rat hippocampus. *The Journal of Physiology*, 334, 33–46.
- Convit, A., De Asis, J., De Leon, M. J., Tarshish, C. Y., De Santi, S., & Rusinek, H. (2000). Atrophy of the medial occipitotemporal, inferior, and middle temporal gyri in non-demented elderly predict decline to Alzheimer's disease. *Neurobiology of Aging*, 21(1), 19–26.
- Cull-Candy, S., Kelly, L., & Farrant, M. (2006). Regulation of Ca<sup>2+</sup>-permeable AMPA receptors: synaptic plasticity and beyond. *Current Opinion in Neurobiology*, 16(3), 288–297.

- Del Vecchio, R. A., Gold, L. H., Novick, S. J., Wong, G., & Hyde, L. A. (2004). Increased seizure threshold and severity in young transgenic CRND8 mice. *Neuroscience Letters*, 367(2), 164–167.
- Delgado, J. Y., Fink, A. E., Grant, S. G. N., O'dell, T. J., & Opazo, P. (2018). Rapid homeostatic downregulation of LTP by extrasynaptic GluN2B receptors. *Journal of Neurophysiology*, 120(5), 2351–2357.
- Derkach, V., Barria, A., & Soderling, T. R. (1999). Ca<sup>2+</sup>/calmodulin-kinase II enhances channel conductance of alpha-amino-3-hydroxy-5-methyl-4-isoxazolepropionate type glutamate receptors. *Proceedings of the National Academy of Sciences of the United States of America*, 96(6), 3269–3274.
- Dietrich, K., Bouter, Y., Mller, M., & Bayer, T. A. (2018). Synaptic Alterations in Mouse Models for Alzheimer Disease—A Special Focus on N-Truncated Abeta 4-42. *Molecules : A Journal of Synthetic Chemistry and Natural Product Chemistry*, 23(4), 718.
- Drummond, E., & Wisniewski, T. (2017). Alzheimer's disease: experimental models and reality. *Acta Neuropathologica*, 133(2), 155–175.
- Dunah, A. W., Sirianni, A. C., Fienberg, A. A., Bastia, E., Schwarzschild, M. A., & Standaert, D. G. (2004). Dopamine D1-Dependent Trafficking of Striatal N-Methyl-D-aspartate Glutamate Receptors Requires Fyn Protein Tyrosine Kinase but Not DARPP-32. *Molecular Pharmacology*, 65(1), 121–129.
- Eguchi, K., Velicky, P., Hollergschwandtner, E., Itakura, M., Fukazawa, Y., Danzl, J. G., & Shigemoto, R. (2020). Advantages of Acute Brain Slices Prepared at Physiological Temperature in the Characterization of Synaptic Functions. *Frontiers in Cellular Neuroscience*, 14–63.
- Erreger, K., Dravid, S. M., Banke, T. G., Wyllie, D. J. A., & Traynelis, S. F. (2005). Subunit-specific gating controls rat NR1/NR2A and NR1/NR2B NMDA channel kinetics and synaptic signalling profiles. *The Journal of Physiology*, 563(Pt 2), 345–358.
- Fadool, D. A., Holmes, T. C., Berman, K., Dagan, D., & Levitan, I. B. (1997). Tyrosine phosphorylation modulates current amplitude and kinetics of a neuronal voltage-gated potassium channel. *Journal of Neurophysiology*, 78(3), 1563–1573.
- Fitzjohn, S. M., Kuenzi, F., Morton, R. A., Rosahl, T. W., Lewis, H., Smith, D., ... Collingridge, G. L. (2010). A study of long-term potentiation in transgenic mice over-expressing mutant forms of both amyloid precursor protein and presenilin-1. *Molecular Brain*, 3(1), 21.

## List of References

- Forner, S., Baglietto-Vargas, D., Martini, A. C., Trujillo-Estrada, L., & LaFerla, F. M. (2017). Synaptic Impairment in Alzheimer's Disease: A Dysregulated Symphony. *Trends in Neurosciences*, 40(6), 347–357.
- Fowler, S. W., Chiang, A. C. A., Savjani, R. R., Larson, M. E., Sherman, M. A., Schuler, D. R., ... Jankowsky, J. L. (2014). Genetic modulation of soluble A $\beta$  rescues cognitive and synaptic impairment in a mouse model of Alzheimer's disease. *Journal of Neuroscience*, 34(23), 7871–7885.
- Gad, S. C., Cassidy, C. D., Aubert, N., Spainhour, B., & Robbe, H. (2006). Nonclinical Vehicle Use in Studies by Multiple Routes in Multiple Species. *International Journal of Toxicology*, 25, 499–521.
- Gao, Y.-L., Wang, N., Sun, F.-R., Cao, X.-P., Zhang, W., & Yu, J.-T. (2018). Tau in neurodegenerative disease. *Annals of Translational Medicine*, 6(10), 175.
- Garcia-Alloza, M., Robbins, E. M., Zhang-Nunes, S. X., Purcell, S. M., Betensky, R. A., Raju, S., ... Frosch, M. P. (2006). Characterization of amyloid deposition in the APPswe/PS1dE9 mouse model of Alzheimer disease. *Neurobiology of Disease*, 24(3), 516–524.
- Giese, K. P., Fedorov, N. B., Filipkowski, R. K., & Silva, A. J. (1998). Autophosphorylation at Thr286 of the  $\alpha$  calcium-calmodulin kinase II in LTP and learning. *Science*, 279, 870–873.
- Giralt, A., Brito, V., Chevy, Q., Simonnet, C., Otsu, Y., Cifuentes-Díaz, C., ... Girault, J. A. (2017). Pyk2 modulates hippocampal excitatory synapses and contributes to cognitive deficits in a Huntington's disease model. *Nature Communications* 2017 8:1, 8(1), 1–16.
- Goedert, M., Spillantini, M. G., Jakes, R., Rutherford, D., & Crowther, R. A. (1989). Multiple isoforms of human microtubule-associated protein tau: sequences and localization in neurofibrillary tangles of Alzheimer's disease. *Neuron*, 3(4), 519–526.
- Gómez-Isla, T., Hollister, R., West, H., Mui, S., Growdon, J. H., Petersen, R. C., ... Hyman, B. T. (1997). Neuronal loss correlates with but exceeds neurofibrillary tangles in Alzheimer's disease. *Annals of Neurology*, 41(1), 17–24.
- Gong, C. X., & Iqbal, K. (2008). Hyperphosphorylation of Microtubule-Associated Protein Tau: A Promising Therapeutic Target for Alzheimer Disease. *Current Medicinal Chemistry*, 15(23), 2321–2328.
- Götz, J., Chen, F., Van Dorpe, J., & Nitsch, R. M. (2001). Formation of neurofibrillary tangles in P301L tau transgenic mice induced by A $\beta$ 42 fibrils. *Science*, 293, 1491–1495.

- Grant, S. G., O'Dell, T. J., Karl, K. A., Stein, P. L., Soriano, P., & Kandel, E. R. (1992). Impaired Long-Term Potentiation, Spatial Learning, and Hippocampal Development in *fyn* Mutant Mice Kandel are in the Center for Neurobiology. *Science*, 258, 1903–1910. Retrieved from <http://science.sciencemag.org/>
- Green, J. L., dos Santos, W. F., & Fontana, A. C. K. (2021). Role of glutamate excitotoxicity and glutamate transporter EAAT2 in epilepsy: Opportunities for novel therapeutics development. *Biochemical Pharmacology*, 193, 114786.
- Green, T. P., Fennell, M., Whittaker, R., Curwen, J., Jacobs, V., Allen, J., ... Costello, G. F. (2009). Preclinical anticancer activity of the potent, oral Src inhibitor AZD0530. *Molecular Oncology*, 3(3), 248–261.
- Greger, I. H., Watson, J. F., & Cull-Candy, S. (2017). Structural and Functional Architecture of AMPA-Type Glutamate Receptors and Their Auxiliary Proteins. *Neuron*, 94(4), 713–730.
- Guglietti, B., Sivasankar, S., Mustafa, S., Corrigan, F., & Collins-Praino, L. E. (2021). Fyn Kinase Activity and Its Role in Neurodegenerative Disease Pathology: a Potential Universal Target? *Molecular Neurobiology*, 58(11), 5986–6005.
- Haas, L. T., & Strittmatter, S. M. (2016). Oligomers of Amyloid  $\beta$  Prevent Physiological Activation of the Cellular Prion Protein-Metabotropic Glutamate Receptor 5 Complex by Glutamate in Alzheimer Disease. *The Journal of Biological Chemistry*, 291(33), 17112.
- Hardingham, G. E., & Bading, H. (2010). Synaptic versus extrasynaptic NMDA receptor signalling: implications for neurodegenerative disorders. *Nature Reviews Neuroscience*, 11(10), 682–696.
- Hardingham, G. E., Fukunaga, Y., & Bading, H. (2002). Extrasynaptic NMDARs oppose synaptic NMDARs by triggering CREB shut-off and cell death pathways. *Nature Neuroscience*, 5(5), 405–414.
- Hardy, J. A., & Higgins, G. A. (1992). Alzheimer's disease: The amyloid cascade hypothesis. *Science*, Vol. 256, pp. 184–185.
- Hartley, D. M., & Choi, D. W. (1989). Delayed rescue of N-methyl-D-aspartate receptor-mediated neuronal injury in cortical culture. *The Journal of Pharmacology and Experimental Therapeutics*, 250(2), 752–758.
- Hatton, C. J., & Paoletti, P. (2005). Modulation of Triheteromeric NMDA Receptors by N-Terminal Domain Ligands. *Neuron*, 46(2), 261–274.

## List of References

- Hawasli, A. H., Benavides, D. R., Nguyen, C., Kansy, J. W., Hayashi, K., Chambon, P., ... Bibb, J. A. (2014). Cyclin-dependent kinase 5 governs learning and synaptic plasticity via control of NMDAR degradation. *Nat Neurosci*, 10(7), 880–886.
- Hayashi, T., & Huganir, R. L. (2004). Tyrosine Phosphorylation and Regulation of the AMPA Receptor by Src Family Tyrosine Kinases. *Journal of Neuroscience*, 24(27), 6152–6160.
- Hayashi, Y., Shi, S. H., Esteban, J. A., Piccini, A., Poncer, J. C., & Malinow, R. (2000). Driving AMPA receptors into synapses by LTP and CaMKII: Requirement for GluR1 and PDZ domain interaction. *Science*, 287, 2262–2267.
- Hebb, D. O. (1949). The Organization of Behavior; A Neuropsychological Theory. In *The Organisation of Behavior*.
- Helboe, L., Egebjerg, J., Barkholt, P., & Volbracht, C. (2017). Early depletion of CA1 neurons and late neurodegeneration in a mouse tauopathy model. *Brain Research*, 1665, 22–35.
- Ho, O. H., Delgado, J. Y., & O'Dell, T. J. (2004). Phosphorylation of proteins involved in activity-dependent forms of synaptic plasticity is altered in hippocampal slices maintained in vitro. *Journal of Neurochemistry*, 91(6), 1344–1357.
- Hsieh, H., Boehm, J., Sato, C., Iwatsubo, T., Tomita, T., Sisodia, S., & Malinow, R. (2006). AMPAR Removal Underlies A $\beta$ -Induced Synaptic Depression and Dendritic Spine Loss. *Neuron*, 52(5), 831–843.
- Huang, Y. Q., Lu, W. Y., Ali, D. W., Pelkey, K. A., Pitcher, G. M., Lu, Y. M., ... MacDonald, J. F. (2001). CAK $\beta$ /Pyk2 kinase is a signaling link for induction of long-term potentiation in CA1 hippocampus. *Neuron*, 29(2), 485–496.
- Inglis, J., Martin, S. J., & Morris, R. G. M. (2013). Upstairs/downstairs revisited: spatial pretraining-induced rescue of normal spatial learning during selective blockade of hippocampal N - methyl- d -aspartate receptors. *European Journal of Neuroscience*, 37(5), 718–727.
- Irizarry, M. C., McNamara, M., Fedorchak, K., Hsiao, K., & Hyman, B. T. (1997). APP(Sw) transgenic mice develop age-related A $\beta$  deposits and neuropil abnormalities, but no neuronal loss in CA1. *Journal of Neuropathology and Experimental Neurology*, 56(9), 965–973.
- Ittner, A., & Ittner, L. M. (2018). Dendritic Tau in Alzheimer's Disease. *Neuron*, 99(1), 13–27.
- Ittner, L. M., Ke, D. Y., Delerue, F., Bi, M., Gladbach, A., van Eersel, J., ... Götz, J. (2010). Dendritic Function of Tau Mediates Amyloid- $\beta$  Toxicity in Alzheimer's Disease Mouse Models. *Cell*,



142(3), 387–397.

- Jackson, H. M., Soto, I., Graham, L. C., Carter, G. W., & Howell, G. R. (2013). Clustering of transcriptional profiles identifies changes to insulin signaling as an early event in a mouse model of Alzheimer's disease. *BMC Genomics*, 14(1), 831.
- Jacobsen, J. S., Wu, C. C., Redwine, J. M., Comery, T. A., Arias, R., Bowlby, M., ... Bloom, F. E. (2006). Early-onset behavioral and synaptic deficits in a mouse model of Alzheimer's disease. *Proceedings of the National Academy of Sciences of the United States of America*, 103(13), 5161–5166.
- Jankowsky, J. L., Slunt, H. H., Gonzales, V., Savonenko, A. V., Wen, J. C., Jenkins, N. A., ... Borchelt, D. R. (2005). Persistent Amyloidosis following Suppression of A $\beta$  Production in a Transgenic Model of Alzheimer Disease. *PLoS Medicine*, 2(12), e355.
- Jarosz-Griffiths, H. H., Noble, E., Rushworth, J. V., & Hooper, N. M. (2016). Amyloid- $\beta$  receptors: The good, the bad, and the prion protein. *Journal of Biological Chemistry*, 291(7), 3174–3183.
- Jazin, E., & Cahill, L. (2010). Sex differences in molecular neuroscience: From fruit flies to humans. *Nature Reviews Neuroscience*, 11(1), 9–17.
- Jolas, T., Zhang, X. S., Zhang, Q., Wong, G., Del Vecchio, R., Gold, L., & Priestley, T. (2002). Long-term potentiation is increased in the CA1 area of the hippocampus of APPswe/ind CRND8 mice. *Neurobiology of Disease*, 11(3), 394–409.
- Jonsson, T., Atwal, J. K., Steinberg, S., Snaedal, J., Jonsson, P. V., Bjornsson, S., ... Stefansson, K. (2012). A mutation in APP protects against Alzheimer's disease and age-related cognitive decline. *Nature*, 488(7409), 96.
- Kaksonen, M., & Roux, A. (2018). Mechanisms of clathrin-mediated endocytosis. *Nature Reviews Molecular Cell Biology* 2018 19:5, 19(5), 313–326.
- Kalia, L. V., Gingrich, J. R., & Salter, M. W. (2004). Src in synaptic transmission and plasticity. *Oncogene* 2004 23:48, 23(48), 8007–8016.
- Kalia, L. V., & Salter, M. W. (2003). Interactions between Src family protein tyrosine kinases and PSD-95. *Neuropharmacology*, 45(6), 720–728.
- Kaufman, A. C., Salazar, S. V., Haas, L. T., Yang, J., Kostylev, M. A., Jeng, A. T., ... Strittmatter, S. M. (2015). Fyn inhibition rescues established memory and synapse loss in Alzheimer mice.

## List of References

- Annals of Neurology*, 77(6), 953–971.
- Kent, S. A., Spires-Jones, T. L., & Durrant, C. S. (2020). The physiological roles of tau and A $\beta$ : implications for Alzheimer's disease pathology and therapeutics. *Acta Neuropathologica* 2020 140:4, 140(4), 417–447.
- Kim, H., Kim, M., Im, S.-K., & Fang, S. (2018). Mouse Cre-LoxP system: general principles to determine tissue-specific roles of target genes. *Laboratory Animal Research*, 34(4), 147.
- Kimura, T., Whitcomb, D. J., Jo, J., Regan, P., Piers, T., Heo, S., ... Cho, K. (2014). Microtubule-associated protein tau is essential for long-term depression in the hippocampus. *Philosophical Transactions of the Royal Society of London. Series B, Biological Sciences*, 369(1633), 20130144.
- Kirov, S. A., Petrak, L. J., Fiala, J. C., & Harris, K. M. (2004). Dendritic spines disappear with chilling but proliferate excessively upon rewarming of mature hippocampus. *Neuroscience*, 127(1), 69–80.
- Kishimoto, Y., Higashihara, E., Fukuta, A., Nagao, A., & Kirino, Y. (2013). Early impairment in a water-finding test in a longitudinal study of the Tg2576 mouse model of Alzheimer's disease. *Brain Research*, 1491, 117–126.
- Klein, M. O., Battagello, D. S., Cardoso, A. R., Hauser, D. N., Bittencourt, J. C., & Correa, R. G. (2019). Dopamine: Functions, Signaling, and Association with Neurological Diseases. *Cellular and Molecular Neurobiology*, 39(1), 31–59.
- Kojima, N., Ishibashi, H., Obata, K., & Kandel, E. R. (1998). Higher Seizure Susceptibility and Enhanced Tyrosine Phosphorylation of N-Methyl-d-Aspartate Receptor Subunit 2B in fyn Transgenic Mice. *Learning & Memory*, 5(6), 429–445.
- Kojima, N., Wang, J., Mansu, I. M., Grant, S. G. N., Mayford, M., & Kandel, E. R. (1997). Rescuing impairment of long-term potentiation in fyn-deficient mice by introducing Fyn transgene. *Proceedings of the National Academy of Sciences of the United States of America*, 94(9), 4761–4765.
- Krämer-Albers, E. M., & White, R. (2011). From axon–glial signalling to myelination: the integrating role of oligodendroglial Fyn kinase. *Cellular and Molecular Life Sciences*, 68(12), 2003–2012.
- Kristensen, A. S., Jenkins, M. A., Banke, T. G., Schousboe, A., Makino, Y., Johnson, R. C., ... Neurosci, N. (2011). Mechanism of Ca<sup>2+</sup>/calmodulin-dependent kinase II regulation of AMPA

- receptor gating. *Nat Neurosci*, 14(6), 727–735.
- Kumar-Singh, S., Theuns, J., Van Broeck, B., Pirici, D., Vennekens, K., Corsmit, E., ... Van Broeckhoven, C. (2006). Mean age-of-onset of familial alzheimer disease caused by presenilin mutations correlates with both increased Abeta42 and decreased Abeta40. *Human Mutation*, 27(7), 686–695.
- Kumar, A. (2011). Long-Term Potentiation at CA3–CA1 Hippocampal Synapses with Special Emphasis on Aging, Disease, and Stress. *Frontiers in Aging Neuroscience*, 3, 7.
- Kumar, A., & Foster, T. C. (2014). Interaction of DHPG-LTD and synaptic-LTD at senescent CA3-CA1 hippocampal synapses. *Hippocampus*, 24(4), 466–475.
- Kurup, P., Zhang, Y., Xu, J., Venkitaramani, D. V., Haroutunian, V., Greengard, P., ... Lombroso, P. J. (2010). A $\beta$ -Mediated NMDA Receptor Endocytosis in Alzheimer's Disease Involves Ubiquitination of the Tyrosine Phosphatase STEP61. *Journal of Neuroscience*, 30(17), 5948–5957.
- Lalonde, R., Kim, H. D., Maxwell, J. A., & Fukuchi, K. (2005). Exploratory activity and spatial learning in 12-month-old APP695SWE/co + PS1/ $\Delta$ E9 mice with amyloid plaques. *Neuroscience Letters*, 390(2), 87–92.
- Lambert, J. C., Ibrahim-Verbaas, C. A., Harold, D., Naj, A. C., Sims, R., Bellenguez, C., ... Seshadri, S. (2013). Meta-analysis of 74,046 individuals identifies 11 new susceptibility loci for Alzheimer's disease. *Nature Genetics*, 45(12), 1452–1458.
- Lambert, M. P., Barlow, A. K., Chromy, B. A., Edwards, C., Freed, R., Liosatos, M., ... Klein, W. L. (1998). Diffusible, nonfibrillar ligands derived from A 1-42 are potent central nervous system neurotoxins. 95, 6448–6453. Retrieved from [www.pnas.org](http://www.pnas.org).
- Lanz, T. A., Carter, D. B., & Merchant, K. M. (2003). Dendritic spine loss in the hippocampus of young PDAPP and Tg2576 mice and its prevention by the ApoE2 genotype. *Neurobiology of Disease*, 13(3), 246–253.
- Larson, J., Lynch, G., Games, D., & Seubert, P. (1999). Alterations in synaptic transmission and long-term potentiation in hippocampal slices from young and aged PDAPP mice. *Brain Research*, 840(1–2), 23–35.
- Larson, M., Sherman, M. A., Amar, F., Nuvolone, M., Schneider, J. A., Bennett, D. A., ... Lesné, S. E. (2012). The complex PrPc-Fyn couples human oligomeric A $\beta$  with pathological tau changes in Alzheimer's disease. *Journal of Neuroscience*, 32(47), 16857–16871.

## List of References

- Lavezzari, G., McCallum, J., Dewey, C. M., & Roche, K. W. (2004). Subunit-specific regulation of NMDA receptor endocytosis. *The Journal of Neuroscience : The Official Journal of the Society for Neuroscience*, 24(28), 6383–6391.
- Lavezzari, G., McCallum, J., Lee, R., & Roche, K. W. (2003). Differential binding of the AP-2 adaptor complex and PSD-95 to the C-terminus of the NMDA receptor subunit NR2B regulates surface expression. *Neuropharmacology*, 45(6), 729–737.
- Lee, G., Thangavel, R., Sharma, V. M., Litersky, J. M., Bhaskar, K., Fang, S. M., ... Ksiezak-Reding, H. (2004). Phosphorylation of Tau by Fyn: Implications for Alzheimer's Disease. *Journal of Neuroscience*, 24(9), 2304–2312.
- Lee, G., Todd Newman, S., Gard, D. L., Band, H., & Panchamoorthy, G. (1998). Tau interacts with src-family non-receptor tyrosine kinases. *Journal of Cell Science*, 111(21), 3167–3177.
- Lee, H. K., Barbarosie, M., Kameyama, K., Bear, M. F., & Huganir, R. L. (2000). Regulation of distinct AMPA receptor phosphorylation sites during bidirectional synaptic plasticity. *Nature*, 405, 955–959.
- Lee, H. K., Takamiya, K., He, K., Song, L., & Huganir, R. L. (2010). Specific Roles of AMPA Receptor Subunit GluR1 (GluA1) Phosphorylation Sites in Regulating Synaptic Plasticity in the CA1 Region of Hippocampus. *Journal of Neurophysiology*, 103(1), 479.
- Lee, S., Salazar, S. V, Cox, T. O., & Strittmatter, S. M. (2019). Pyk2 Signaling through Graf1 and RhoA GTPase Is Required for Amyloid-Oligomer-Triggered Synapse Loss. *J Neurosci*, 39(10), 1910.
- Lewis, J., Dickson, D. W., Lin, W. L., Chisholm, L., Corral, A., Jones, G., ... McGowan, E. (2001). Enhanced neurofibrillary degeneration in transgenic mice expressing mutant tau and APP. *Science*, 293(5534), 1487–1491.
- Li, C., & Götz, J. (2018). Pyk2 is a Novel Tau Tyrosine Kinase that is Regulated by the Tyrosine Kinase Fyn. *Journal of Alzheimer's Disease*, 64(1), 205.
- Li, S., Jin, M., Koeglsperger, T., Shepardson, N. E., Shankar, G. M., & Selkoe, D. J. (2011). Soluble  $\beta$  oligomers inhibit long-term potentiation through a mechanism involving excessive activation of extrasynaptic NR2B-containing NMDA receptors. *Journal of Neuroscience*, 31(18), 6627–6638.
- Lindwall, G., & Cole, R. D. (1984). Phosphorylation affects the ability of tau protein to promote microtubule assembly. *Journal of Biological Chemistry*, 259(8), 5301–5305.

- Liu, Shi Jie, Gasperini, R., Foa, L., & Small, D. H. (2010). Amyloid- $\beta$  decreases cell-surface AMPA receptors by increasing intracellular calcium and phosphorylation of GluR2. *Journal of Alzheimer's Disease*, 21(2), 655–666.
- Liu, Siqiong June, & Zukin, R. S. (2007).  $\text{Ca}^{2+}$ -permeable AMPA receptors in synaptic plasticity and neuronal death. *Trends in Neurosciences*, 30(3), 126–134.
- Liu, X. B., Murray, K. D., & Jones, E. G. (2004). Switching of NMDA Receptor 2A and 2B Subunits at Thalamic and Cortical Synapses during Early Postnatal Development. *Journal of Neuroscience*, 24(40), 8885–8895.
- Lott, I. T., & Head, E. (2019, March 1). Dementia in Down syndrome: unique insights for Alzheimer disease research. *Nature Reviews Neurology*, Vol. 15, pp. 135–147.
- Lu, W., Shi, Y., Jackson, A. C., Bjorgan, K., During, M. J., Sprengel, R., ... Nicoll, R. A. (2009). Subunit composition of synaptic AMPA receptors revealed by a single-cell genetic approach. *Neuron*, 62(2), 254–268.
- Lu, Y. F., Kojima, N., Tomizawa, K., Moriwaki, A., Matsushita, M., Obata, K., & Matsui, H. (1999). Enhanced synaptic transmission and reduced threshold for LTP induction in fyn-transgenic mice. *The European Journal of Neuroscience*, 11(1), 75–82.
- Lu, Y. M., Roder, J. C., Davidow, J., & Salter, M. W. (1998). Src activation in the induction of long-term potentiation in CA1 hippocampal neurons. *Science*, 279(5355), 1363–1367.
- Lynch, G., Larson, J., Kelso, S., Barrionuevo, G., & Schottler, F. (1983). Intracellular injections of EGTA block induction of hippocampal long-term potentiation. *Nature*, 305, 719–721.
- Lynch, M. A. (2004). Long-Term Potentiation and Memory. *Physiological Reviews*, 84(1), 87–136.
- Macdermott, A. B., Mayer, M. L., Westbrook, G. L., Smith, S. J., & Barker, J. L. (1986). NMDA-receptor activation increases cytoplasmic calcium concentration in cultured spinal cord neurones. *Nature*, 321, 519–522.
- Madisen, L., Zwingman, T. A., Sunkin, S. M., Oh, S. W., Zariwala, H. A., Gu, H., ... Zeng, H. (2010). A robust and high-throughput Cre reporting and characterization system for the whole mouse brain. *Nature Neuroscience*, 13(1), 133–140.
- Maloney, J. A., Bainbridge, T., Gustafson, A., Zhang, S., Kyauk, R., Steiner, P., ... Atwal, J. K. (2014). Molecular Mechanisms of Alzheimer Disease Protection by the A673T Allele of Amyloid Precursor Protein. *The Journal of Biological Chemistry*, 289(45), 30990.

## List of References

- Marcello, E., Epis, R., Saraceno, C., & Di Luca, M. (2012). Synaptic dysfunction in Alzheimer's disease. *Advances in Experimental Medicine and Biology*, 970, 573–601.
- Mastrolia, V., al Massadi, O., de Pins, B., & Girault, J. A. (2021). Pyk2 in dorsal hippocampus plays a selective role in spatial memory and synaptic plasticity. *Scientific Reports*, 11(1), 16357.
- Mawuenyega, K. G., Sigurdson, W., Ovod, V., Munsell, L., Kasten, T., Morris, J. C., ... Bateman, R. J. (2010). Decreased clearance of CNS  $\beta$ -amyloid in Alzheimer's disease. *Science*, 330(6012), 1774.
- Mayer, M. L., Westbrook, G. L., & Guthrie, P. B. (1984). Voltage-dependent block by  $Mg^{2+}$  of NMDA responses in spinal cord neurones. *Nature*, 309, 261–263.
- McKean, N. E., Handley, R. R., & Snell, R. G. (2021). A Review of the Current Mammalian Models of Alzheimer's Disease and Challenges That Need to Be Overcome. *International Journal of Molecular Sciences*, 22(23), 13168.
- Mehta, A., Prabhakar, M., Kumar, P., Deshmukh, R., & Sharma, P. L. (2013). Excitotoxicity: Bridge to various triggers in neurodegenerative disorders. *European Journal of Pharmacology*, 698(1–3), 6–18.
- Meisl, G., Yang, X., Hellstrand, E., Frohm, B., Kirkegaard, J. B., Cohen, S. I. A., ... Knowles, T. P. J. (2014). Differences in nucleation behavior underlie the contrasting aggregation kinetics of the A $\beta$ 40 and A $\beta$ 42 peptides. *Proceedings of the National Academy of Sciences of the United States of America*, 111(26), 9384–9389.
- Meng, Y., Zhang, Y., & Jia, Z. (2003). Synaptic transmission and plasticity in the absence of AMPA glutamate receptor GluR2 and GluR3. *Neuron*, 39(1), 163–176.
- Minkeviciene, R., Ihalaenen, J., Malm, T., Matilainen, O., Keksa-Goldsteine, V., Goldsteins, G., ... Tanila, H. (2008). Age-related decrease in stimulated glutamate release and vesicular glutamate transporters in APP/PS1 transgenic and wild-type mice. *Journal of Neurochemistry*, 105(3), 584–594.
- Mitchell, A. J., & Shiri-Feshki, M. (2008). Temporal trends in the long term risk of progression of mild cognitive impairment: A pooled analysis. *Journal of Neurology, Neurosurgery and Psychiatry*, 79(12), 1386–1391.
- Miyakawa, T., Yagi, T., Tateishi, K., & Niki, H. (1996). Susceptibility to drug-induced seizures of Fyn tyrosine kinase-deficient mice. *NeuroReport*, 7(15), 2723–2726.

- Moncaut, N., & Hart-Johnson, S. (2021). The impact of COVID-19 lockdowns on the genetic integrity of your mouse colonies. *Lab Animal* 2021 50:11, 50(11), 301–302.
- Monyer, H., Burnashev, N., Laurie, D. J., Sakmann, B., & Seeburg, P. H. (1994). Developmental and regional expression in the rat brain and functional properties of four NMDA receptors. *Neuron*, 12(3), 529–540.
- Morris, M., Knudsen, G. M., Maeda, S., Trinidad, J. C., Ioanoviciu, A., Burlingame, A. L., & Mucke, L. (2015). Tau post-translational modifications in wild-type and human amyloid precursor protein transgenic mice. *Nature Neuroscience*, 18(8), 1183–1189.
- Mucke, L., Masliah, E., Yu, G. Q., Mallory, M., Rockenstein, E. M., Tatsuno, G., ... McConlogue, L. (2000). High-level neuronal expression of A $\beta$ (1-42) in wild-type human amyloid protein precursor transgenic mice: Synaptotoxicity without plaque formation. *Journal of Neuroscience*, 20(11), 4050–4058.
- Mufson, E. J., Ikonov, M. D., Counts, S. E., Perez, S. E., Malek-Ahmadi, M., Scheff, S. W., & Ginsberg, S. D. (2016, September 15). Molecular and cellular pathophysiology of preclinical Alzheimer's disease. *Behavioural Brain Research*, Vol. 311, pp. 54–69.
- Murphy, P. M., Beckett, T. L., Ding, Q., Patel, E., Markesbery, W. R., St Clair, D. K., ... Keller, J. N. (2007). A $\beta$  solubility and deposition during AD progression and in APP  $\times$  PS-1 knock-in mice. *Neurobiology of Disease*, 27(3), 301–311.
- Nakazawa, K., Quirk, M. C., Chitwood, R. A., Watanabe, M., Yeckel, M. F., Sun, L. D., ... Tonegawa, S. (2002). Requirement for Hippocampal CA3 NMDA Receptors in Associative Memory Recall. *Science*, 297(5579), 211–218.
- Nakazawa, T., Komai, S., Tezuka, T., Hisatsune, C., Umemori, H., Semba, K., ... Yamamoto, T. (2001). Characterization of Fyn-mediated Tyrosine Phosphorylation Sites on GluR $\epsilon$ 2 (NR2B) Subunit of the N-Methyl-D-aspartate Receptor. *Journal of Biological Chemistry*, 276(1), 693–699.
- Nakazawa, T., Komai, S., Watabe, A. M., Kiyama, Y., Fukaya, M., Arima-Yoshida, F., ... Manabe, T. (2006). NR2B tyrosine phosphorylation modulates fear learning as well as amygdaloid synaptic plasticity. *EMBO Journal*, 25(12), 2867–2877.
- National Institute for Health and Clinical Excellence. (2011). Donepezil, galantamine, rivastigmine, and memantine for the treatment of Alzheimer's Disease. In *National Institute for Health and Clinical Excellence*.

## List of References

- Nguyen, T. H., Liu, J., & Lombroso, P. J. (2002). Striatal enriched phosphatase 61 dephosphorylates Fyn at phosphotyrosine 420. *Journal of Biological Chemistry*, 277(27), 24274–24279.
- Nicoll, R. A. (2017). A Brief History of Long-Term Potentiation. *Neuron*, 93(2), 281–290.
- Nicoll, R. A., & Schmitz, D. (2005). Synaptic plasticity at hippocampal mossy fibre synapses. *Nature Reviews Neuroscience* 2005 6:11, 6(11), 863–876.
- Nishi, A., Kuroiwa, M., & Shuto, T. (2011). Mechanisms for the modulation of dopamine D 1 receptor signaling in striatal neurons. *Frontiers in Neuroanatomy*, 0(JULY), 43.
- Nowak, L., Bregestovski, P., Ascher, P., Herbet, A., & Prochiantz, A. (1984). Magnesium gates glutamate-activated channels in mouse central neurones. *Nature*, 307, 462–465.
- Nozaki, C., Vergnano, A. M., Filliol, D., Ouagazzal, A.-M., Goff, A. Le, Carvalho, S., ... L Kieffer, B. (2011). Zinc alleviates pain through high-affinity binding to the NMDA receptor NR2A subunit. *Nat Neurosci*, 14(8), 1017–1022.
- Nussbaum, R. L., & Ellis, C. E. (2003). Alzheimer's Disease and Parkinson's Disease. *New England Journal of Medicine*, 348(14), 1356–1364.
- Nygaard, H. B., Wagner, A. F., Bowen, G. S., Good, S. P., MacAvoy, M. G., Strittmatter, K. A., ... Van Dyck, C. H. (2015). A phase Ib multiple ascending dose study of the safety, tolerability, and central nervous system availability of AZD0530 (saracatinib) in Alzheimer's disease. *Alzheimer's Research and Therapy*, 7(1), 35.
- O'Dell, T. J., Kandel, E. R., & Grant, S. G. N. (1991). Long-term potentiation in the hippocampus is blocked by tyrosine kinase inhibitors. *Nature*, 353, 558–560.
- Orgogozo, J. M., Gilman, S., Dartigues, J. F., Laurent, B., Puel, M., Kirby, L. C., ... Hock, C. (2003). Subacute meningoencephalitis in a subset of patients with AD after A $\beta$ 42 immunization. *Neurology*, 61(1), 46–54.
- Owen, D. J., & Evans, P. R. (1998). A structural explanation for the recognition of tyrosine-based endocytotic signals. *Science*, 282(5392), 1327–1332.
- Padmanabhan, P., Martínez-Mármol, R., Xia, D., Götz, J., & Meunier, F. A. (2019). Frontotemporal dementia mutant Tau promotes aberrant Fyn nanoclustering in hippocampal dendritic spines. *ELife*, 8, e45040.
- Paoletti, P., Bellone, C., & Zhou, Q. (2013). NMDA receptor subunit diversity: Impact on receptor properties, synaptic plasticity and disease. *Nature Reviews Neuroscience*, 14(6), 383–400.



- Papouin, T., & Haydon, P. G. (2018). Obtaining Acute Brain Slices. *Bio-Protocol*, 8(2).
- Paul, S., Snyder, G. L., Yokakura, H., Picciotto, M. R., Nairn, A. C., & Lombroso, P. J. (2000). The Dopamine/D1 Receptor Mediates the Phosphorylation and Inactivation of the Protein Tyrosine Phosphatase STEP via a PKA-Dependent Pathway. *J Neurosci*, 20(15), 5630–5638. Retrieved from <https://www.jneurosci.org/content/jneuro/20/15/5630.full.pdf>
- Petit, T. L., & LeBoutillier, J. C. (1990). Quantifying synaptic number and structure: effects of stain and post-mortem delay. *Brain Research*, 517(1–2), 269–275.
- Pettit, D. L., Perlman, S., & Malinow, R. (1994). Potentiated Transmission and Prevention of Further LTP by Increased CaMKII activity in Postsynaptic Hippocampal Slice Neurons. *Science*, 266, 1881–1885.
- Pham, E., Crews, L., Ubhi, K., Hansen, L., Adame, A., Cartier, A., ... Masliah, E. (2010). Progressive accumulation of amyloid- $\beta$  oligomers in Alzheimer's disease and in amyloid precursor protein transgenic mice is accompanied by selective alterations in synaptic scaffold proteins. *FEBS Journal*, 277(14), 3051–3067.
- Philpot, B. D., K, S. A., Shouval, H. Z., & Bear, M. F. (2001). Visual Experience and Deprivation Bidirectionally Modify the Composition and Function of NMDA Receptors in Visual Cortex. *Neuron*, 29(1), 157–169.
- Pitera, A. P., Asuni, A. A., O'Connor, V., & Deinhardt, K. (2019). Pathogenic tau does not drive activation of the unfolded protein response. *Journal of Biological Chemistry*, 294(25), 9679–9688.
- Prybylowski, K., Chang, K., Sans, N., Kan, L., Vicini, S., & Wenthold, R. J. (2005). The synaptic localization of NR2B-containing NMDA receptors is controlled by interactions with PDZ proteins and AP-2. *Neuron*, 47(6), 845–857.
- Quinlan, E., Philpot, B. D., Huganir, R. L., & Bear, M. F. (1999). Rapid, experience-dependent expression of synaptic NMDA receptors in visual cortex in vivo. *Nature Neuroscience*, 2(4), 352–357.
- Rapoport, M., Dawson, H. N., Binder, L. I., Vitek, M. P., & Ferreira, A. (2002). Tau is essential to  $\beta$ -amyloid-induced neurotoxicity. *Proceedings of the National Academy of Sciences of the United States of America*, 99(9), 6364–6369.
- Roberson, E. D., Scarce-Levie, K., Palop, J. J., Yan, F., Cheng, I. H., Wu, T., ... Mucke, L. (2007). Reducing Endogenous Tau Ameliorates Amyloid -Induced Deficits in an Alzheimer's Disease

## List of References

- Mouse Model. *Science*, 316(5825), 750–754.
- Roberson, Erik D, Halabisky, B., Yoo, J. W., Yao, J., Chin, J., Yan, F., ... Mucke, L. (2011). Amyloid- $\beta$ /Fyn-Induced Synaptic, Network, and Cognitive Impairments Depend on Tau Levels in Multiple Mouse Models of Alzheimer's Disease NIH Public Access. *J Neurosci*, 31(2), 700–711.
- Roche, K. W., Standley, S., McCallum, J., Dune Ly, C., Ehlers, M. D., & Wenthold, R. J. (2001). Molecular determinants of NMDA receptor internalization. *Nature Neuroscience*, 4(8), 794–802.
- Roder, S., Danober, L., Pozza, M. F., Lingenhoehl, K., Wiederhold, K. H., & Olpe, H. R. (2003). Electrophysiological studies on the hippocampus and prefrontal cortex assessing the effects of amyloidosis in amyloid precursor protein 23 transgenic mice. *Neuroscience*, 120(3), 705–720.
- S. Maltera, J. (2011). Effect of Anticoagulants on Amyloid-Protein Precursor and Amyloid Beta Levels in Plasma. *Journal of Alzheimer's Disease & Parkinsonism*, 1, 101.
- Saganich, M. J., Schroeder, B. E., Galvan, V., Bredesen, D. E., Koo, E. H., & Heinemann, S. F. (2006). Deficits in synaptic transmission and learning in amyloid precursor protein (APP) transgenic mice require C-terminal cleavage of APP. *Journal of Neuroscience*, 26(52), 13428–13436.
- Salazar, S. V., Cox, T. O., Lee, S., Brody, A. H., Chyung, A. S., Haas, L. T., & Strittmatter, S. M. (2019). Alzheimer's Disease Risk Factor Pyk2 Mediates Amyloid- $\beta$ -Induced Synaptic Dysfunction and Loss. *The Journal of Neuroscience : The Official Journal of the Society for Neuroscience*, 39(4), 758–772.
- Salter, M. W., & Kalia, L. V. (2004). SRC kinases: A hub for NMDA receptor regulation. *Nature Reviews Neuroscience*, 5(4), 317–328.
- Sasahara, M., Fries, J. W. U., Raines, E. W., Gown, A. M., Westrum, L. E., Frosch, M. P., ... Collins, T. (1991). PDGF B-chain in neurons of the central nervous system, posterior pituitary, and in a transgenic model. *Cell*, 64(1), 217–227.
- Scheff, S. W., Price, D. A., Schmitt, F. A., Dekosky, S. T., & Mufson, E. J. (2007). Synaptic alterations in CA1 in mild Alzheimer disease and mild cognitive impairment. *Neurology*, 68(18), 1501–1508.
- Scheff, S. W., Price, D. A., Schmitt, F. A., & Mufson, E. J. (2006). Hippocampal synaptic loss in early Alzheimer's disease and mild cognitive impairment. *Neurobiology of Aging*, 27(10), 1372–

1384.

- Scheff, S. W., Price, D. A., Schmitt, F. A., Scheff, M. A., & Mufson, E. J. (2011). Synaptic loss in the inferior temporal gyrus in mild cognitive impairment and Alzheimer's disease. *Journal of Alzheimer's Disease*, 24(3), 547–557.
- Scott, D. B., Michailidis, I., Mu, Y., Logothetis, D., & Ehlers, M. D. (2004). Endocytosis and Degradative Sorting of NMDA Receptors by Conserved Membrane-Proximal Signals. *The Journal of Neuroscience*, 24(32), 7096.
- Serneels, L., Van Biervliet, J., Craessaerts, K., Dejaegere, T., Horr  , K., Van Houtvin, T., ... De Strooper, B. (2009).  $\gamma$ -Secretase heterogeneity in the aph1 subunit: Relevance for alzheimer's disease. *Science*, 324, 639–642.
- Seubert, P., Vigo-Pelfrey, C., Esch, F., Lee, M., Dovey, H., Davis, D., ... Schenk, D. (1992). Isolation and quantification of soluble Alzheimer's  $\beta$ -peptide from biological fluids. *Nature*, 359(6393), 325–327.
- Shankar, G. M., Bloodgood, B. L., Townsend, M., Walsh, D. M., Selkoe, D. J., & Sabatini, B. L. (2007). Natural oligomers of the Alzheimer amyloid- $\beta$  protein induce reversible synapse loss by modulating an NMDA-type glutamate receptor-dependent signaling pathway. *Journal of Neuroscience*, 27(11), 2866–2875.
- Shankar, G. M., Li, S., Mehta, T. H., Garcia-Munoz, A., Shepardson, N. E., Smith, I., ... Selkoe, D. J. (2008). Amyloid- $\beta$  protein dimers isolated directly from Alzheimer's brains impair synaptic plasticity and memory. *Nature Medicine*, 14(8), 837–842.
- Shipton, O. A., Leitz, J. R., Dworzak, J., Acton, C. E. J., Tunbridge, E. M., Denk, F., ... Vargas-Caballero, M. (2011). Tau Protein Is Required for Amyloid -Induced Impairment of Hippocampal Long-Term Potentiation. *Journal of Neuroscience*, 31(5), 1688–1692.
- Shipton, O. A., & Paulsen, O. (2013). GluN2A and GluN2B subunit-containing NMDA receptors in hippocampal plasticity. *Philosophical Transactions of the Royal Society B: Biological Sciences*, 369(1633), 20130163–20130163.
- Shirazi, S. K., & Wood, J. G. (1993). The protein tyrosine kinase, fyn, in Alzheimer's disease pathology. *Neuroreport*, 4(4), 435–437.
- Silbering, A. F., & Benton, R. (2010). Ionotropic and metabotropic mechanisms in chemoreception: Chance or design? *EMBO Reports*, 11(3), 173–179.

## List of References

- Smith, L. M., Zhu, R., & Strittmatter, S. M. (2018). Disease-modifying benefit of Fyn blockade persists after washout in mouse Alzheimer's model. *Neuropharmacology*, 130, 54–61.
- Song, B., Ao, Q., Niu, Y., Shen, Q., Zuo, H. C., Zhang, X. F., & Gong, Y. D. (2013). Amyloid beta-peptide worsens cognitive impairment following cerebral ischemia-reperfusion injury. *Neural Regeneration Research*, 8(26), 2449.
- Sperling, R. A., Aisen, P. S., Beckett, L. A., Bennett, D. A., Craft, S., Fagan, A. M., ... Phelps, C. H. (2011). Toward defining the preclinical stages of Alzheimer's disease: Recommendations from the National Institute on Aging-Alzheimer's Association workgroups on diagnostic guidelines for Alzheimer's disease. *Alzheimer's and Dementia*, 7(3), 280–292.
- Sri, S. (2018). *Emergence of synaptic and cognitive dysfunction in an inducible mouse model of Alzheimer's disease*. University of Southampton.
- Sri, S., Pegasiou, C. M., Cave, C. A., Hough, K., Wood, N., Gomez-Nicola, D., ... Vargas-Caballero, M. (2019). Emergence of synaptic and cognitive impairment in a mature-onset APP mouse model of Alzheimer's disease. *Acta Neuropathologica Communications*, 7(1), 25.
- Stevens, C. F., & Wang, Y. (1995). Facilitation and depression at single central synapses. *Neuron*, 14(4), 795–802.
- Strack, S., & Colbran, R. J. (1998). Autophosphorylation-dependent Targeting of Calcium/Calmodulin-dependent Protein Kinase II by the NR2B Subunit of the N-Methyl-D-aspartate Receptor. *Journal of Biological Chemistry*, 273(33), 20689–20692.
- Stramiello, M., & Wagner, J. J. (2008). D1/5 receptor-mediated enhancement of LTP requires PKA, Src family kinases, and NR2B-containing NMDARs. *Neuropharmacology*, 55(5), 871–877.
- Sturchler-Pierrat, C., Abramowski, D., Duke, M., Wiederhold, K. H., Mistl, C., Rothacher, S., ... Sommer, B. (1997). Two amyloid precursor protein transgenic mouse models with Alzheimer disease-like pathology. *Proceedings of the National Academy of Sciences of the United States of America*, 94(24), 13287–13292.
- Tang, T. T. T., Badger, J. D., Roche, P. A., & Roche, K. W. (2010). Novel approach to probe subunit-specific contributions to N-methyl-D-aspartate (NMDA) receptor trafficking reveals a dominant role for NR2B in receptor recycling. *The Journal of Biological Chemistry*, 285(27), 20975–20981.
- Taubenfeld, S. M., Stevens, K. A., Pollonini, G., Ruggeiro, J., & Alberini, C. M. (2002). Profound molecular changes following hippocampal slice preparation: loss of AMPA receptor subunits

- and uncoupled mRNA/protein expression. *Journal of Neurochemistry*, 81(6), 1348–1360.
- Terry, R. D., Masliah, E., Salmon, D. P., Butters, N., DeTeresa, R., Hill, R., ... Katzman, R. (1991). Physical basis of cognitive alterations in Alzheimer's disease: Synapse loss is the major correlate of cognitive impairment. *Annals of Neurology*, 30(4), 572–580.
- Thomson, A. M., & Bannister, A. P. (1999). Release-independent depression at pyramidal inputs onto specific cell targets: dual recordings in slices of rat cortex. *The Journal of Physiology*, 519 Pt 1(Pt 1), 57–70.
- Tovar, K. R., & Westbrook, G. L. (2002). Mobile NMDA Receptors at Hippocampal Synapses. *Neuron*, 34(2), 255–264.
- Trabzuni, D., Wray, S., Vandrovcova, J., Ramasamy, A., Walker, R., Smith, C., ... Ryten, M. (2012). MAPT expression and splicing is differentially regulated by brain region: relation to genotype and implication for tauopathies. *Human Molecular Genetics*, 21(18), 4094–4103.
- Traynelis, S. F., Lonnie P, W., McBain, C. J., Menniti, F. S., Vance, K. M., Ogden, K. K., ... Dingledine, R. (2010). Glutamate receptor ion channels: structure, regulation, and function. *Pharmacological Reviews*, 62(3), 405–496.
- Trinchese, F., Liu, S., Battaglia, F., Walter, S., Mathews, P. M., & Arancio, O. (2004). Progressive age-related development of Alzheimer-like pathology in APP/PS1 mice. *Annals of Neurology*, 55(6), 801–814.
- Tsien, J. Z., Huerta, P. T., & Tonegawa, S. (1996). The Essential Role of Hippocampal CA1 NMDA Receptor–Dependent Synaptic Plasticity in Spatial Memory. *Cell*, 87(7), 1327–1338.
- Um, J. W., Kaufman, A. C., Kostylev, M., Heiss, J. K., Stagi, M., Takahashi, H., ... Strittmatter, S. M. (2013). Metabotropic Glutamate Receptor 5 Is a Coreceptor for Alzheimer A $\beta$  Oligomer Bound to Cellular Prion Protein. *Neuron*, 79(5), 887–902.
- Um, J. W., Nygaard, H. B., Heiss, J. K., Kostylev, M. A., Stagi, M., Vortmeyer, A., ... Strittmatter, S. M. (2012). Alzheimer amyloid- $\beta$  oligomer bound to postsynaptic prion protein activates Fyn to impair neurons. *Nature Neuroscience*, 15(9), 1227–1235.
- Valdivielso, J. M., Eritja, À., Caus, M., & Bozic, M. (2020). Glutamate-Gated NMDA Receptors: Insights into the Function and Signaling in the Kidney. *Biomolecules*, 10(7), 1051.
- Van Dam, D., D'Hooge, R., Staufenbiel, M., Van Ginneken, C., Van Meir, F., & De Deyn, P. P. (2003). Age-dependent cognitive decline in the APP23 model precedes amyloid deposition.

## List of References

- European Journal of Neuroscience*, 17(2), 388–396.
- Van Dyck, C. H., Nygaard, H. B., Chen, K., Donohue, M. C., Raman, R., Rissman, R. A., ... Strittmatter, S. M. (2019). Effect of AZD0530 on Cerebral Metabolic Decline in Alzheimer Disease: A Randomized Clinical Trial. *JAMA Neurology*, 76(10), 1219–1229.
- Vanderwolf, C. H. (1969). Hippocampal electrical activity and voluntary movement in the rat. *Electroencephalography and Clinical Neurophysiology*, 26(4), 407–418.
- Vargas-Caballero, M., Denk, F., Wobst, H. J., Arch, E., Pegasiou, C.-M., Oliver, P. L., ... Wade-Martins, R. (2017). Wild-Type, but Not Mutant N296H, Human Tau Restores A $\beta$ -Mediated Inhibition of LTP in Tau-/- mice. *Frontiers in Neuroscience*, 11, 201.
- Vargas-Caballero, M., Willaime-Morawek, S., Gomez-Nicola, D., Perry, V. H., Bulters, D., & Mudher, A. (2016, April 2). The use of human neurons for novel drug discovery in dementia research. *Expert Opinion on Drug Discovery*, Vol. 11, pp. 355–367.
- Venkitaramani, D. V, Moura, P. J., Picciotto, M. R., & Lombroso, P. J. (2011). Striatal-enriched protein tyrosine phosphatase (STEP) knockout mice have enhanced hippocampal memory. *European Journal of Neuroscience*, 33(12), 2288–2298.
- Volianskis, A., Køstner, R., Mølgaard, M., Hass, S., & Jensen, M. S. (2010). Episodic memory deficits are not related to altered glutamatergic synaptic transmission and plasticity in the CA1 hippocampus of the APP<sup>swe</sup>/PS1 $\Delta$ E9-deleted transgenic mice model of  $\beta$ -amyloidosis. *Neurobiology of Aging*, 31(7), 1173–1187.
- Vorhees, C. V., & Williams, M. T. (2006). Morris water maze: procedures for assessing spatial and related forms of learning and memory. *Nature Protocols*, 1(2), 848.
- Wan, Q., Man, H. Y., Braunton, J., Wang, W., Salter, M. W., Becker, L., & Wang, Y. T. (1997). Modulation of GABAA Receptor Function by Tyrosine Phosphorylation of  $\beta$  Subunits. *Journal of Neuroscience*, 17(13), 5062–5069.
- Wang, Y., Ma, Y., Hu, J., Cheng, W., Jiang, H., Zhang, X., ... Li, X. (2015). Prenatal chronic mild stress induces depression-like behavior and sex-specific changes in regional glutamate receptor expression patterns in adult rats. *Neuroscience*, 301, 363–374.
- Wang, Yan, & Qin, Z. (2010). Molecular and cellular mechanisms of excitotoxic neuronal death. *Apoptosis in the Aging Brain*, 15(11), 1382–1402.
- Wang, Yipeng, & Mandelkow, E. (2016, January 1). Tau in physiology and pathology. *Nature*

*Reviews Neuroscience*, Vol. 17, pp. 5–21.

- Waxman, E. A., & Lynch, D. R. (2005). N-methyl-D-aspartate receptor subtype mediated bidirectional control of p38 mitogen-activated protein kinase. *The Journal of Biological Chemistry*, 280(32), 29322–29333.
- Weggen, S., & Beher, D. (2012). Molecular consequences of amyloid precursor protein and presenilin mutations causing autosomal-dominant Alzheimer's disease. *Alzheimer's Research and Therapy*, Vol. 4, p. 9.
- Wentholt, R. J., Petralia, R. S., J. B. I., & Niedzielski, A. (1996). Evidence for multiple AMPA receptor complexes in hippocampal CA1/CA2 neurons. *J Neurosci*, 16(6), 1982–1989.
- Wittenberg, R., Hu, B., Barraza-Araiza, L., & Rehill, A. (2019). *Projections of older people with dementia and costs of dementia care in the United Kingdom, 2019–2040*.
- Wright, A. L., Zinn, R., Hohensinn, B., Konen, L. M., Beynon, S. B., Tan, R. P., ... Vissel, B. (2013). Neuroinflammation and Neuronal Loss Precede A $\beta$  Plaque Deposition in the hAPP-J20 Mouse Model of Alzheimer's Disease. *PLoS ONE*, 8(4), e59586.
- Wyllie, D. J. A., Livesey, G. E., & Hardingham, G. E. (2013). Influence of GluN2 subunit identity on NMDA receptor function. *Neuropharmacology*, 74, 4–17.
- Xia, D., & Götz, J. (2014). Premature lethality, hyperactivity, and aberrant phosphorylation in transgenic mice expressing a constitutively active form of Fyn. *Frontiers in Molecular Neuroscience*, 7, 40.
- Xiao, M. Y., Zhou, Q., & Nicoll, R. A. (2001). Metabotropic glutamate receptor activation causes a rapid redistribution of AMPA receptors. *Neuropharmacology*, 41(6), 664–671.
- Yagi, T. (1994). Src Family Kinases Control Neural Development and Function. *Development, Growth & Differentiation*, 36(6), 543–550.
- Yang, K., Trepanier, C., Sidhu, B., Xie, Y. F., Li, H., Lei, G., ... MacDonald, J. F. (2012). Metaplasticity gated through differential regulation of GluN2A versus GluN2B receptors by Src family kinases. *EMBO Journal*, 31(4), 805–816.
- Yu, X. M., Askalan, R., Keil, G. J., & Salter, M. W. (1997). NMDA channel regulation by channel-associated protein tyrosine kinase Src. *Science*, 275(5300), 674–678.
- Zamanillo, D., Sprengel, R., Hvalby, Ø., Jensen, V., Burnashev, N., Rozov, A., ... Sakmann, B. (1999). Importance of AMPA receptors for hippocampal synaptic plasticity but not for spatial

## List of References

- learning. *Science*, 284, 1805–1811.
- Zanetti, L., Regoni, M., Ratti, E., Valtorta, F., & Sassone, J. (2021). Presynaptic AMPA receptors in health and disease. *Cells*, 10(9), 2260.
- Zhao, M., Finlay, D., Zharkikh, I., & Vuori, K. (2016). Novel role of Src in priming Pyk2 phosphorylation. *PLoS ONE*, 11(2), e0149231.
- Zhao, M. G., Toyoda, H., Lee, Y. S., Wu, L. J., Ko, S. W., Zhang, X. H., ... Zhuo, M. (2005). Roles of NMDA NR2B subtype receptor in prefrontal long-term potentiation and contextual fear memory. *Neuron*, 47(6), 859–872.
- Zheng, H., & Koo, E. H. (2006). The amyloid precursor protein: beyond amyloid. *Molecular Neurodegeneration*, 1(1), 5.
- Zhou, Y., Takahashi, E., Li, W., Halt, A., Wiltgen, B., Ehninger, D., ... Silva, A. J. (2007). Interactions between the NR2B receptor and CaMKII modulate synaptic plasticity and spatial learning. *The Journal of Neuroscience : The Official Journal of the Society for Neuroscience*, 27(50), 13843–13853.



